

**Micellar Lyotropic Gels:  
The interplay between gel network and liquid-crystalline order**

Von der Fakultät Chemie der Universität Stuttgart zur Erlangung der Würde eines  
Doktors der Naturwissenschaften (Dr. rer. nat.) genehmigte Abhandlung

Vorgelegt von  
**Sonja Dieterich**  
aus Ludwigsburg

Hauptberichter: Prof. Dr. Frank Gießelmann

Mitberichter: Prof. Dr. Jan Lagerwall

Tag der mündlichen Prüfung: 30.07.2021

Institut für Physikalische Chemie der Universität Stuttgart

2021





## **Declaration of Authorship**

I hereby certify that the dissertation entitled

Micellar Lyotropic Gels - The interplay between gel network and liquid-crystalline order

is entirely my own work except where otherwise indicated. Passages and ideas from other sources have been clearly indicated.

Name/Name: \_\_\_\_\_

Unterschrift/Signed: \_\_\_\_\_

Datum/Date: \_\_\_\_\_

This doctoral thesis has been prepared in the framework of the DFG-funded project "Lyotropic Gels" (DFG Gi 243/9-1) at the Institute of Physical Chemistry of the University of Stuttgart. In addition, measurements were performed at the Institute Laue-Langevin (ILL) in Grenoble, France, and at the Physical and Biophysical Research Group (PC III) at Bielefeld University.

My cumulative thesis is based on the following three publications:

- (I) S. Dieterich, T. Sottmann, F. Giesselmann, Gelation of Lyotropic Liquid-Crystal Phases-The Interplay between Liquid Crystalline Order and Physical Gel Formation, *Langmuir* **2019**, *35*, 16793.
- (II) S. Dieterich, F. Stemmler, N. Preisig, F. Giesselmann, Micellar Lyotropic Nematic Gels, *Adv. Mater.* **2021**, *33*, 2007340.
- (III) S. Dieterich, S. Prévost, C. Dargel, T. Sottmann, F. Giesselmann, Synergistic structures in lyotropic lamellar gels, *Soft Matter* **2020**, *16*, 10268.

Furthermore, the results have contributed to the following publications:

- (IV) S. Koitani, S. Dieterich, N. Preisig, K. Aramaki, C. Stubenrauch, Gelling Lamellar Phases of the Binary System Water-Didodecyldimethylammonium Bromide with an Organogelator, *Langmuir* **2017**, *33*, 12171.
- (V) K. Steck, S. Dieterich, C. Stubenrauch, F. Giesselmann, Surfactant-based lyotropic liquid crystal gels – the interplay between anisotropic order and gel formation, *J. Mater. Chem. C* **2020**, *8*, 5335.

---

The results have also been presented at national and international conferences as follows:

*Oral contributions*

- Sonja Dieterich, Natalie Preisig, Thomas Sottmann, Cosima Stubenrauch, Frank Giesselmann, “Gelled Lyotropic Liquid Crystals - the interplay between liquid-crystalline order and gel morphology”, *13<sup>th</sup> European Detergents Conference*, Berlin, Germany, **2017**
- Sonja Dieterich, Natalie Preisig, Thomas Sottmann, Cosima Stubenrauch, Frank Giesselmann, “Gelled Lyotropic Liquid Crystals - Impact of gelator on liquid-crystalline self-organization”, *45<sup>th</sup> German Liquid Crystal Conference*, Luxembourg, Luxembourg, **2018**
- Sonja Dieterich, Thomas Sottmann, Frank Giesselmann, “Synergistic structures in lyotropic lamellar gels”, *47<sup>th</sup> German Liquid Crystal Conference*, Magdeburg, Germany, **2021**

*Poster Contributions*

- Sachi Koitani, Sonja Dieterich, Natalie Preisig, Kenji Aramaki, Cosima Stubenrauch, “Gelling Lamellar Phases of the Binary System Water – Didodecyldimethylammonium Bromide with an Organogelator”, *13<sup>th</sup> European Detergents Conference*, Berlin, Germany, **2017**
- Sonja Dieterich, Thomas Sottmann, Frank Giesselmann, “Gelled Lyotropic Liquid Crystals”, *2<sup>nd</sup> German British Liquid Crystal Conference*, Würzburg, Germany, **2017**
- Sonja Dieterich, Natalie Preisig, Thomas Sottmann, Cosima Stubenrauch, Frank Giesselmann, “Gelled Lyotropic Liquid Crystals - impact of gelator on liquid crystalline self-organization”, *27<sup>th</sup> International Liquid Crystal Conference*, Kyoto, Japan, **2018**
- Sonja Dieterich, Thomas Sottmann, Sylvain Prévost and Frank Giesselmann, “SANS Investigations on Gelled Lamellar Liquid Crystals”, *46<sup>th</sup> German Liquid Crystal Conference*, Paderborn, Germany, **2019**

## Acknowledgements

Many people helped and supported me during my doctorate. All of them contributed to the realization of this thesis. Words cannot express how grateful I am for the support I received in the last years, the experiences I gained and the great memories I made, but I will try it anyway.

My special thanks go to:

- Prof. Dr. Frank Gießelmann for the opportunity to investigate a fascinating topic in liquid crystal research, and more importantly for his expert advice and constant support. The combination of his joy to teach, thorough supervision while letting one develop and the creation of a pleasant working atmosphere is invaluable.
- Prof. Dr. Jan Lagerwall for preparing the second assessment of this thesis, but also for his engagement setting up the Bandol Summer School and his eagerness to introduce young scientists to the world of liquid crystals.
- Prof. Dr. Sabine Laschat for taking over the post of chairperson in the examination.
- Prof. Dr. Thomas Sottmann for the introduction into the world of neutron scattering and all the invaluable help with interpreting scattering data.
- Prof. Dr. Cosima Stubenrauch for the fruitful discussions in our DFG project and the enabling of the cooperation with the group of Prof. Aramaki in Yokohama.
- Prof. Dr. Kenji Aramaki, for the possibility to stay at his research group at the Yokohama National University.
- Dr. Ralf Schweins, Dr. Sylvain Prévost and David Bowyer, the local contacts at the D11 instrument at ILL, who helped with the SANS experiments and the data reduction.
- Diana Zauser, Kristina Schneider, Stefan Lülldorf, Julian Fischer, Shih-yu Tseng and Johanna Bruckner for the help with SANS measurements and the good times during night shifts at the ILL.
- Prof. Dr. Thomas Hellweg and Dr. Carina Dargel for the possibility to use the Xeuss facility at the University of Bielefeld and the help with carrying out SAXS measurements there.
- Dr. Katja Steck for all the fruitful discussion regarding the experimental handling of LLC gels.
- Dr. Natalie Preisig for taking the freeze-fracture electron microscopy images.

- 
- Gabriele Bräuning for the help with DSC measurements. Moreover, she and Diana Zauser ensure smooth processes in the lab.
  - Dr. Carsten Müller, Dr. Nadia Kapernaum and Dr. Johanna Bruckner for the help and discussions regarding X-ray scattering at the Nanostar and SAXSess systems.
  - Dr. Christian Häge, who taught me to program with Python and for setting up a python script.
  - Dr. Clarissa Dietrich and Dr. Friederike Knecht for the thorough proof reading.
  - My bachelor students and research intern Styliani Varytimiadou, Friedrich Stemmler and Michael Herbst for their participation in research projects and their engagement and curiosity in exploring LLC gels.
  - The mechanical and electrical workshop members, especially Boris Tschertsche, for the construction of various sample holders and other repair work. Additionally, thanks go to our secretaries Inge Blankenship and Elisa Ilg for the help with all the administrative hurdles during a doctorate and Stefan Jagiella for the technical support.
  - All present and former members of the work group, for the great working atmosphere, their eagerness to help, the scientific (and non-scientific) discussions and the good times at conferences or group retreats.
  - Deutsche Forschungsgemeinschaft for funding our project "Lyotropic Gels" (DFG Gi 243/9-1).
  - Fond der Chemischen Industrie for financial support in form of a scholarship.
  - All my friends and roommates, who cheered me up in bad times and celebrated the good times.
  - My parents Michael and Andrea, sister Julia and brother Fabian, for their support, encouragement and love. None of this would be possible without you!

# Table of Contents

<b>Acronyms .....</b>	<b>XI</b>
<b>Kurzzusammenfassung.....</b>	<b>XIII</b>
<b>Abstract .....</b>	<b>XV</b>
<b>1 Introduction into the world of anisotropic gels .....</b>	<b>1</b>
1.1 Anisotropic chemically cross-linked hydrogels .....	5
1.2 Anisotropic physically cross-linked hydrogels.....	7
1.3 Liquid-crystalline chemical gels.....	10
1.4 Liquid-crystalline physical gels.....	12
<b>2 Scope of this thesis .....</b>	<b>15</b>
2.1 Motivation and scope .....	15
2.2 Overview.....	16
<b>3 General Background .....</b>	<b>18</b>
3.1 Surfactant-based lyotropic liquid crystals .....	18
3.2 Self-assembled fibrillar networks .....	33
<b>4 Preparation and stability of micellar lyotropic LC physical gels</b> <b>(Publication I).....</b>	<b>38</b>

---

<b>4.1</b>	<b>Specific background</b> .....	<b>38</b>
4.1.1	The lyotropic system H <sub>2</sub> O – <i>n</i> -decanol – SDS .....	38
4.1.2	The LMWG 12-HOA .....	39
<b>4.2</b>	<b>Results and Discussion</b> .....	<b>42</b>
4.2.1	General preparation route .....	42
4.2.2	Gelling nematic, lamellar and hexagonal phases.....	46
4.2.3	Coexistence and mutual impact of gel network and lamellar structure.....	56
<b>4.3</b>	<b>Conclusion</b> .....	<b>62</b>
<b>5</b>	<b>Lyotropic nematic gels (Publication II)</b> .....	<b>64</b>
<b>5.1</b>	<b>Specific background</b> .....	<b>65</b>
5.1.1	The lyotropic system H <sub>2</sub> O – <i>n</i> -decanol – CDEAB .....	65
5.1.2	The low molecular weight gelators DBS, DBC and HG1 .....	66
<b>5.2</b>	<b>Results and Discussion</b> .....	<b>70</b>
5.2.1	Preparation of lyotropic nematic gels .....	71
5.2.2	Structures and properties of lyotropic nematic gels .....	72
<b>5.3</b>	<b>Conclusion</b> .....	<b>82</b>
<b>6</b>	<b>Synergistic structures in lyotropic lamellar gels (Publication III)</b> .....	<b>84</b>
<b>6.1</b>	<b>Specific background</b> .....	<b>85</b>
6.1.1	Small-angle neutron and X-ray scattering – a comparison.....	85
6.1.2	Data reduction and analysis of Neutron Scattering Data.....	89
6.1.3	Neutron scattering from lamellar phases .....	92
6.1.4	Neutron scattering from fibrillar networks .....	95

---

<b>6.2</b>	<b>Results and Discussion .....</b>	<b>97</b>
6.2.1	Indications of a new synergistic structure in lyotropic lamellar gels .....	98
6.2.2	Detailed analysis of SANS data.....	100
6.2.3	Model for the new synergistic structure .....	104
<b>6.3</b>	<b>Conclusion.....</b>	<b>110</b>
<b>7</b>	<b>Concluding discussion and outlook.....</b>	<b>111</b>
<b>8</b>	<b>References.....</b>	<b>114</b>
<b>9</b>	<b>Appendix.....</b>	<b>134</b>
9.1	Comparative study on the cosurfactant effect of 12-HOA .....	134
9.2	Publications.....	138



## Acronyms

12-HOA	12-hydroxyoctadecanoic acid
C <sub>10</sub> E <sub>4</sub>	tetraethyleneglycol monodecylether
C <sub>12</sub> E <sub>7</sub>	heptaethyleneglycol monododecylether
CDEAB	<i>N,N</i> -dimethyl- <i>N</i> -ethylhexadecylammonium bromide
cgc	critical gelation concentration
CMC	critical micelle concentration
DBC	<i>N,N'</i> -dibenzoyl-L-cystine
DBS	1,3:2,4-dibenzylidene-D-sorbitol
DFG	Deutsche Forschungsgemeinschaft
DOH	<i>n</i> -decanol
DSC	differential scanning calorimetry
FFEM	freeze-fracture electron microscopy
FWHM	full width at half maximum
H <sub>1</sub>	lyotropic hexagonal liquid-crystalline phase
HG1	hydrogelator 1
ILL	Institut Laue Langevin
iso	isotropic
IUPAC	International Union of Pure and Applied Chemistry
LC	liquid crystal
LCE	liquid-crystalline elastomer
LLC	lyotropic liquid crystal
LMWG	low molecular weight gelator

---

$L_{\alpha}$	lyotropic lamellar phase with molten alkyl chains (fluid)
$L_{\beta}$	lyotropic lamellar phase with frozen alkyl chains (gel-like)
$L_{\beta'}$	tilted lamellar phase with frozen alkyl chains (gel-like)
$N_{bx}$	lyotropic biaxial nematic phase
$N_c$	lyotropic nematic phase composed of cylindrical micelles
$N_d$	lyotropic nematic phase composed of disk-like micelles
NIST	National Institute of Standards and Technology
PEG	poly(ethylene glycol)
POM	polarized optical microscopy
SAFiN	self-assembled fibrillar network
SANS	small-angle neutron scattering
SAXS	small-angle X-ray scattering
SDS	sodium dodecylsulfate
$T_{gel-sol}$	gel-sol transition temperature
$T_{sol-gel}$	sol-gel transition temperature
UV	ultraviolet
$V_2O_5$	vanadium pentoxide
wt%	weight percent

## Kurzzusammenfassung

Im Rahmen dieser Arbeit wurden mizellare lyotrop-flüssigkristalline Gele als eine neue Klasse komplexer, weicher Materialien etabliert. In diesen lyotrop-flüssigkristallinen (LFK) Gelen wird die Anisotropie einer tensidbasierten lyotrop-flüssigkristallinen Phase mit der Elastizität und der mechanischen Stabilität eines selbstassemblierten, fibrillarem Gelnetzwerk, welches von einem niedermolekularen Gelator gebildet wird, kombiniert. Solche LFK Gele sind von Interesse, da sie als wasserbasierte Systeme einen Einsatz in biomedizinischen Anwendungen finden könnten. Außerdem können LFK Gele als lyotropes Pendant zu thermotropen flüssigkristallinen Elastomeren (FKE) betrachtet werden, welche heutzutage das Rückgrat des bedeutenden Gebiets der biomimetischen Aktuation und weichen Robotik darstellen. Im Gegensatz zu FKEs sind lyotrop-flüssigkristalline Gele einfach in ihrer Herstellung und verträglich mit wässrigen Systemen. Daher sind LFK Gele eine vielversprechende neue Art flüssigkristalliner Netzwerke, die auf eine Vielzahl externer Stimuli, wie Dampfdruck, pH-Wert oder Ionenkonzentration reagieren könnten.

Der Ausgangspunkt dieser Dissertation waren die folgenden zwei grundlegenden Fragestellungen:

- 1) Ist es möglich alle vier flüssigkristallinen Phasen (lamellare  $L_\alpha$ , nematische  $N_d$  oder  $N_c$ , hexagonale  $H_1$  Phase) des lyotropen Systems  $H_2O - n\text{-decanol} - SDS$  in den Gelzustand zu überführen, während die jeweilige flüssigkristalline Ordnung bei der Gelierung erhalten bleibt?
- 2) Wie beeinflussen sich Gelnetzwerk und flüssigkristalline Phase gegenseitig in ihrer Struktur und ihren Eigenschaften?

Zunächst wurde ein kontrolliertes und reproduzierbares Verfahren für die Herstellung von LFK Gelen entwickelt. Dadurch war es möglich lyotrop lamellare, nematische und hexagonale Gele zu erhalten, vorausgesetzt der Gelator erfüllt gewisse Anforderungen. Zum Beispiel ist der Schlüssel zu lyotrop-nematischen Gelen die Verwendung eines Gelators, dessen Molekülstruktur nicht amphiphil ist und der daher nicht in die Mizellen eingelagert werden kann und so die Mizellform weitestgehend unverändert lässt.

Die zweite Erkenntnis die im Rahmen dieser Arbeit gewonnen wurde ist, dass das Verhältnis von Fibrillendurchmesser und intermizellarem Abstand, bzw. lamellarer Wiederholungseinheit entscheidend die Struktur des LFK Gels bestimmt. In lyotrop-lamellaren Gelen bilden sich neue synergistische Strukturen, die weder in der gelatorfreien lamellaren Phase noch in einem isotropen mizellaren Gel auftreten. Jedoch bilden sich diese nur wenn die Dicke der Gelfibrillen die lamellare

Schichtdicke deutlich übersteigt. In einer elastischen Antwort der lamellaren Phase auf die dicken Gelfibrillen biegen sich die lamellaren Schichten zu Zylindern, die koaxial die Fibrille umschließen. Ähnliche Strukturen werden auch in Nervenzellen beobachtet, in denen Axons von zylindrischen Myelinschichten umschlossen werden.

Auch die eukaryotische Zelle kann als komplexes Biogel angesehen werden, da die Zellmembran, welche eine selbstorganisierte Phospholipiddoppelschicht darstellt, mit dem Zytoskelett koexistiert, welches ein ausgefeiltes Gelnetzwerk ist. Mizellare lyotrop-flüssigkristalline Gele können daher als eine neue Art geliertes komplexer weicher Materie betrachtet werden, welche spontan biomimetische Strukturen bilden können.

## Abstract

Within the scope of this work micellar lyotropic liquid-crystalline (LLC) gels were established, which are a new category of complex soft materials. In LLC gels the anisotropy of a surfactant-based lyotropic liquid-crystalline phase is combined with the elasticity and mechanical stability of a self-assembled fibrillar network formed by a low molecular weight gelator (LMWG). Such LLC gels are of interest since they constitute water-based systems very likely usable in biomedical applications. Additionally, they can be considered as the lyotropic counterpart to the thermotropic liquid-crystalline elastomers (LCEs), which are today the backbone of the much-noticed field of biomimetic actuation and soft robotics. In contrast to LCEs, LLC gels are easy and cheap in fabrication and compatible to aqueous systems. Thus, LLC gels are promising new LC networks which might respond to a broad range of external stimuli, such as vapor pressure, pH-value or ion concentration. The starting point of this dissertation were the following two fundamental research questions:

1) is it possible to transfer all four liquid-crystalline phases (lamellar  $L_\alpha$ , nematic  $N_d$  or  $N_c$ , hexagonal  $H_1$ ) of the lyotropic model system  $H_2O - n$ -decanol – SDS into the gelled state with the respective LC order conserved during gelation? And 2) how does the gel network influence structure and properties of the liquid-crystalline phase and vice versa?

First, a controlled and reproducible procedure for the fabrication of LLC gels was developed. By doing so, lyotropic lamellar, nematic and hexagonal gels were obtained, if the gelator fulfills certain requirements. For example, the key to achieve lyotropic nematic gels is the use of LMWGs, which have a non-amphiphilic molecular structure and thus cannot be incorporated into the micelles leaving the shape and composition of the micelles essentially unmodified.

The second conclusion of this work is that the relation of the gel fiber diameter and the interlayer distance crucially determines the structure of the formed LLC gel. If the fiber thickness considerably exceeds the lamellar repeat unit new synergistic structures are formed in lyotropic lamellar gels, which neither appear in the gelator-free  $L_\alpha$  phase nor in a micellar isotropic gel. As an elastic response to the thick gel fibers, the lamellar layers bend into closed cylinders which coaxially enclose the fiber. Similar structures are also found in neural cells, where axons are cylindrically enclosed by lamellar myelin sheets.

Additionally, the eukaryotic cell can be regarded as a complex biogel, since the cell membrane, a self-assembled fluid phospholipid bilayer, coexists with the cytoskeleton, which is a sophisticated gel

network. Micellar lyotropic liquid-crystalline gels can thus be considered as a new kind of gelled complex soft matter spontaneously forming biomimetic structures.

# 1 Introduction into the world of anisotropic gels

The focus of this thesis is on micellar lyotropic liquid-crystalline gels, which are formed by the combination of micellar lyotropic liquid crystals and self-assembled fibrillar networks. Hence, an anisotropic gel results. Different types of anisotropic gels are nowadays known, in which the gel formation and the anisotropy of the gels are achieved via different ways. This chapter is intended to give an overview of the various kinds of anisotropic gels, classify them and emphasize what is new and interesting about our approach to implement micellar lyotropic liquid crystalline physical gels as a special type of anisotropic gels.

Before dealing with anisotropic gels, the fundamental question: “What is a gel?” has first to be answered. Textbooks and review articles on gels often start with the famous quote of Dr. Dorothy Jordan Lloyd from 1926: “The colloid condition, the gel, is one which is easier to recognize than to define”.<sup>[1]</sup> This quote simultaneously refers to the complexity of gels, as well as to their most striking property, which is the fact that gels, although dilute systems, do not exhibit steady state flow. Testing for this characteristic is till today often applied to recognize gels and is also used in this work to determine whether or not a sample is gelled. Another phenomenological definition for gels, which is also a part of the IUPAC definition<sup>[2]</sup>, is that gels “exhibit mechanical properties characteristic of the solid state”<sup>[3]</sup>, *i.e.* “a gel has a finite, usually rather small yield stress.”<sup>[2]</sup> Due to the variety of gel types, it is often preferred to define a gel by its properties, rather than by its structural characteristics. However, most definitions refer to both, the properties and the structure of a gel.<sup>[1,3-5]</sup>

The first applicable structural definition of a gel was made by Jordan Lloyd: [Gels] “must be build up from two components, one of which is a liquid at the temperature under consideration, and the other of which, the gelling substance, often spoken of as the gelator, is a solid”.<sup>[1]</sup> Even though this definition does not apply for all systems, which are today considered as gels, it is still useful since it covers all gels, in which a gelator forms a three-dimensional network, which macroscopically immobilizes the solvent molecules giving rise to its solid-like appearance and properties, like *e.g.* elasticity.<sup>[6]</sup> Flory states that the common feature of all gels is “the presence of a continuous structure”, which is permanent.<sup>[4]</sup> Based on this, Weiss and T  rech classify gels as systems that meet the following two conditions: “(1) [A gel] has a continuous microscopic structure with macroscopic dimensions that is permanent on the time scale of an analytical experiment and (2) is solid-like in its rheological behavior (no flow but elasticity) despite being mostly liquid.”<sup>[5]</sup>

Today, the general IUPAC definition for a gel is a “non-fluid colloidal network or polymer that is

expanded throughout its whole volume by a fluid”.[2] With this definition the IUPAC follows Kramer *et al.*, who claim that in a gel one of the components has to be a liquid, simultaneously excluding xero- and aerogels (dried out open structure with a collapsed or retained network, respectively), as well as dried silica gels and unswollen cross-linked rubber from the term “gel”.<sup>[7]</sup> Contrary, Flory<sup>[4]</sup>, as well as Weiss and T  rech<sup>[5]</sup>, don’t make a statement on number and nature of components in the gel system.

The large number of different gel types makes it necessary to classify them. Flory<sup>[4]</sup> distinguished between four types of gels; the same classification is still used by IUPAC<sup>[2]</sup>, which added a fifth category as follows:

- 1) Polymeric network formed by covalent cross-linked
- 2) Polymeric network formed by physical aggregation of polymer chains
- 3) Polymeric network formed by glassy junction points. (This category is added by IUPAC to complete the list of Flory)
- 4) Lamellar structures, including mesophases
- 5) Particulate disordered structures

The last category covers all gels where a percolation of particles with large geometrical anisotropy occurs. This includes fibrillar protein gels<sup>[8,9]</sup> and neurofilament physical gel networks<sup>[10]</sup>, as well as artificial gel networks comprised of supramolecular fibrils<sup>[11]</sup>, which is the type of gel used in this work. The category also contains all gels formed by anisometric colloidal particles, such as clay platelets<sup>[12]</sup>, rod-like cellulose nanocrystals<sup>[13,14]</sup> and long, flat vanadium pentoxide ( $V_2O_5$ ) ribbons<sup>[15,16]</sup>.

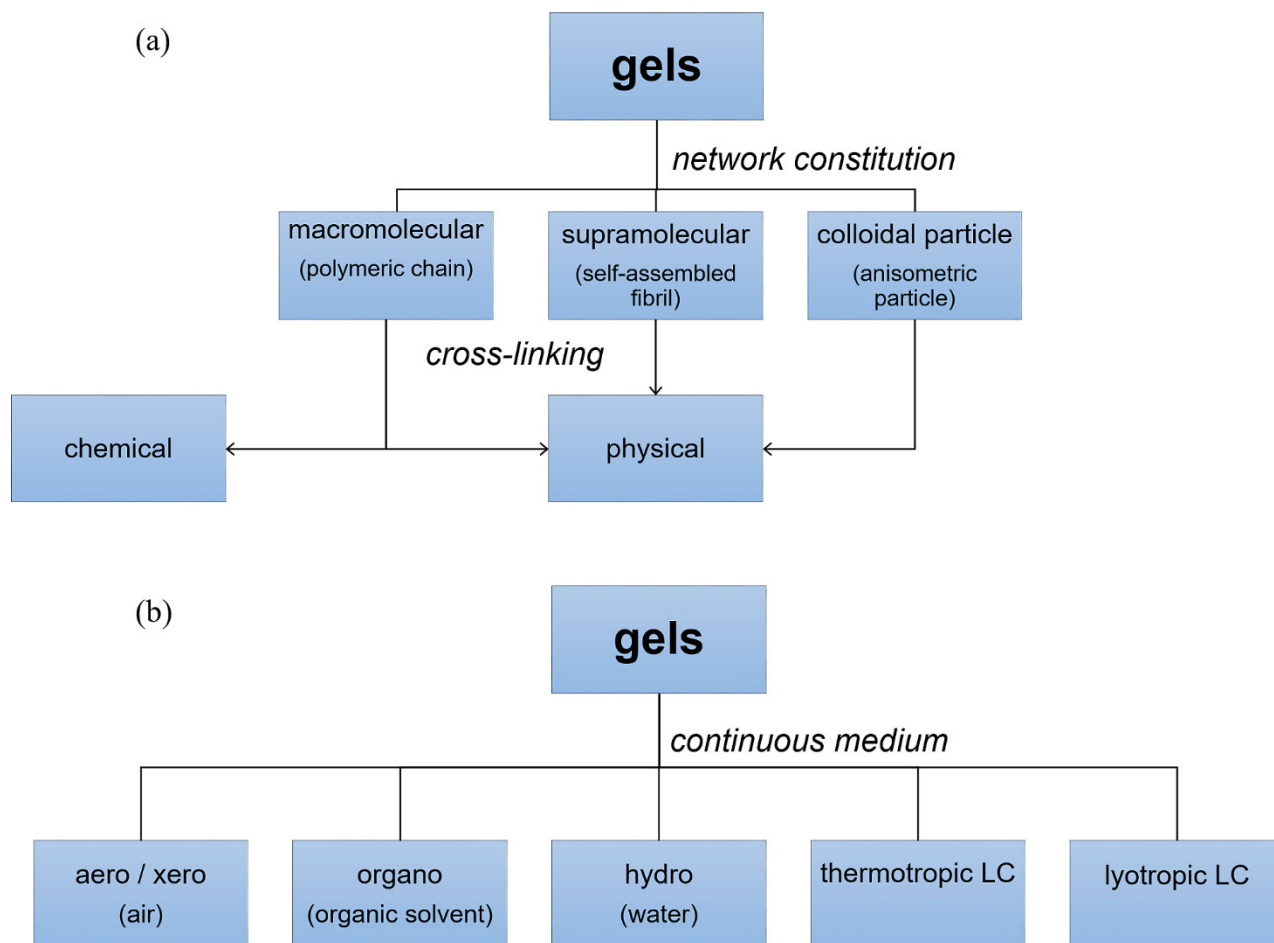
At this point it is important to clarify the difference between a *gel* and a *glass*, since both are non-equilibrium systems showing solid-like behavior. They can be experimentally difficult to distinguish since both show no flow in inverted test tubes, they have similar mechanical properties (elastic storage modulus larger than loss modulus) and dynamical behavior (large relaxation times).<sup>[17,18]</sup> Nevertheless, there is a crucial difference. In a gel the solid-like character stems from the aggregation of particles into an infinite percolated network, while in a glass a caging effect by the surrounding particles limits the mobility of the included particle, preventing the structure from re-organization.<sup>[19,20]</sup> Thus, during the liquid-glass transition the system is vitrified, but both liquid and



glass have intrinsically the same structure characterized by the interparticle distance.<sup>[18]</sup> The glass structure is homogenous at length scales larger than the interparticle distance and the corresponding liquid contains just the single particles and no precursors.<sup>[18]</sup> The interactions in a glass are predominantly repulsive (caging effect),<sup>[17,18]</sup> although also attractive glasses were reported.<sup>[18,21]</sup> In contrast, the sol-gel transition is characterized by the formation of a continuous network due to attractive interactions between the particles.<sup>[18]</sup> Already in the sol, clusters with a finite life time are present, hence there are in principal liquid (monomeric particles) to sol (small clusters that not span the volume) transitions possible.<sup>[18]</sup> A gel is characterized by the length between two adjacent junctions in the network (mesh size), which is much larger than the interparticle distance. Thus, to distinguish between a glass and a gel small-angle scattering techniques can be applied.<sup>[18]</sup>

The fourth category, gels with lamellar structures, includes the lamellar gel phases  $L_\beta$  and  $L_\beta'$ . In these phases, the gel-like properties result from frozen dynamics of the lipid chains within the bilayer.<sup>[22,23]</sup> Although these phases are generally referred to as gel phases, there is *no network* formation. But there are other types of gelled lamellar structures, in which a network exists, even though it is not apparent at first glance. Hydrogels of space-filling multilamellar vesicles are known, where “the interlocked multilamellar vesicles form a sturdy network that holds the solution and imparts the solidlike behavior”.<sup>[24]</sup> Another type of gels that belongs into this category are so-called  $L_{\alpha,g}$  ( $\alpha$  = fluid membranes,  $g$  = gelled lamellar phase) phases. Here, the  $L_\alpha$  phase is gelled by the introduction of topological defects, which are simultaneously promoted and stabilized by (a) short poly(ethylene glycol)-based (PEG) amphiphilic block copolymers decorating the membrane<sup>[25–27]</sup> or (b) ionic surfactants like SDS<sup>[28]</sup>, or partly caboxylated head groups of a glucolipid surfactant<sup>[29]</sup>. In (a) and (b), the larger head group areas of PEG lipids and ionic surfactants compared to the one of non-ionic surfactants result into an increase of the membrane curvature (see chapter 3.1). The PEG lipids and ionic surfactants segregate into the regions with high-curvature, which are defects, thus proliferating and stabilizing other defects. Around the topological defects, small domains oriented in all directions are formed creating an effective 3D structure, *i.e.* connected membranes percolate throughout the sample. Since no flow occurs along the layer normal a gel phase is formed.<sup>[25–29]</sup>

From a more practical point of view, it is reasonable to classify gels according to the medium in which the network is formed (water, organic solvent, liquid crystal), according to the constitution of the networks' backbone (polymeric chains, supramolecular fibrils, anisometric colloidal particles) and the type of the cross-linking (chemical/physical), as it is shown in Figure 1.1. In principal, when the network is formed by physical cross-linking, the gel formation is reversible.



**Figure 1.1:** *a)* Classification of gels according to the type of network. *b)* Classification of gels according to the medium in which network formation takes place. Modified from Ref.<sup>[11]</sup>

According to Flory, the polymer chains or particles are disordered.<sup>[4]</sup> However, polymer chains, fibrils or particles can be ordered, giving rise to anisotropic gels with the fibrils, polymeric chains or nanoparticles themselves being the mesogenic building blocks. A second way to achieve anisotropic gels is by forming an isotropic 3D network in an anisotropic solvent, *i.e.* in either a thermotropic liquid crystal, a micellar lyotropic liquid crystal or a particle-based lyotropic liquid crystal. Due to the long-range orientational order of the liquid-crystalline solvent, the fibers can align and orient themselves, a mechanism which is called templating.<sup>[30]</sup>

In the following paragraph, examples for different kinds of anisotropic gels are listed, without any claim for completeness and with the focus rather on the gel structure than on applications.

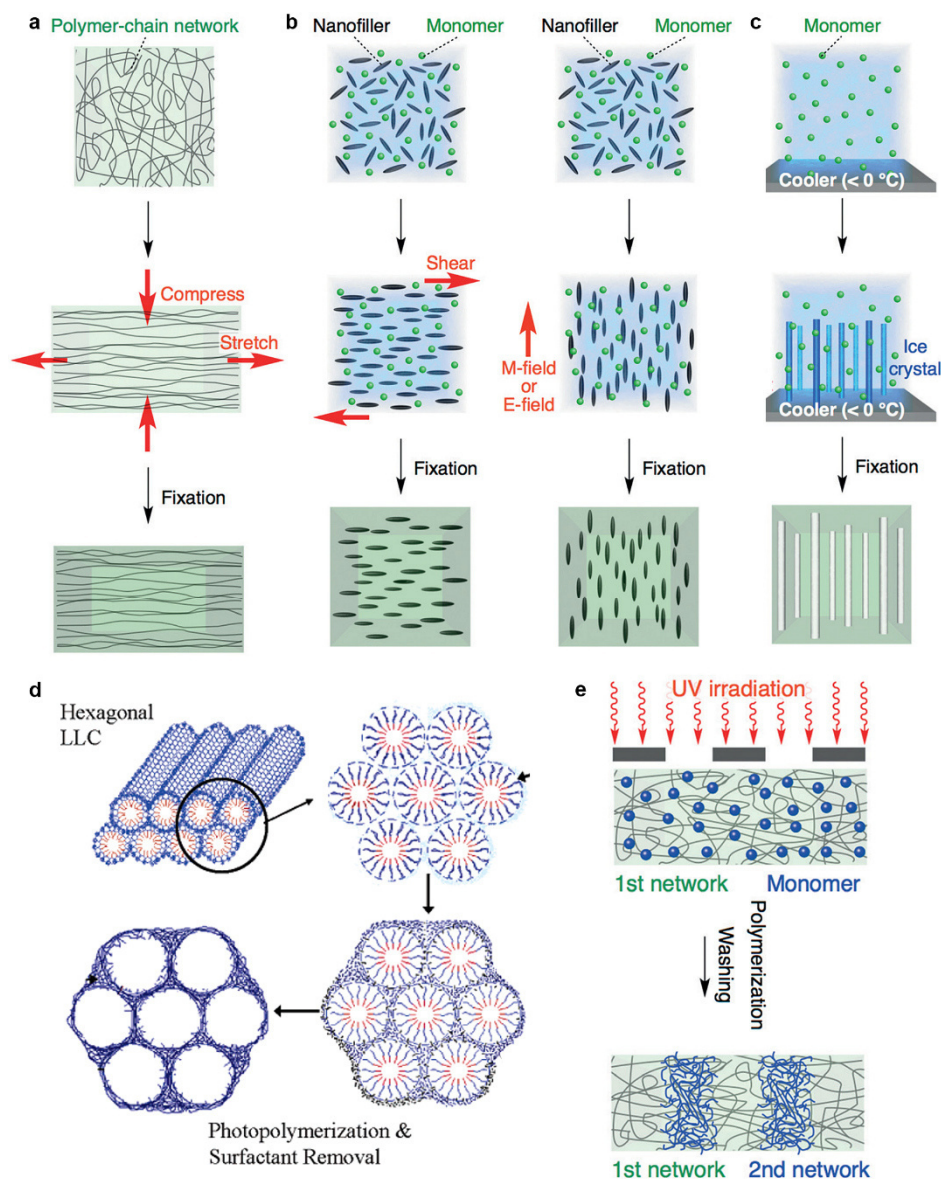
## 1.1 Anisotropic chemically cross-linked hydrogels

In a chemically cross-linked hydrogel, the 3D network component is a cross-linked hydrophilic polymer (*e.g.* polyacrylamide) that has the ability to adsorb large amounts of water. Their striking feature is a stimuli-responsive swelling behavior, *i.e.* a swelling or deswelling due to the formation or breaking of hydrogen bonds between water and the polar functional groups of the polymer, induced by *e.g.* a change in temperature. Thus, hydrogels are applied in soft biomimetic actuating systems.<sup>[31–33]</sup> Their water-rich structure makes hydrogels promising candidates for the fabrication of artificial tissues or organs. Nevertheless, most biological systems have anisotropic structures necessary for particular functions. Thus, there is an ongoing research interest in anisotropic hydrogels to achieve biomimetic structures.<sup>[34]</sup>

The different routes to anisotropic hydrogels are summarized in Figure 1.2. One way is to align single polymer chains by stretching or compressing them unidirectionally and fix the induced anisotropy subsequently by in situ polymerization (UV-light induced) as shown in Figure 1.2a. Another approach is to carry out the polymerization in a solution of 1D or 2D nanofillers, which are mostly colloidal lyotropic liquid crystals (see Figure 1.2b). Colloidal LLCs can be formed from *e.g.* inorganic nanosheets<sup>[35,36]</sup>, clay nanosheets<sup>[37]</sup>, graphene oxide nanosheets<sup>[38]</sup>, carbon nanotubes<sup>[39]</sup>, or collagen nanofibers<sup>[40]</sup>, which are macroscopically aligned by either mechanical methods (shear) or field-assisted methods (electric or magnetic field) prior to photopolymerization.<sup>[34]</sup> Additionally, anisotropic hydrogels can be obtained from alternating stacks of uniaxially aligned rigid bilayers from polymerizable surfactant and intermediate soft hydrogel matrices.<sup>[41–44]</sup> Another possibility is to use a liquid-crystalline polymer network and a hydrogel network which interpenetrate each other.<sup>[45]</sup> The entrapment of a thermotropic liquid crystal in a hydrogel matrix leads to an anisotropic hydrogel as well.<sup>[46]</sup>

Even more obvious is the combination of micellar lyotropic liquid crystals with hydrogels. Liquid single crystal hydrogels are formed by aligning micelles or membranes consisting of polymerizable surfactants and subsequent polymerization with cross-linkers.<sup>[47,48]</sup> Nanostructured hydrogels are likewise accessible by the polymerization of a non-surfactant monomer in the continuous water region of a LLC, such that the properties of the LLC are transferred to the hydrogel.<sup>[49]</sup> The LLC can either remain in the hydrogel matrix (confined LLC)<sup>[50,51]</sup> or can be removed (washing with water) after the polymerization, *i.e.* the micellar LLC serves as a template.<sup>[52–54]</sup> If a larger size of the water channels is desired, LLCs formed by amphiphilic block-copolymers are used.<sup>[55,56]</sup> Additionally, anisotropic

hydrogels with large void channels can be achieved using unidirectionally grown ice crystals as template.<sup>[57]</sup> Last, a top down approach to anisotropic hydrogels is available. In a fabrication process via photolithography, selected regions of a hydrogel containing a second monomer and a photo-initiator are exposed to UV-light.<sup>[58]</sup>



**Figure 1.2:** Different methods for the fabrication of anisotropic chemically cross-linked hydrogels. *a)* Oriented polymer networks via mechanical stretching or compression forces; *b)* shear or field aligned nanofillers; oriented void channels via *c)* unidirectional crystallization or *d)* micellar LLC templates; *e)* photolithography as a top down approach. In all cases the anisotropic alignment is permanently fixed by a UV-light induced photopolymerization giving rise to a hydrophilic polymer network, *i.e.* the hydrogel matrix. *a), b), c), e)* are reprinted with permission from K. Sano *et al.*, *Angew. Chem. Int. Ed.* **2018**, *57*, 2532.<sup>[34]</sup> Copyright 2018 Wiley-VCH Verlag GmbH & Co. KGaA, Weinheim. *d)* is adapted with permission from J. D. Clapper *et al.*, *Macromolecules* **2007**, *40*, 1101.<sup>[55]</sup> Copyright 2007 American Chemical Society.

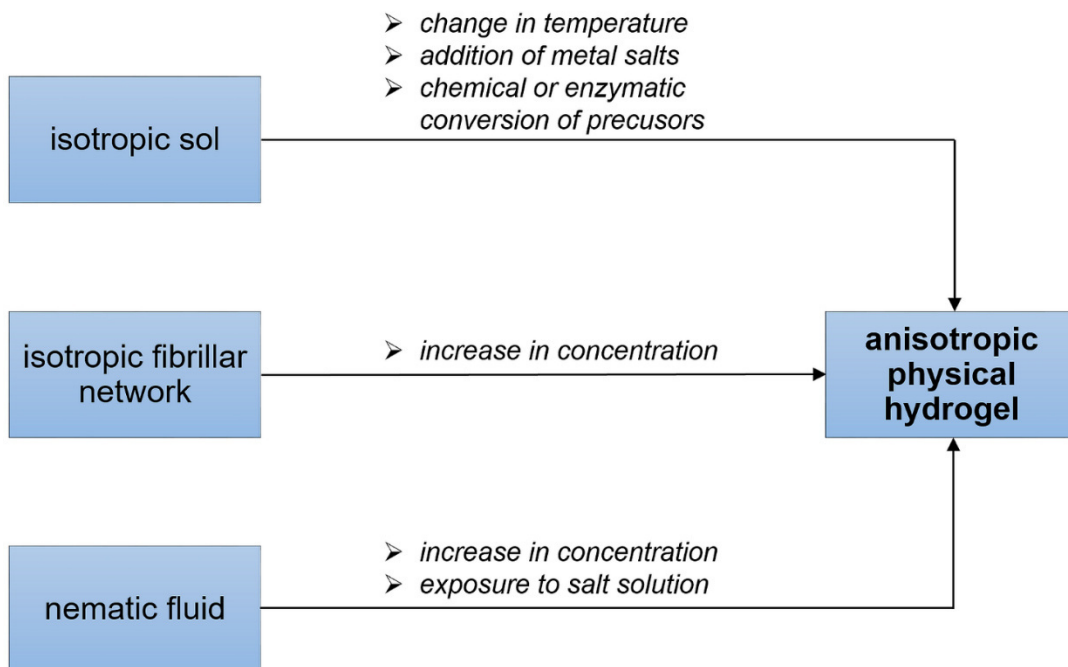
## 1.2 Anisotropic physically cross-linked hydrogels

Physically cross-linked hydrogels are formed by macromolecular polymer chains, self-assembled supramolecular fibers and colloidal nanoparticles. Actually, IUPAC recommends to refer to a colloidal network in water as aquagel<sup>[2]</sup>; a suggestion that is mostly not followed in literature. Anisotropic colloidal hydrogels were reported for *e.g.* clay platelets<sup>[59,60]</sup>, vanadium pentoxide ribbons<sup>[15]</sup> and neurofilaments<sup>[10]</sup>.

Additionally, nanocomposite hydrogels in which polymer chains are physically cross-linked with silicate nanoparticles exist. Long poly(ethylene oxide) chains adsorb onto clay platelets, which act as multifunctional cross-linkers, or in other words: the polymer chains bridge the nanoparticles. Shear orientation leads to anisotropic gels.<sup>[61,62]</sup>

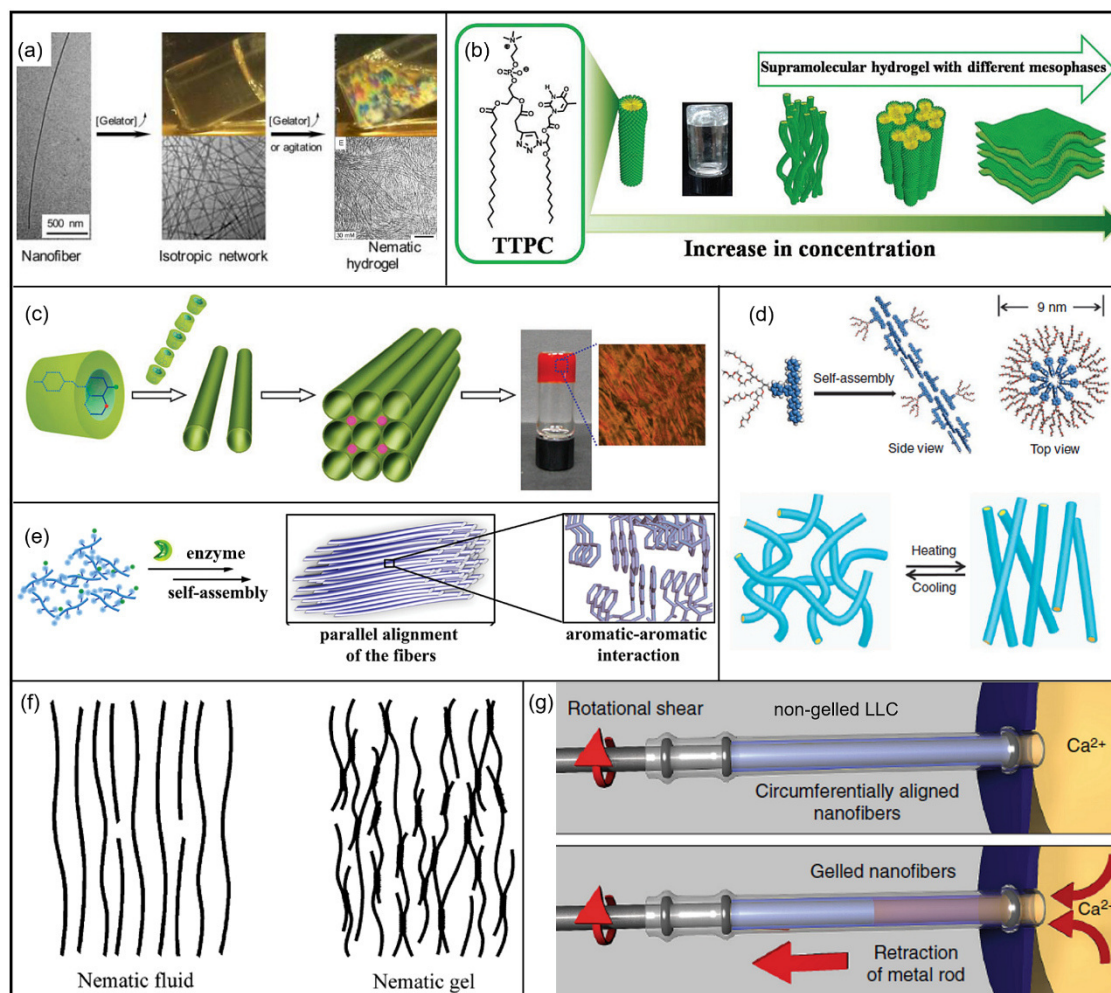
Another anisotropic physically cross-linked hydrogel consists of polymeric micelles. Amphiphilic coil-rod-coil triblock copolymers self-assemble in water into discrete micellar nanocylinders. The isotropic fluid is transferred into a nematic gel by the addition of rod-coil-rod molecules, which bridge the nanocylinders reversibly, forming an interconnected network resulting in an anisotropic gel.<sup>[63]</sup>

A large class of physical hydrogels are gels formed by low molecular weight hydrogelators, which self-assemble in water into supramolecular fibers resulting in a fibrillar network. Different ways to anisotropic self-assembled fibrillar networks were reported, which are listed in Figure 1.3.



**Figure 1.3:** Classification of different ways to form an anisotropic physical hydrogel from low molecular weight gelators.





**Figure 1.4:** Examples for the formation of anisotropic self-assembled fibrillar networks. For an *a*) bile acid dimer (adapted with permission from M. Zhang *et al.*, *Langmuir* **2017**, 33, 1084.<sup>[64]</sup> Copyright 2017 American Chemical Society) and *b*) artificial nucleolipid (Reproduced from Ref.<sup>[65]</sup> with permission from The Royal Society of Chemistry, Copyright 2018) an isotropic fibrillar network is formed at low concentrations, while increasing the gelator concentration leads to an anisotropic gel. *c*) For fibrous rods of cyclodextrin the gelation is completed by the addition of lithium salt. Reproduced from Ref.<sup>[66]</sup> with permission from The Royal Society of Chemistry, Copyright 2011. *d*) Self-assembled tubules reversibly form a nematic gel upon increasing the temperature. Reprinted by permission from Springer Nature, Z. Huang *et al.*, *Nat. Commun.* **2011**, 2, 459.<sup>[67]</sup> Copyright 2011. *e*) Hydrogelator-precursors are converted into hydrogelators by an enzyme catalyzed reaction, the formed hydrogelators immediately self-assemble into aligned fibers due to interfiber  $\pi$ - $\pi$  interactions. Adapted from J. Zhou *et al.*, *J. Am. Chem. Soc.* **2014**, 136, 2970.<sup>[68]</sup> ACS Authors Choice, Copyright 2014 American Chemical Society. This is an unofficial adaptation of an article that appeared in an ACS publication. ACS has not endorsed the content of this adaptation or the context of its use. *f*) Increasing the peptide concentration in a fibrillar nematic fluid results in a nematic gel due to the formation of fiber-like junctions. Reprinted with permission from A. Aggeli *et al.*, *J. Am. Chem. Soc.* **2003**, 125, 9619.<sup>[69]</sup> Copyright 2003 American Chemical Society. *g*) Filaments from self-assembled peptide amphiphile molecules form a lyotropic liquid crystal, which can be circumferentially aligned by rotational shear. Gelation is mediated by  $\text{Ca}^{2+}$  ions flowing into the glass tube. Adapted from S. M. Chin *et al.*, *Nat. Commun.* **2018**, 9, 2395.<sup>[70]</sup> Open Access, Copyright 2018 S. M. Chin *et al.*

The transition from an isotropic fibrillar network to an anisotropic network with increasing gelator concentration was reported for a bile acid dimer<sup>[64]</sup> and a thymine containing artificial nucleolipid<sup>[65]</sup>. In case of the bile acid dimer, the anisotropy of the gel arises due to a parallel arrangement of the fibrils (Figure 1.4a).<sup>[64]</sup> The same holds for the artificial nucleolipid system, in which at increasing concentration an ordering of the fibers leads to a nematic hydrogel. At very high nucleolipid concentrations (> 60 wt%) a fusion of the fibers results in a lamellar phase, as shown in Figure 1.4b.<sup>[65]</sup> Another way to anisotropic hydrogels is the direct formation from an isotropic sol with a change in temperature<sup>[67]</sup>, the addition of a metal salt<sup>[66]</sup>, or the either chemical or enzymatic conversion of precursor-hydrogelators. For fibrous rods of cyclodextrin, which are formed by head-to-head association due to azo-dye molecules in the cavities of the cyclodextrin, the gelation is completed by the addition of lithium salt. The lithium ions induce a tetragonal packing of the cyclodextrin fibers giving rise to an anisotropic gel (Figure 1.4c).<sup>[66]</sup> Amphiphiles, laterally grafted with a dendritic oligoether-chain, self-assemble into tubules with a nematic substructure. At low concentrations, the isotropic solution of tubules is reversibly transferred into a nematic gel with aligned nanofibers by increasing the temperature. With increasing concentration, the sol-gel transition temperature decreases and the alignment of the nanofibers is spontaneously fixed at room temperature, *i.e.* a nematic gel is formed (see Figure 1.4d).<sup>[67]</sup> The either chemical (*e.g.* by a base<sup>[71]</sup>) or enzymatic (dephosphorylation<sup>[68]</sup> or hydrolysis<sup>[71]</sup> reaction catalyzed by a phosphatase or an esterase, respectively) conversion of hydrogel precursors leads to the formation of anisotropic hydrogels. Alignment of nanofibers is induced by interfiber interactions, which can be enhanced by using strong and directed  $\pi$ - $\pi$  interactions (see Figure 1.4e).<sup>[68]</sup>

The third way to anisotropic physical hydrogels is the conversion of nematic fluids comprising of aligned fibrils into anisotropic fibrillar networks. In self-assembling peptide gels, nematic hydrogels are formed from nematic fluids by increasing the peptide concentration. Peptides in a  $\beta$ -strand conformation, which can be considered as chiral rod-like units, self-assemble at a given concentration into semi-rigid fibrils. Due to excluded volume interactions a nematic fluid results. At higher concentrations a nematic gel is formed. The gel formation is associated with the onset of the building of thicker fibers out of thin fibrils. Hence, the fibrils in the self-assembled network are linked via fiber-like junctions (see Figure 1.4f).<sup>[69,72]</sup> Additionally, the formation of a nematic gel, a nematic fluid and an isotropic fluid can be reversibly controlled by changing the pH-value.<sup>[69]</sup> Amphiphilic peptides are known to self-assemble into nanofibers in aqueous solution.<sup>[73,74]</sup> Heating and cooling of the solution leads to long filaments of bundled nanofibers. The entropically driven dehydration or

rehydration of the nanofibers upon heating or cooling results in the fusion of the nanofibers into plaques and the subsequent rupture gives rise to thicker bundles of nanofibers.<sup>[75]</sup> The long filaments form a lyotropic liquid-crystalline phase which can be macroscopically aligned by low shear forces. Monodomain gels were obtained by the exposure to a salt solution through cross-linking with divalent ions ( $\text{Ca}^{2+}$ ) (see Figure 1.4g).<sup>[70,75,76]</sup>

Anisotropic physical gels can occur in organic solvents as well. A nonaqueous lyotropic nematic gel is formed by fatty acid substituted urea in decane. The nematic gel is composed of extended inverse micelles which are held together by dipolar and dispersion forces.<sup>[77]</sup> A low molecular weight steroid organogelator forms a birefringent organogel in cyclohexane. The long fibers build up a nematic gel by increasing the steroid concentration as a consequence of excluded volume effects. Applying a magnetic field at the sol-gel transition leads to a gel with even higher orientational order.<sup>[78,79]</sup> The addition of water to an ionic liquid results in the spontaneous self-organization into a liquid-crystalline ionogel.<sup>[80]</sup>

All examples of anisotropic physically cross-linked gels discussed in this chapter have in common that the building blocks of the LLC phase simultaneously constitute (at least part of) the gel network. This prevents an independent tailoring of liquid-crystalline and gel network properties.

### 1.3 Liquid-crystalline chemical gels

Liquid-crystalline chemical gels are formed by photoreactive molecules which are dispersed in a thermotropic liquid crystal matrix. A subsequent photopolymerization leads to the formation of a cross-linked network with the thermotropic LC as solvent.<sup>[81,82]</sup> Since the polymer chains preferentially grow along (or perpendicular) the liquid crystal director, the director field is mimicked by the polymer network.<sup>[83]</sup> The monomers contain one or two reactive groups (mainly acrylate groups) and usually possess a part which is structurally related to a liquid crystal, *i.e.* exhibits form anisometry. The monomers can be even liquid-crystalline mesogens themselves (reactive LC, see Figure 1.5a for typical components for the preparation of LC chemical gels).<sup>[81,82]</sup> The mesogenic units facilitate the orientation of the monomers in the thermotropic LC. The liquid crystal system including the polymerizable (LC) molecules can be oriented in various desired configurations prior to photopolymerization.<sup>[84]</sup> The LC order is then templated by the final polymer network leading to an anisotropic network, which stabilizes the structure and the properties of the monomeric LC such as their heat and shock resistance; *i.e.* since the configuration of the thermotropic mesogens is



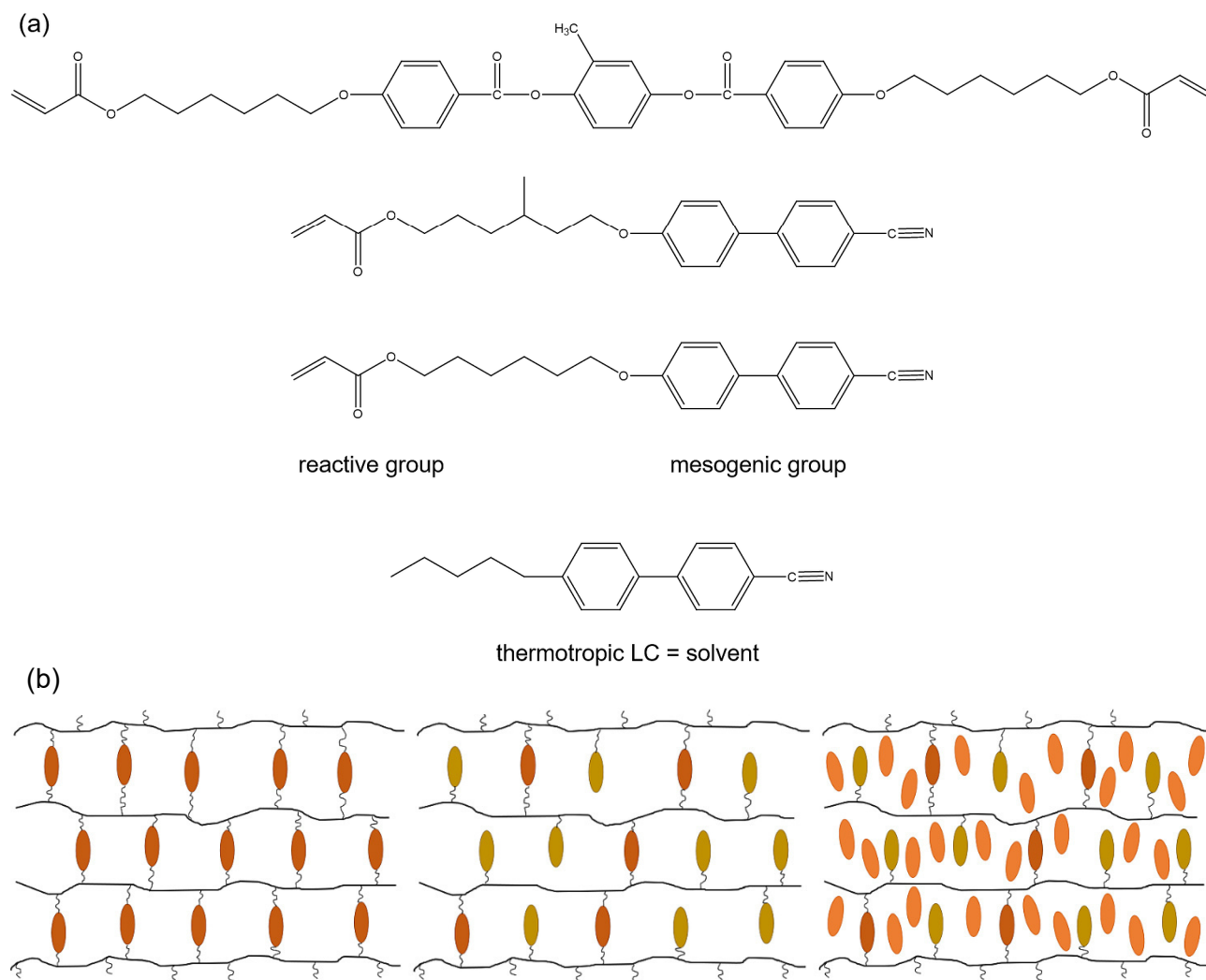
permanently fixed, temperature dependent effects are considerably reduced.<sup>[85–87]</sup> Thus, LC chemical gels are often called polymer-stabilized liquid crystals and find applications in liquid crystal displays (LCDs).<sup>[83,84,88]</sup>

The cross-linking density of the network can be controlled by the concentration of those monomers carrying two reactive groups. In a slightly cross-linked network the mono-functional molecules bound to the polymer backbone (mesogenic unit in side chain) can be switched together with the small-molecule mesogens upon applying an electric field.<sup>[89]</sup> The gel network provides the system with a “memory” ensuring the recovery of the original configuration when removing the electric field due to the elastic interactions between the polymer network and the liquid crystal.<sup>[82,88,89]</sup> So far, mostly nematic gels<sup>[86,90,91]</sup> and cholesteric gels<sup>[92–95]</sup> have been reported, but also polymer-stabilized ferroelectric SmC\* phases<sup>[81,96–98]</sup> were obtained.

Closely related to liquid-crystalline chemical gels are liquid-crystalline elastomers (LCEs) and liquid-crystalline networks, which are slightly cross-linked or densely cross-linked polymer networks, respectively, in which the mesogenic units are covalently linked to the polymer network.<sup>[31,88]</sup> LC chemical gels can be considered as LCEs swollen in a thermotropic LC solvent. A schematic drawing of a LC elastomer, network and gel is shown in Figure 1.5b. In LCEs, the mesogenic units are either linked to the polymer backbone via flexible alkyl spacers (side-chain polymers), or they are part of the polymer backbone itself (main-chain polymers).<sup>[88,99]</sup> The coupling of the macroscopic shape to the global orientational order is the prominent feature of LCEs.<sup>[100,101]</sup> External stimuli, such as light, temperature or electric fields modify or destroy the LC orientational order leading to macroscopic shape changes in response. Hence, LCEs find their application in stimuli-responsive actuators, since they can convert external energy into directed mechanical motion.<sup>[102,103]</sup> Applications of LCEs in micropumps<sup>[104]</sup> or motors<sup>[105]</sup>, as well as in biomimetic actuation (*e.g.* artificial muscles)<sup>[106,107]</sup> or locomotion<sup>[108,109]</sup> were reported. Additionally, LCEs can be swollen in organic solvents<sup>[110,111]</sup> or water<sup>[112]</sup> resulting in lyotropic LC phases, but also macroscopic shape changes were observed due to solvent concentration as external stimuli.

Interestingly, liquid-crystalline physical gels consisting of physically cross-linked polymers have been reported as well.<sup>[113–115]</sup> End associating ABA triblock copolymers with two polystyrene end-blocks and a side chain LC polymer midblock form a physically interconnected micellar network in a small molecule nematic LC due to the different solubilities of the different blocks. While the polystyrene blocks are rather insoluble (LC-phobic) in the thermotropic LC, the side chain LC polymer swells in the LC solvent. The anisotropic LC gel forms at very low polymer concentration, the cross-links in

the gel can break and reconnect, and the homogenous gel exhibits high optical clarity.<sup>[114]</sup> Similarly, self-assembled fibrillar networks can form in a thermotropic LC, which will be described in the next chapter.

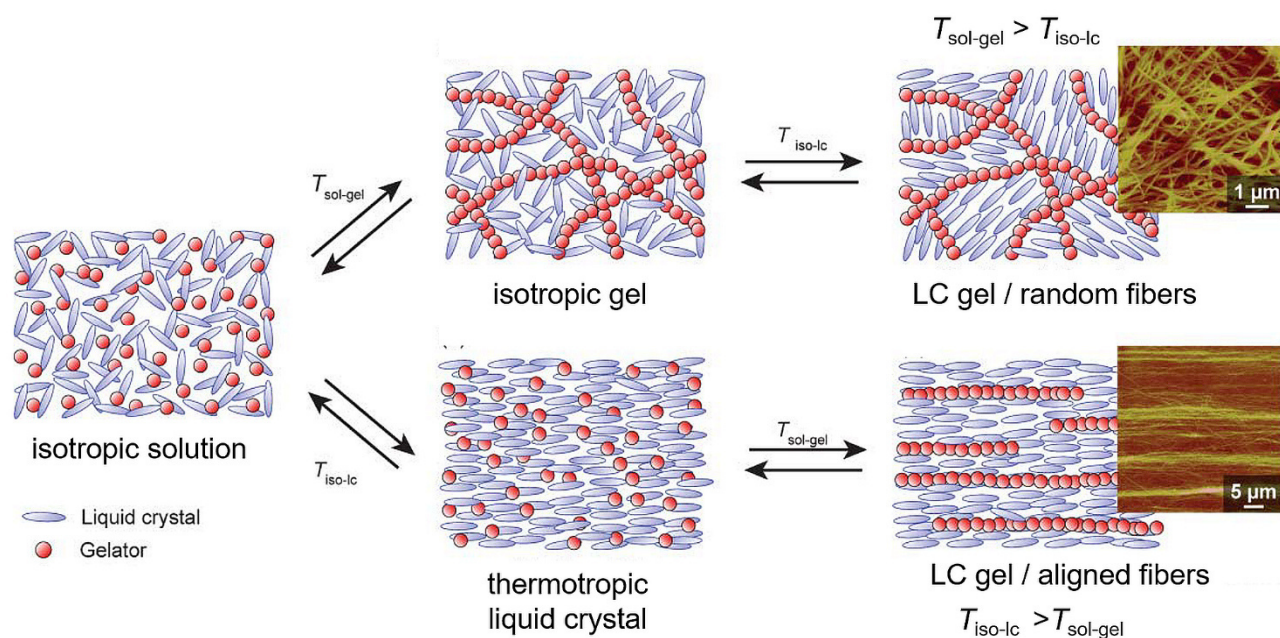


**Figure 1.5:** *a)* Molecular structure of typical reactive mesogens and thermotropic LC used for the preparation of liquid-crystal chemical gels. Sketch is redrawn based on Ref.<sup>[89]</sup> *b)* Schematic drawing of the structure of a liquid-crystal network (*left*), a liquid-crystal elastomer (*middle*) and a liquid-crystal gel (*right*). Sketch is redrawn based on Ref.<sup>[88]</sup>

## 1.4 Liquid-crystalline physical gels

In order to achieve thermotropic liquid-crystalline gels with a reversible and externally controlled gel formation, thermotropic LC physical gels were developed. In thermotropic LC physical gels a self-assembled fibrillar network formed from low molecular weight (organo)gelators is combined

with a thermotropic liquid-crystalline phase.<sup>[116,117]</sup> The structure of the resulting LC gel crucially depends on the sequence of the isotropic-LC transition ( $T_{\text{iso-lc}}$ ) and the sol-gel transition ( $T_{\text{sol-gel}}$ ). If with decreasing temperature the LC forms first, the liquid-crystalline phase can act as a soft template leading to aligned gel fibers.<sup>[30,118]</sup> On the contrary, if a randomly oriented gel network forms first, a polydomain LC morphology emerges (see Figure 1.6).<sup>[119]</sup>



**Figure 1.6:** The consecutive formation of a thermotropic liquid-crystalline gel from an isotropic solution leads to different structures of the resulting gel, depending on whether the gel network or the liquid-crystalline phase forms first upon cooling. Adapted from Ref.<sup>[119]</sup> with permission from The Royal Society of Chemistry, Copyright 2007.

Applying an electric field to a polydomain LC physical gel leads to a macroscopic alignment of the LC director causing a light-scattering material to switch into a transparent one.<sup>[120–123]</sup> Moreover, the gel network can stabilize the LC alignment and director patterns.<sup>[124,125]</sup> Anisotropic properties such as the electro-optical response in twisted nematic cells<sup>[126–129]</sup> or hole mobility<sup>[130]</sup> can be enhanced due to the presence of the gel structure. The use of chiral gelators allows to receive cholesteric phases above the sol-gel transition temperature (for  $T_{\text{iso-lc}} > T_{\text{sol-gel}}$ ) where the monomeric gelator acts as a chiral dopant.<sup>[131]</sup> Additionally, cholesteric thermo-reversible LC gels can be achieved.<sup>[132]</sup> With a photoresponsive gelator undergoing a trans-cis isomerization upon UV light exposure, the system can be switched between an isotropic solution, a nematic gel, a fluid cholesteric phase and a cholesteric gel, since only the trans-isomer has gelation ability.<sup>[133]</sup> Thermotropic liquid-crystalline colloidal gels were obtained by confining the LC phase in a colloidal silica gel.<sup>[134,135]</sup>

The next step is to extend the field of anisotropic physical gels to aqueous systems, namely to evolve micellar lyotropic liquid-crystalline physical gels. Since biological tissues are water-rich structures, water-based supramolecular gels with anisotropic order and a reversible network formation are desirable for applications in the field of artificial tissues or biomimetic actuation.

Lyotropic liquid-crystalline gels, in the sense that genuine LLC phases formed by anisometric micelles coexist with self-assembled fibrillar networks, were not known until 2015. Then, Xu *et al.* reported the successful gelation of the lyotropic lamellar and hexagonal phase of the system  $D_2O - n\text{-decane} - C_{10}E_4$  with the low molecular weight gelator 12-hydroxyoctadecanoic acid (12-HOA).<sup>[136]</sup> To the best of our knowledge, except for this “proof of principle” work<sup>[136]</sup>, no micellar LLC physical gels were reported in literature until 2016.

Hence, in the field of anisotropic gels, micellar lyotropic physical gels have long been a blind spot on the map and a systematic access to micellar lyotropic liquid-crystalline gels was missing. It was the mission of the DFG (*Deutsche Forschungsgemeinschaft*) project “Gelled lyotropic liquid crystals – orthogonal self-assembly or soft templating” and the topic of this thesis to fundamentally establish micellar lyotropic LC gels of various liquid-crystalline phases and elucidate their structure.

## 2 Scope of this thesis

### 2.1 Motivation and scope

As described in the introduction, LLC gels are a new kind of anisotropic gels. Until 2016, only one example of a successfully gelled LLC system was reported.<sup>[136]</sup> The goal of this thesis is thus to fill the gap to LLC gels in order to provide a systematic route to micellar lyotropic liquid-crystalline gels and to elucidate their structure. The concept of LLC gels is to combine two systems: one system introduces the gel network forming ability (self-assembled fibrillar network), the other one contributes the liquid-crystalline order (micellar lyotropic LC phase).

Why are micellar lyotropic liquid-crystalline gels interesting and beneficial to other types of anisotropic gels discussed in chapter 1? Due to their compatibility to aqueous systems, LLC gels might find biomedical applications, as it was reported for other types of anisotropic hydrogels.<sup>[34,137–139]</sup> Additionally, LLC gels can be considered as the lyotropic counterpart to the thermotropic liquid crystal elastomers, which nowadays dominate the field of soft robotics and biomimetic actuation.<sup>[99,106,140,141]</sup> In addition to temperature and light, LLC gels and may respond to a broad range of chemical stimuli such as pH-value, vapor pressure, ion and solute concentration. Third, a responsive and reversible gel formation initiated by external stimuli is achieved by using responsive low molecular weight gelators forming self-assembled fibrillar networks (SAFiNs), as it was reported for SAFiNs in isotropic solvents.<sup>[142–146]</sup> The new class of micellar lyotropic liquid-crystalline physical gels under study combines all three features mentioned above within one system.

Another advantage of LLC gels is that the thermal (LC-isotropic and gel-sol transition) and structural properties of LLC gels can be tailored individually. Additionally, the two coexisting structures, namely the LLC phase and the gel network, can take over different specific functions. Usually, the role of the gel network is to provide long-term mechanical stability. For example, LLCs are used as templates for macroscopically aligned nanostructured materials.<sup>[147,148]</sup> The structure of macroscopically aligned LLC phases may be arrested by the gel network and the enhanced mechanical stability of a gelled template may facilitate the synthesis of *e.g.* nanoporous monoliths. Additionally, LLC gels can be used in electrochemical applications, in which the anisotropic electrolyte gels offer channels for efficient ion migration.<sup>[149]</sup>

Biomedical applications of LLC gels may be in transdermal drug delivery, where membrane-embedded biologically active proteins or water-insoluble drugs solubilized in the micelles of a LLC

may be delivered via a stable gel.<sup>[150,151]</sup> As mentioned above, the thermoreversible gel formation in SAFiNs can be reversibly triggered by external stimuli such as light<sup>[152,153]</sup>, pH-value<sup>[154,155]</sup>, enzymes<sup>[156,157]</sup> or ion concentration<sup>[152]</sup>, which creates possibilities for on-demand drug release.<sup>[158,159]</sup> Another biomedical application may be the design of artificial tissues from LLC gels, as it was shown for anisotropic chemically cross-linked hydrogels.<sup>[137,139]</sup> Last but not least, LLC gels find a famous analogue in nature. The eukaryotic cell can be regarded as a membrane-based LC biogel since the cell membrane, which is a fluid phospholipid bilayer coexists with the cytoskeleton, which is a sophisticated gel network where protein filaments form a 3D scaffold.<sup>[160,161]</sup>

All these fascinating potential applications however require a rational design and a deeper knowledge of micellar LLC gels. In view of this challenge, this thesis on LLC gels addresses the following fundamental research questions:

- Are we able to successfully gel lyotropic liquid-crystalline phases? Which of the common LLC phases (lamellar  $L_\alpha$ , nematic  $N_d$  or  $N_c$ , hexagonal  $H_1$ ) can be transferred into a lyotropic lamellar, nematic or hexagonal gel, respectively? A successful gelation implies that the particular liquid-crystalline order of the respective LLC phase is preserved in the gelled state, where the LLC phase coexists with the physical 3D network.
- If yes, how does the LLC phase and the gel network mutually influence each other's structure?

## 2.2 Overview

First, the general background considering the structure and properties of micellar lyotropic liquid crystals and self-assembled fibrillar networks is reviewed in chapter 3. The results corresponding to the three publications on which this cumulative thesis is based on are discussed in chapters 4 - 6. In chapter 7, a summarizing discussion puts the results in a larger context.

Chapter 4 is based on the publication "Gelation of Lyotropic Liquid-Crystalline Phases – the Interplay between Liquid-Crystalline Order and Physical Gel Formation" (*Publication I*)<sup>[162]</sup>. It covers investigations on the gelation of the lamellar  $L_\alpha$ , the nematic  $N_d$  and  $N_c$ , as well as the hexagonal  $H_1$  phase of the system  $H_2O - n$ -decanol – sodium dodecylsulfate (SDS) with the low molecular weight gelator 12-HOA. The main result presented in chapter 4 is that only lamellar gels could be obtained. Due to the amphiphilic nature of the gelator 12-HOA, it additionally acts as a cosurfactant thus preventing

the formation of lyotropic nematic gels.

Hence, in chapter 5 the subsequent question that is answered is: How is it possible to obtain lyotropic nematic gels? Pathways to lyotropic nematic gels were studied using a second lyotropic model system and different LMWGs. The key to lyotropic nematic gels was the use of gelators, whose non-amphiphilic molecular structure leaves the shape of the anisometric micelles essentially unchanged, as reported in the second publication contributing to this thesis with the title “Micellar Lyotropic Nematic Gels” (*Publication II*)<sup>[163]</sup>.

Since lyotropic lamellar gels are the most straightforward to obtain, chapter 6 of this thesis deals with a thorough structural analysis of gelled lamellar phases. By means of small angle neutron scattering, the mutual interactions between gel network and lamellar phase are examined more closely. As reported in the third scientific paper “Synergistic Structures in Lyotropic Lamellar Gels” (*Publication III*)<sup>[164]</sup> contributing to this cumulative thesis, synergistic structures are formed in lyotropic lamellar gels, which neither exist in the non-gelled  $L_\alpha$  phase nor in an isotropic micellar gel.

### 3 General Background

In this section I will review the necessary background information for all following sections, namely the structures and properties of micellar lyotropic liquid crystals (3.1) and self-assembled fibrillar networks (3.2). More specific background is found at the beginning of each of the following chapters 4 – 6.

#### 3.1 Surfactant-based lyotropic liquid crystals

The liquid-crystalline state of matter is, according to IUPAC, “a mesomorphic state having long-range orientational order and either partial positional order or complete positional disorder.”<sup>[165]</sup> As the term “mesomorphic” (*mesos*, ancient Greek for middle) expresses, the order of a mesomorphic state ranges between the 3D long-range positional and orientational order of solid crystals and the absence of any long-range order in isotropic liquids. LC phases, which are also called mesophases, thus occur between the crystalline state and the liquid state on changing variables of state such as temperature or concentration. They combine properties of ordinary liquids like fluidity with the anisotropic properties of crystals, *e.g.* optical birefringence.<sup>[165]</sup>

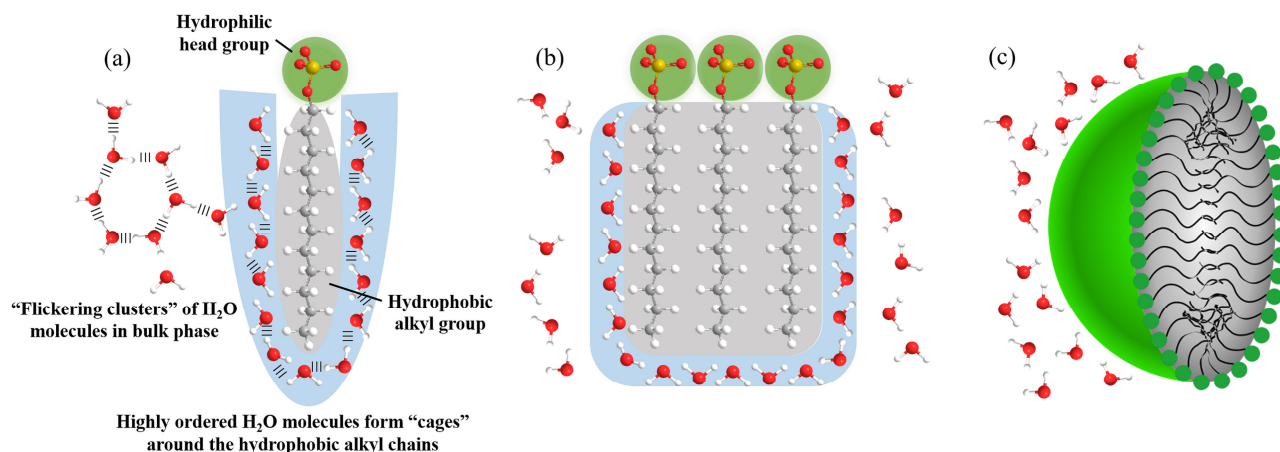
The building blocks of LC phases (also called mesogens) are required to have an anisometric (non-spherical) shape since otherwise long-range orientational order remains undefined. In principal, one can distinguish between two types of liquid crystals, thermotropic and lyotropic liquid crystals. In thermotropic liquid crystals the building blocks are typically anisometric molecules and the stability of a thermotropic LC phase is given within a certain temperature range at constant pressure. Lyotropic liquid crystals however, require a solvent in which nanoparticles (particle-based LLCs), long polymeric chains (polymeric LLCs), stack of dye molecules (chromonic LLCs) or supramolecular assemblies of surfactant molecules (micellar LLCs) of anisotropic shape are dispersed and thus constitute the building blocks in LLCs. The latter class - micellar LLCs - are the longest known and most common class of LLCs and are also subject in this thesis. Depending on the concentration, amphiphilic surfactant molecules self-assemble into bilayers or micelles of different shape. Therefore, the occurrence of lyotropic liquid-crystalline phases depends not only on temperature but more importantly on the relative concentrations of the compounds in the mixture.

Amphiphilic (*amphi*, Greek: both and *phil*, Greek: like or love) molecules consist of one hydrophilic/lipophobic (water-loving, fat-hating) part and another hydrophobic/lipophilic (water-hating, fat-loving) part. In many cases amphiphilic molecules dissolved in a solvent such as water



spontaneously self-assemble into micelles above a certain concentration, the critical micelle concentration (CMC). These amphiphiles are also called surfactants (from surface active agent). Typical surfactant molecules consist of a polar, water-soluble head group attached to a non-polar, water-insoluble hydrocarbon chain. According to the charge of the head group, surfactants can be classified into anionic, cationic, zwitterionic or non-ionic surfactants. Amphiphilic molecules which do not form micelles on their own but can be incorporated into micelles are called cosurfactants. Usually, cosurfactants have a small and non-ionic head group; typical examples are long- and medium-chain alcohols.<sup>[166]</sup>

As of now, water is considered to be the solvent. The driving force of micelle formation is the hydrophobic effect, which is of entropic nature since an aggregation of the surfactant molecules in water increases the water entropy in comparison to a system of monomerically dissolved surfactants. In more detail, if an amphiphilic molecule is brought into water, the water's hydrogen bond network is disrupted. Since the hydrogen bonding energy is quite high (1 - 50 kJ/mol)<sup>[167]</sup> the maximum number of hydrogen bonds is retained in the system by the water molecules arranging around the non-polar alkyl chain forming a "cage" around it (Figure 3.1a). This reduces the configurational freedom of the water molecules and thus their entropy. By an aggregation of surfactant molecules into micelles the hydrophobic hydrocarbon chains are shielded from the surrounding water, which reduces the number of ordered water molecules significantly and hence reduces the entropy loss (Figure 3.1c).<sup>[167,168]</sup>



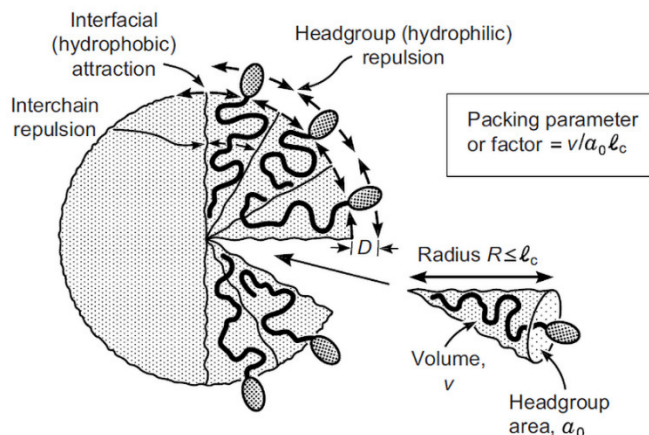
**Figure 3.1:** Schematic explanation of the hydrophobic effect. (a) To maintain the number of hydrogen bonds in water, amphiphiles enforce the formation cages of highly ordered water molecules around each alkyl chain, which leads to a loss in entropy. (b) An aggregation of the hydrophobic chains reduces the number of water molecules in the cage, the entropy loss is reduced. (c) In the ideal case of a micelle, the hydrophobic tails are not in contact with water, thus the number of ordered water molecules is minimized and so is the entropy loss. Redrawn from Ref.<sup>[168]</sup>.

At surfactant concentrations much larger than the CMC, lyotropic liquid-crystalline phases can be formed. The molecular shape of the surfactant and the relative concentrations of the components of the lyotropic mixtures determine the micellar shape, which in turn determines which LLC phase is formed under these conditions.

An elegant way to correlate the micellar shape with the required space of the monomeric surfactant is the principle of the packing parameter introduced by Israelachvili.<sup>[169]</sup> As illustrated in Figure 3.2, the packing parameter  $\Pi$  compares the area requirement of the hydrophobic head group with the one of the hydrophobic chain

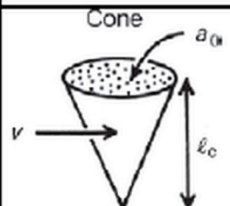


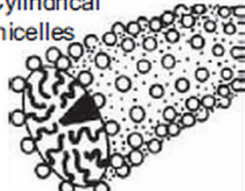

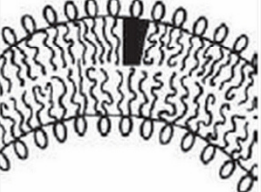
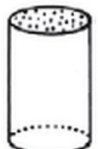

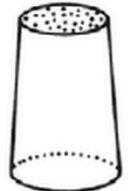
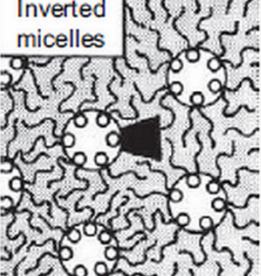
$$\Pi = \frac{v}{a_0 \cdot l_c}, \quad (3.1)$$

with the optimum head group area  $a_0$ , the effective volume of the hydrophobic alkyl chain  $v$  and the length of the alkyl chain  $l_c$  (Figure 3.2). Hence  $\frac{v}{l_c}$  is the cross-sectional area of the hydrophobic part.



**Figure 3.2:** Schematic representation of the area requirements of the hydrophilic and hydrophobic parts of a surfactant in a spherical micelle. The optimum head group  $a_0$  is determined by the repulsion of the head groups and hydrophobic interfacial forces (attractive) which prevent gaps between the headgroups, which in turn would lead to water - alkyl tail contacts. The volume  $v$  and length  $l_c$  of the alkyl chain determine how closely the hydrophobic chains can pack inside the micelle (interchain repulsion). Hence,  $a_0$ ,  $v$ ,  $l_c$  determine the favored micellar shape. Reprinted from Ref.<sup>[170]</sup> with permission, Copyright Elsevier 2011.

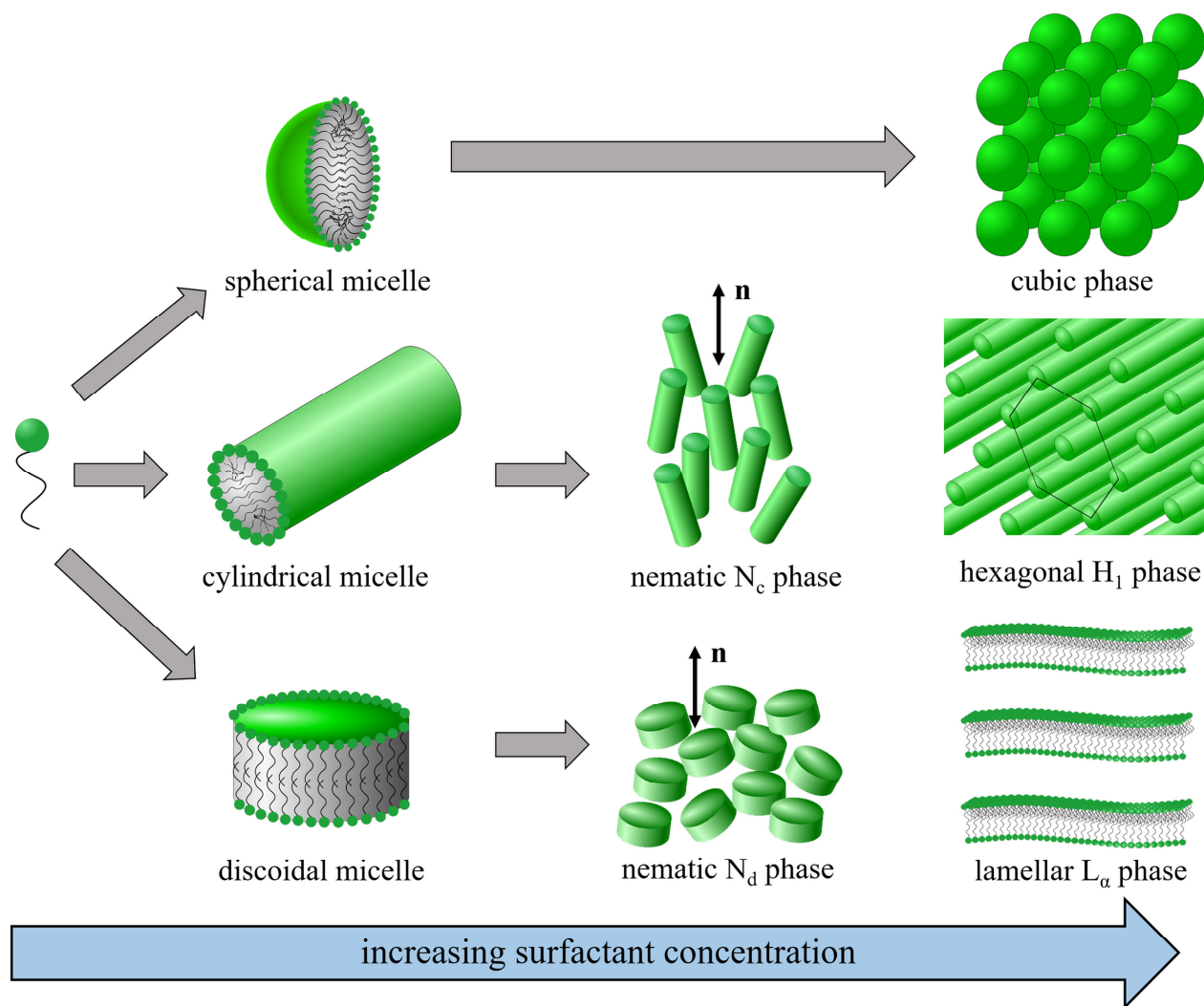
If the space requirement of the polar head group is larger than of the hydrophobic tail, the micelle has a positive curvature. For  $\Pi$  smaller than  $1/3$  spherical micelles (Figure 3.3a) and for  $\Pi$  between  $1/3$  and  $1/2$  cylindrical micelles (Figure 3.3b) are expected. If the head group occupies as much space as the alkyl chain,  $\Pi = 1$  holds true and planar bilayers are formed (Figure 3.3d). For the cross-section area of the hydrophobic tail being larger than of the head group,  $\Pi > 1$  is valid and inverted micelles are formed (Figure 3.3e), which happens at very high surfactant concentrations or in non-polar solvents.<sup>[167,170]</sup>

Critical packing parameter $v/a_0\ell_c$	Critical packing shape	Structures formed
(a) $< 1/3$	Cone 	Spherical micelles 
(b) $1/3-1/2$	Truncated cone 	Cylindrical micelles 
(c) $1/2-1$	Truncated cone 	Flexible bilayers, vesicles 
(d) $\sim 1$	Cylinder 	Planar bilayers 
(e) $> 1$	Inverted truncated cone or wedge 	Inverted micelles 

**Figure 3.3:** Packing parameter, packing shape of the surfactant and the formed micelle type for (a) spherical micelles, (b) cylindrical micelles, (c) vesicles, (d) planar bilayers and (e) inverted micelles. Reprinted from Ref.<sup>[170]</sup> with permission, Copyright Elsevier 2011.

Lyotropic liquid-crystalline phases form at relatively high surfactant concentration, *i.e.* a high volume fraction of micelles. Then the repulsive interactions between the micelles, which can be of steric,

electrostatic or entropic nature, lead to an ordering of the anisotropic micelles into the different LLC phases.<sup>[171]</sup> The two-step self-assembly of surfactants into lyotropic liquid-crystalline phases, where micelles of different shape build-up LLC phases of the different structure is shown in Figure 3.4.

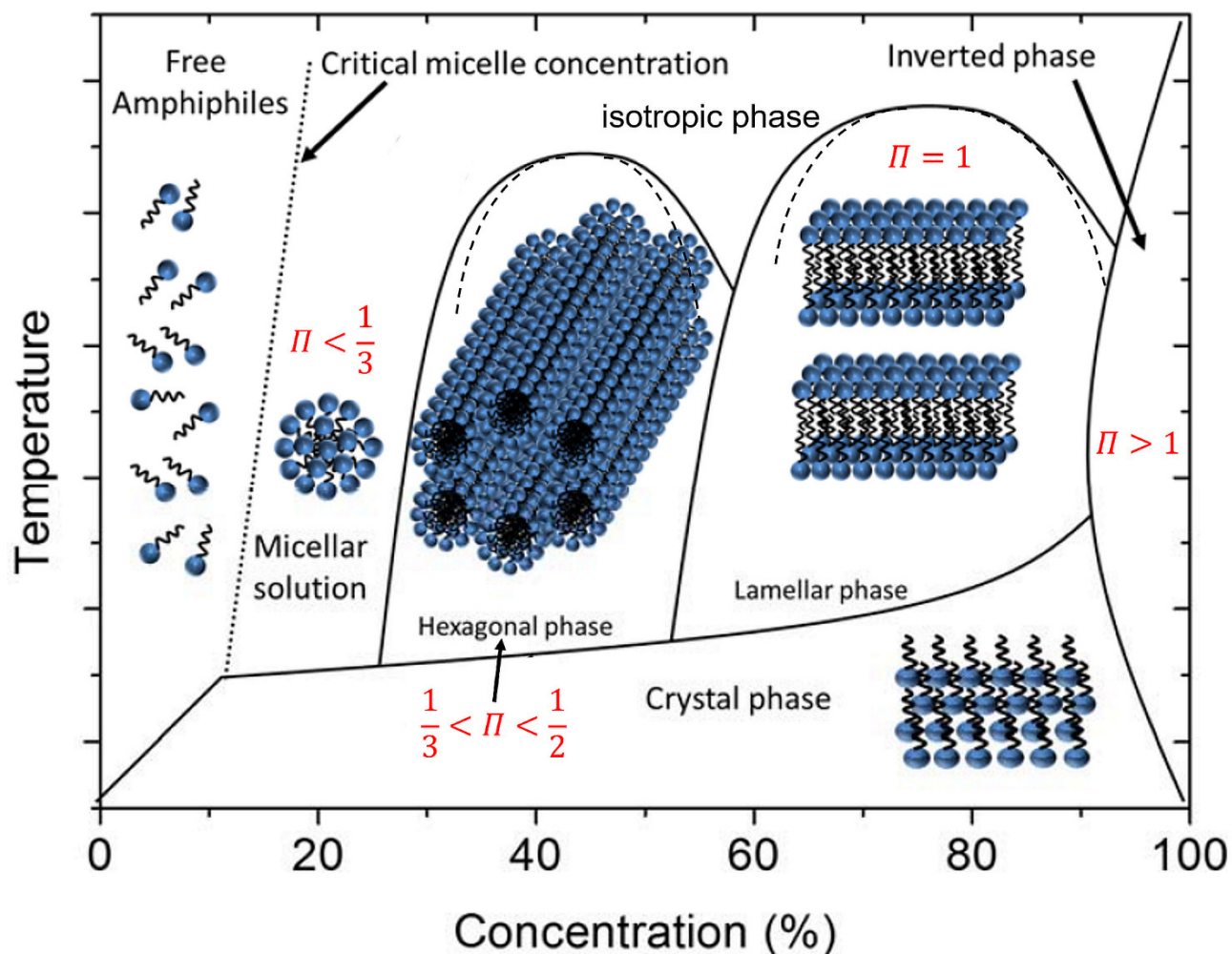


**Figure 3.4:** Schematic representation of the two-step self-assembly of amphiphilic molecules into LLC phases. The different micellar shapes and the lyotropic liquid-crystalline phases formed in dependence of surfactant concentration are shown. Redrawn after Ref.<sup>[166]</sup>

As mentioned before, the concentration is the fundamental variable of state for the appearance of lyotropic liquid-crystalline phases. There is a typical sequence of the LLC phases with increasing surfactant concentration, which is shown in the generic phase diagram in Figure 3.5. The lyotropic hexagonal  $H_1$  phase occurs in a wide range between the isotropic or cubic phase and the lamellar phase. The lamellar  $L_\alpha$  phase is typically found at high surfactant concentrations and occurs over a broad concentration and temperature range.<sup>[171]</sup> The reason for the sequence hexagonal phase



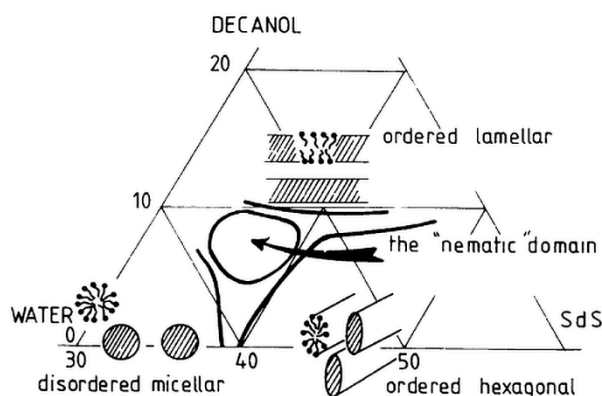
– lamellar phase with increasing surfactant concentration in a binary surfactant/water mixture is the size of the optimum head group area  $a_0$ . The head group area includes the amount of water bound to the polar head groups, *i.e.* the hydration shell. The size of the hydration shell decreases with increasing surfactant concentration since less water molecules per surfactant are available for the solvation of the head groups. Hence, the packing parameter  $\Pi$  increases and micelles with a smaller curvature are formed.<sup>[167]</sup>



**Figure 3.5:** Generic phase diagram of a binary amphiphile/water system. Above the critical micelle concentration, a solution of spherical micelles is formed. With increasing surfactant concentration the micellar shape changes (increasing packing parameter  $\Pi$ ) and the micelles aggregate into lyotropic hexagonal and at even higher concentrations lyotropic lamellar phases. Between the micellar solution and the hexagonal phase also cubic phases from spherical micelles (see also Figure 3.4) are possible. Adapted from I. Dierking, S. Al-Zangana, *Nanomaterials* **2017**, 7(10), 305.<sup>[172]</sup> (Open Access).

While the nematic phase is most common in thermotropic liquid crystals, lyotropic nematic phases are rather rare. In contrast to the frequent and broad hexagonal and lamellar phases, the nematic regime

in the phase diagram of lyotropic mixtures is often very narrow. Usually, the appearance of lyotropic nematic phases requires the use of an ionic surfactant and additionally a cosurfactant or an electrolyte.<sup>[173]</sup> In the case of ionic surfactants, repulsive Coulomb interaction mainly determine the area requirement of the polar head group.<sup>[167]</sup> The addition of salts shields the ionic head group, thus decreasing the repulsive interaction and leading to a smaller effective head group area. A similar effect can be achieved by the addition of cosurfactants, where the small non-ionic head groups reduce the Coulomb repulsion and thus the micelle curvature. Hence, the lyotropic nematic phases appear in a typical ternary (surfactant/cosurfactant/water) phase diagram (Figure 3.6) with increasing cosurfactant concentration between the lyotropic hexagonal and lamellar phase.



**Figure 3.6:** Draft of the partial phase diagram of the lyotropic system sodium decylsulfate (SdS) – *n*-decanol – water. Reprinted from Ref.<sup>[174]</sup> with the permission of EDP Sciences, Copyright 1981.

In the following, the lyotropic mesophases relevant for this thesis are introduced with regard to their properties and their characterization.

### ***Lyotropic nematic $N_d$ and $N_c$ phase***

As mentioned above, lyotropic nematic phases are rare and appear only in a limited temperature and concentration range. Hence, lyotropic nematic phases were not discovered until 1967.<sup>[175]</sup>

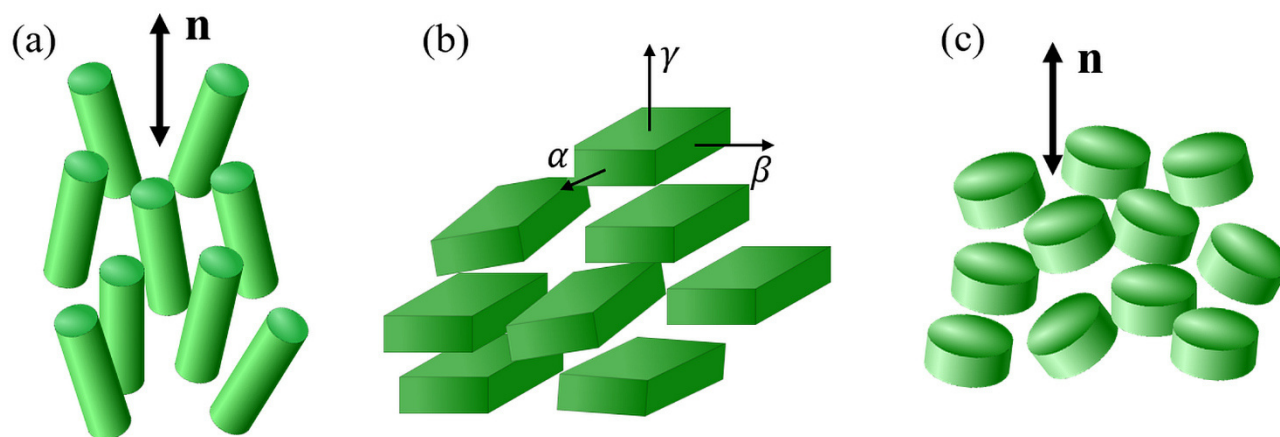
Lyotropic nematic phases are characterized by the presence of long-range orientational order and the absence of any long-range translational order. Nevertheless, short-range translational order, *i.e.* a pseudo-lamellar structure has been reported for lyotropic nematic phases.<sup>[176]</sup> Orientational order means that the principal axes of the micelles are on spatial and temporal average oriented along a preferred direction. This preferred direction is called the director  $\mathbf{n}$ , with the directions  $+\mathbf{n}$  and  $-\mathbf{n}$

being physically indistinguishable. To quantify the quality of orientational order, the orientational order parameter  $S_2$  is defined as

$$S_2 = \frac{1}{2} \langle 3 \cos^2 \beta_i - 1 \rangle, \quad (3.2)$$

where  $\beta_i$  is the angle between the director and the principal axis of all building blocks (micelles, mesogens)  $i$  and the brackets denote the ensemble average over many building blocks at the same time or a temporal average for a single building block. If there is no long-range orientational order, meaning that the micelles are oriented in all directions with the same probability as in the isotropic phase,  $S_2$  is zero. For a perfectly oriented system  $S_2$  increases to  $+1$ .<sup>[177]</sup>

Three different types of lyotropic nematic phases are known and their structures are shown in Figure 3.7. Two of them are uniaxial ( $N_c$  and  $N_d$  phase), while the third is biaxial ( $N_{bx}$ ). In the uniaxial phases, the director corresponds to the optical axis of the system and all directions perpendicular to the director are equivalent ( $D_{\infty h}$  symmetry). In the biaxial phase all three directions are inequivalent due to orientational ordering along the directions of the longest and shortest axes of the micelles. There are 3 two-fold symmetry axes and two optical axes ( $D_{2h}$  symmetry).<sup>[178]</sup>



**Figure 3.7:** Schematic representation of the lyotropic nematic (a)  $N_c$  phase, (b)  $N_{bx}$  phase and (c)  $N_d$  phase. In the  $N_c$  phase the micelles have cylindrical shape, in the  $N_{bx}$  phase the micellar shape is brick-like and in the  $N_d$  phase is build-up by disk-like micelles. In the uniaxial  $N_c$  phase and  $N_d$  phase the principal micellar axes are on average oriented along the director  $\mathbf{n}$ . In the biaxial  $N_{bx}$  phase the  $\alpha$ - and  $\gamma$ -axes are orientationally ordered. Redrawn after Ref.<sup>[173]</sup>

In a “micellar frame”  $\alpha, \beta, \gamma$  (see Figure 3.7), a tensor property  $\vec{T}$  such as the electric or magnetic susceptibility is written as<sup>[177]</sup>



$$\vec{T} = \begin{pmatrix} T_{\alpha\alpha} & 0 & 0 \\ 0 & T_{\beta\beta} & 0 \\ 0 & 0 & T_{\gamma\gamma} \end{pmatrix}, \quad (3.3)$$

with  $T_{\alpha\alpha} = T_{\beta\beta} \neq T_{\gamma\gamma}$  in case of a uniaxial phase and  $T_{\alpha\alpha} \neq T_{\beta\beta} \neq T_{\gamma\gamma}$  in case of a biaxial phase. Hence, in case of a uniaxial phase the 2<sup>nd</sup> rank tensor becomes<sup>[177]</sup>

$$\vec{T} = \begin{pmatrix} T_{\perp} & 0 & 0 \\ 0 & T_{\perp} & 0 \\ 0 & 0 & T_{\parallel} \end{pmatrix}, \quad (3.4)$$

with  $T_{\perp}$  and  $T_{\parallel}$  being the principal value of the property  $\vec{T}$  perpendicular and parallel to the director, respectively. Similarly, the anisotropy<sup>[177]</sup>

$$\Delta T = T_{\gamma\gamma} - \frac{(T_{\alpha\alpha} + T_{\beta\beta})}{2}, \quad (3.5)$$

can be written as

$$\Delta T = T_{\parallel} - T_{\perp}. \quad (3.6)$$

By means of small angle X-ray scattering, the micellar shape was claimed to be cylindrical in case of the  $N_c$  phase (calamitic nematic phase) and disk-like in case of the  $N_d$  phase (discotic nematic phase).<sup>[174,179]</sup> Additionally, it was noticed that  $N_c$  phases from amphiphiles with hydrocarbon chains align with the director parallel to the magnetic field (positive anisotropy of the diamagnetic susceptibility,  $\Delta\chi^d > 0$ , often called type I mesophases and indicated with a “+”), while  $N_d$  phases are aligned with the director perpendicular to the magnetic field direction (negative anisotropy of the diamagnetic susceptibility,  $\Delta\chi^d < 0$ , often called type II mesophases and indicated with a “-“).<sup>[180]</sup> Since hydrocarbon chains are known to align perpendicular to the magnetic field<sup>[181]</sup>, a cylindrical micelle shape in case of the  $N_c$  and a disc-like shape in case of a  $N_d$  phase was proposed.<sup>[182]</sup> In case of perfluorinated chains the signs of  $\Delta\chi^d$  are inverted in comparison to those in the case of alkyl chains.<sup>[180]</sup> Hence, to distinguish between a  $N_c$  and a  $N_d$  phase, the sign of  $\Delta\chi^d$  is a distinctive property to be tested.

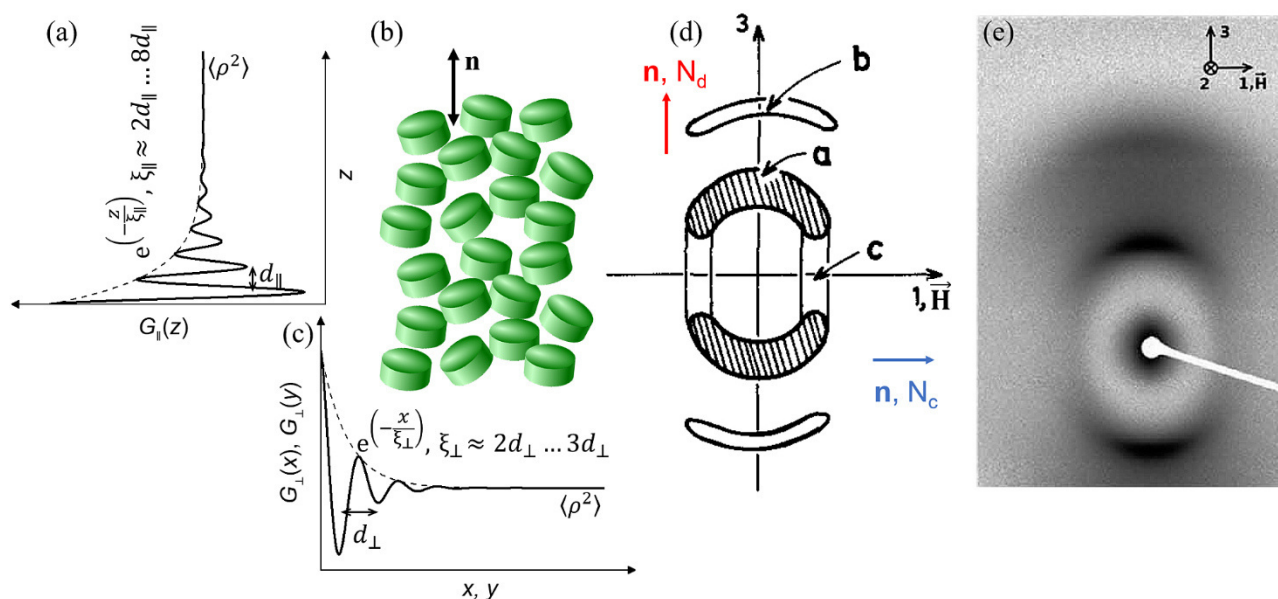
To identify lyotropic nematic phases, polarized optical microscopy (POM) and X-ray scattering can be used. General information on the POM technique and the characteristic textures of the different (thermotropic) liquid-crystalline phases can be found in respective textbooks<sup>[183,184]</sup>. For further

information on the X-ray technique and X-ray scattering on soft matter, Ref.<sup>[185]</sup> and Ref.<sup>[186]</sup> are recommended, respectively.

Under a polarizing microscope nematic phases usually show a *schlieren* texture with typical point defects of topological strengths  $\pm\frac{1}{2}$  and  $\pm 1$ , from which two or four black brushes emerge, respectively.<sup>[184]</sup> For lyotropic nematic phases, the schlieren texture is the characteristic texture for freshly prepared samples.<sup>[171]</sup> If a micellar solution is filled into a capillary with an untreated hydrophilic glass surface, the surface is covered by a mono- or bilayer of surfactant. For lyotropic nematic phases, this leads to a slow alignment of the cylindrical or disk-like micelles with their long axes parallel to the glass surface.<sup>[167,187]</sup> In case of the  $N_d$  phase filled into flat glass capillaries, this results in an homeotropic alignment with the director oriented parallel to the path of light propagation. Hence, a pseudo-isotropic texture results, which appears greyish when the capillary is tilted.<sup>[187],[171]</sup> In case of a  $N_c$  phase the calamitic shaped micelles align in a planar way, such that the director is oriented perpendicular to the path of travelling light. If the alignment is not uniform, the typical schlieren texture is observed between crossed polarizers. For a complete uniform alignment, the assistance of a magnetic field is often necessary.<sup>[171]</sup>

Due to the lack of long-range translational order in lyotropic nematic phases, only diffuse scattering maxima can be observed in X-ray scattering patterns.<sup>[174,188]</sup> In Figure 3.8 the characteristic scattering patterns for an aligned  $N_d$  phase is shown. Rather strong arcs (a-band in Figure 3.8d) are seen in the direction parallel to the director. These maxima are present due to the short-range intermicellar positional correlation in this direction (Figure 3.8a), which is the direction of the short intermicellar distance  $d_{\parallel}$ .<sup>[179]</sup> The arc-shape of these maxima arises since orientational fluctuations of the micelles smear these bands out.<sup>[176]</sup> In a perfectly oriented sample ( $S_2 = 1$ ) these maxima would appear as points, while in the isotropic phase (no orientational ordering,  $S_2 = 0$ ) would appear as a circle. For lyotropic nematic phases often a second scattering maxima in the same direction can be observed, which is the second order maxima of the stronger first maxima (b-band in Figure 3.8d). This indicates a pseudo-lamellar ordering of the micelles, *i.e.* a lamellar ordering over only a few (up to 8) intermicellar distances.<sup>[176,189]</sup> Perpendicular to this direction very broad and weak bands are observed (c-band in Figure 3.8d), which can appear rather rectilinear<sup>[176]</sup> or as a diffuse ring<sup>[171]</sup>. These maxima correspond to the long intermicellar distance  $d_{\perp}$  and thus appear at lower  $q$ -values than in the direction perpendicular to it (Bragg relation  $d_c = 2\pi/q_c$ ).<sup>[179]</sup> Due to the shape anisotropy of the micelles, the 2D scattering pattern (Figure 3.8e) is elliptical. For an aligned  $N_c$  phase, a similar scattering patterns

emerges. But now, the rather strong a- and b-arcs are oriented perpendicular to the director  $\mathbf{n}$  representing the short intermicellar distance  $d_{\perp}$ .<sup>[179]</sup>

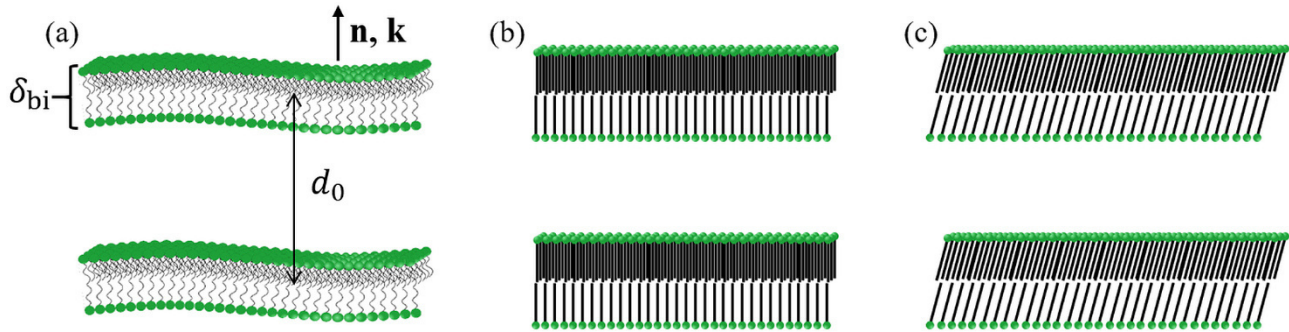


**Figure 3.8:** Emergence of the X-ray diffraction pattern of an aligned lyotropic nematic phase, exemplary shown for the  $N_d$  phase. The exponential decay of the correlation functions ( $G_{\parallel}(z)$ ,  $G_{\perp}(x)$ ,  $G_{\perp}(y)$ ) shows the short-range translational order (a) parallel and (c) perpendicular to the director  $\mathbf{n}$ . In the direction of the director the correlation length  $\xi_{\parallel}$  can range over several intermicellar distances  $d_{\parallel}$  indicating a pseudo-lamellar order. In b) a schematic structure of the  $N_d$  phase is shown. A theoretical and a real X-ray diffraction pattern are presented in d) and e), respectively. The magnetic field is applied in the 1-direction, thus the director of the  $N_d$  phase points along the 3-direction (for a uniform alignment, rotation of the capillary around the 3-axis is required). The broad and rather weak maxima denoted with **a** and **c** arise due to the short ( $d_{\parallel}$ ) and long ( $d_{\perp}$ ) intermicellar distance, respectively. The **b**-band is the second order of the **a**-band and appears due to the pseudo-lamellar order. The arc-shape of the **a** and **b**-band results from the long-range orientational order of the nematic phase. In case of a  $N_c$  phase, the X-ray diffraction pattern looks similar, but now the director  $\mathbf{n}$  points along the 1-direction. d) is adapted from Y. Galerne *et al.*, *J. Chem. Phys.* **1987**, 87, 1851.<sup>[189]</sup>, with the permission of AIP Publishing. e) is reprinted from Ref.<sup>[190]</sup> with permission of Taylor & Francis.

### *Lyotropic lamellar $L_{\alpha}$ phase*

The lyotropic lamellar  $L_{\alpha}$  phase consists of equidistant flat surfactant bilayers (lamellae) with a large shape anisotropy (ideally infinite, usually larger than 1:50)<sup>[171]</sup> separated by a water sub-layer. In addition to the orientational order, the  $L_{\alpha}$  phase is characterized by a long-range one-dimensional positional ordering of the lamellae along the layer normal  $\mathbf{k}$ , which is parallel to the director  $\mathbf{n}$ .<sup>[191]</sup> As indicated by the index “ $\alpha$ ”, the alkyl chains of the amphiphilic molecules are oriented perpendicular

to the surface of the bilayer and are in a liquid-like state making the  $L_\alpha$  phase a 2D fluid (Figure 3.9a).<sup>[171]</sup> In contrast, the hydrocarbon chains of  $L_\beta$  (Figure 3.9b) and  $L_{\beta'}$  (Figure 3.9c) phases are in an all-trans configuration and either parallel or tilted with respect to the layer normal. The surfactant molecules possess an in-plane 2D (hexatic) bond orientational order and due to the stiff alkyl chains the  $L_\beta$  and  $L_{\beta'}$  phases exhibit very high viscosity.<sup>[171,192,193]</sup>

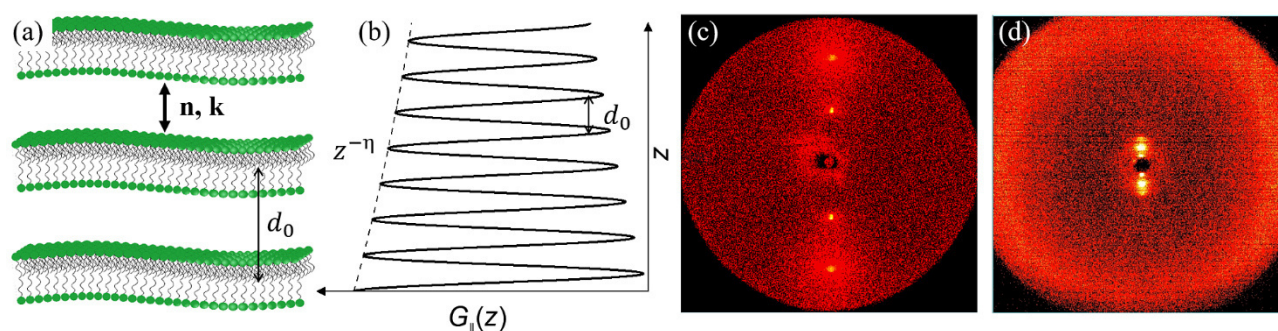


**Figure 3.9:** Schematic drawing of the lamellar (a)  $L_\alpha$  phase, (b)  $L_\beta$  phase and (c)  $L_{\beta'}$  phase. In a lamellar phase, surfactant bilayers (called lamellae) of a thickness  $\delta_{bi}$  are regularly positioned along the layer normal  $\mathbf{k}$  with a periodicity  $d_0$  (called lamellar repeat unit), i.e. lamellar phases show 1D-translational order. In the  $L_\alpha$  phase the alkyl chains are in a liquid-like state, while in the  $L_\beta$  and  $L_{\beta'}$  phase, stiff alkyl chains are oriented parallel or tilted to the layer normal.

As the lyotropic nematic  $N_d$  phase, the  $L_\alpha$  phase has a negative anisotropy of the diamagnetic susceptibility ( $\Delta\chi^d < 0$ )<sup>[194]</sup> and tends to slowly align with the bilayers parallel to a hydrophilic glass surface.<sup>[171]</sup> Thus, with POM often pseudo-isotropic textures (appear black between crossed polarizers) are observed where in case of an imperfect alignment so-called oily-streaks are visible. In case of a planar alignment, the mosaic texture and the focal-conic fan-shaped texture are typical for the  $L_\alpha$  phase.<sup>[195]</sup> With freeze-fracture electron microscopy (FFEM), the layered structure can be visualized by smooth lamellar fracture faces, so-called layer steps.<sup>[167,196,197]</sup>

A typical X-ray image from the structure of a  $L_\alpha$  phase is shown in Figure 3.10. The one-dimensional periodic structure of the  $L_\alpha$  phase is reflected by the appearance of sharp pseudo-Bragg peaks indicating a large correlation length of the 1D-translational order of the bilayers of over 100 nm (Figure 3.10b).<sup>[171]</sup> Often further peaks appear with the relation of the relative  $q$ -positions of the peaks being 1:2:3:4...with respect to the position of the principal peak, i.e. these peaks are higher order peaks. The positions of these peaks are reciprocal (Bragg relation  $d_0 = 2\pi m/q_m$  with  $m$  being  $m^{\text{th}}$  diffraction order) to the lamellar repeat unit  $d_0$ , which is the sum of the bilayer thickness  $\delta_{bi}$  and the thickness of the water sub-layer (Figure 3.9a).<sup>[198]</sup> In case of an aligned sample, sharp spots appear in the X-ray diffractions pattern along the direction perpendicular to the lamellae (parallel to  $\mathbf{n}$  and  $\mathbf{k}$ )

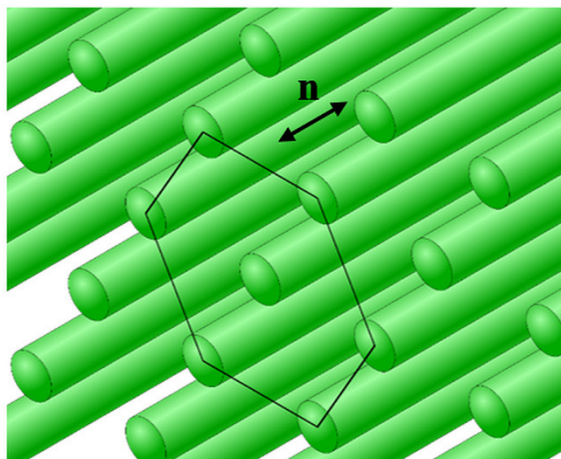
(Figure 3.10c). In the wide-angle region, a diffuse scattering maximum confirms the presence of “molten” liquid-like paraffinic chains, where the maximum indicates the mean distance between the alkyl chains (approximately 0.46 nm, Figure 3.10d).<sup>[167]</sup> In contrast, rather sharp maxima are present in the X-ray curve of  $L_\beta$  and  $L_\beta'$  phases.<sup>[192,193]</sup> Due to the liquid-like character of the alkyl tails in the  $L_\alpha$  phase, the wide-angle scattering appears as a diffuse ring in the 2D diffraction pattern.<sup>[199]</sup>



**Figure 3.10:** Emergence of the typical 2D X-ray diffraction pattern of an aligned lyotropic lamellar  $L_\alpha$  phase. *a)* Sketch of the  $L_\alpha$  structure with director  $\mathbf{n}$  and layer normal  $\mathbf{k}$  aligned in vertical direction ( $z$ -direction). The lamellar repeat unit  $d_0$  is indicated. *(b)* Correlation function  $G_{\parallel}(z)$  with period  $d_0$  of the lamellar structure in *(a)*. True long-range translational order is destroyed by thermal fluctuations of the bilayers. The amplitude of  $G_{\parallel}(z)$  thus slowly decays algebraically with an exponent  $\eta$  called the Caillé parameter (see chapter 6.1.3). In an X-ray scattering experiment this quasi long-range translational order leads to multiple orders  $m$  of sharp pseudo-Bragg peaks at relatively small scattering vectors  $|\vec{q}_{\parallel}| = \frac{2\pi}{d_0}m$  in the direction of  $\mathbf{k}$ . Experimental 2D diffraction patterns of the same shear aligned  $L_\alpha$  phase at different sample-to-detector distances showing the small-angle regime *(c)* and the wide-angle regime *(d)*. In *(c)* the pseudo-Bragg peaks of the lamellar structure are seen as sharp spots in the direction of  $z$ . In *(d)* an additional ring of diffuse scattering from the fluid intra-lamellar order is observed in the wide-angle regime. Here, the pseudo-Bragg peaks are overexposed.

### *Lyotropic hexagonal $H_1$ phase*

In a hexagonal phase the amphiphiles form long cylinders with a circular cross-section and a large shape anisotropy (diameter to length at least 1:50, often called infinite cylinders).<sup>[171]</sup> Parallel cylinders are arranged on a two-dimensional hexagonal lattice with the water in between. Hence, the director  $\mathbf{n}$  indicating the long-range orientational order points along the long axes of the cylindrical micelles and there is a two-dimensional long-range translational order in the plane perpendicular to  $\mathbf{n}$  (see Figure 3.11).<sup>[167]</sup>



**Figure 3.11:** Schematic drawing of the structure of a lyotropic hexagonal  $H_1$  phase. Long cylindrical micelles are oriented parallel to each other on a 2D hexagonal lattice with the director  $\mathbf{n}$  along the long cylinder axes.

The hydrocarbon chains of the amphiphiles are in a liquid-like state, thus the hexagonal phase is also often labelled as  $H_a$ . The designation “ $H_1$ ” phase denotes that the alkyl tails point inside the micelles with the polar head groups facing the surrounding water (“normal” hexagonal phase). In contrast, at very high surfactant concentrations or when large concentrations of non-polar solvents are added, the cylindrical micelles are inverted, with the alkyl chains pointing outwards and the water placed inside the cylinders. This phase is called the inverse hexagonal phase  $H_2$ .<sup>[171]</sup>

The  $H_1$  phase is highly viscous since the only easy direction of flow is normal to the 2D lattice in the direction of  $\mathbf{n}$ . In addition, defects can further increase the effective viscosity.

Similar to the calamitic nematic  $N_c$  phase, the hexagonal phase exhibits a positive anisotropy of the diamagnetic susceptibility ( $\Delta\chi^d > 0$ ), but its high viscosity needs higher magnetic fields and/or a long period of time to get the  $H_1$  phase uniformly aligned.<sup>[194,200]</sup> Under a polarizing microscope the  $H_1$  phase typically shows fan-like textures. Additionally, the observation of non-geometric textures with or without striations is characteristic.<sup>[195]</sup>

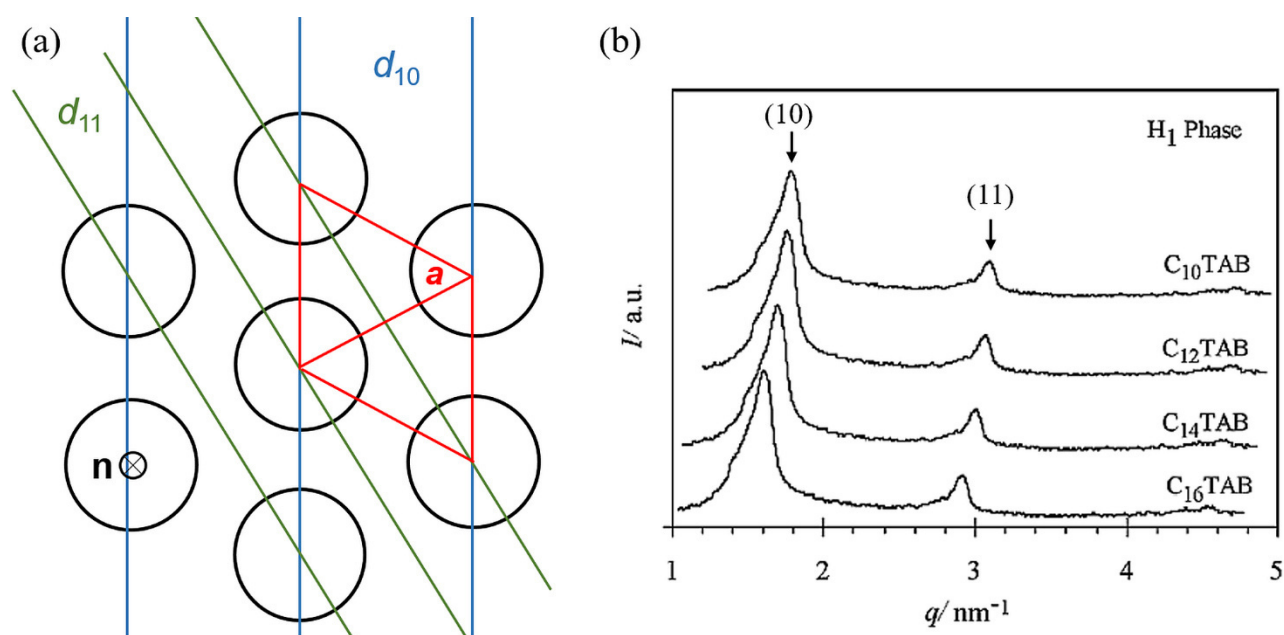
A typical X-ray scattering profile of the hexagonal phase shows pseudo-Bragg peaks with  $q$ -ratios of  $1:\sqrt{3}:2:\sqrt{7}\dots$ , reflecting the two-dimensional hexagonal symmetry of the  $H_1$  phase (see Figure 3.12).<sup>[167]</sup> However, often only the first scattering maximum is visible. The lattice parameter  $a$  of the hexagonal structure can be obtained from the X-ray data using

$$a = \frac{2}{\sqrt{3}} d_{10}, \quad (3.7)$$



where  $d_{10}$  is the distance between adjacent rows of cylinders obtained from the position of the first scattering maximum  $q_{10}$  via the Bragg equation (Figure 3.12).<sup>[198]</sup>

In the rare case that the X-ray beam is oriented along the long cylinder axes, the six-fold symmetry of the hexagonal lattice is reflected in a 2D diffraction pattern by the appearance of the symmetrical distribution of six spots which ideally have the same intensity.<sup>[201]</sup> At high  $q$ -values a broad and diffuse band at approximately  $q = \frac{2\pi}{0.45 \text{ nm}}$  can be observed<sup>[167]</sup>, which indicates that the alkyl chains are in a liquid-like state. Even if the  $H_1$  phase is uniformly aligned, this maximum appears as a diffuse ring in a 2D X-ray diffraction pattern.<sup>[171]</sup>



**Figure 3.12:** Emergence of the X-ray scattering profile  $I(q)$  of a lyotropic hexagonal phase. *a)* Schematic drawing of the hexagonal phase with view along the director  $\mathbf{n}$ . The 2D hexagonal translational order characterized by the periodic distances  $d_{10}$  and  $d_{11}$  and the lattice parameter  $a$  leads to the appearance of (10) and (11) peaks in the corresponding X-ray profile, as shown in *b)*. *b)* is reprinted from D. Varade *et al.*, Phase diagrams of water–alkyltrimethylammonium bromide systems, *Colloids Surf., A* **2008**, 315, 205.<sup>[202]</sup>, Copyright 2008, with permission from Elsevier.

### 3.2 Self-assembled fibrillar networks

Self-assembled fibrillar networks (SAFiNs) are formed when a sol consisting of a small content of so-called low molecular weight gelator (LMWG, molecular weight usually  $\leq 2000$  Da) molecules in a solvent is cooled below its characteristic sol-gel transition temperature  $T_{\text{sol-gel}}$  (Figure 3.5). The gelator molecules self-assemble via physical interactions, such as hydrogen bonds,  $\pi$ - $\pi$  interactions or

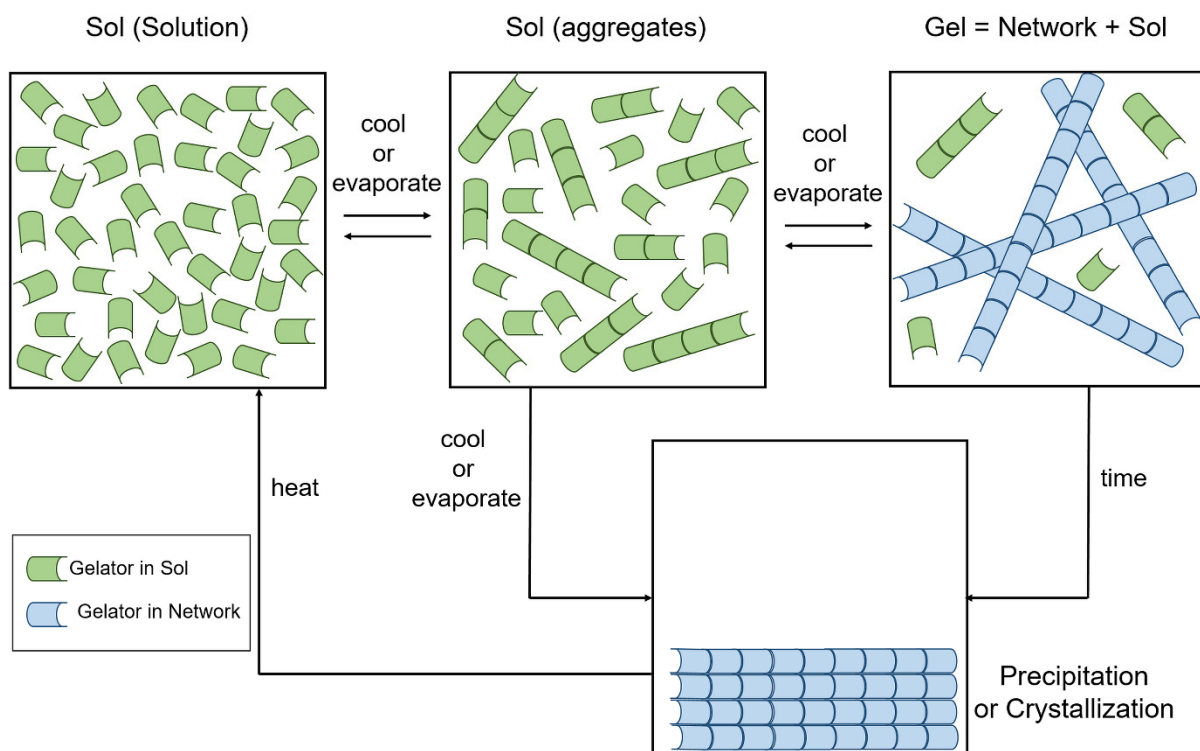
London dispersion interactions.<sup>[5,11,203]</sup> These interactions are highly specific with anisotropic tendencies, which highly favor one-dimensional aggregation into fibers, ribbons, tubules, strands or tapes.<sup>[142,204]</sup> The aggregate morphology depends on the molecular structure of the LMWG as well as on the gelator-solvent interaction and the procedure of gel formation. To result in a gel, the 1D aggregates (from now on simply called fibers) have to build up a three-dimensional network of large surface area, which permeates the volume and thereby immobilizes the solvent macroscopically due to adhesion and surface tension, although the solvent molecules are still able to diffuse microscopically.<sup>[205]</sup> Therefore, macroscopic flow under gravity is inhibited.<sup>[11,142,206]</sup> In the network, the fibers are interconnected in so-called junction zones, which can be of permanent or transient nature.<sup>[143,207,208]</sup> Permanent junction zones originate from mismatches during the fiber growth leading to a branched network.<sup>[209,210]</sup> Transient junction zones emerge from physical interactions between the fibers as well as from the mechanical contact of the entangled fibers.<sup>[210,211]</sup> The junction zones provide rigidity to the microstructure and are thus responsible for the solid-like, elastic properties of the gel.<sup>[5,142]</sup>

Since all interactions (intra- as well as interfiber) are of the non-covalent kind, the resulting physical gels are thermoreversible, meaning that the network can be repeatedly disassembled and reassembled upon heating or cooling, respectively.<sup>[5,11,212]</sup> The process of supramolecular gel formation is summarized in Figure 3.13.

LMWGs which are able to gel water are called hydrogelators, whereas LMWGs that gel organic solvents are called organogelators, the resulting gels are called hydrogels or organogels, respectively.<sup>[5,203]</sup>

The molecular structure of LMWGs is often based on naturally occurring biomolecules, such as steroids, sugars, fatty acids, amino acids and nucleobases. Especially for hydrogels, this can lead to biocompatibility as well as biodegradability important for biological applications such as biosensors, tissue engineering, drug delivery etc.<sup>[213–215]</sup> The inherent molecular chirality of these gelator molecules is often reflected in a supramolecular chirality, *i.e.* in twisted fibers or helical ribbons, with a pitch between 10 nm and several microns.<sup>[216]</sup> The handedness of the chiral fiber is directly linked to the molecular chirality of the gelator, with one enantiomer forming only left-handed fibers and the other one only right-handed fibers.<sup>[216]</sup>





**Figure 3.13:** Process of the gel formation by a low molecular weight gelator (LMWG). The LMWG is dissolved in a solvent by heating (sol formation). Cooling the sol leads to an aggregation of the LMWG molecules into small fibers and further cooling leads to the formation of the fiber network, which immobilizes the solvent. Depending on the lifetime stability of the gel, precipitation or crystallization of the gelator occurs sooner or later. Adapted and redrawn from Ref.<sup>[203]</sup>

To be able to form a network in a solvent, a minimum gelator concentration, which is called the critical gelator concentration ( $c_{gc}$ , usually  $\leq 2$  wt%) is necessary.<sup>[142]</sup> The  $c_{gc}$  is thus a measure for the efficiency of a gelator in the respective solvent. The efficiency of a LMWG as organogelator can also be evaluated by the range of different solvents the gelator is able to gel. Measures for the stability of a gel are its thermal stability (gel-sol transition temperature  $T_{gel-sol}$ ), its mechanical stability (rheological criteria like its yield stress or the values and ratio of the elastic  $G'$  and the loss  $G''$  moduli), as well as its long-term stability (between a few hours and several decades).<sup>[5,207]</sup> Since most SAFiNs are thermodynamically metastable, macroscopic phase separation, *i.e.* crystallization or precipitation of the gelator takes place with time.<sup>[5,217]</sup>

As it will become more clear below, the structure of the network (*e.g.* fiber diameter, network mesh size, junction zone density) and thus the properties of the gel depend on its age, the gelator concentration, the solvent and the gels' history, *i.e.* its formation (*e.g.* slow or fast cooling rate), the temperature at which it is kept and the application of mechanical stresses.<sup>[5,143,217]</sup>

The fiber can be either of crystalline or amorphous nature depending on the gelator and the

solvent.<sup>[206,218]</sup> Fiber and network growth are either described via a percolation<sup>[219]</sup> model characterized by a divergence of the connectivity correlation length<sup>[143]</sup> or a nucleation and growth mechanism,<sup>[209,220–222]</sup> mostly assuming the fiber to have a crystalline nature.

The solvent-gelator relationship crucially influences the ability to form a gel in the first place, as well as the fiber morphology and the gels' properties. 1D aggregation into a fiber and subsequent network formation is on a delicate balance between dissolution of the gelator molecules and precipitation of aggregates from the solution.<sup>[223]</sup> The solvent may compete with the gelator for the functional groups responsible for the fiber formation (*e.g.* hydrogen bond donors or acceptors), thus preventing inter-gelator interactions and leading to dissolution of the LMWG molecules rather than to fiber formation. Hence, stable gels are usually achieved by choosing a solvent with limited interactions with the LMWG molecules.<sup>[224,225]</sup> Contrary, if the inter-fiber interactions are too strong and not reduced by fiber-solvent interactions precipitation of the aggregates results.<sup>[223]</sup>

Moreover, the fiber structure formed by a certain LMWG can be different in different solvents.<sup>[224,226,227]</sup> If for example several different interactions are responsible for the fiber formation, one specific interaction can be the main driving force in polar solvents and another one can be the main driving force in non-polar solvents resulting in different arrangements of the gelator molecules in polar or non-polar solvents.<sup>[228]</sup> To rationalize the gel formation, the gel forming ability and certain gel properties are often correlated with different solubility parameters of the solvent.<sup>[224,229–231]</sup> For example, Hansen solubility parameters, which dissect the gelator-solvent interactions into dispersive, polar and hydrogen bonding interactions, are used to predict whether dissolution, gel formation or precipitation occurs for a gelator in different solvents.<sup>[232]</sup>

It was shown that a certain degree of undercooling (or supersaturation) is necessary to enforce gel formation.<sup>[233]</sup> Thus, the morphology of the gel depends on the gelation temperature (for isothermal gelling conditions)<sup>[220,234]</sup> or the cooling rate (for non-isothermal gelling conditions)<sup>[209,221,222]</sup>, since the degree of supersaturation determines the number of formed nuclei, the nucleation rate and the formation of permanent junction zones, which determine the fiber length and the cross-linking density. Cooling the sol below  $T_{\text{sol-gel}}$  leads to a supersaturated solution far from the thermodynamic equilibrium, a situation which is the key to the formation of a metastable, well-organized network structure, meaning that a micro-phase separated structure occurs rather than precipitation or crystallization.<sup>[233]</sup> A higher cooling rate or a lower gelation temperature lead to a higher degree of undercooling and thus to an increased supersaturation, as does a higher gelator concentration. An increased gelator-solvent compatibility requires a higher degree of undercooling necessary to start

gelation, giving another reason why the solvent influences the fiber and network morphology.<sup>[235]</sup> The higher the degree of supersaturation, the higher the driving force for (micro)phase separation, *i.e.* fiber formation which might also result in a higher degree of mismatching leading to a highly branched network.<sup>[208,209,220,221,234,236,237]</sup>

A final note regarding the nomenclature of the fibrous aggregates in SAFiNs. In biological fibrillar materials such as cellulose or collagen the term fiber means a large fiber in the micrometer range that is composed of smaller fibrils in the nanometer range. In turn, the fibrils can be composed of even smaller fibrils called nanofibrils or microfibrils.<sup>[238,239]</sup> However, the fibrous aggregates in SAFiNs are usually less than 100 nm in diameter, but still mostly called fibers, *e.g.* in the references<sup>[240–242]</sup>. To emphasize that the fibrous aggregate is in the nanometer range the term nanofiber is also used.<sup>[64,68,74]</sup> Moreover, there are examples where finer fibrils entwine to compose the final gel fiber. To underline this behavior the terms fibril (for the thin fibers building up the bigger fiber) and fiber (for the final fiber) are used,<sup>[72,79]</sup> regardless whether the diameter of the final fiber is the nanometer or micrometer range. From now on the term fiber is used in this thesis to describe the fibrous aggregates formed by LMWGs.

## 4 Preparation and stability of micellar lyotropic LC physical gels (Publication I)

In this chapter, the experimental procedure of transferring the lyotropic liquid-crystalline phases (lamellar  $L_\alpha$ , nematic  $N_d$  or  $N_c$ , hexagonal  $H_1$ ) of the system  $H_2O - n$ -decanol – SDS into the corresponding gelled state using the gelator 12-hydroxyoctadecanoic acid (12-HOA) is presented. The choice of 12-HOA was based on successful preliminary tests to gel the lamellar phases of the lyotropic systems  $D_2O - n$ -decane –  $C_{10}E_4$ <sup>[136]</sup> and  $H_2O -$  didodecyldimethylammonium bromide.<sup>[243]</sup> After describing an easy and reproducible gelling procedure for LLC gels, insights how the gelator and the fiber network influence the LLC phases and vice versa are reported. Furthermore, it is demonstrated why the obtained lyotropic liquid-crystalline gels are not orthogonal self-assembled systems, *i.e.* the two structures – lyotropic liquid-crystalline phase and gel fiber network – do not form independently of each other within the same system.

### 4.1 Specific background

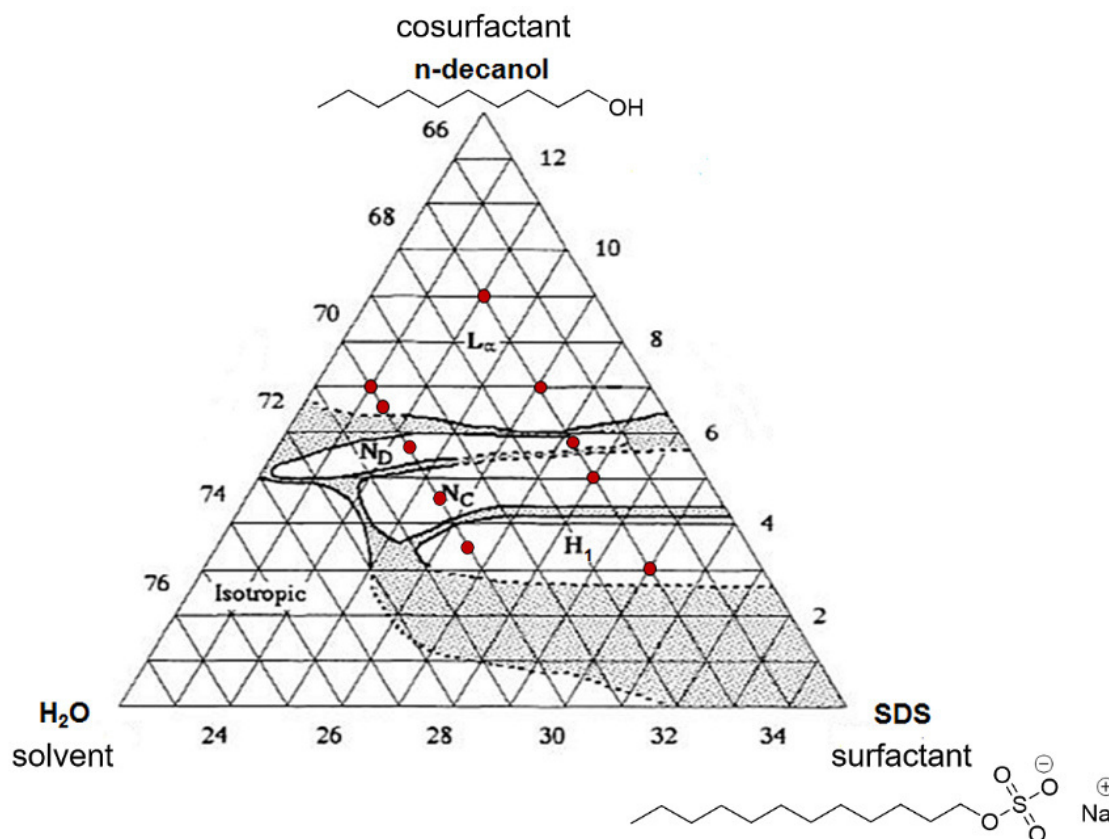
#### 4.1.1 The lyotropic system $H_2O - n$ -decanol – SDS

The micellar lyotropic system containing sodium dodecylsulfate as anionic surfactant,  $n$ -decanol as cosurfactant and water as solvent was chosen as “solvent” for gelation since, depending on the composition, it exhibits four different lyotropic phases at room temperature, namely the lamellar  $L_\alpha$  phase, the nematic  $N_d$  and  $N_c$  phases and the hexagonal  $H_1$  phase (see Figure 4.1).

To be exact, also small islands of the biaxial nematic  $N_{bx}$  phase were observed in the room temperature phase diagram<sup>[244]</sup> and temperature dependent  $N_{bx} - N_c$ <sup>[244,245]</sup> and  $N_d - N_{bx}$ <sup>[190]</sup> phase sequences were observed at different compositions. To keep it simple, compositions aside those biaxial phase regions were chosen for further investigations. The identification of the  $N_c$  and  $N_d$  phase was performed as described in the chapter 3.1. In order to fully rule out the possibility that a biaxial nematic gel has been formed, the birefringences ( $n_2 - n_1$  and  $n_3 - n_2$ ) would need to be measured by *e.g.* laser conoscopy.<sup>[190,246]</sup> But since the  $N_{bx}$  phase appears only in a very narrow regime in the phase diagram, the formation of a biaxial nematic gel is highly unlikely.

A pseudo-lamellar arrangement of the micelles in the nematic phases of this system was reported by Berger *et al.*<sup>[188]</sup> As shown by POM<sup>[247]</sup> and SAXS<sup>[248]</sup> studies, the ratio  $n$ -decanol / SDS crucially

defines the formed phase. SAXS investigations proved that the micellar shape depends on the *n*-decanol / SDS ratio showing that the transition from a cylindrical to a discotic micellar shape almost coincides with the  $N_c - N_d$  transition at increasing cosurfactant / surfactant ratio.<sup>[248]</sup>

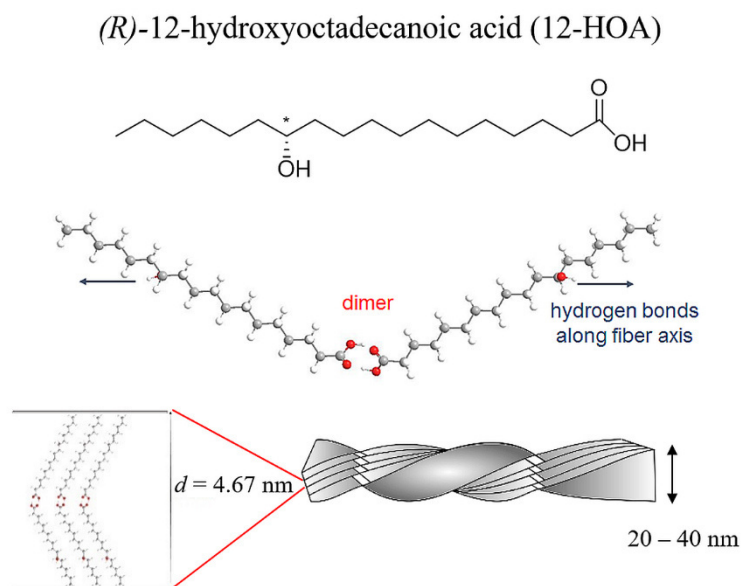


**Figure 4.1:** Phase diagram of the system  $H_2O - n\text{-decanol} - SDS$  including the molecular structures of the surfactant SDS and the cosurfactant *n*-decanol. The red dots indicate the examined sample compositions. Adapted with permission from P.-O. Quist *et al.*, *Phys. Rev. E* **1993**, 47, 3374.<sup>[249]</sup> Copyright 1993 by the American Physical Society.

#### 4.1.2 The LMWG 12-HOA

12-HOA is known to gel various organic solvents and is thus an organogelator.<sup>[250,251]</sup> The self-assembled structure of 12-HOA fibers in non-polar solvents is shown in Figure 4.2 and constitutes as follows: The 12-HOA molecules form cyclic bend dimers via hydrogen bonds between the carboxylic head groups.<sup>[252,253]</sup> Due to hydrogen bonds between the hydroxyl-groups at the C12-position, the dimers aggregate into a one-dimensional fiber with a zig-zag chain of H-bonds along the fiber axis.<sup>[254]</sup>

Moreover, the fibers exhibit an internal layer structure with layers of 4.67 nm thickness, as proven by X-ray investigations.<sup>[255]</sup>

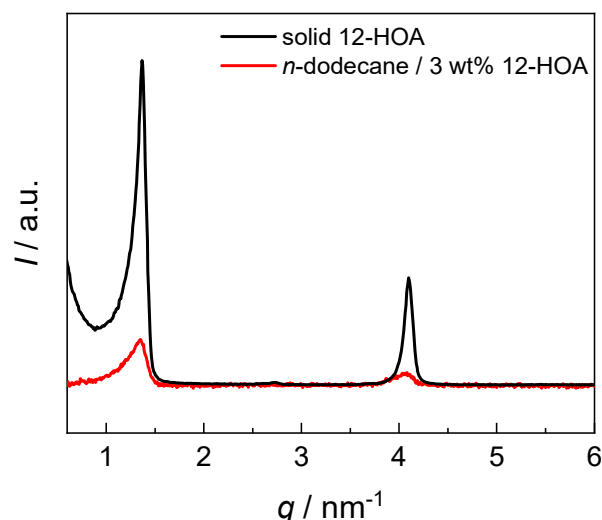


**Figure 4.2:** Molecular structure of the organogelator *(R)*-12-hydroxyoctadecanoic acid and its self-assembly into a one-dimensional gel fiber. Reprinted with permission from S. Dieterich *et al.*, *Langmuir* **2019**, *35*, 16793.<sup>[162]</sup> Copyright 2019 American Chemical Society.

The fibers form a 3D interconnected network via transient and permanent junction zones, where the former are formed by neighboring gelator strands which expose their hydrogen bonds to the fiber surface<sup>[211]</sup> and the latter occur due to crystallographic mismatching during fiber growth.<sup>[256]</sup> The self-assembled fiber network structures are considered to be composed of crystalline structures reminiscent of the one found in crystalline 12-HOA.<sup>[257,258]</sup> Both, the scattering profiles (see Figure 4.3) of the solid 12-HOA powder and the binary gel *n*-dodecane / 12-HOA show two peaks which were assigned to be the (001) and (003) reflections arising from the layer-structured fibers and the crystalline monoclinic microdomains which interconnect the fibers in the junction zones.<sup>[257,259]</sup>

The chirality of the 12-HOA molecule expresses itself in the formation of twisted gel fibers, in which *(R)*-12-HOA forms left-handed fibers and the fibers formed by *(S)*-12-HOA show a right-handed twist.<sup>[260]</sup> There is an ongoing scientific discussion whether the racemic form is able to gel organic solvents or not. Sakurai *et al.* claim that the racemic form does not form gels<sup>[261]</sup>, whereas Douglas *et al.* describe the gelation ability of the racemic form as significantly worse than of the enantiopure compound.<sup>[262]</sup> The reason for this are different H-bond configurations which leads in

organic solvents to twisted fibers in the case of enantiopure 12-HOA and platelets in the case of the racemate.<sup>[262]</sup>



**Figure 4.3:** X-ray diffraction profiles of the solid 12-HOA powder (black) and the binary gel *n*-dodecane / 3 wt% 12-HOA (red). Reflections are observed at the same  $q$ -values indicating that the arrangement of the 12-HOA molecules in the gel fibers and in the junction zones is similar to the one in the crystalline state.

It was verified that the gelator used in this study is (*R*)-12-HOA by measuring its melting point and its optical activity. By means of differential scanning calorimetry (DSC) the melting point was measured to be at  $79.5^\circ\text{C}$ , which is in good agreement with the literature value of  $79.8^\circ\text{C}$  and clearly higher than the value of  $76.2^\circ\text{C}$  for the racemate.<sup>[261]</sup> The specific rotation of 12-HOA  $[\alpha]$  was measured with a polarimeter (PerkinElmer, 241 MC) at room temperature in pyridine at  $\lambda = 589 \text{ nm}$  (Na-D line) and in benzene at  $\lambda = 365 \text{ nm}$  (Hg-lamp). The specific rotation was found to be  $[\alpha]_{\text{D}} = -0.39$  (literature  $[\alpha]_{\text{D}} = -0.46$ )<sup>[255]</sup> and  $[\alpha]_{365} = -0.99$  (literature  $[\alpha]_{365} = -0.84$  (Kanto Chemicals, purified) and  $[\alpha]_{365} = -1.0$  (SigmaAldrich))<sup>[261]</sup>. Hence, the used 12-HOA is clearly present in its *R*-configuration.

The type of the solvent considerably influences the 12-HOA network properties, *i.e.* the network microstructure. Macroscopic physical properties such as the critical gelator concentration, the thermal and viscoelastic properties, as well as the opacity of the gel depend on the used solvent.<sup>[251]</sup> As described before in chapter 3.2, the solvent-gelator interaction determines the gel formation, in which proper gelation is only possible for a solvent that has limited interactions with the gelator. Due to this solvent-gelator interplay, polar solvents and especially hydrogen-bonding solvents rather dissolve 12-HOA and thus prevent gel formation. The critical gelator concentration increases with increasing

polarity and hydrogen-bonding ability of the solvent.<sup>[263]</sup> Moreover, the addition of polar additives like alcohols<sup>[264]</sup> or lecithin<sup>[265]</sup> suppresses the gelation process and leads to higher critical gelator concentrations and a reduced mechanical strength since the additives compete with 12-HOA for the specific gelator-gelator interactions. In rather polar solvents, 12-HOA forms a less-effective spherulitic network instead of elongated fibers.<sup>[226,251]</sup>

If 12-HOA is so sensitive to the hydrogen bonding ability of the solvent, why was it chosen to gel lyotropic liquid crystals, which mainly contain water? The reason are the successful efforts to gel microemulsions<sup>[266,267]</sup> and LLC phases<sup>[136]</sup> of the system  $D_2O - n\text{-decane} - C_{10}E_4$ , the gel properties of which were shown to be not significantly changed in comparison to the gel formed in *n*-decane. Additionally, our own preliminary test gelling the  $L_\alpha$  phase of the system  $H_2O - \text{didodecyldimethylammonium bromide}$  was successful as well.<sup>[243]</sup> We assume that in surfactant containing systems a surfactant monolayer around the gel fiber protects the intra-fiber hydrogen bonding and mediates the compatibility between the mainly non-polar fiber and water.<sup>[164]</sup> Furthermore, 12-HOA was already used in the successful gelation of thermotropic LC phases.<sup>[132,268,269]</sup>

Finally, it has to be mentioned that salts of 12-HOA with proper counterions (*e.g.* alkanolamines) act like surfactants in water. Cooling down an isotropic micellar solution, tubules with walls of concentrically stacked bilayers separated by water are formed.<sup>[270,271]</sup> At high concentrations, these multilamellar tubules are mechanically jammed into a glassy state<sup>[272]</sup> (sometimes called hydrogels<sup>[273]</sup>). For certain counterions such as hexanolamines, a transition from tubules to twisted ribbons occurs, which entangle to form a network and thus a hydrogel formation arises at low 12-HOA salt concentration (0.1 wt%).<sup>[273,274]</sup>

## 4.2 Results and Discussion

### 4.2.1 General preparation route

At first, a general preparation protocol for lyotropic liquid-crystalline gels was developed. As explained in chapter 3.1 the amount of water as well as the ratio between cosurfactant and surfactant crucially determine the shape of the micelles and thus the resulting LLC phase. To avoid changes in the micellar shape by adding the gelator, the water mass fraction  $\omega_{H_2O}$



$$\omega_{H_2O} = \frac{m_{H_2O}}{m_{H_2O} + m_{SDS} + m_{DOH} + m_{gelator}} \quad (4.1)$$

with  $m_{H_2O}$ ,  $m_{SDS}$ ,  $m_{DOH}$  and  $m_{gelator}$  being the masses of water, SDS, *n*-decanol and 12-HOA, respectively, and the cosurfactant to surfactant ratio  $\gamma_{DOH/SDS}$

$$\gamma_{DOH/SDS} = \frac{m_{DOH}}{m_{SDS}} \quad (4.2)$$

is kept constant in both the non-gelled LLC phase and the corresponding gel obtained thereof.

The amount of added gelator is specified by the gelator mass fraction  $\mu$

$$\mu = \frac{m_{LMWG}}{m_{H_2O} + m_{SDS} + m_{DOH} + m_{LMWG}} \quad (4.3)$$

or by the respective weight percent

$$wt\%_{LMWG} = \frac{m_{LMWG}}{m_{tot}} \cdot 100. \quad (4.4)$$

A possible orthogonal self-assembly requires the simultaneous formation of the LLC phase and the fibrillar network. To meet this condition, the gelator 12-HOA was dissolved in *n*-decanol at 80°C. Likewise, SDS was dissolved in water at 40°C. Subsequently, the two solutions were combined by adding the SDS/H<sub>2</sub>O solution to 12-HOA/DOH at 80°C by means of a syringe with a thick needle and ensuring a proper homogenization via steady and cautious mixing. The mixture was quenched in an ice bath for half an hour to achieve fast network growth. Afterwards, the sample was kept at room temperature for one day to complete gel formation. The sample was considered as gelled if the macroscopic sample does not flow for at least eight hours when turning the vial upside down.

The cooling procedure has a distinct influence on the formed gel, as shown in Figure 4.4. If the sample is cooled down quickly by quenching in an ice bath, a homogenous gel is formed which exhibits blueish light scattering due to the Tyndall effect.<sup>[275]</sup> Contrary, if the sample is cooled down slowly by leaving it at room temperature, visible white areas which are either very large network regions (large crystalline junction zones) or part of the gelator precipitating. This finding is supported by the phenomenological observation that a gel which has been cooled down slowly is a mechanically weaker gel, either due to a reduced number of net points or a reduced amount of available gelator. In literature it was found that the cooling rate significantly influences the morphology of the fiber

network.<sup>[209,221]</sup> Under the assumption of a nucleation-fiber growth-branching mechanism<sup>[276]</sup>, a higher cooling rate leads to a lower onset of nucleation and therefore a higher degree of undercooling (and thus supersaturation) at the moment of nucleation. This leads to an increased number of smaller nuclei. Additionally, an increased cooling rate results in a higher degree of fiber branching (mainly due to an increased rate of crystallographic mismatching leading to permanent junction zones).<sup>[209,221]</sup> Moreover, for isothermal network formation it was also shown that a higher degree of undercooling leads to a denser network of thinner and shorter (*i.e.* more branched network) fibers resulting in a mechanically more stable gel of higher elasticity.<sup>[276]</sup>



**Figure 4.4:** Comparison of a gelled lamellar phase cooled down either rapidly (*left*) or slowly (*right*).

The second observation regarding the gelling procedure is that the LLC phase is forming significantly faster (within seconds) than the gel network (in the range of minutes to hours, depending on the gelator concentration). Although a simultaneous formation of LLC phase and network was envisaged, the gel network is formed in the presence of the LLC phase.

To evaluate the liquid-crystalline as well as the gel properties of the gelled LLC phases and to clarify whether or not the gelled LLC phases are orthogonal self-assembled systems, the gelled samples are compared with two parent systems: *i*) the gelator-free LLC with the same  $\omega_{H_2O}$  and  $\gamma_{DOH/SDS}$  as the gelled LLC and *ii*) the binary gel formed by *n*-dodecane and the same amount  $\mu$  of 12-HOA as in the gelled LLC. Dodecane was chosen for comparison since it has the same chain length than the hydrophobic part of the surfactant SDS.

The first diagnostic test to determine whether a gel has formed is the tube-inversion test. The vial containing the sample is turned upside down and either the sample is self-supporting (gel) or flows under its own weight (sol). A gel is a material having a yield stress, below which the material shows

elastic behavior (soft but rigid solid). The sample begins to flow if the external forces acting on the sample exceed the internal structural forces, which are given by the strength of the bonds in the network and the rigidity of the network.<sup>[277]</sup> In the tube-inversion test, the external force is the weight force  $F_g$  of the sample due to gravity. A schematic drawing of the experiment is shown in Figure 4.5. The weight of the sample is

$$m = \pi R^2 \cdot L \cdot \rho \quad (4.5)$$

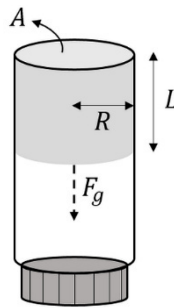
where  $R$  is the vial radius,  $L$  is the sample height and  $\rho$  is the sample density.

The yield stress  $\sigma_y$  is then

$$\sigma_y = \frac{F_g}{A} = L \cdot \rho \cdot g \quad (4.6)$$

with the vial base area  $A$  and the acceleration due to gravity  $g$ .<sup>[278,279]</sup>

Since the column height of the sample depends on the sample mass and the diameter of the vial, it is of great importance to always conduct the test under the same experimental conditions (sample weight, vial type). Additionally, one has to be careful to not misclassify highly viscous fluids as gels. The distance a sample flows down over a certain time under the action of gravity is inversely proportional to the viscosity of the sample.<sup>[279]</sup> Thus, a sufficiently long period of observation is necessary to distinguish between a highly viscous fluid and a gel, which we chose to be eight hours.

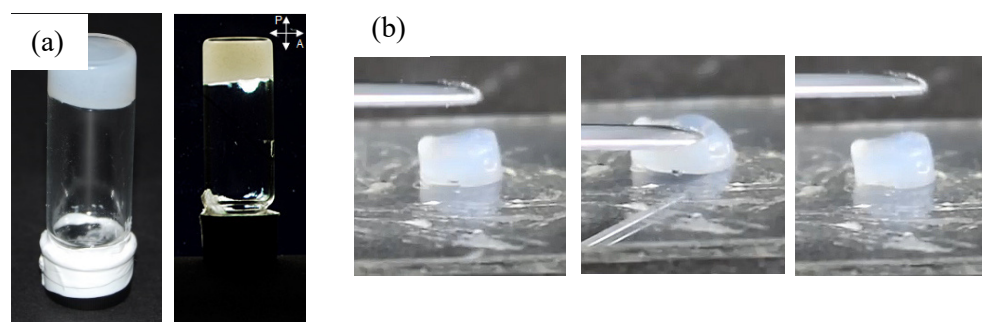


**Figure 4.5:** Schematic drawing of the tube-inversion experiment. The sample is considered as a cylinder of radius  $R$  and length  $L$  and base area  $A$ . The weight force  $F_g$  due to gravity is balanced by internal structural forces of the gel, *i.e.* the yield stress. Redrawn after Ref.<sup>[278]</sup>

Using the tube-inversion test, it was confirmed that gelling all four examined LLC phases (lamellar  $L_\alpha$ , nematic  $N_d$  and  $N_c$ , hexagonal  $H_1$ ) with 12-HOA led to a stable gel above a certain critical gelation concentration (cgc). At least 1.5 wt% 12-HOA are required to gel the  $L_\alpha$  phase. For the lyotropic

nematic phases and hexagonal phase 1.8 wt% and 2.0 wt% are needed to transfer the sample into the gel state, respectively. Contrary, only 0.2 wt% 12-HOA are sufficient to obtain the binary gel *n*-dodecane / 12-HOA. This observation can be explained with the fact that interactions between gelator and solvent molecules reduce the ability of a gelator to form a gel network. It was thus found that the critical gelation concentration for 12-HOA increases with increasing polarity of the solvent and increasing ability of the solvent to form hydrogen bonds.<sup>[251]</sup>

As shown in Figure 4.6, the gelled  $L_\alpha$  phase shows optical birefringence between crossed polarizers, elastic response to external stress and exhibits no flow, all clearly proving the formation of an anisotropic gel.



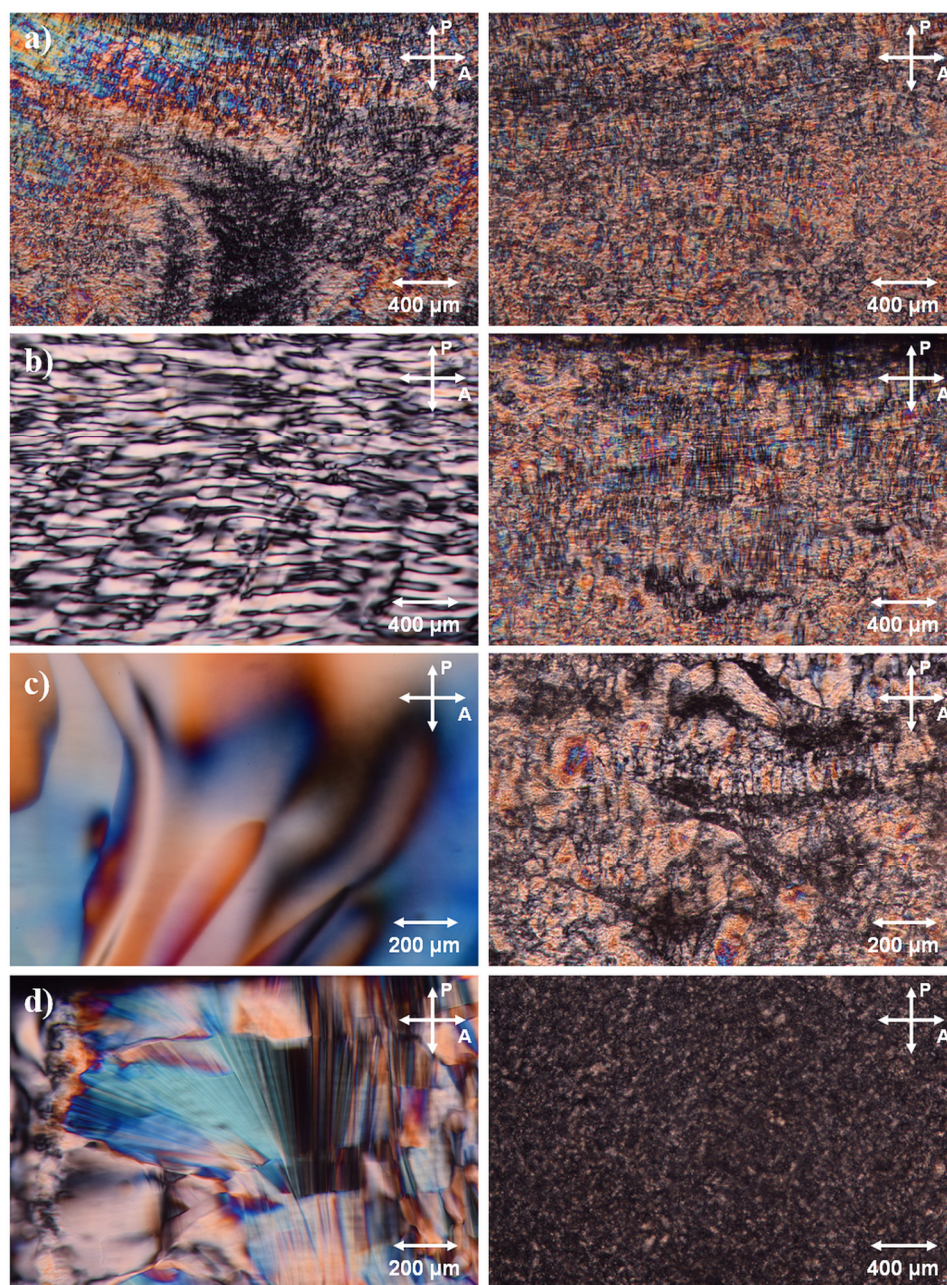
**Figure 4.6:** *a)* Picture of the gelled lyotropic lamellar phase outside and between crossed polarizers. The gel shows no flow but strong optical birefringence. *b)* The gel returns to its original shape when the stress is released proving its elasticity. Adapted with permission from S. Dieterich *et al.*, *Langmuir* **2019**, 35, 16793.<sup>[162]</sup> Copyright 2019 American Chemical Society.

#### 4.2.2 Gelling nematic, lamellar and hexagonal phases

As a second step, it has to be examined whether the order of the respective LLC phases is preserved during gelation. The liquid-crystalline properties were investigated using polarized optical microscopy (Figure 4.7) and small-angle X-ray scattering (Figure 4.8). The textures of the gelator-free and gelled  $L_\alpha$  phase resemble each other; both show an oily-streaks texture in a planar matrix proving that the lamellar order is maintained in the gelled state. Contrary, the POM images of the other LLC phases gelled with 12-HOA provide evidence that no lyotropic nematic or hexagonal gel was obtained. While the textures of the gelator-free  $N_d$  and  $N_c$  phase show schlieren textures typical of the nematic phase, the corresponding gelled samples ( $\mu = 0.018$ ) exhibit textures similar to the lamellar gel. The image of the gelator-free  $H_1$  phase shows a typical fanlike texture, but the corresponding gelled sample ( $\mu = 0.02$ ) is not birefringent anymore. Large junction zones in the gel



network with an extension of hundreds of nanometers (range of the wavelength of visible light) cause local spots of weak birefringence (see Figure 4.7d), otherwise an isotropic gel is obtained.

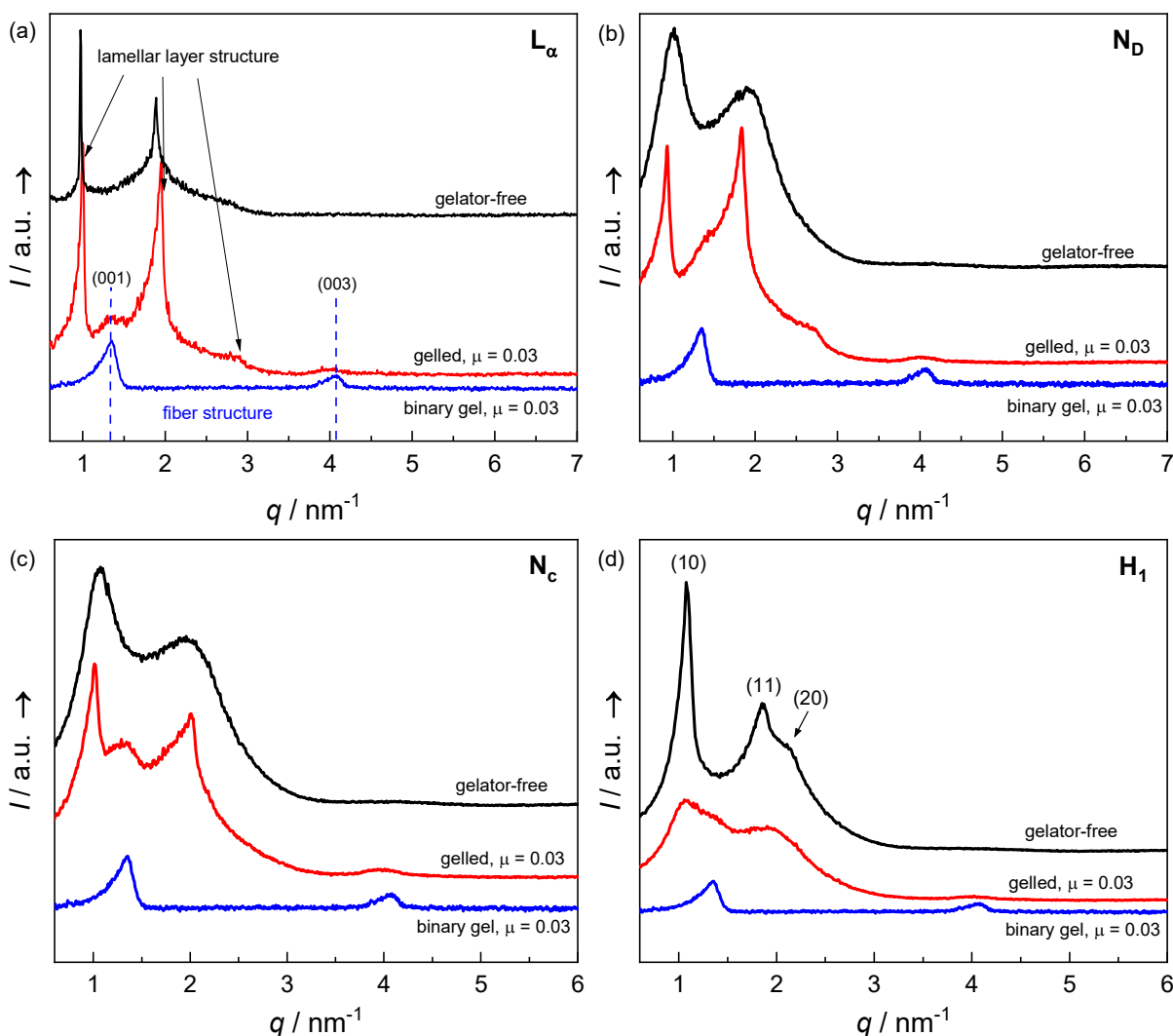


**Figure 4.7:** (Left) Texture images obtained by polarized optical microscopy of the gelator-free *a*)  $L_\alpha$ , *b*)  $N_d$ , *c*)  $N_c$  and *d*)  $H_1$  phase and their gelled counterparts ( $\omega_{H_2O} = 0.70$  for all samples) (right). While the gelator-free nematic phases show a typical schlieren texture, the corresponding gelled phases exhibit characteristics of the lamellar phase. The hexagonal phase is not birefringent in the gelled state; the observed texture arises from aggregation of gel fibers. Reprinted with permission from S. Dieterich *et al.*, *Langmuir* **2019**, *35*, 16793.<sup>[162]</sup> Copyright 2019 American Chemical Society.

The findings obtained by POM are confirmed by small-angle X-ray scattering. In Figure 4.8 the X-ray diffractograms of the gelled ( $\mu = 0.03$ ) and gelator-free  $L_\alpha$ ,  $N_d$ ,  $N_c$  and  $H_1$  phase as well as of the binary gel are shown. For the gelled and gelator-free  $L_\alpha$  phase two orders of pseudo-Bragg peaks due to the lamellar layer structure emerge (Figure 4.8a). Additionally, small scattering maxima at  $q = 1.33 \text{ nm}^{-1}$  and  $q = 3.99 \text{ nm}^{-1}$  appear in the SAXS curve of the gelled  $L_\alpha$  phase as well as of the binary gel. These maxima are known to be the (001) and (003) reflections due to the layered structure of the 12-HOA fibers<sup>[255,259]</sup> (see Figure 4.3). The limited number of layers per twisted fiber give rise to the considerable width of these “intra-fiber” scattering maxima which are weak in intensity due to the small fraction of fibers in the sample. To conclude, the X-ray diffractograms in Figure 4.8a prove the formation and coexistence of a lamellar layer and a gel fiber structure in the gelled  $L_\alpha$  phase.

In contrast, the SAXS results for the nematic and hexagonal phases contradict the existence a gel with nematic or hexagonal order. On the one hand, for the gelator-free  $N_d$  and  $N_c$  phases broad scattering maxima are visible in Figure 4.8b,c due to the short-range translational order present in nematic phases. On the other hand, in the corresponding gelled materials a scattering profile typical of a lyotropic lamellar profile with two orders of sharp layer peaks with a  $q$ -ratio of 1 : 2 are observed. The POM and SAXS results thus clearly demonstrate that gelling a nematic phase with 12-HOA leads to the formation of a lamellar gel.

The  $I(q)$  profile of the gelator-free  $H_1$  phase (Figure 4.8d) exhibits three sharp peaks with a  $q$ -ratio of 1 :  $\sqrt{3}$  : 2 which is characteristic for 2D hexagonal order. However, in case of the gelled material just two diffuse scattering maxima remain, indicating that only short-range translational order is left. In summary, the fact that the gelled material shows no birefringence between crossed polarizers along with the SAXS results demonstrate that gelling a  $H_1$  phase with 12-HOA results in an isotropic gel and not in a lyotropic hexagonal gel.

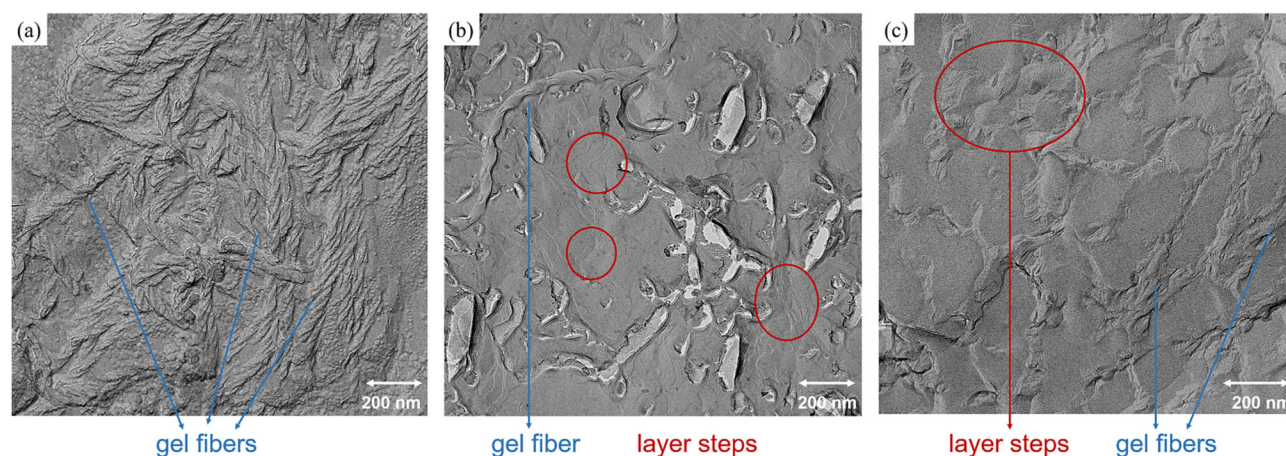


**Figure 4.8:** X-ray diffraction profiles of the gelator-free (black) and gelled (red) *a*)  $L_\alpha$ , *b*)  $N_D$ , *c*)  $N_c$  and *d*)  $H_1$  phases ( $\omega_{H_2O} = 0.70$  for all samples). In the binary gel (blue), the diffuse and weak (001) and (003) peaks from the layered structure of the 12-HOA fibers are seen. Reprinted with permission from S. Dieterich *et al.*, *Langmuir* **2019**, 35, 16793.<sup>[162]</sup> Copyright 2019 American Chemical Society.

Further evidence for the coexistence of a fiber network and a lamellar layer structure in the gelled  $L_\alpha$  phase, but also in the gels obtained by gelling a nematic phase is given by the freeze-fracture electron microscopy (FFEM) pictures in Figure 4.9. For the  $L_\alpha$ , as well as for the  $N_c$  phase gelled with 12-HOA, twisted gel fibers as well as layer steps typical of a  $L_\alpha$  phase are observed. For the gelled  $L_\alpha$  phase this is further evidence that both “parent” structures have actually formed and exist next to each other. In all cases, all fibers observed in the replica show a right-handed twist meaning that all fibers are actually left-handed, as expected for (*R*)-12-HOA gels<sup>[260]</sup>. However, this result for the lamellar gel is in clear contrast to the  $L_\alpha$  phase of the system  $D_2O$ –*n*-decane– $C_{10}E_4$  gelled with 12-HOA, where non-twisted fibers were observed.<sup>[136]</sup> The fiber thickness is in the same range for all



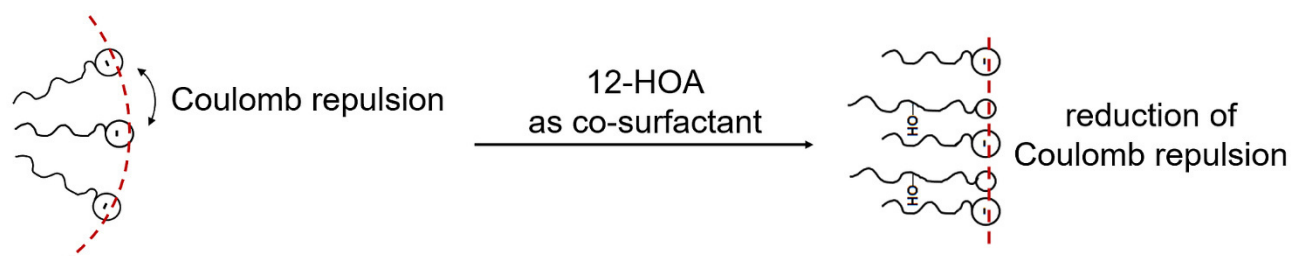
investigated gels, 20 – 60 nm for the binary gel, 30 – 50 nm for the gelled  $L_\alpha$  phase and 20 – 40 nm for the lamellar gel obtained by gelling the  $N_c$  phase.



**Figure 4.9:** Freeze fracture electron microscopy image of the *a*) binary gel *n*-dodecane / 3 wt% 12-HOA, *b*) the gelled  $L_\alpha$  phase ( $\omega_{H_2O} = 0.67$ ,  $\gamma_{DOH/SDS} = 0.375$ ,  $\mu = 0.03$ ) and *c*) the nematic  $N_c$  phase ( $\omega_{H_2O} = 0.67$ ,  $\gamma_{DOH/SDS} = 0.18$ ) after gelling the sample with 3 wt% 12-HOA. The observed layer steps indicate the presence of a lamellar structure which coexists with twisted gel fibers. Adapted with permission from S. Dieterich *et al.*, *Langmuir* **2019**, *35*, 16793.<sup>[162]</sup> Copyright 2019 American Chemical Society.

What is the reason for the strong stabilization of the lamellar regime? Why is it not possible to transfer lyotropic nematic phases into the state of a nematic gel using the gelator 12-HOA? An explanation may lie in the molecular structure of 12-HOA (Figure 4.2). Disregarding the 12-hydroxy group, 12-HOA has a typical amphiphilic structure with a non-polar alkyl tail and a polar head group. Hence, the gelator is likely incorporated into the amphiphilic film also acting as a cosurfactant. As described in chapter 3.1, the curvature of the micelle and thus the formed lyotropic liquid-crystalline phase depends on the packing parameter introduced by Israelachvili.<sup>[169]</sup> The effective head group area of anionic surfactants like SDS is determined by repulsive Coulomb interactions between the charged head groups. Thus, the ratio of the effective cross section area occupied by the alkyl tail and the effective cross section area occupied by the head group is increased when 12-HOA is incorporated into the micelles since a non-ionic cosurfactant leads to a smaller effective head group area by reducing the Coulomb repulsion between the charged head groups of the anionic surfactant molecules. As shown in Figure 4.10 the incorporation of 12-HOA into the amphiphilic film flattens the micelle curvature and results in the transition from a nematic phase into a lamellar gel. The surface activity of 12-HOA was already observed for gelled bicontinuous microemulsions and other gelled lyotropic liquid crystals.<sup>[243,267,280]</sup>

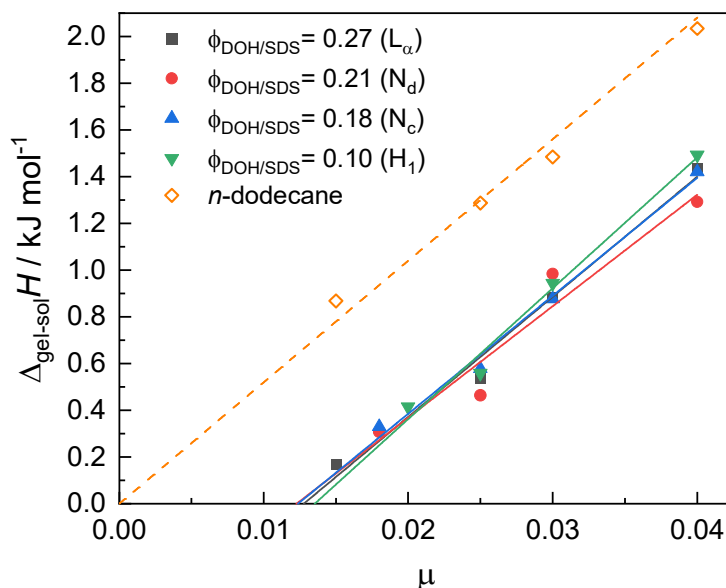




**Figure 4.10:** Schematic representation how the incorporation of the non-ionic 12-HOA into the micelles leads to a decreased film curvature by reducing the Coulomb repulsion between the charged head groups of the anionic SDS molecules. Reprinted with permission from S. Dieterich *et al.*, *Langmuir* **2019**, *35*, 16793.<sup>[162]</sup> Copyright 2019 American Chemical Society.

The subsequent question to be answered is how high actually the gelator concentration incorporated into the micelles is? Differential scanning calorimetry was used to roughly determine the amount of 12-HOA acting as cosurfactant as follows:

With increasing gelator concentration more (or thicker) gelator fibers are formed and a stronger gel network is build up. The enthalpy of the gel melting  $\Delta_{\text{gel-sol}}H$  is thus expected to increase with increasing gelator amount and it is observed in Figure 4.11 that this relationship is linear for all samples, the binary gel *n*-dodecane / 12-HOA (and additionally shown in literature for a different binary gel *n*-decane / 12-HOA<sup>[281]</sup>) as well as the gelled lyotropic liquid-crystalline phases. While the linear regression for the binary gel passes through the origin as expected, the linear regression for all gelled LLC phases independent of the cosurfactant to surfactant ratio  $\gamma_{\text{DOH/SDS}}$  intersects the abscissa at a gelator content between 1.23 and 1.35 wt.% of 12-HOA. For clarification, the corresponding gelator-free phase is given in parenthesis in Figure 4.11, even if the samples are in a different state after gelation. This offset indicates the amount of gelator incorporated into the amphiphilic film, which is thus estimated to be between 1.2 to 1.4 wt% 12-HOA. A view on the ternary phase diagram (Figure 4.1) reveals that the nematic  $N_d$  and  $N_c$  phases differ in cosurfactant (*n*-decanol) concentration by roughly 1 wt.%. Hence, it is reasonable to assume that 1.2 to 1.4 wt% 12-HOA integrated into the micelles are enough to substantially change the micellar curvature and thus the phase behavior upon gelation.

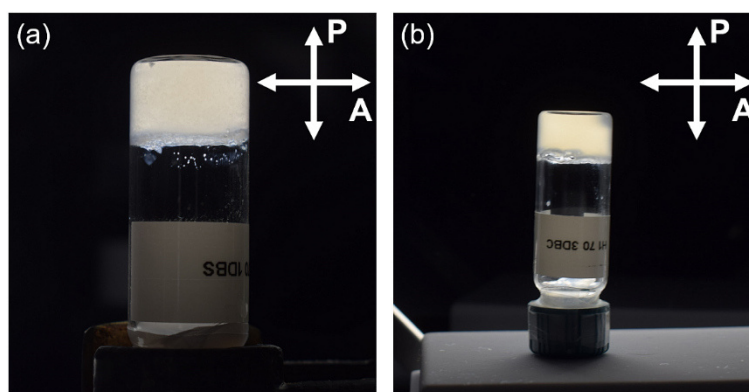


**Figure 4.11:** Gel-sol transition enthalpy versus the gelator mass fraction  $\mu$  for the gelled phases of the composition  $\omega_{H_2O} = 0.67$  and  $\gamma_{DOH/SDS} = 0.27$  (black squares),  $\gamma_{DOH/SDS} = 0.21$  (red circles),  $\gamma_{DOH/SDS} = 0.18$  (blue triangles up) and  $\gamma_{DOH/SDS} = 0.10$  (green triangles down), and for the binary gel *n*-dodecane / 12-HOA (orange diamonds). The linear extrapolation to  $\Delta_{\text{gel-sol}}H = 0$  leads to an intersection with the abscissa for a gelator content between 1.23 and 1.35 wt.% for the LLC sample. Since  $\Delta_{\text{gel-sol}}H = 0$  is found at  $\mu = 0$  for the binary gel as expected, the obtained value for the gelled LLC samples can be interpreted as a rough estimate of the fraction of 12-HOA incorporated into the micelles. Adapted with permission from S. Dieterich *et al.*, *Langmuir* **2019**, 35, 16793.<sup>[162]</sup> Copyright 2019 American Chemical Society.

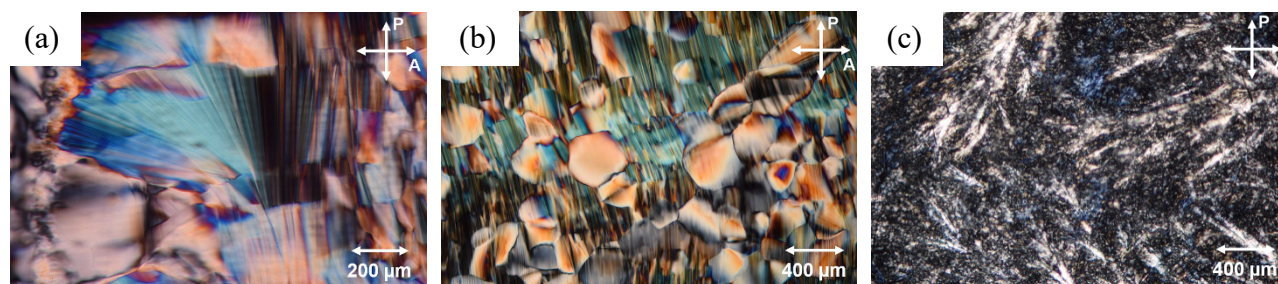
However, the formation of an isotropic gel upon gelation of the hexagonal phase cannot be explained with the cosurfactant effect of 12-HOA, since an increase in cosurfactant content should drive the hexagonal phase into the nematic or lamellar regimes (see the effect of *n*-decanol in Figure 4.1). Actually, the addition of stearic acid, which has almost the same molecular structure as 12-HOA but misses the 12-hydroxy group responsible for gel formation (see appendix, Figure 9.1), lead to the formation of a  $N_c$  phase at room temperature, which is the result of stearic acid acting as cosurfactant. What is then the reason for the transformation of the  $H_1$  phase into an isotropic gel during gelation? We believe that the formation of a 3D network of comparatively thick fibers is not compatible with the 2D translational order in the hexagonal phase. The network formation destroys the high degree of translational order present in a lyotropic  $H_1$  phase. Thus, other low molecular weight gelators, namely DBS and DBC (see chapter 5.1.2) which are known to form thinner gel fibers, were tested in order to obtain micellar lyotropic hexagonal gels. The results on gelling the hexagonal phase with the gelators DBS and DBC are reported in the following.

Between crossed polarizers the gels obtained with DBS and DBC show optical birefringence (see

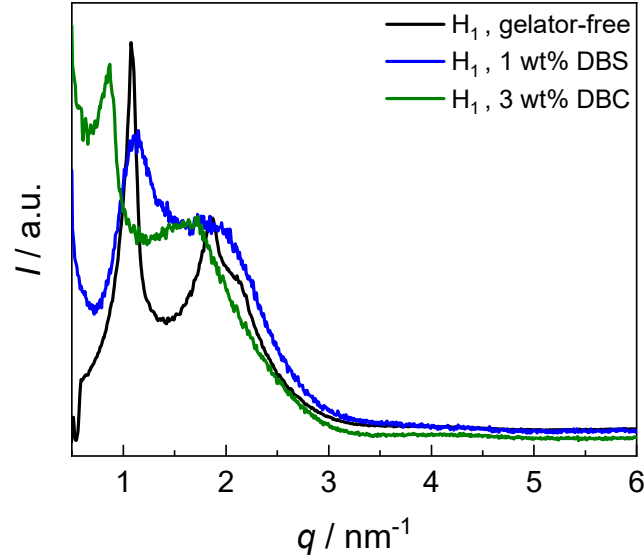
Figure 4.12). To confirm that the anisotropic gels indeed exhibit a hexagonal structure, POM and SAXS measurements were executed (Figure 4.13 and Figure 4.14). For both, the gelator-free  $H_1$  phase and the  $H_1$  phase gelled with 1 wt% DBS a striated texture and a mosaic texture was observed, both characteristic of the hexagonal phase. For the  $H_1$  phase gelled with 2 wt% DBC a rather non-characteristic texture was found. In the X-ray curve of this sample the first scattering maximum appears quite sharp and the second maximum is very broad and might contain the (11) and (20) reflections typical of a hexagonal phase. However, the scattering maxima observed in the gel obtained with DBS are rather broad indicating only short-range translational order. Nevertheless, the results obtained with POM demonstrate that a hexagonal gel is formed upon gelation of the  $H_1$  phase with DBS and the hexagonal nature of the gel obtained with DBC is confirmed by X-ray scattering. Thus in contrast to gelation with 12-HOA, gelling the  $H_1$  phase with the gelators DBS or DBC successfully transfers the hexagonal structure into the gelled state.



**Figure 4.12:** Optical birefringence between crossed polarizers and the absence of flow confirm the formation of an anisotropic gel for *a*) the  $H_1$  phase gelled with 1 wt% DBS and *b*) the  $H_1$  phase gelled with 3 wt% DBC.



**Figure 4.13:** Images of the textures observed with polarized optical microscopy of *a*) the gelator-free  $H_1$  phase, *b*) the  $H_1$  phase gelled with 1 wt% DBS and *c*) the  $H_1$  phase gelled with 3 wt% DBC.



**Figure 4.14:** X-ray diffraction profiles of the gelator-free  $H_1$  phase (black), the  $H_1$  phase gelled with 1 wt% DBS (blue) and the  $H_1$  phase gelled with 3 wt% DBC (green).

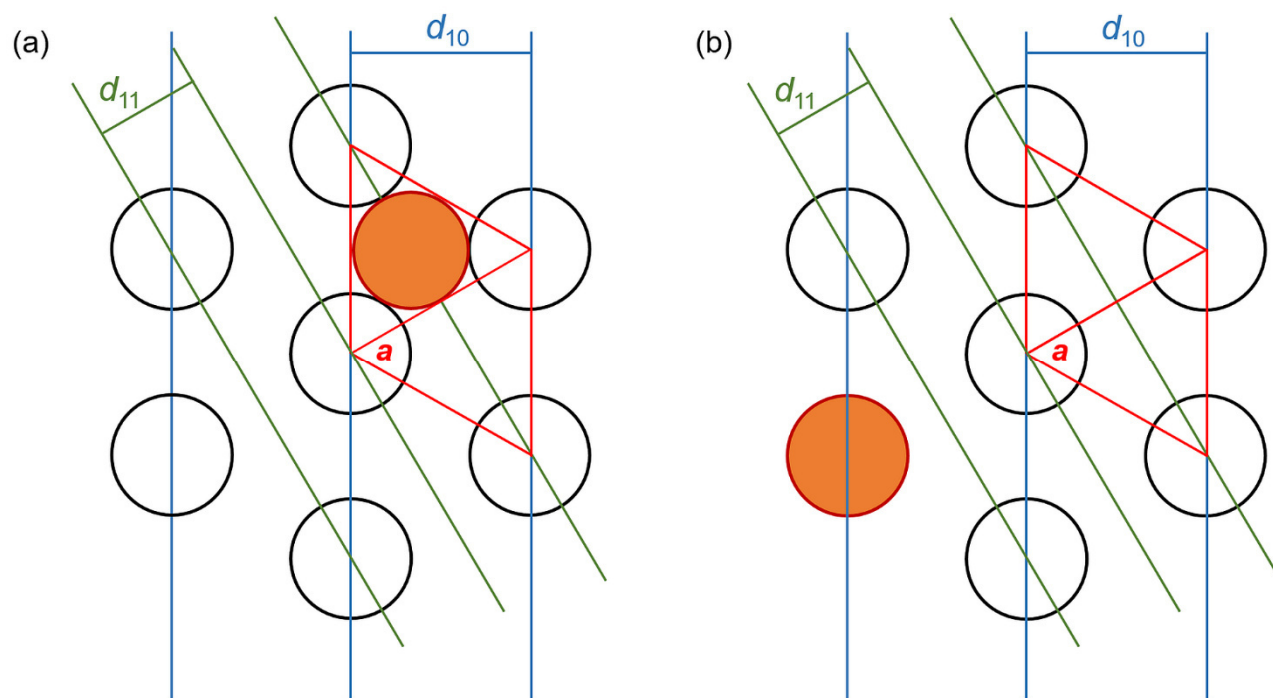
For the hexagonal gel obtained with DBC a shift of the scattering maxima to lower  $q$ -values in comparison with the gelator-free  $H_1$  phase is observed. The  $d_{10}$  distance between the cylindrical micelles and the lattice constant  $a$  ( $a = \frac{2}{\sqrt{3}}d_{10}$ ) obtained from Lorentz fits to the X-ray curves (Bragg relation  $d_{10} = \frac{2\pi}{q_{10}}$ ) are listed in Table 4.1.

**Table 4.1:** Distance  $d_{10}$  between the cylindrical micelles and lattice constant  $a$  obtained from the analyses of the first order scattering maxima of the SAXS data shown in Figure 4.14 for the studied gelator-free  $H_1$  phase and the corresponding hexagonal gels.

Sample	$d_{10}$ / [nm]	$a$ / [nm]
Gelator-free $H_1$	5.8	6.7
$H_1$ , 1 wt% DBS	5.4	6.4
$H_1$ , 3 wt% DBC	7.4	8.6

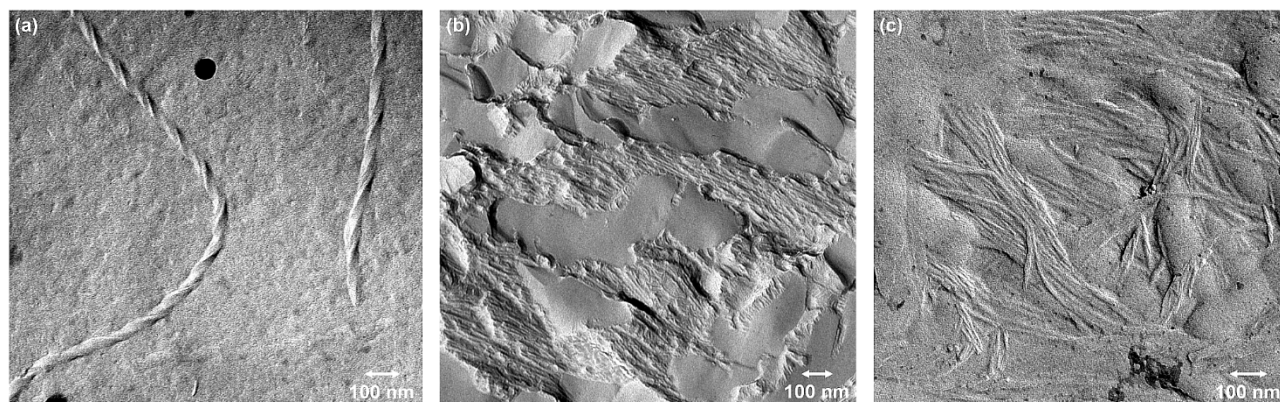
What is the reason of the considerable widening of the hexagonal structure in case of gelation with DBC? First, one has to consider how the gel fibers can coexist with the 2D hexagonal order of the  $H_1$  phase. To not destroy the hexagonal structure, the gel fiber can either run between the cylindrical micelles or one gel fiber can replace one micelle in the hexagonal lattice. Both possibilities are sketched in Figure 4.15. Thus, most of the fibers have to run parallel to the director. Nevertheless, for gel formation the formation of a 3D network is necessary. Thus, the average length of the cylindrical micelles is assumed to be considerable shorter than in the gelator-free case since cross connections

between the fibers are inevitable. If the diameter of the formed gel fibers is larger than the diameter of the micelles or than the space between the micelles the hexagonal structure must expand. Above a certain threshold, the fibers are too thick to be compatible with the hexagonal structure and an isotropic gel is formed.



**Figure 4.15:** Schematic drawing of a hexagonal gel. The gel fiber (orange) can *a*) either run between the micelles or *b*) replace one micelle.

The fiber diameter observed with electron microscopy is 20 – 35 nm in case of the isotropic gel obtained with 12-HOA, 4 – 7 nm for fibers made of DBS in the hexagonal gel and 8 – 14 nm for DBC gel fibers in the hexagonal gel (see Figure 4.16). While gel fibers from DBS can be easily incorporated in the hexagonal structure, the hexagonal structure has to expand to include the DBC fibers. In case of 12-HOA the fibers are too large to be integrated in the 2D hexagonal structure and thus an isotropic gel is formed.



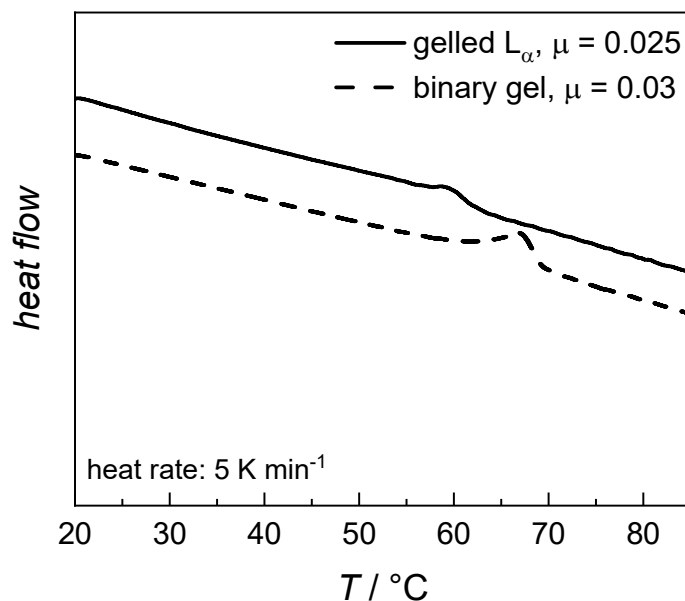
**Figure 4.16:** The gel fibers are visible in the FFEM images of *a)* the isotropic gel obtained with 3 wt% 12-HOA, *b)* the hexagonal gel obtained with 1 wt% DBS and *c)* the hexagonal gel obtained with 3 wt% DBC.

To conclude, similar as in lyotropic lamellar gels (see chapter 6) the ratio of the fiber diameter to the hexagonal lattice constant is the crucial parameter whether or not the hexagonal structure is conserved during gelation. If the fiber diameter is too large, an isotropic gel results. In case of a hexagonal gel, the fiber thickness considerably determines the hexagonal structure.

### 4.2.3 Coexistence and mutual impact of gel network and lamellar structure

Since the  $L_\alpha$  phase is the only lyotropic phase whose structure is preserved during gelation with 12-HOA, we focused on the  $L_\alpha$  phase to investigate the mutual influence of gel fiber network and lamellar layer structure on each other in the lamellar gel.

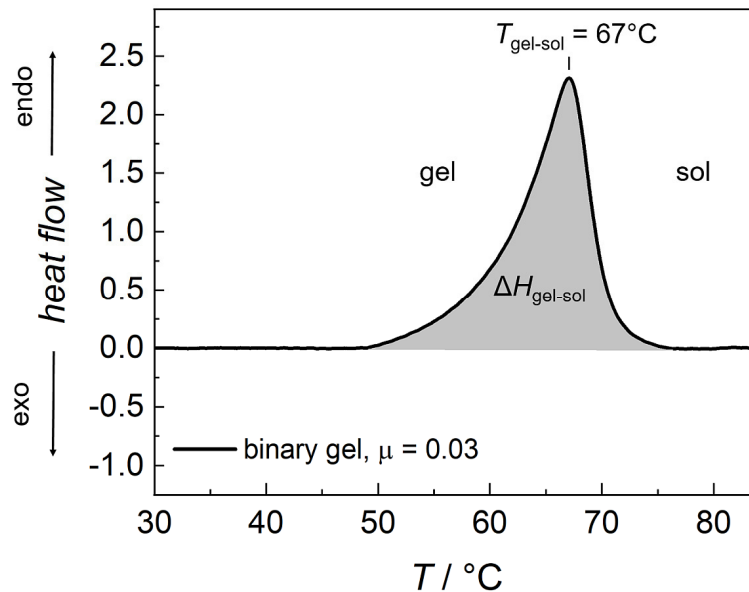
A measure for the strength of the formed network is the gel-sol transition temperature  $T_{\text{gel-sol}}$ , as well as the amount of energy necessary to break the interactions in the fiber network. Thus, DSC measurements were used to study the thermal behavior of the gels. The observed endothermic peaks while heating are related to a “melting” of the gel network. It was noticed that the peaks are more pronounced for the binary gel than for the lamellar gel, as can be seen in the heating curves in Figure 4.17.



**Figure 4.17:** DSC heating curves for a lamellar gel ( $\omega_{H_2O} = 0.67$ ,  $\gamma_{DOH/SDS} = 0.27$ ,  $\mu = 0.025$ , solid line) and a binary gel *n*-dodecane / 12-HOA ( $\mu = 0.03$ , dashed line), both obtained with a heating rate of 5 Kmin<sup>-1</sup>.

The fact that the calorimetry peaks span a large range of about (or even more) than 10 K shows that several processes take place during the melting of the gel. On the one hand, the cross-links between the fibers have to be broken (interfiber interactions), on the other hand the H-bonds holding together a single fiber have to be overcome (intrafiber interactions). Therefore, not the onset but the maximum of a peak was taken as gel-sol transition temperature, as suggested in literature.<sup>[278]</sup> After subtracting a baseline, the area under the curve yields the enthalpy of the gel melting  $\Delta_{\text{gel-sol}}H$  (see Figure 4.18). A hysteresis was noticed between the gel melting and the gel formation, as was observed for SAFINs before.<sup>[143,282,283]</sup> The hysteresis and  $\Delta_{\text{gel-sol}}H$  are increasing with increasing heating rate and thus the lowest heating rate that still allowed a sufficient detection of the gel melting peaks was used, which was a rate of 5 Kmin<sup>-1</sup>. Solely the transition from gel to the fluid sol while heating was considered. By that the gel-sol transition temperature for one sample was found to have a reproducibility in the order of  $T_{\text{gel-sol}} \pm 1.5$  K.



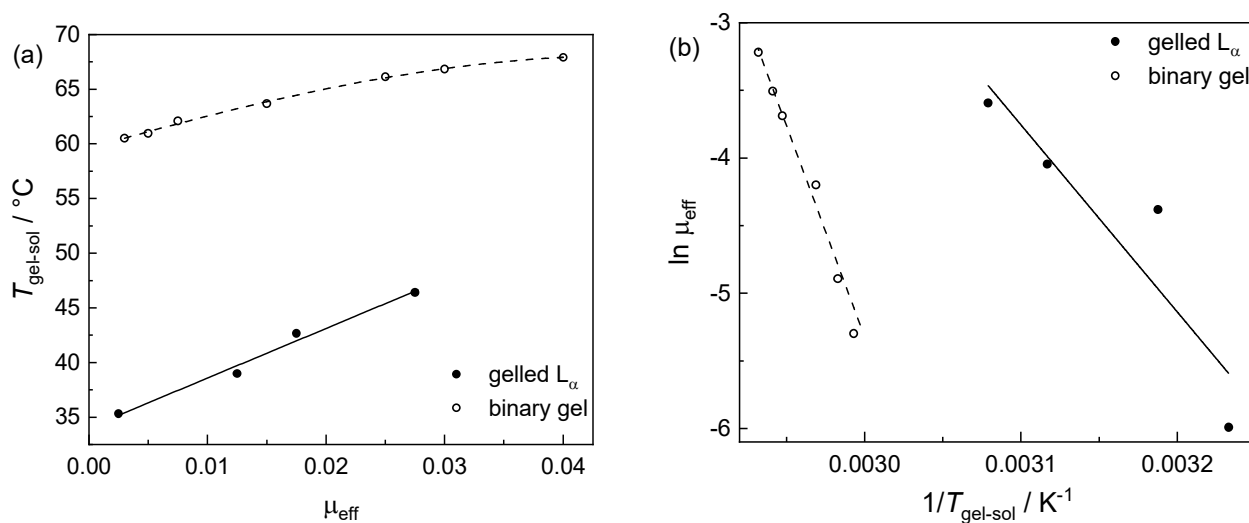


**Figure 4.18:** Baseline-subtracted DSC heating curve for the binary gel *n*-dodecane / 12-HOA ( $\mu = 0.03$ ). The gel-sol transition temperature  $T_{\text{gel-sol}}$  is obtained from the peak maximum and the gel melting enthalpy  $\Delta H_{\text{gel-sol}}$  from the area under the calorimetry peak.

The gel-sol transition temperature dependent on the gelator content is compared for the lamellar gel with the one of the binary gel. To only consider the fraction of gelator actually forming fibers, the amount of gelator acting as cosurfactant in the lamellar gel was neglected and an effective gelator mass fraction  $\mu_{\text{eff}} = \mu_{\text{weighed in}} - 0.0125$  was used. As expected, the gel-sol transition temperature increases with increasing gelator amount for the lamellar and the binary gel due to the presence of more fibers. Since  $T_{\text{gel-sol}}$  of the gelled lamellar phase is about 25 K lower than for the binary gel, the gelled  $L_{\alpha}$  phase is the weaker gel.

As reported in literature for various gelators (molecular as well as polymeric ones)<sup>[153,284,285]</sup>, the plot of  $\ln \mu_{\text{eff}}$  versus  $T_{\text{gel-sol}}^{-1}$  shows a linear behavior (see Figure 4.19b). The physical meaning behind this behavior is still discussed in two contradictive models.





**Figure 4.19:** *a*) Gel-sol transition temperature in dependence of the effective (fiber-forming) mass fraction of 12-HOA for the lamellar gel ( $\omega_{\text{H}_2\text{O}} = 0.67$ ,  $\gamma_{\text{DOH}/\text{SDS}} = 0.27$ , filled circles) and the binary gel *n*-dodecane / 12-HOA (open circles). *b*) The plot of  $\ln \mu_{\text{eff}}$  versus  $T_{\text{gel-sol}}^{-1}$  shows a linear dependence for both, the gelled  $L_\alpha$  phase ( $\omega_{\text{H}_2\text{O}} = 0.67$ ,  $\gamma_{\text{DOH}/\text{SDS}} = 0.375$ ) and the binary gel.

The first model assumes that the sol to gel transition is of second order and gelation is interpreted as a percolation process, in which the molecules first assemble into small clusters before they assemble further into a space-filling network at the gelation point. Typical of a second order transition, the molecules undergo changes well before the transition point and the clusters cooperatively grow in size such that the cluster size, *i.e.* the correlation length, increases with a power law dependence in the vicinity of the gelation point.<sup>[278]</sup> This model is supported by the fact that the rheological properties follow a power law as the gelation point is approached.<sup>[241,286,287]</sup> The thermal properties of such a transition were first described for the gelation of biopolymers such as gelatin by Eldridge and Ferry, which assumed that gelation proceeds via an exothermic pairwise cross-linking process.<sup>[285]</sup> The dimerization of biopolymer chains (or gelator fibers in the case of SAFINs) provides the following relationship between the gelator concentration and  $T_{\text{gel-sol}}$

$$\ln \mu = \frac{-\Delta H_{\text{cr}}}{RT_{\text{gel-sol}}} + \text{constant}, \quad (4.7)$$

with  $R$  being the gas constant.  $\Delta H_{\text{cr}}$  is the enthalpy connected to the cross-linking process and can be interpreted as the energy necessary to break one mole of cross-links, *i.e.* nodes of the gel network.<sup>[281]</sup> From the slope of the linear fits in Figure 4.19b an enthalpy of  $\Delta H_{\text{cr}} = 260 \text{ kJ mol}^{-1}$  for the binary gel and  $\Delta H_{\text{cr}} = 115 \text{ kJ mol}^{-1}$  for the lamellar gel is obtained. The fact that less energy is required to break

the nodes in the gelled  $L_\alpha$  phase than in the binary gel confirms again that the gel formed in a lamellar phase is weaker than the one formed in dodecane. Interactions of 12-HOA with the surrounding polar water may reduce the gel forming ability of 12-HOA since the number of “inter-gelator” hydrogen bonds is reduced.

The second model assumes the sol to gel transition to be a first order transition which proceeds via a nucleation and growth mechanism.<sup>[278]</sup> The gel to sol transition is interpreted as the melting of gelator crystals and the relation between gelator concentration  $\mu$  and  $T_{gel-sol}$  is

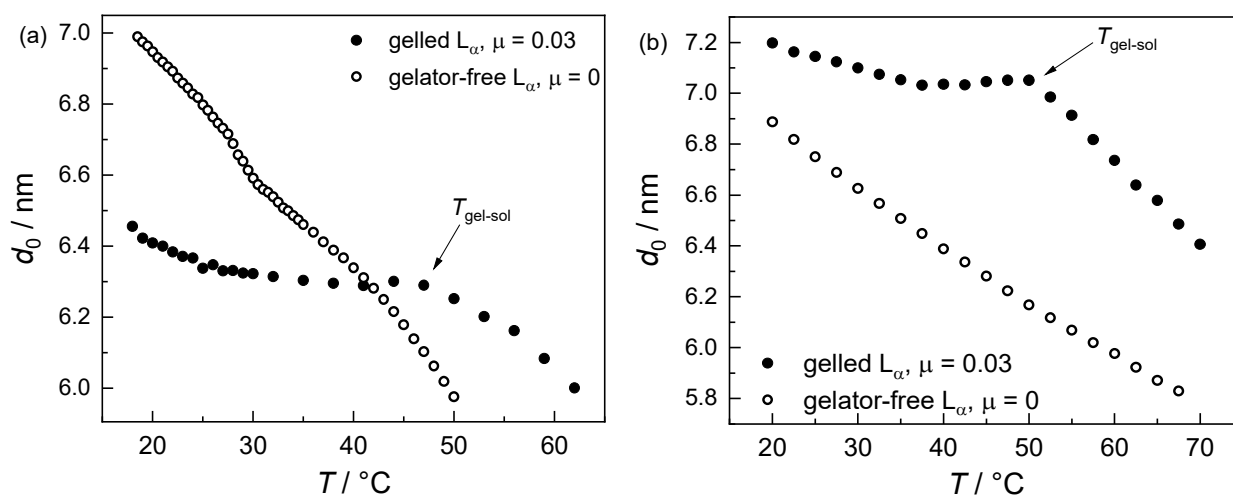
$$\ln \mu = \frac{-\Delta H_m}{R} \cdot (T_{gel-sol} - T_m), \quad (4.8)$$

where  $\Delta H_m$  is the melting enthalpy of neat gelator and  $T_m$  is the melting temperature of neat gelator. From the linear fits in Figure 4.19b, the 12-HOA melting temperatures of 80.3°C and 80.4°C are obtained for the case of the binary gel and the lamellar gel, respectively. Thus, the obtained melting temperatures are close to the value of 79.5°C obtained from a DSC measurement of neat 12-HOA and the value of 79.8°C found in literature,<sup>[261]</sup> which supports to treat the dissolution of 12-HOA gels as a melting of gelator crystals. However, the enthalpy obtained from the fits ( $\Delta H_m = 260 \text{ kJ mol}^{-1}$  for the binary gel and  $\Delta H_m = 115 \text{ kJ mol}^{-1}$  for the lamellar gel) is significantly larger than the melting enthalpy of neat 12-HOA received from DSC measurements, which is  $\Delta H_m = 49.5 \text{ kJ}\cdot\text{mol}^{-1}$ .

The observed broad calorimetry peaks in the DSC heating curves suggest a weakly first order transition. In fact, the gel network formation of small molecule gelators is nowadays interpreted as a two-step process.<sup>[278,288]</sup> First, the gelator molecules self-assemble into fibers via a first-order process, which is mainly observed in DSC measurements due to the discontinuous enthalpy change related to the fiber formation. In a second step, the fibers link together to form clusters and finally the 3D network, the cross-linking between the fibers is a second order process with a diverging cluster size at the gelation point. This explains the fact that gel-sol transition temperatures which are measured via rheology or the “table-top” method (a gel in an inversed vial is placed in a heated water bath and checked for flow) are often found to be below the ones measured with DSC.<sup>[281]</sup> The first probes the mechanical stability of the gel which is connected to its cross-linking density, and the second rather measures the melting of the single gel fibers.

A striking difference between the gelator-free  $L_\alpha$  phase and the lamellar gel becomes obvious by a look at the temperature dependent lamellar layer spacing (see Figure 4.20). For the gelator-free  $L_\alpha$  phase the lamellar repeat unit  $d_0$  is decreasing with increasing temperature. Such behavior is

expected due to the enhanced fluctuations of the surfactant molecules and thus decreasing orientational order with increasing temperature.<sup>[289]</sup> In contrast, the gelled  $L_\alpha$  phase shows an almost temperature-independent layer spacing at low temperatures. Above a certain temperature a decrease of the layer spacing as in the gelator-free case can be observed. The temperature from which the behavior changes coincides with the gel-sol transition temperature. Below the gel-sol transition temperature the lamellar layer spacing is arrested, while above  $T_{\text{gel-sol}}$  the layer spacing is free to change with temperature. The gel network seems to freeze the lamellar liquid crystalline order leading to stiffer lamellar bilayers.

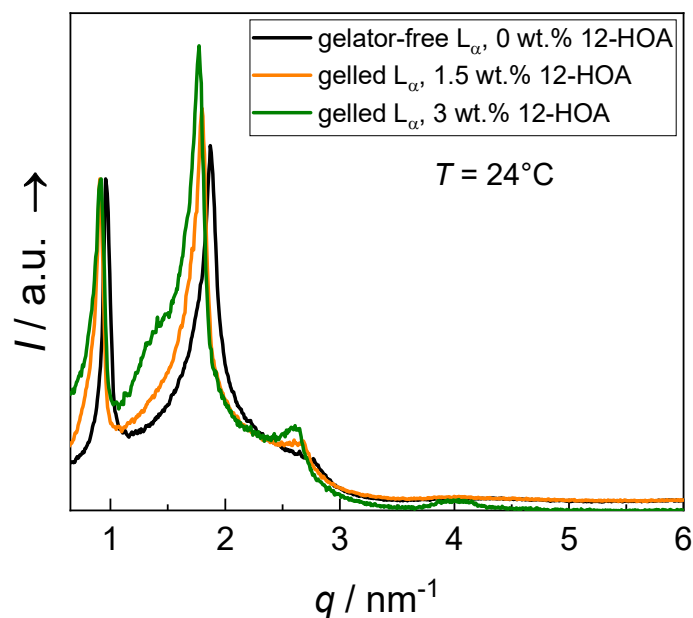


**Figure 4.20:** Lamellar repeat unit  $d_0$  in dependence of temperature for the gelator-free  $L_\alpha$  phase (for *a*)  $\omega_{\text{H}_2\text{O}} = 0.70$ ,  $\gamma_{\text{DOH/SDS}} = 0.28$ , and *b*)  $\omega_{\text{H}_2\text{O}} = 0.70$ ,  $\gamma_{\text{DOH/SDS}} = 0.30$ , open circles) and the corresponding gelled  $L_\alpha$  phase ( $\mu = 0.03$ , filled circles) measured by small angle X-ray scattering. For the gelled  $L_\alpha$  phase an arrested layer spacing is observed below the gel-sol transition temperature  $T_{\text{gel-sol}}$ . *a*) is adapted with permission from S. Dieterich *et al.*, *Langmuir* **2019**, *35*, 16793.<sup>[162]</sup> Copyright 2019 American Chemical Society.

Another indication that the lamellar structure is influenced by the presence of the gel network gives a detailed comparison of the diffraction profiles of the gelator-free  $L_\alpha$  phase and the lamellar gel (see Figure 4.21). For the gelled  $L_\alpha$  phases a shift of the layer peaks to lower  $q$  in comparison with the corresponding gelator-free  $L_\alpha$  phase as in Figure 4.21 is often observed. This is a common, but not the general behavior and this trend is not systematic in its magnitude. One reason for the increase in the layer spacing might be that the incorporation of the “cosurfactant” 12-HOA with a C18 chain broadens the bilayer formed by the C12 surfactant SDS. Additionally, an increase in the layer repeat unit points towards a higher degree of orientational order.

More important, for the gelled  $L_\alpha$  phase the intensity of the second order peak is enhanced and a third

order layer peak emerges, which indicates that the quality of lamellar ordering is clearly enhanced by the presence of the gel network fibers. This leads to the general conclusion that both structures, lamellar layers and gel fibers, do not coexist independently of each other.



**Figure 4.21:** Comparison of the X-ray profiles obtained for the gelator-free  $L_\alpha$  phase (black) and for the  $L_\alpha$  phases gelled with 1.5 wt.% (orange) and 3 wt.% (green) 12-HOA. The intensity is normalized to the intensities of the first order layer peaks. With increasing gelator amount an enhancement of the second order layer peak and even a third order layer peak due to the lamellar structure can be observed. This indicates a higher translational order for the gelled than for the gelator-free  $L_\alpha$  phase. Reprinted with permission from S. Dieterich *et al.*, *Langmuir* **2019**, *35*, 16793.<sup>[162]</sup> Copyright 2019 American Chemical Society.

### 4.3 Conclusion

In this section of the thesis one of the first examples of surfactant-based lyotropic liquid-crystalline physical gels is presented. The development of a reproducible procedure for the fabrication of such LLC gels is described. The combination of a lamellar liquid crystal and a low molecular weight gelator leads to a new kind of a mechanically stable, elastic and anisotropic soft solid.

In conclusion, the obtained results clearly demonstrate that the two combined structures, liquid crystalline phase and gel fiber network, do not coexist independently of each other meaning that the gelled lyotropic liquid crystalline phases are not orthogonal self-assembled systems.

It is possible to transform all observed LLC phases into the gelled state using the gelator 12-HOA, but only for the  $L_\alpha$  phase its lamellar structure is maintained. In contrast, nematic phases have a lamellar

structure in the gelled state and the hexagonal phase was found to be isotropic after gelation. It seems that the high order of the hexagonal phase is incompatible with the gel network structure. However, it turned out that hexagonal gels could be obtained using different low molecular weight gelators, which form considerably thinner gel fibers as 12-HOA, which allows the fiber network and the hexagonal phase to coexist with each other. Hence, the gel fiber diameter is the crucial criterion whether micellar lyotropic hexagonal gels can be formed.

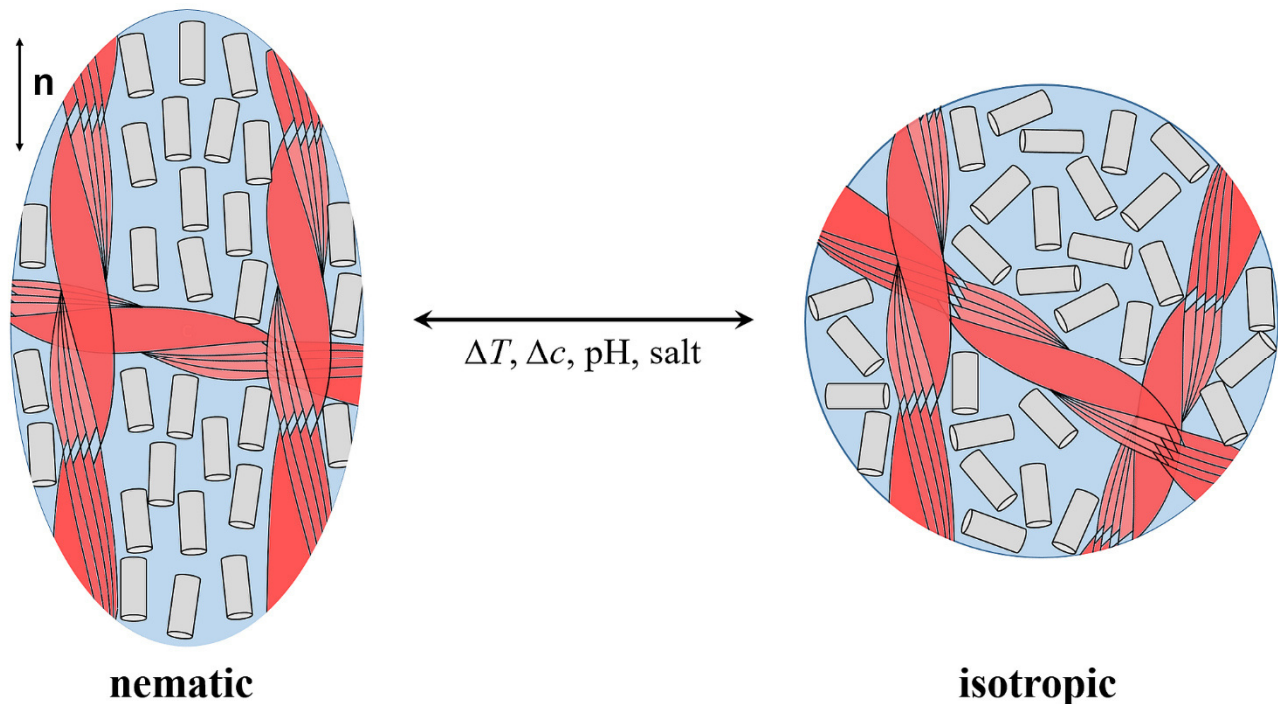
All in all, the gel network interacts with the lyotropic phases in such a way that the lamellar structure is stabilized, as additionally shown by an increased translational order in the lamellar gel in comparison to the gelator-free  $L_\alpha$  phase.

Due to the strong preference of the lamellar phase, the structures of non-layered phases, such as the nematic phases, could not be preserved during gelation with 12-HOA. In addition, the gelator 12-HOA was found to be surface active and thus acting partly as cosurfactant in the LLC system. This leads to a flattening of the micelle curvature and thus to a broadening of the lamellar regime. Hence, in the next step, low molecular weight gelators which are not surface active were investigated in order to obtain lyotropic nematic gels. The results are presented in the next part of this thesis (chapter 5).

Gelling the  $L_\alpha$  phase is most straightforward. The behavior of the examined lamellar gels deviates from the one of the gelator-free  $L_\alpha$  phase since an arrested lamellar layer spacing and an enhanced lamellar order were found. Thus, the structure of the lamellar gels and the mutual influence of lamellar layer structure and gel fiber network on each other is studied in more detail in a systematic SANS study, the results of which are discussed in section 6 of this thesis.

## 5 Lyotropic nematic gels (Publication II)

Nematics are the structurally simplest LC phase, which makes lyotropic nematic gels essential for demonstrating fundamental principles in LLC gels. The absence of any long-range translational order is also the reason for their low viscosity enabling easy alignment of lyotropic nematics before gelation. As described in chapter 1 lyotropic nematic gels can be considered as the lyotropic counterpart to thermotropic nematic elastomers. Likewise, the orientational order of the lyotropic nematic phase can be coupled to the orientation of the physical gel network. A change in the order (order-disorder transition) of a macroscopically aligned (monodomain) lyotropic nematic gel may thus lead to a change in the shape of the gel if the fiber network relaxes into an isotropic state, as shown in Figure 5.1. Hence, lyotropic nematic gels are promising materials for the application in water-based stimuli-responsive actuators.



**Figure 5.1:** Schematic drawing of the expected actuation principle in lyotropic nematic ( $N_c$ ) gels. Since the topology of a gel network is coupled to the orientation and order of the LLC, the shape of a macroscopically aligned sample changes (*i.e.* contraction in the direction of the director  $\mathbf{n}$  and expansion perpendicular to it) when the nematic to isotropic phase transition is induced by external stimuli such as temperature, solvent concentration, pH-value or the addition of salts.

In comparison to lamellar and hexagonal lyotropics, lyotropic nematic phases are rather rare. Gelling lyotropic nematic phases is challenging due to the small range of the nematic regime in the phase

diagram. In addition we found in chapter 4 that gelling LLC phases leads to a strong preference of the lamellar structure. Probably as a result of these problems, no micellar nematic physical gels were reported in literature before this study. This chapter describes how the first examples of micellar lyotropic nematic gels were found and it is shown that gelators which are not amphiphilic and are thus not able to act as a cosurfactant are essential to obtain these gels. Furthermore, first results regarding monodomains of micellar nematic gels are presented.

## 5.1 Specific background

### 5.1.1 The lyotropic system H<sub>2</sub>O – *n*-decanol – CDEAB

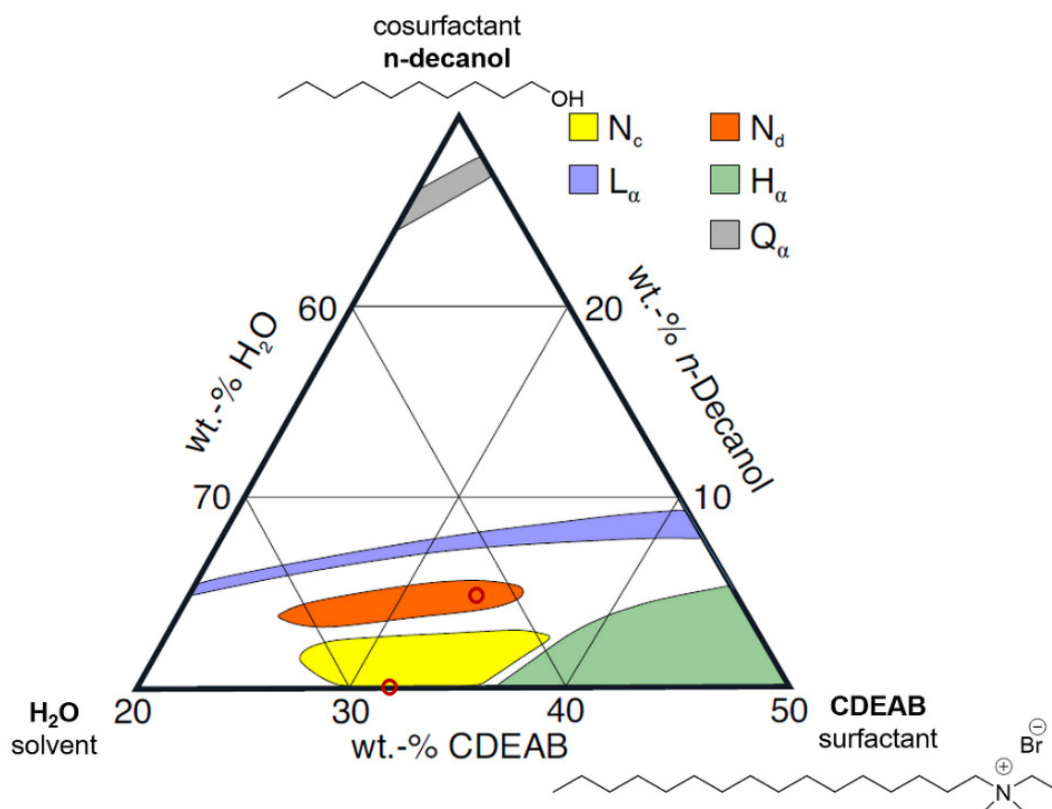
In addition to the lyotropic system H<sub>2</sub>O – *n*-decanol – SDS (see chapter 4.1.1), the nematic phases of the lyotropic system consisting of *N,N*-dimethyl-*N*-ethylhexadecylammonium bromide (CDEAB) as surfactant, *n*-decanol as cosurfactant and water was used to obtain lyotropic nematic gels. The molecular structures of the components and the phase diagram of the system H<sub>2</sub>O – *n*-decanol – CDEAB are shown in Figure 5.2. In the binary system water/CDEAB, a nematic N<sub>c</sub> phase exists at surfactant concentrations lower than for the hexagonal phase. This is one of the rare cases that a nematic phase exists in a binary water/surfactant system. However, the formation of the rather flat, disk-like micelles in the N<sub>d</sub> phase requires the use of the cosurfactant *n*-decanol.

As demonstrated by X-ray studies, the addition of *n*-decanol leads to structures with a smaller interfacial curvature since for a *n*-decanol molecule solubilized in the micelle, the surface increase is small in comparison to the volume increase. Additionally, the hydroxyl groups of *n*-decanol reduce the electrostatic repulsion between the positively charged CDEAB head groups leading to a denser micelle surface.<sup>[290]</sup>

It was shown that in the isotropic phase of the ternary system the micelles already have an anisotropic rod-like shape. A reduction of the water concentration at constant CDEAB/*n*-decanol ratio transforms the micellar shape into a weakly anisotropic elliptical one (still isotropic phase). Due to an increased micelle density, a further decrease of the water content leads to anisotropic disk-like micelles which are uniaxially ordered (N<sub>d</sub> phase). By further decreasing the water content, the anisotropy and ordering of the micelles increases until an expanded bilayer structure is formed (L<sub>α</sub> phase).<sup>[291]</sup> In the N<sub>c</sub> phase the addition of *n*-decanol results in a growth in length and in a slight increase in diameter of the micelles. For both nematic phases it was shown that the temperature induced nematic to isotropic

transition is not caused by a change of the micellar shape, but a sudden reduction in the degree of ordering of the micelles.<sup>[291]</sup>

The composition we chose to obtain a nematic  $N_d$  phase was  $\omega_{H_2O} = 0.632$ ,  $\gamma_{DOH/CDEAB} = 0.15$ , and for the nematic  $N_c$  phase  $\omega_{H_2O} = 0.68$ ,  $\gamma_{DOH/CDEAB} = 0$  was used.

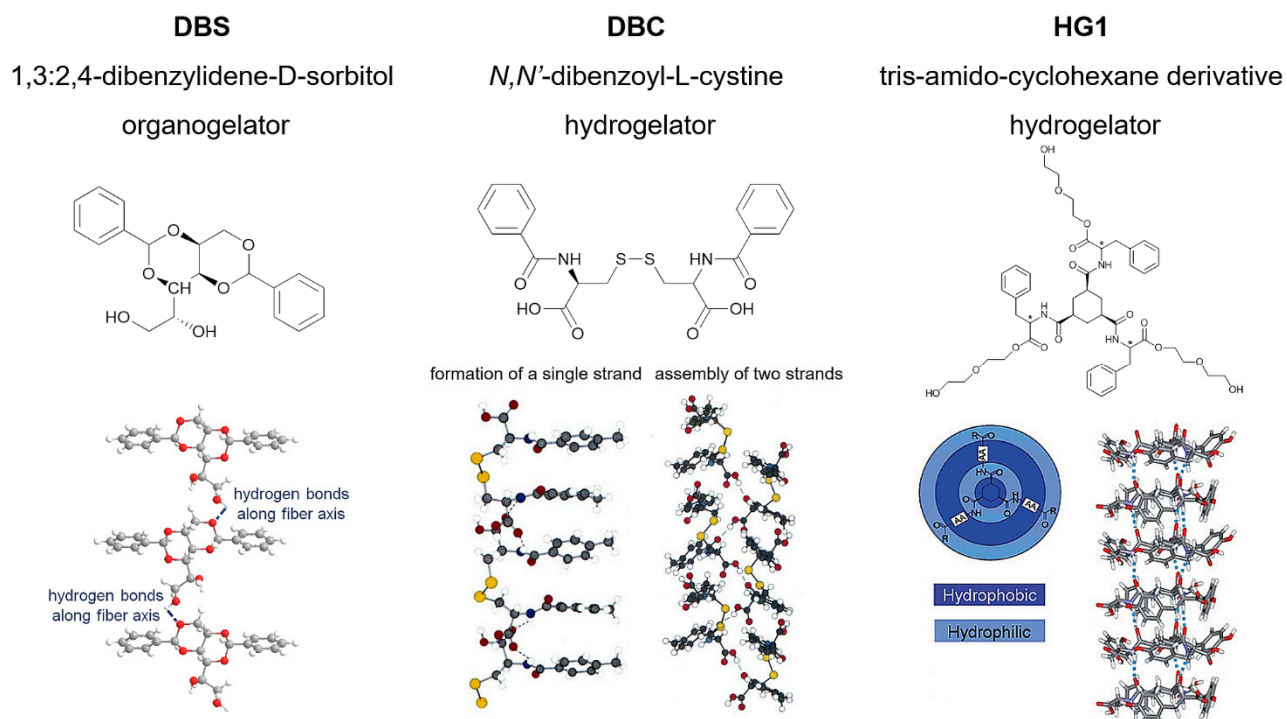


**Figure 5.2:** Room temperature phase diagram of the ternary system H<sub>2</sub>O – *n*-decanol – CDEAB (schematically redrawn from Ref.<sup>[292]</sup> by Prof. F. Gießelmann) including the molecular structures of the surfactant CDEAB and the cosurfactant *n*-decanol, as well as the used compositions which are indicated by red circles.

### 5.1.2 The low molecular weight gelators DBS, DBC and HG1

Instead of the amphiphilic LMWG 12-HOA used in the previous study (chapter 4) we now examined the capability of the non-amphiphilic LMWGs 1,3:2,4-dibenzyliden-D-sorbitol (DBS), *N,N'*-dibenzoyl-L-cystine (DBC) and the tris-amido-cyclohexane derivative HG1 to gel lyotropic nematic phases. The molecular structures of these gelators and the corresponding fiber formation is shown in Figure 5.3.





**Figure 5.3:** Molecular structure and fiber growth of the LMWGs DBS, DBC (fiber formation is actually shown for the compound ditoluoyl-L-cystine, which crystals are assumed to have the same intermolecular interactions than a DBC gel fiber, reprinted with permission from Ref.<sup>[293]</sup> Copyright 1995 Wiley-VCH) and HG1 (reproduced from Ref.<sup>[294]</sup> with permission from The Royal Society of Chemistry, Copyright 2009).

DBS is known for its ability to gel organic solvents for over 100 years.<sup>[295]</sup> The special feature of DBS is the broad range of solvents it is able to gel, non-polar ones as well as polar protic ones. Since the self-complementary non-covalent interactions holding together the 1D stack are hydrogen bonds as well as  $\pi$ - $\pi$  interactions, each of the interactions can predominantly be responsible for the gelation.<sup>[295]</sup> It was shown by selective conversion of either the 5-OH or the 6-OH group with a methoxy group that the 6-OH group is intermolecularly bonded to an acetal oxygen leading to gel formation (*i.e.* no gel was formed when the terminal 6-OH group was protected). However, if the 5-OH group was protected gelation still occurred proving that the 5-OH group is not involved in the self-assembly of the fiber.<sup>[296]</sup> In contrast, for alcoholic solvent solvents a  $\pi$ - $\pi$  stacking of the DBS molecules building up the gel fiber was observed.<sup>[282]</sup> The competition between “DBS-DBS” and “DBS-solvent” hydrogen bonds leads to a higher importance of  $\pi$ - $\pi$  interactions in protic solvents. Additionally, it was shown that the morphology of the gel fibers is different for solvents of different polarity. In nonpolar solvents helical fibers are observed, while the planar  $\pi$ - $\pi$  interactions in polar solvents lead to non-helical fibers.<sup>[228]</sup> However, the ability of a solvent to accept or donate hydrogen bonds determines the physical properties of the resulting gel more than the solvent polarity.<sup>[227]</sup>

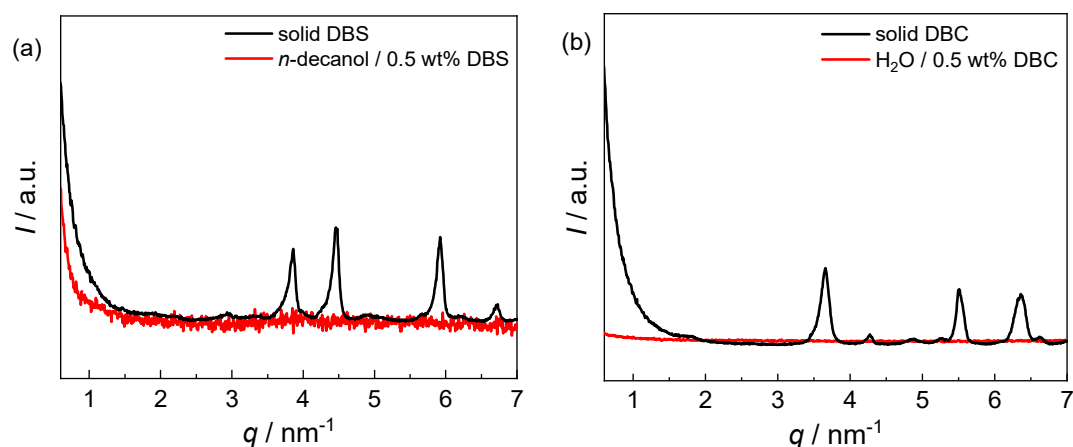
The gelator DBS was already used to gel thermotropic LC phases<sup>[122]</sup> and in our DFG project “Gelled lyotropic liquid crystals – orthogonal self-assembly or soft templating”, see chapter 2) other lyotropic LC phases were gelled with DBS as well.<sup>[297,298]</sup> For gelling the  $L_\alpha$  and  $H_1$  phases of the system  $H_2O - C_{12}E_7$  (heptaethyleneglycol monododecylether) with DBS it was found that the structure of the formed LLC gel is the same, independent on whether the gel network or the LLC phase has formed first. The sol-gel transition temperature of the DBS gel network was customized by changing the gelator content in a way that the network forms at either higher or lower temperatures than the LLC phase, but all obtained LLC gels behave similar and are orthogonal self-assembled systems.<sup>[297,298]</sup>

The ability of DBC to gel water is known since the early 1920s.<sup>[299,300]</sup> In water, DBC forms fibers with a diameter of 20 – 60 nm.<sup>[155]</sup> As shown in Figure 5.3 the DBC molecules stack linearly, with hydrogen-bonds between the amide NH and the carboxyl carbonyl with the donor-acceptor combination on one side of the S-S linkage linking to the molecule below and the other one to the molecule above. A  $\pi$ - $\pi$  stacking of the aromatic rings further stabilizes the gel fibers.<sup>[242,293]</sup> The interactions relevant for the DBC fiber formation were investigated by modifying single groups of the molecule and observing the change in the gelation ability. If the S-S linkage is replaced by  $CH_2-CH_2$  or  $CH=CH$  groups, the gelating properties are destroyed.<sup>[300]</sup> The  $CH_2-S-S-CH_2$  dihedral angle of about  $90^\circ$  is required for the directed intermolecular hydrogen-bonds and the  $\pi$ - $\pi$  interactions. The importance of aromatic groups is shown since the diacetyl-L-cystine compound shows no gelation (too water-soluble), but for naphthalene instead of benzyl groups an increased gelation ability (lower cgc, faster gel formation) is observed.<sup>[242]</sup> That the carboxyl-proton is not essential for gel formation (not included in the intra-fiber hydrogen bonding) is proven since the methyl ester derivative can form gels.<sup>[242]</sup> However, under alkaline conditions DBC is not able to form gels, probably due to an electrostatic repulsion between the carboxylate groups. Moreover, the carboxylic acid proton is believed to promote interfiber hydrogen bonds with the amide carbonyl.<sup>[293]</sup> If the  $\alpha$ -carboxyl is converted into a primary  $\alpha$ -carboxamide group the hydrogen-acceptor ability of the carbonyl oxygen is increased resulting in an improved gel forming performance proving the importance of the carbonyl oxygen for the intrafiber hydrogen bonding.<sup>[242]</sup> If however an electron withdrawing nitro-group is added to the aromatic ring, no improvement in the hydrogen-donor ability of the amide NH was noticed, instead a crystallization from solution was observed before gel formation. The same is noticed if the benzoyl-groups are replaced by toluoyl-groups. This shows the delicate balance between gelation and crystallization. DBC single crystals allow an X-ray analysis on

the atomic level and the observed ‘fibrous’ crystals confirm the above-mentioned assumed interactions between the molecules.<sup>[242]</sup>

The responsiveness of DBC gels to the pH-value allows an controlled release of (drug) molecules when the gel dissolution is triggered in alkaline solutions.<sup>[155]</sup> In case of a pH-gradient a directed self-assembly with gel fibers oriented parallel to the gradient is achieved.<sup>[301]</sup>

In contrast to the gel fibers of 12-HOA (see chapter 4.1.2), the gel fibers of DBS and DBC are non-crystalline as proved by the absence of diffraction maxima in the SAXS curves of the respective binary gels (see Figure 5.4).



**Figure 5.4:** X-ray diffractions profiles (own measurements) of the solid powder (black) and a binary gel (red) of the gelators *a*) DBS and *b*) DBC. In both cases, no diffraction maximum can be observed in the gel proving the non-crystalline nature of the gel fibers.

In contrast to the “old” gelators DBS and DBC, HG1 was only developed in 2003 as a LMWG in a series of cyclohexane-based hydrogelators in the group of Prof. van Esch.<sup>[302]</sup> HG1 is a highly effective hydrogelator able to gel water at concentrations as low as 0.033 wt%.<sup>[240]</sup> The formed fibers are thin (5 - 25 nm), have a long aspect ratio (length ~ 500 nm) and presumably consist of twisted bundles of stacked HG1 molecules. A rigid gel from long and stiff fibers which entangle and stabilize the network by mainly mechanical contacts between the fibers results.<sup>[294]</sup> The high gelation ability of HG1 arises from the anisotropic self-assembly of the gelator molecules, in which the 1D array is stabilized by six hydrogen-bonds between the carboxamide groups (see Figure 5.3).<sup>[302]</sup> The uniaxial interactions between the 1,3,5 triamide cyclohexane cores were also shown for derivatives of HG1, for which 1D crystals<sup>[303]</sup> or organogels<sup>[304]</sup> (if the residues are long alkyl chains, *i.e.* trialkyl 1,3,5 cyclohexanetricarboxamide derivatives) were observed. In case of HG1, the hydrophobic amino acid L-phenylalanine is connected to the core. The phenyl-rings were shown to fold inwards shielding

the 1D hydrogen bonds between the amides from competitive interactions with water. Additionally, hydrophobic interactions are added as an aggregation force (alternating hydrophobic and hydrophilic building blocks, but due to bulky “circular” molecular shape HG1 shows no surface/interface activity) supporting the 1D stack of gelator molecules.<sup>[240]</sup> Self-assembled fibrillar networks with encapsulated vesicles or spherical micelles and interpenetrating networks with elongated entangled micelles are formed from solutions of HG1 and various surfactants in water.<sup>[294,302,305]</sup>

## 5.2 Results and Discussion

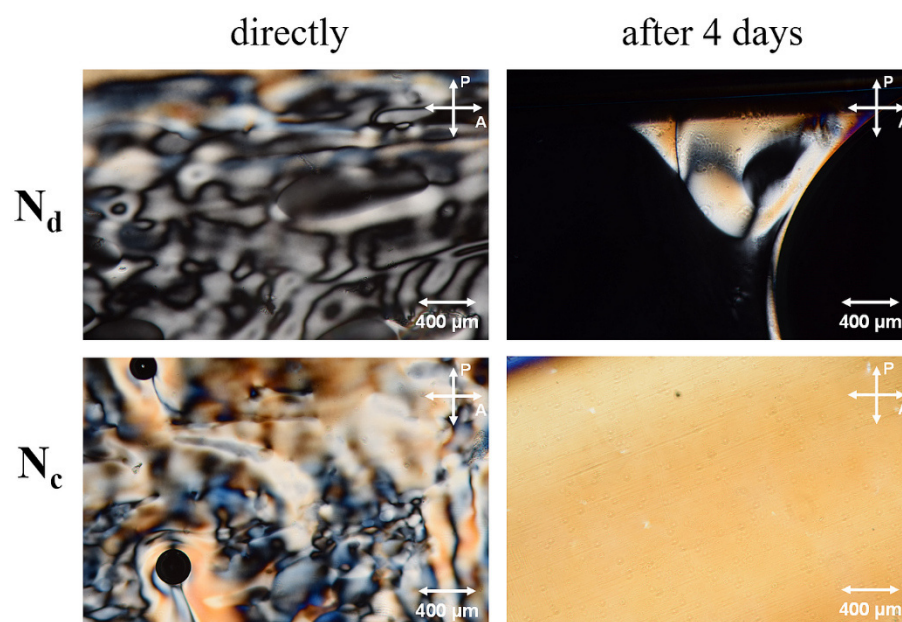
Using the three low molecular weight gelators DBS, DBC and HG1 the first examples of micellar lyotropic nematic gels with a self-assembled 3D fiber network were achieved. Besides the nematic phases of the lyotropic system H<sub>2</sub>O – *n*-decanol – SDS, the N<sub>d</sub> and N<sub>c</sub> phases of the lyotropic system H<sub>2</sub>O – *n*-decanol – CDEAB were gelled as well (see Bachelor thesis of Friedrich Stemmler<sup>[306]</sup>). Gels were achieved for all combinations with the exception of the nematic phases of the system H<sub>2</sub>O – *n*-decanol – CDEAB with the gelator DBC. All obtained gels were nematic with the exception of the system H<sub>2</sub>O – *n*-decanol – SDS gelled with HG1, where starting from the N<sub>c</sub> phase an isotropic gel was received. A complete overview on the experiments to obtain lyotropic nematic gels with these surfactant systems and gelators is given in Table 5.1. The properties of the lyotropic nematic gels of the system H<sub>2</sub>O – *n*-decanol – CDEAB are reported in Ref<sup>[306]</sup>. All in all, we were able to obtain nine different lyotropic nematic gels, which are to the best of our knowledge the first examples of this new kind of anisotropic hydrogels.

**Table 5.1:** Overview on the nematic phases (N<sub>d</sub> and N<sub>c</sub>) of the two lyotropic systems and the three low molecular weight gelators used in this study to obtain lyotropic nematic gels. The symbols ✓ and ✗ indicate whether or not the gelation was successful. The numbers in the brackets is the critical gelator concentration (cgc) in wt%, necessary to obtain a nematic gel. Reprinted from the Supporting Information of Ref.<sup>[163]</sup>

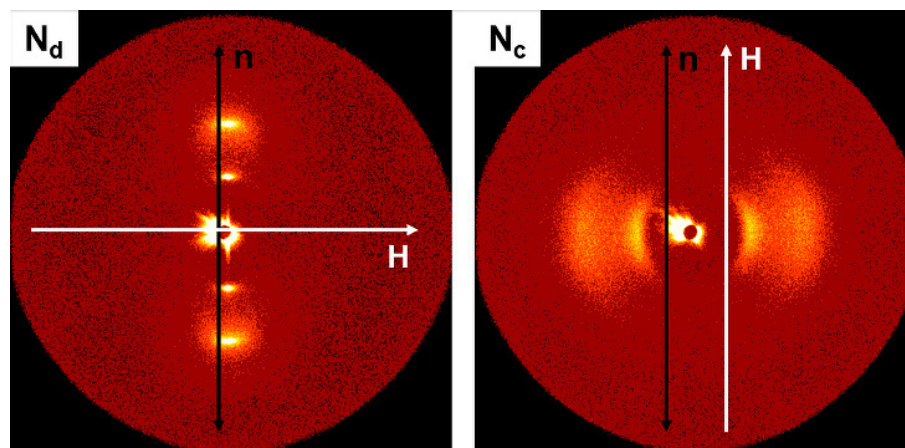
System		LMWG (cgc / wt%)		
		DBS	DBC	HG1
H <sub>2</sub> O - <i>n</i> -decanol - SDS	N <sub>d</sub>	✓ (0.75)	✓ (2.0)	✓ (1.75)
	N <sub>c</sub>	✓ (0.75)	✓ (2.0)	(✗) N <sub>c</sub> → isotropic, gelled
H <sub>2</sub> O - <i>n</i> -decanol - CDEAB	N <sub>d</sub>	✓ (2.0)	✗	✓ (1.5)
	N <sub>c</sub>	✓ (3.5)	✗	✓ (1.0)

### 5.2.1 Preparation of lyotropic nematic gels

The  $N_d$  phase (disk-shaped micelles as mesogenic units) and the  $N_c$  phase (cylindrical micelles as mesogenic units) were distinguished by the way they attach to a polar glass surface and align in a magnetic field. As seen in Figure 5.5, the  $N_d$  phase aligns homeotropic in flat glass capillaries, while for the  $N_c$  phase a uniform planar director alignment can be observed after four days. While the  $N_d$  phase has a negative anisotropy of diamagnetic susceptibility ( $\Delta\chi^d < 0$ ), for the  $N_c$  phase  $\Delta\chi^d > 0$  applies. Hence, the director is oriented either perpendicular ( $N_d$ ) or parallel ( $N_c$ ) to an external magnetic field as confirmed by 2D SAXS patterns in Figure 5.6.



**Figure 5.5:** Polarizing microscopy images of (above) the  $N_d$  and (below) the  $N_c$  phase of the system  $H_2O - n$ -decanol – SDS, (left) directly after filling the sample into flat glass capillaries and (right) four days after filling. After 4 days the  $N_d$  phase appears black between crossed polarizers (with the exception of the sample to air interface) indicating a homeotropic alignment (appears grey upon tilting), while for the  $N_c$  phase a non-disturbed uniform director alignment can be observed. Reprinted from the Supporting Information of Ref.<sup>[163]</sup>



**Figure 5.6:** 2D SAXS diffractograms of (left) the gelator-free  $N_d$  phase and (right) the gelator-free  $N_c$  phase. The samples were oriented for 8 hours in an external magnetic field of 1 T before measuring. While the director  $\mathbf{n}$  of the  $N_d$  phase is oriented perpendicular to the magnetic field direction, the director of the  $N_c$  phase is oriented parallel to it. Reprinted from the Supporting Information of Ref.<sup>[163]</sup>

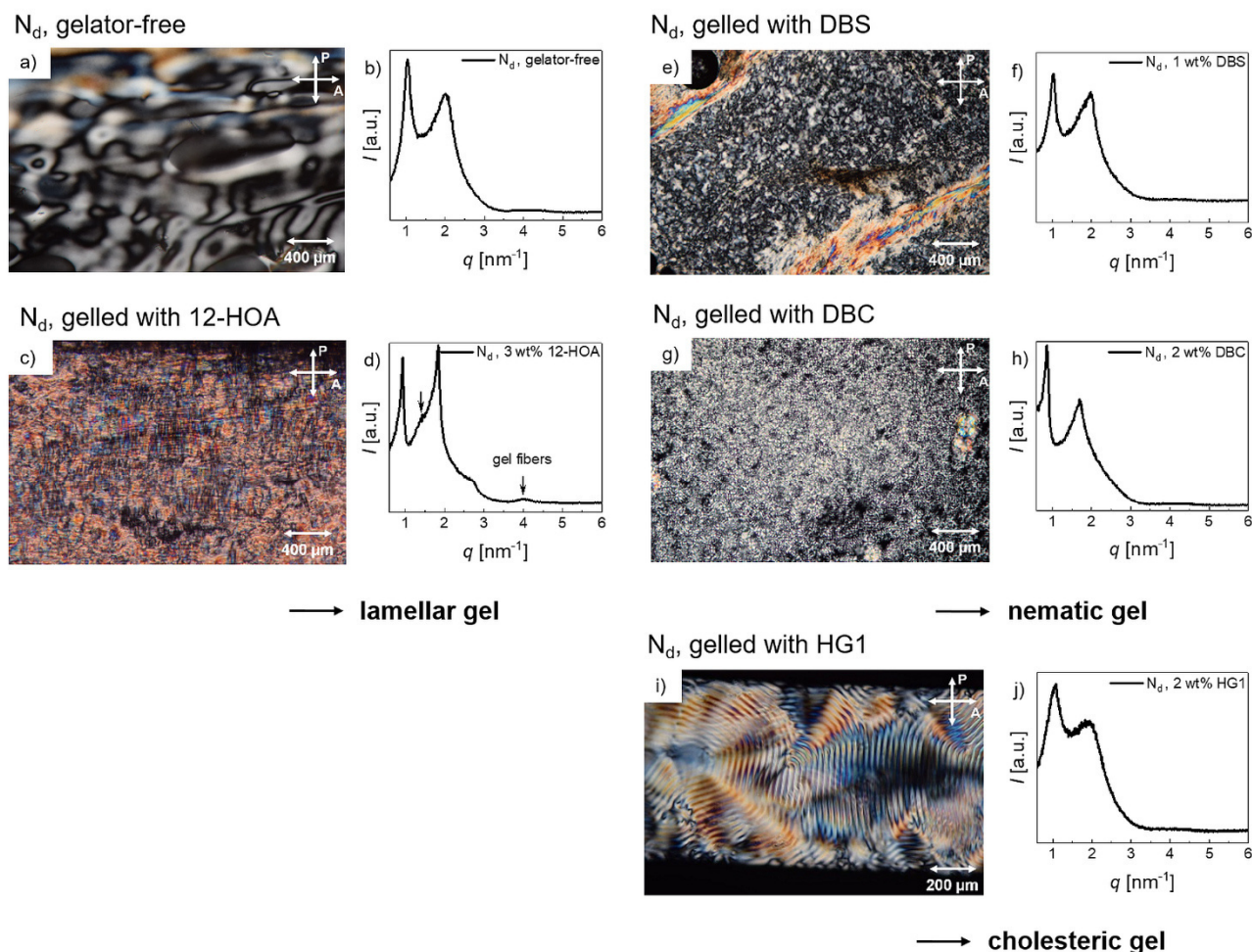
Gels made of DBS, DBC or HG1 were prepared slightly different than described in section 4 for the gelator 12-HOA. All three gelators could not be dissolved in *n*-decanol. Hence, they were added directly to an already prepared nematic phase. For dissolving the gelator in the ternary system, high temperatures (95 - 100°C) were needed. No clear optical difference could be observed for gels cooled down either rapidly or slowly.

### 5.2.2 Structures and properties of lyotropic nematic gels

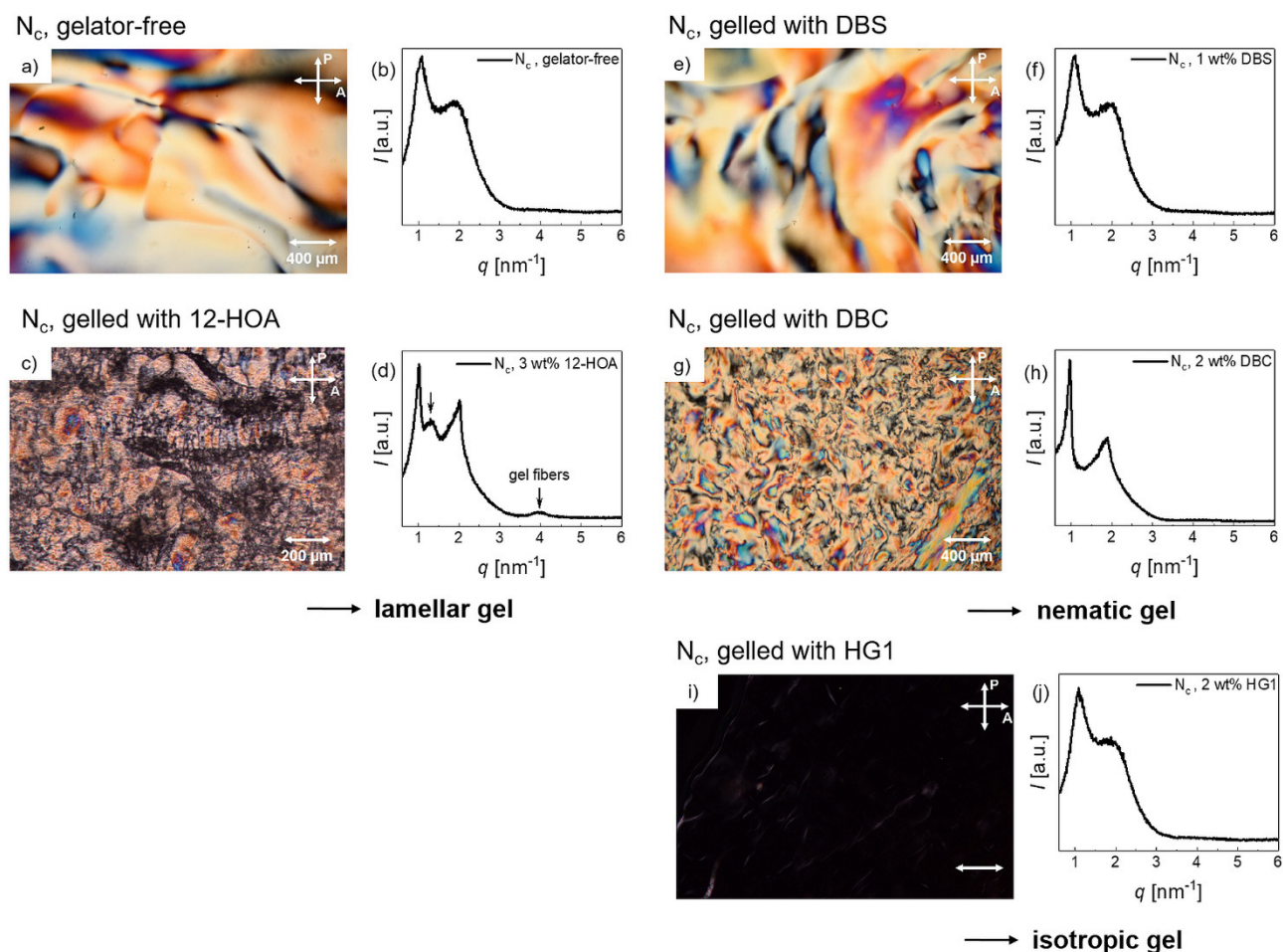
In comparison to the gelator 12-HOA the gelators DBS, DBC and HG1 are bulky and non-amphiphilic. Due to its amphiphilic nature 12-HOA is partly incorporated into the micelles acting as a cosurfactant and thus reduces the micelle curvature leading to a lamellar gel (see chapter 4). In contrast DBS, DBC and HG1 are likely to leave the micelle curvature unchanged upon gelation.

Indeed, POM and X-ray investigations confirm the nematic nature of the gels obtained when gelling the  $N_d$  (Figure 5.7) and  $N_c$  (Figure 5.8) phases with DBS and DBC, since *schlieren* textures in POM examinations and X-ray profiles that resemble the one of the gelator-free  $N_d$  phase were observed. The X-ray intensity profile of the  $N_d$  phase gelled with HG1 also clearly proves the absence of translational order and its POM image reveals a *fingerprint* texture, typical of a chiral nematic phase (see Figure 5.7i). Obviously, gelation of the  $N_d$  phase with HG1 leads to a lyotropic cholesteric gel, due to (heterogeneous) chiral induction by the twisted gel fibers. However, gelling the  $N_c$  phase with HG1 leads to the formation of an isotropic gel (see Figure 5.8i). (see also Figure 5.4).





**Figure 5.7:** Comparison of the gelator-free  $N_d$  phase with the  $N_d$  phase gelled with the different LMWGs. (left) POM images of a) the gelator-free  $N_d$  phase and of the gels obtained with c) 12-HOA, e) DBS, g) DBC and i) HG1. (right) X-ray diffraction profiles of b) the gelator-free  $N_d$  phase and of the gels obtained with d) 12-HOA, f) DBS, h) DBC and j) HG1. Gelation of the lyotropic nematic  $N_d$  phase with the gelator 12-HOA leads to a lamellar gel. Contrary, gelation of the  $N_d$  phase with the LMWGs DBS and DBC results in a nematic gel. When using HG1 to gel the  $N_d$  phase, the formation of a chiral nematic gel is observed. The layered structure of the 12-HOA fibers<sup>[255,259]</sup> reveals itself by two small and broad maxima at  $q = 1.35 \text{ nm}^{-1}$  and  $q = 4.04 \text{ nm}^{-1}$  in the X-ray profile in (d). Contrary, the presence of gel fibers of DBS and DBC is not reflected in the X-ray profiles. Adapted with permission from S. Dieterich *et al.*, *Adv. Mater.* **2021**, *33*, 2007340.<sup>[163]</sup> Copyright 2021 John Wiley & Sons.



**Figure 5.8:** Comparison of the gelator-free  $N_c$  phase with the  $N_c$  phase gelled with the different LMWGs. (left) POM images of a) the gelator-free  $N_c$  phase and of the gels obtained with c) 12-HOA, e) DBS, g) DBC and i) HG1. (right) X-ray diffraction profiles of b) the gelator-free  $N_c$  phase and of the gels obtained with d) 12-HOA, f) DBS, h) DBC and j) HG1. Gelation of the lyotropic nematic  $N_c$  phase with the gelator 12-HOA leads to a lamellar gel. Contrary, gelation of the  $N_c$  phase with the LMWGs DBS and DBC results in a nematic gel. When using HG1 to gel the  $N_c$  phase, the formation of an isotropic gel is observed. Adapted from the Supporting Information of Ref.<sup>[163]</sup>

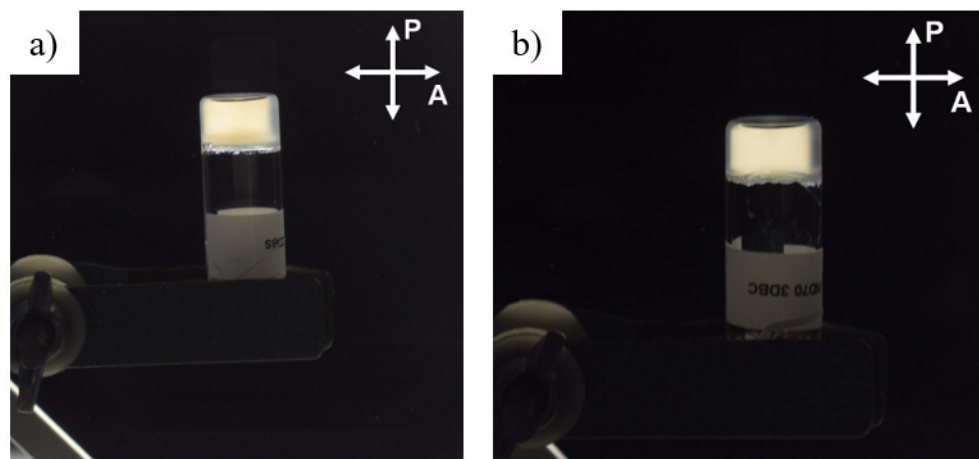


All thermal properties of the micellar nematic gels, namely the LLC sequences and the gel-sol transition temperatures  $T_{\text{gel-sol}}$  are listed in Table 5.2.

**Table 5.2:** Phase sequences of the gelator-free and gelled nematic phases of the system  $\text{H}_2\text{O} - n\text{-decanol} - \text{SDS}$  (studied up to  $105^\circ\text{C}$  by means of POM and X-ray scattering, for the sample  $\text{N}_d$ , 2 wt% DBC the  $L_\alpha$ -isotropic phase transition is above  $105^\circ\text{C}$ ), as well as  $T_{\text{gel-sol}}$  of the nematic gels.  $T_{\text{gel-sol}}$  is measured by inversion of the test tube at different temperatures in a water basin and checking for flow. A transition of the  $\text{N}_d$  phase into a lyotropic lamellar  $L_\alpha$  phase with increasing temperature is found. The appearance of a phase with long-range translational order at higher temperatures than a phase with solely long-range orientational order is highly untypical but already reported for the studied system  $\text{H}_2\text{O} - n\text{-decanol} - \text{SDS}$ .<sup>[190,307]</sup> Reprinted from the Supporting Information of Ref.<sup>[163]</sup>

sample	Phase Sequence [ $^\circ\text{C}$ ]	$T_{\text{sol-gel}}$ [ $^\circ\text{C}$ ]
Gelator-free $\text{N}_d$	$\text{N}_d$ 33 $L_\alpha$ 90 isotropic	-
$\text{N}_d$ , 1 wt% DBS	$\text{N}_d$ 36 $L_\alpha$ 94 isotropic	78
$\text{N}_d$ , 2 wt% DBC	$\text{N}_d$ 40 $L_\alpha$	69
Gelator-free $\text{N}_c$	$\text{N}_c$ 30 isotropic	-
$\text{N}_c$ , 1 wt% DBS	$\text{N}_c$ 31 isotropic	85
$\text{N}_c$ , 2 wt% DBC	$\text{N}_c$ 42 isotropic	75

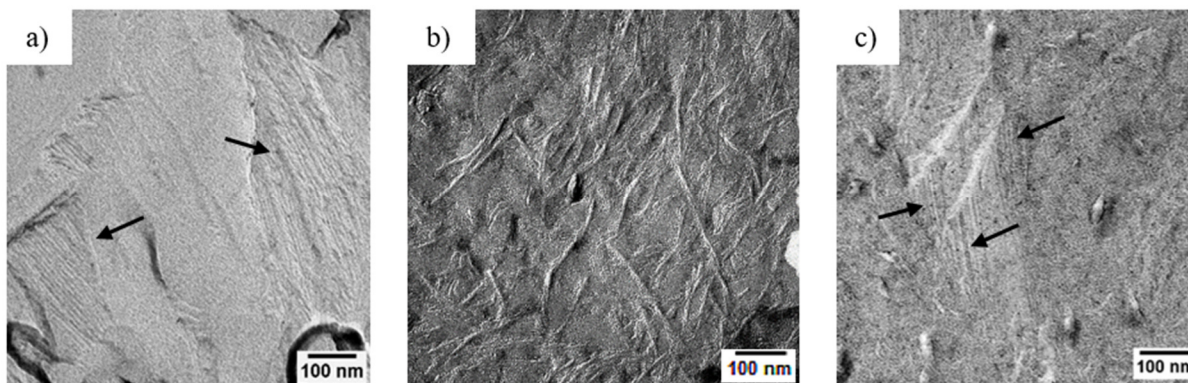
The anisotropic and self-sustaining properties of the lyotropic nematic gels were demonstrated since the gels show optical birefringence between crossed polarizers and no flow when turning the vial upside down (see Figure 5.9). To further examine the gel network properties, exemplary FFEM and rheology measurements were performed. The FFEM images in Figure 5.10 show twisted gel fibers in the nematic gels (in case of HG1 meaningful images were obtained for the binary gel  $\text{H}_2\text{O} / 0.5 \text{ wt}\% \text{ HG1}$  only). The fibers have an average thickness of 6.5 nm for DBS, 10 nm for DBC and 4.5 nm for HG1. In case of the  $\text{N}_c$  phase gelled with DBC an arbitrary fiber network is observed, while in the  $\text{N}_d$  phase gelled with DBS the fibers show orientational alignment. One has to keep in mind that FFEM probes the local structure of a sample and not enough images were taken to generalize the observed behavior.



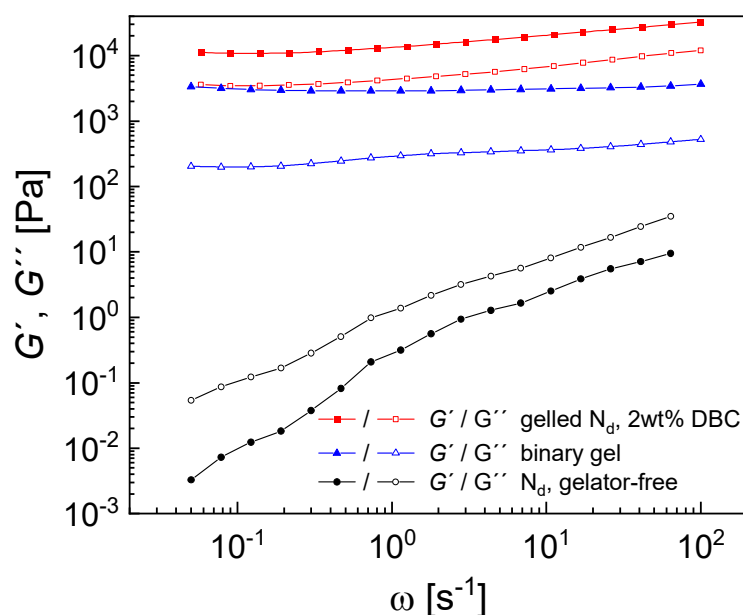
**Figure 5.9:** Gel formation and anisotropy are confirmed for the nematic gels *a)*  $N_d$  phase gelled with 2 wt% DBS and *b)*  $N_d$  phase gelled with 3 wt% DBC, since no flow is observed when turning the sample upside down and the samples show optical birefringence between crossed polarizers. Adapted with permission from S. Dieterich *et al.*, *Adv. Mater.* **2021**, 33, 2007340.<sup>[163]</sup> Copyright 2021 John Wiley & Sons.

Rheology measurements shown in Figure 5.11 clearly reveal the gel character of the nematic gel. For the nematic  $N_d$  phase gelled with 2 wt% DBC the storage modulus  $G'$  (which represents the elastic solid-like behavior) is over the whole frequency range about one order of magnitude larger than the loss modulus  $G''$ , (which represents the viscous liquid-like behavior). The behavior of the nematic gel is quite similar to the one of the isotropic binary gel ( $H_2O$  gelled with 0.5 wt% DBC), demonstrating that the gel properties are not considerably changed when an isotropic solvent is replaced with a micellar lyotropic nematic phase. In contrast, the fluid gelator-free nematic phase exhibits  $G'' > G'$  showing typical liquid-like behavior with both moduli at least three orders of magnitude smaller than in the nematic gel.

How are the lyotropic nematic phase and the fiber network influencing each other and what is the resulting morphology of the nematic gel? These questions were investigated by 2D small-angle X-ray experiments in a magnetic field, the direction of which is normal to the axis of the glass capillary with the LLC gel sample.

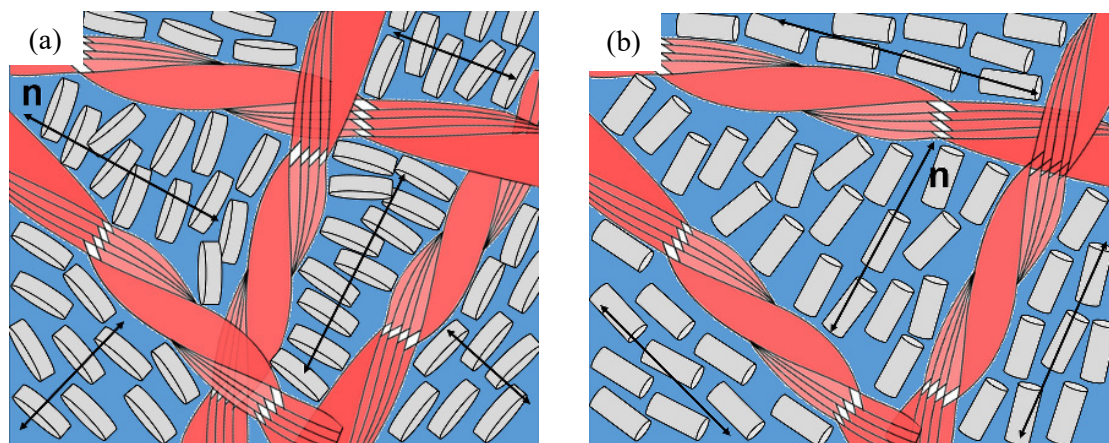


**Figure 5.10:** The gel fibers are visible in freeze-fracture electron microscopy images. Exemplary shown for the *a*) the  $N_d$  phase gelled with 1 wt% DBS, *b*)  $N_c$  phase gelled with 2 wt% DBC and *c*) the binary gel  $H_2O / 0.5$  wt% HG1. Please note the orientational alignment of the fibers in *a*) and the arbitrary running fibers in *b*). Adapted with permission from S. Dieterich *et al.*, *Adv. Mater.* **2021**, 33, 2007340.<sup>[163]</sup> Copyright 2021 John Wiley & Sons.



**Figure 5.11:** Storage modulus  $G'$  (filled symbols) and loss modulus  $G''$  (open symbols) for the gelator-free  $N_d$  phase (black circles), the nematic gel ( $N_d$  phase gelled with 2 wt% DBC, red squares) and the binary gel ( $H_2O$  gelled with 0.5 wt% DBC, blue triangles), obtained via oscillation frequency ( $\omega$ ) sweeps at constant shear stress ( $\tau = 2$  Pa for the gelator-free  $N_d$  phase and  $\tau = 40$  Pa for the gelled  $N_d$  phase and the binary gel) and temperature ( $T = 24^\circ\text{C}$ ). Reprinted with permission from S. Dieterich *et al.*, *Adv. Mater.* **2021**, 33, 2007340.<sup>[163]</sup> Copyright 2021 John Wiley & Sons.

If the sample is slowly cooled down from the isotropic sol state two scenarios must be distinguished: In the first scenario we assume that the gel network forms first. Given the negligible magnetic interactions with the fibers, a random isotropic network will form, which will disturb any macroscopic alignment if the micellar nematic phase forms at lower temperatures. As a result, a polydomain structure of the  $N_c$  and  $N_d$  gels is expected, as shown in Figure 5.12.



**Figure 5.12:** Model for the polydomain structure of a micellar nematic gel in case of *a*) the  $N_d$  phase and *b*) the  $N_c$  phase. Reprinted with permission from S. Dieterich *et al.*, *Adv. Mater.* **2021**, *33*, 2007340.<sup>[163]</sup> Copyright 2021 John Wiley & Sons.

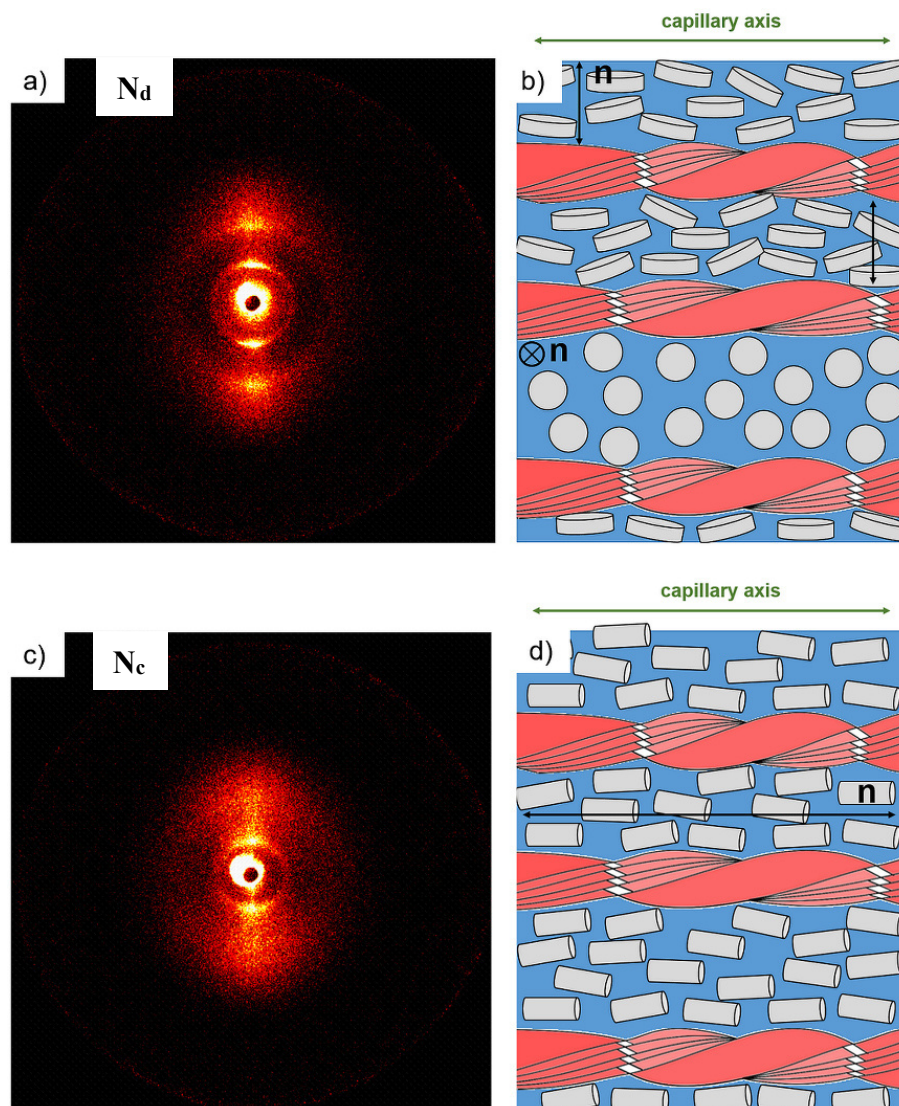
In the second scenario we assume that the LLC phase forms first. Likewise to the cases observed for gelator-free  $N_c$  and  $N_d$  phases, the action of the magnetic field will align the nematic director parallel ( $N_c$ ,  $\Delta\chi^d > 0$ ) or normal ( $N_d$ ,  $\Delta\chi^d < 0$ ) to the field direction (see Figure 5.14). The aligned nematic phases will act as a soft template for the growth of the fiber network and, as a result, macroscopically aligned nematic gels should be obtained.

Most surprisingly, our experiments did not follow either of these two scenarios. On the one hand the 2D diffraction patterns shown in Figure 5.13a and c clearly indicate the formation of macroscopically aligned nematic gels (second scenario), but on the other hand the alignment of the nematic directors do not follow the expectations. Instead, the  $N_c$  director is found normal to magnetic field direction and parallel to the capillary axis while the  $N_d$  director aligns normal to the capillary axis.

These rather unexpected observations can be readily explained if we assume that the fiber network forms first (see Table 5.2) and that the fibers preferentially grow in the directions parallel to the glass surface of the thin cylindrical capillaries (700 $\mu$ m in diameter). This will lead to an anisotropic, uniaxially aligned fiber network which now acts as a soft template for the formation of the micellar nematic phases at lower temperature. If the templating effect exceeds the aligning action of the



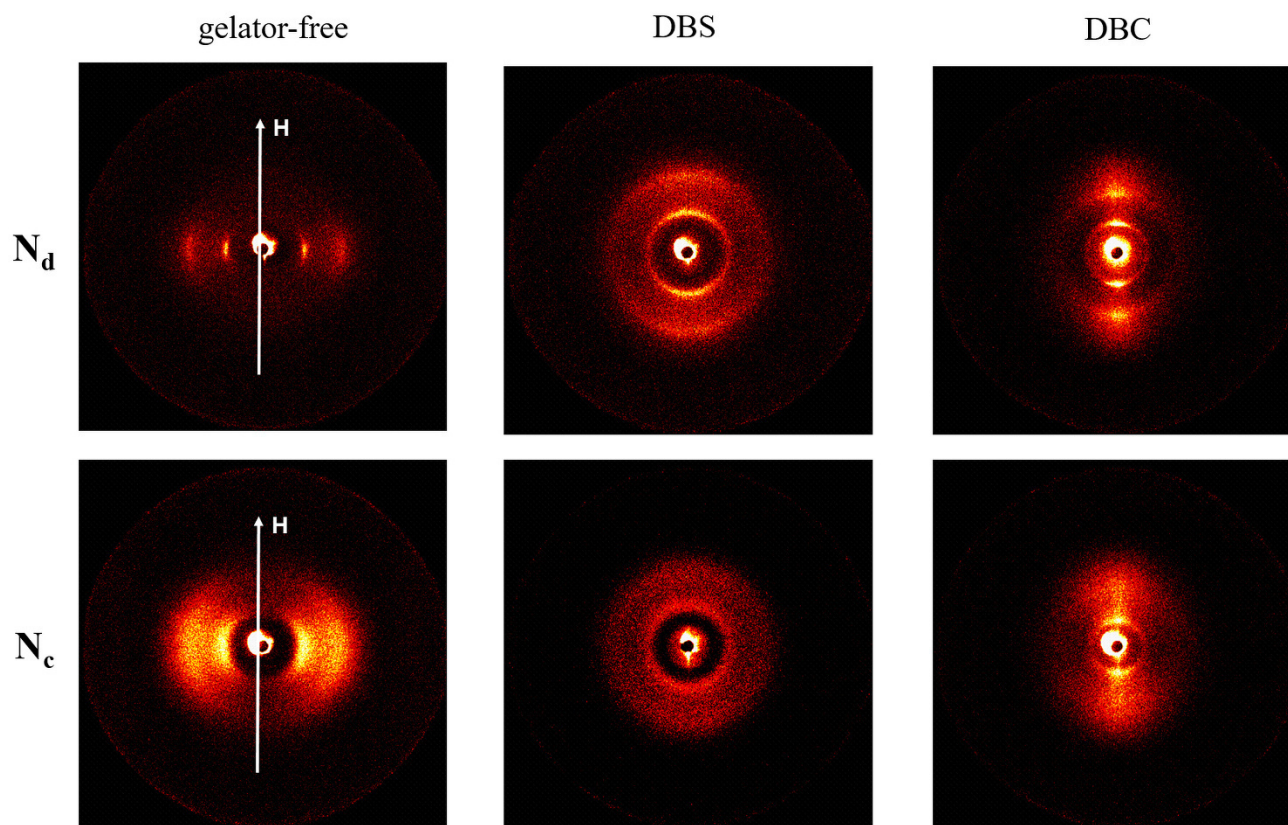
magnetic field effect, this scenario will exactly lead to the gel configurations shown in Figure 5.13b for the  $N_d$  gel and in Figure 5.13d for the  $N_c$  gel. Each of these configurations is in full agreement with the corresponding 2D X-ray patterns actually observed in the experiment.



**Figure 5.13:** 2D SAXS diffractograms of the DBC gelled a)  $N_d$  phase and c)  $N_c$  phase. The model derived from the 2D SAXS measurements is schematically shown in b) for the  $N_d$  phase and in d) for the  $N_c$  phase. Although the gel fibers form first, an oriented director configuration is observed. Probably, the capillary surface guides a linear growth of the gel fibers which in turn serve as a soft template for the nematic phase. Reprinted with permission from S. Dieterich *et al.*, *Adv. Mater.* **2021**, *33*, 2007340.<sup>[163]</sup> Copyright 2021 John Wiley & Sons.

A uniform alignment of the nematic gels is easier to achieve for nematic phases gelled with DBC than with DBS (see Figure 5.14). Such monodomains of lyotropic nematic networks are essential for the potential use of LLC gels as actuators and sensors. However, a director alignment as shown in

Figure 5.13 is not always reproducible. In some cases, nematic polydomain gels were observed as well.



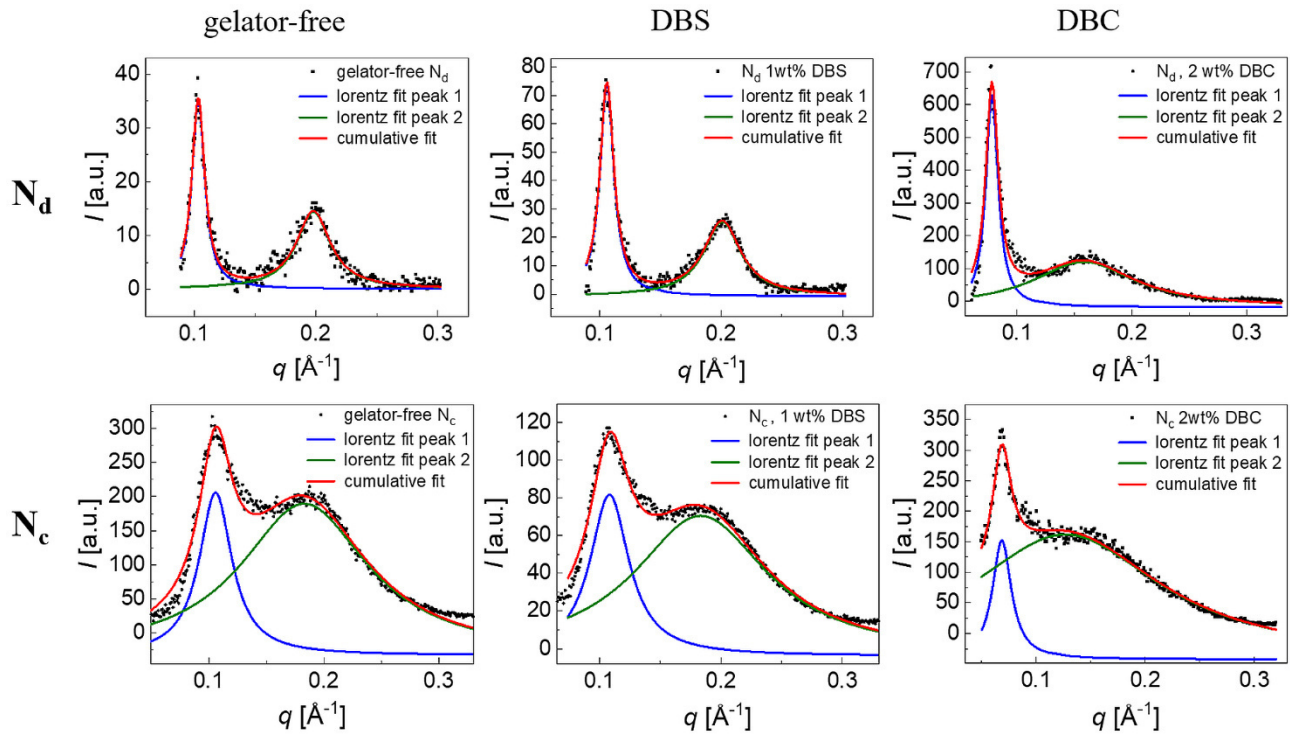
**Figure 5.14:** 2D SAXS diffractograms of (left) the gelator-free, (middle) the DBS gelled and (right) the DBC gelled  $N_d$  (above) and  $N_c$  (below) phases. While the gelator-free nematic phases are oriented by the magnetic field, the orientation of the nematic gels is presumably determined by the orientation of the gel fibers. Reprinted from the Supporting Information of Ref.<sup>[163]</sup>

For all samples, the nematic fluids and the nematic gels, the X-ray profile exhibits a relatively sharp first order and a diffuse second order scattering maxima at  $q_2 \approx 2q_1$  indicating the presence of a pseudo-lamellar structure, *i.e.* clusters with short-range translational order. A previous study on the nematic phases of the same system reports a local pseudo-lamellar arrangement of the micelles.<sup>[188]</sup> Additionally, a pseudo-lamellar structure was found for the  $N_d$ ,  $N_c$  and  $N_{bx}$  (biaxial nematic) phases of two further lyotropic systems.<sup>[176]</sup> Such smectic clusters are also known to appear in nematic phases of thermotropic LCs when approaching the nematic-smectic phase transition.<sup>[308–310]</sup>

To determine the correlation length, a peak shape analysis was carried out using a cumulative fit of two Lorentz fits (see Figure 5.15) according to

$$I(q) = \frac{2A}{\pi} \frac{FWHM}{4(q - q_0)^2 + FWHM^2}, \quad (5.1)$$

where  $q_0$  is the position of the scattering maximum, FWHM is the full width at half maximum and  $A$  is the area of the peak. As shown by the Lorentzian shape of the diffraction maxima the positional correlation function decays exponentially, with  $\xi$  being the correlation length obtained from the width of the peak ( $\xi = \frac{2}{FWHM}$ ). For the  $N_d$  phase the correlation length is about 150 Å and remains practically in the same range in the gelled state. In the  $N_c$  phase the correlation length is significantly lower, about 55 Å, and a clear increase for the  $N_c$  phase gelled with DBC ( $\xi = 95$  Å) is noted.



**Figure 5.15:** Intensity vs  $q$  profiles obtained from radial averaging of the 2D X-ray diffractograms shown in Figure 5.14 for (left) the gelator-free, (middle) the DBS gelled and (right) the DBC gelled (above)  $N_d$  and (below)  $N_c$  phases. All experimental data is fitted by a cumulative fit of two Lorentz fits. Reprinted from the Supporting Information of Ref.<sup>[163]</sup>

**Table 5.3:** The mean intermicellar distance  $d_c$  and the positional correlation length  $\xi$  obtained from the analyses of the first order diffuse scattering maxima of the SAXS data shown in Figure 5.5 for the studied gelator-free nematic phases and the corresponding nematic gels. Reprinted from the Supporting Information of Ref.<sup>[163]</sup>

Sample	$d_c$ / [Å]	$\xi$ / [Å]
Gelator-free $N_d$	60.8	156.6
$N_d$ , 1 wt% DBS	59.4	142.5
$N_d$ , 2 wt% DBC	80.6	154.5
Gelator-free $N_c$	59.0	57.8
$N_c$ , 1 wt% DBS	57.7	51.3
$N_c$ , 2 wt% DBC	90.9	94.9

The mean micellar to micellar distance (for the  $N_d$  phase along the director, for the  $N_c$  phase perpendicular to it) is calculated from the SAXS data using the Bragg equation  $d_c = 2\pi/q_c$ . For the nematic gels obtained with DBS the intermicellar distance is in the same range as for the gelator-free nematic phases. Contrary, a pronounced increase of the intermicellar distance in the order of 20 - 30 Å is noticed for the nematic gels obtained with DBC. An explanation for the enlargement of the intermicellar distance due to gelation with DBC might be the thickness of the DBC gel fibers. As revealed by FFEM, the DBS fiber diameter is  $\sim 6.5$  nm, which is in the range of the intermicellar distance (6.1 nm and 5.9 nm for the gelator-free  $N_d$  and  $N_c$  phases, respectively). The fibers formed from DBC however are about 10 nm thick which exceeds the intermicellar distance of the gelator-free nematic phases. While the DBS fibers can easily be incorporated into the nematic phases, a local widening of micellar arrangement is necessary to incorporate the DBC fibers into the nematic structure significantly. However, it is questionable whether the fraction of gel fibers formed by the addition of only 2 wt% DBC is sufficient to explain the observed increase in the intermicellar distance.

### 5.3 Conclusion

For the first time, micellar lyotropic nematic gels were obtained by adding low molecular weight gelators to micellar nematic phases. The key to obtain micellar nematic gels turned out to be the use of gelators which have a bulky and non-amphiphilic molecular structure and are thus unable to change the shape of the anisometric micelles. A chirality transfer from the twisted gel fibers to the nematic phase leading to cholesteric gels is noticed in certain cases. By means of 2D X-ray scattering the

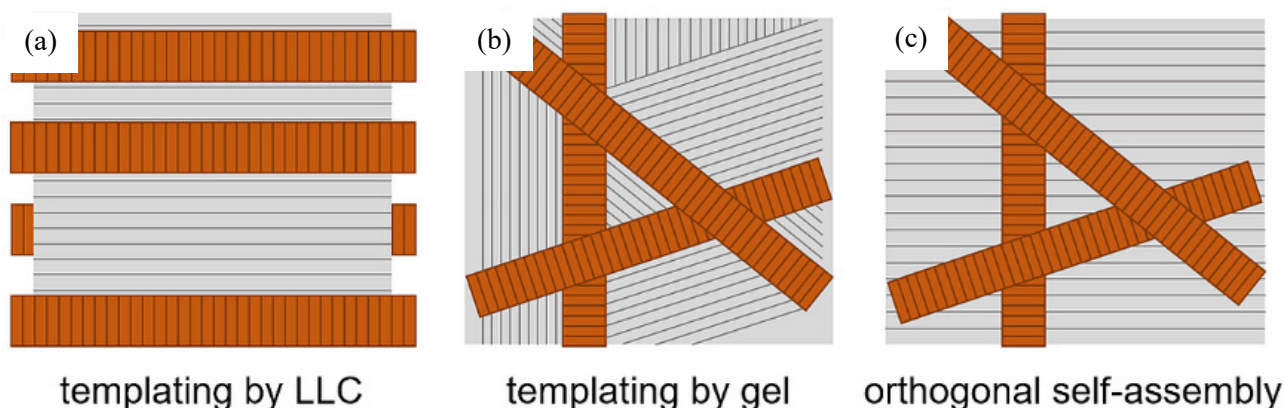


existence of macroscopically aligned nematic gels was demonstrated. This new kind of anisotropic hydrogels is most interesting for applications in stimuli-responsive water-based actuation and sensing systems. The fabrication of large monodomains of lyotropic nematic gels and the investigation of their stimuli-responsive behavior is the next important and most promising step in the research of lyotropic liquid-crystalline gels.

## 6 Synergistic structures in lyotropic lamellar gels (Publication III)

As presented in chapter 4 the lyotropic lamellar phase is most straightforward to gel. In this chapter the mutual influence of the  $L_\alpha$  phase and the fiber network will be discussed. Furthermore, the structure of the lamellar gels obtained with 12-HOA with those obtained using the gelator DBS will be compared. While both gelators form twisted gel fibers, they substantially differ in the thickness of the fibers. DBS forms rather thin fibers (4 – 8 nm)<sup>[297]</sup>, whereas 12-HOA forms rather thick fibers (21 – 33 nm)<sup>[281]</sup>.

Before starting this study, three possible scenarios on the resulting structure of the lamellar gels were anticipated (see Figure 6.1). Two scenarios are based on a soft-templating mechanism, in which either the  $L_\alpha$  phase directs the orientation of the gel network resulting in an anisotropic fiber network or the gel network guides the orientation of the lamellar phase leading to a polydomain morphology. Similar to what was found in thermotropic LC physical gels the structure that forms first might determine the morphology of the second structure.<sup>[119]</sup> A third option could be that the two structures form simultaneously and independent of each other, a scenario that is called orthogonal self-assembly.<sup>[6,311,312]</sup>



**Figure 6.1:** Possible structures of a lyotropic lamellar gel. *a), b)* One of the two structures guides the orientation of the other one due to a templating mechanism. *c)* Both structures form independently of each other resulting in an orthogonal self-assembled system. Adapted with permission from S. Dieterich *et al.*, *Langmuir* **2019**, *35*, 16793.<sup>[162]</sup> Copyright 2019 American Chemical Society.

Other studies presented in the course of our DFG project on gelled lyotropic liquid crystals conclude that structure and properties of gel network and LLC remain essentially unchanged by the presence of each other.<sup>[136,243,297,298]</sup> It was shown that the chronology of DBS gel and LLC formation has no significant influence on the actual LLC gel structure.<sup>[297]</sup> All these studies have in common that

structural investigations were limited on length scales of up to 10 nm. To solve the question whether the gel network or the LLC morphologies are changed by the presence of the other, also investigations on larger length scales are necessary.

Since length scales up to 500 nm are accessible with small angle neutron scattering, a systematic SANS study was carried out. Furthermore, the possibility of contrast variation experiments allows to observe the individual contributions of the fiber network and the lamellar phase to the scattering profile. The results of the SANS study are reported in this chapter leading to the conclusion that none of the three scenarios shown in Figure 6.1 apply for lamellar gels with 12-HOA as gelator, but instead a new synergistic structure is formed in the lyotropic lamellar gel, which do not exist in the two parent systems, namely the non-gelled  $L_\alpha$  phase and the binary gel.

## 6.1 Specific background

### 6.1.1 Small-angle neutron and X-ray scattering – a comparison

Please note that this chapter is not intended to give a comprehensive introduction into elastic scattering and instrumentation of SANS experiments. For scattering theory, textbooks like in Ref.<sup>[185,313]</sup> are recommended and details on the used instruments (D11 at ILL and NG7 at NIST) can be found on the facilities' webpages.<sup>[314,315]</sup>

The mechanism of scattering is quite different for neutrons and X-rays since it depends on the nature of the interaction between the radiation probe and the sample. However, the emergence of the interference pattern from the scattered waves and its calculation is similar for both, neutron and X-ray scattering.

With the approximation that the interaction with a scatterer does not depend on the scattering by other scatterers (no multiple scattering, Born approximation), the amplitude  $A(\mathbf{q})$  of the scattered wave as received by the detector at the scattering vector  $\mathbf{q}$  is<sup>[316,317]</sup>

$$A(\mathbf{q}) = \int_V \rho(\mathbf{r}) e^{-i\mathbf{q}\mathbf{r}} d\mathbf{r}, \quad (6.1)$$

with  $A(\mathbf{q})$  being the Fourier transform of the scattering length density distribution  $\rho(\mathbf{r}) = \sum_i \rho_i(\mathbf{r}) \cdot b_i$ . Thereby,  $\rho_i(\mathbf{r})$  is the local density of scatterers of type  $i$  and  $b_i$  is called the scattering length which is a measure of the scattering power of a scattering center for the used radiation

probe.<sup>[317,318]</sup>

In the case of a two-component system including one phase (*e.g.* colloidal particles) with a volume fraction  $\phi$  and a scattering length density  $\rho_1$  and a second phase (*e.g.* solvent) with a scattering length density  $\rho_2$  and a volume fraction  $(1 - \phi)$ , the scattering length density distribution reads<sup>[318,319]</sup>

$$\rho(\mathbf{r}) = \begin{cases} \rho_1 & \text{in } V_1 = \phi \cdot V \\ \rho_2 & \text{in } V_2 = (1 - \phi) \cdot V \end{cases} \quad (6.2)$$

Then the amplitude is<sup>[318]</sup>

$$A(\mathbf{q}) = \int_{\phi V} \rho_1 e^{-i\mathbf{q}\mathbf{r}} d\mathbf{r} + \int_{(1-\phi)V} \rho_2 e^{-i\mathbf{q}\mathbf{r}} d\mathbf{r} \quad (6.3)$$

which can be rewritten as

$$A(\mathbf{q}) = \int_{\phi V} (\rho_1 - \rho_2) e^{-i\mathbf{q}\mathbf{r}} d\mathbf{r} + \rho_2 \int_V e^{-i\mathbf{q}\mathbf{r}} d\mathbf{r}. \quad (6.4)$$

The second term is not measured in a scattering experiment since the mean density of scatterers leads to a signal in forward direction ( $q = 0$ ) only. Scattering is solely caused by variations in the scattering length density.<sup>[318]</sup>

Since the scattering intensity per unit volume is

$$I(\mathbf{q}) = \frac{A(\mathbf{q})A^*(\mathbf{q})}{V}, \quad (6.5)$$

the scattering intensities for discrete inhomogeneities (*e.g.* particles) in the scattering length density distribution can be described as<sup>[317,319]</sup>

$$I(\mathbf{q}) = \frac{N}{V} \cdot (\Delta\rho)^2 \cdot P(\mathbf{q}) \cdot S(\mathbf{q}). \quad (6.6)$$

The measured scattering intensity is proportional to the number density  $\frac{N}{V}$  of scatterers, the contrast factor  $(\Delta\rho)^2$ , the form factor  $P(\mathbf{q})$  and the structure factor  $S(\mathbf{q})$ .

The form factor<sup>[185]</sup>

$$P(\mathbf{q}) = \left\langle \left[ \int_{V_p} \rho(\mathbf{r}) e^{-i\mathbf{q}\mathbf{r}} d\mathbf{r} \right]^2 \right\rangle \quad \text{“intraparticle interference”} \quad (6.7)$$

describes the size and shape of the scattering object with volume  $V_p$  while the structure factor<sup>[316,318]</sup>

$$S(\mathbf{q}) = 1 + \frac{N-1}{V} \cdot \int_V [g(\mathbf{r}) - 1] e^{-i\mathbf{q}\mathbf{r}} d\mathbf{r} \quad \text{“interparticle interference”} \quad (6.8)$$

considers the interference between different scattering objects with the pair-correlation function  $g(\mathbf{r})$ .

According to equation (6.6), the scattering intensity depends on the scattering contrast, which reflects the interaction between the probing radiation and the investigated sample of matter. In X-ray scattering, the electromagnetic radiation is scattered by the electrons of the atoms (Thomson scattering), where the scattering arises like for free electrons. The fraction of incoming unpolarized radiation scattered by one electron is given by the Thomson scattering length  $b_e$ <sup>[317,320]</sup>

$$b_e^2 = r_e^2 \left( \frac{1 + \cos^2(2\theta)}{2} \right) \quad (6.9)$$

with the classical electron radius  $r_e$ . For small scattering angles the scattering length of the electron cloud of an atom is

$$b = r_e \cdot Z \quad (6.10)$$

with  $Z$  being the number of electrons in the atom. Hence, the scattering amplitude  $A(q)$  corresponds to the Fourier transform of the electron probability density and the contrast arises from the differences in the electron density in the probed matter.<sup>[320]</sup>

In neutron scattering the neutrons interact with the atomic nuclei via the strong nuclear force (and the magnetic moment of the neutron interacts with magnetization density fluctuations of the sample, this magnetic scattering is not discussed in the following). The neutron scattering length  $b$  is a measure for the interaction of the neutrons with nuclei and has a coherent and an incoherent part. The coherent scattering results from the interference of waves scattered at different nuclei and thus contains information about the structure. Additionally, the variation of the nucleus position and spin state causes a fluctuation of the scattering length around its mean value that is uncorrelated with the scattering length fluctuations from another nucleus. The incoming neutron wave is then scattered from

an ensemble of uncorrelated fluctuating scattering lengths which leads to incoherent scattering. This flat incoherent background is independent of  $q$  and thus contains no information about the structure.<sup>[320,321]</sup>

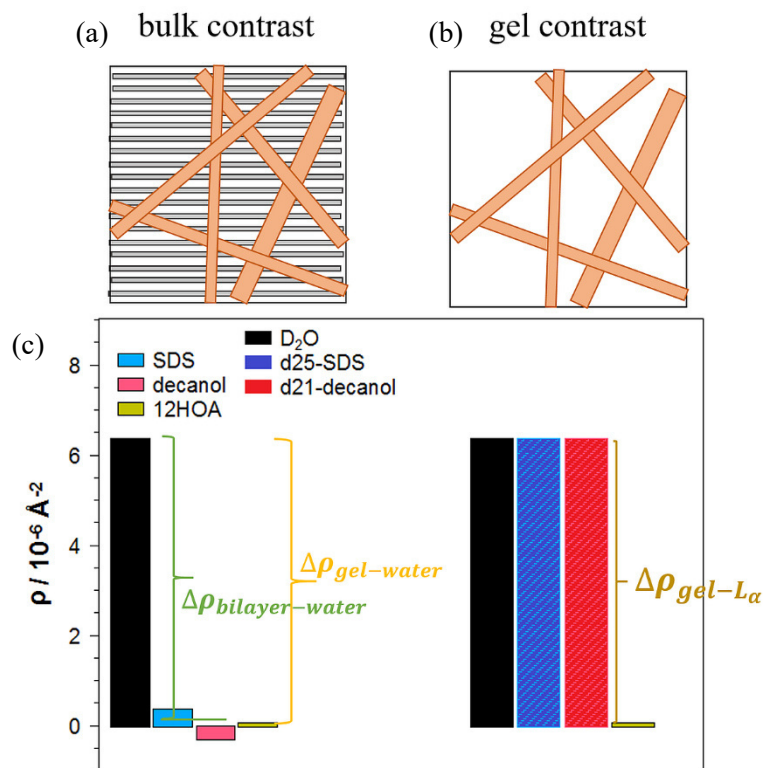
While in X-ray scattering the scattering length increases with increasing atomic number, the magnitude of the neutron scattering length  $b$  varies in an unsystematic way from element to element and even dramatic variations in  $b$  are found for isotopic substitution. In the absence of a theory for nuclear forces, the scattering length has to be determined experimentally.<sup>[317]</sup> The two hydrogen isotopes  $^1\text{H}$  and  $^2\text{H}$  show a large difference in the coherent scattering length with  $b_{^1\text{H}} = -0.374 \cdot 10^{-12} \text{cm}$  and  $b_{^2\text{H}} = 0.668 \cdot 10^{-12} \text{cm}$ ,<sup>[321]</sup> in which a negative value for  $b$  indicates an attractive interaction potential for nucleus and neutron and signifies a shift of  $\pi$  in the phase scattering.<sup>[316,319]</sup> Additionally,  $^1\text{H}$  has an extremely long incoherent scattering length that exceeds the one of  $^2\text{H}$ .

The scattering length density of a molecule is<sup>[316]</sup>

$$\rho_p = \frac{\sum_i x_i b_i}{V_p} = \frac{N_A \rho_p^0}{M_p} \sum_i x_i b_i \quad (6.11)$$

with  $x_i$  atoms of kind  $i$  with the scattering length  $b_i$  and the molecular volume  $V_p = \frac{M_p}{\rho_p^0}$ , with the bulk density  $\rho_p^0$  and the molar mass  $M_p$ .

In colloidal systems of organic materials (polymers, micelles, ...) an excellent contrast is achieved when either the solute or the solvent is deuterated. More important for this study, in a multicomponent system one structure can be highlighted by matching the scattering length density of the other structure with the one of the solvent.<sup>[316,320]</sup> Such kind of a contrast matching experiment is shown in case of a lamellar gel in Figure 6.2. In the so-called bulk contrast, there is a contrast between the bilayers and  $\text{D}_2\text{O}$  and another contrast between the gel fibers and  $\text{D}_2\text{O}$ . If the scattering length of the surfactant and the cosurfactant are adjusted to match the one of  $\text{D}_2\text{O}$  by using mainly deuterated and partly protonated surfactant and cosurfactant, the contrast between the bilayers and  $\text{D}_2\text{O}$  vanishes and only the contrast between the gel fibers and the surrounding  $L_\alpha$  phase remains. In this ‘gel contrast’, the structure of the gel network in the lamellar gel can be studied separately. The possibility to vary the contrast by isotopic substitution is the great advantage of SANS over other scattering techniques.



**Figure 6.2:** The *a)* bulk and *b)* gel scattering contrast of the SANS experiments on lamellar gels and *c)* the scattering length densities  $\rho$  of the components and the respective scattering contrasts  $\Delta\rho$  are shown. The use of  $D_2O$  leads to the observation of the gel network and the surfactant bilayers. Only the gel network is seen when all components (solvent and surfactant) of the lyotropic liquid crystal are deuterated.

### 6.1.2 Data reduction and analysis of Neutron Scattering Data

Data reduction is the crucial step before data analysis. A calibration to absolute scaling ( $I(q) / \text{cm}^{-1}$ ) allows a comparison between data obtained with different scattering sources, at different neutron facilities or at the same instrument but at different  $q$ -ranges (different sample-to-detector distance or different wavelengths).

In an elastic scattering experiment, the quantitative expression for the interaction between the radiation and the sample is the differential scattering cross-section  $\frac{d\sigma}{d\Omega}$  which contains all information on the structure of the sample. As shown in Figure 6.3, the detector counts the number of neutrons scattered in the direction  $2\theta$  into the solid angle  $d\Omega$  and thus the differential scattering cross-section is<sup>[319]</sup>

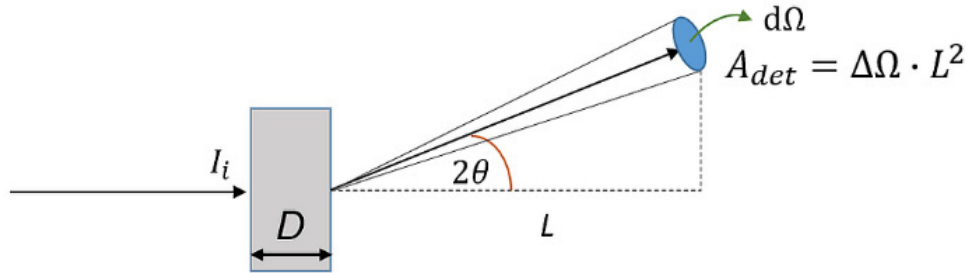
$$\frac{d\sigma}{d\Omega}(q) = \frac{\text{number of neutrons scattered per second in } d\Omega \text{ in direction } 2\theta}{\Phi_0 d\Omega} \quad (6.12)$$

with the incident flux  $\Phi_0$ , *i.e.* the number of incident neutrons per unit area per second. This means that in a scattering experiment the scattered intensity  $I(q)$  measured at an angle  $2\theta$  and a sample-to-detector distance  $L$  is compared with the incident intensity  $I_i$  according to<sup>[321]</sup>

$$\frac{d\sigma}{d\Omega}(q) = \frac{I(q)_{\text{measured}} \cdot L^2}{I_i} \quad (\text{cm}^2). \quad (6.13)$$

Normalization to unit sample volume  $V$  results in the differential scattering cross-section per unit sample volume  $\frac{d\Sigma}{d\Omega}$ , which is the key quantity to obtain in the data reduction procedure since it specifies the probability of a neutron being scattered out from the unit sample volume in the direction  $2\theta$  into the solid angle  $d\Omega$

$$\frac{d\Sigma}{d\Omega}(q) = \frac{1}{V} \cdot \frac{d\sigma}{d\Omega}(q) \quad (\text{cm}^{-1}). \quad (6.14)$$



**Figure 6.3:** Geometry of a scattering experiment with a neutron beam of incident intensity  $I_i$ , sample thickness  $D$  and detector surface area  $A_{det} = \Delta\Omega \cdot L^2$  at sample-to-detector distance  $L$  and scattering angle  $2\theta$ . Redrawn from Ref.<sup>[321]</sup>

The scattering intensity depends on the sample thickness  $D$  and the transmission  $Tr$  of the sample.  $Tr$  is defined as the ratio of the intensities between the neutron beam through the sample and the empty beam (no sample in beam path) at  $q = 0$

$$Tr = \frac{I_{\text{sample}}(0)}{I_{\text{empty beam}}(0)}. \quad (6.15)$$

These intensities are measured by removing the beam stop and bringing an attenuator (neutron absorber such as perforated Cadmium sheets or PMMA) into the direct beam and subsequent



integration of the intensity of the direct beam. The measurement of the empty beam also allows the determination of the beam center, which is crucial for radial averaging. Since neutrons fall under gravity, the beam center position depends on the sample-to-detector distance and the wavelength. Natural radiation and electronic noise from the detection device produce an electronic background, which has to be subtracted from the measured intensity. The electronic background is obtained by bringing a strong neutron absorber (Cadmium or boron carbide  $B_4C$ ) into the beam path in order to stop the incoming beam. The residual measured intensity stems from the electronic background. Additionally, the quartz cell which contains the sample scatters the incoming beam. Thus, the scattering from the empty cell has to be subtracted from the total scattering.<sup>[316,321]</sup>

To calibrate to absolute units, a standard sample with a known scattering cross-section has to be measured

$$\left(\frac{d\Sigma}{d\Omega}\right)_{sample} = \frac{I_{sample}}{I_{standard}} \cdot \left(\frac{d\Sigma}{d\Omega}\right)_{standard} \quad (6.16)$$

Water is commonly used as standard since it shows a flat scattering practically independent from the scattering angle (mainly incoherent scattering). For large sample-to-detector distances no water measurements are performed due to the small scattering intensity and thus long acquisition time necessary for a good signal to noise ratio. Instead, a scaling factor  $F_{sc}$  is used to transfer the calibration measurement from a shorter sample-to-detector distance (*e.g.* 8 m) to the large one (*e.g.* 39 m).<sup>[316,321]</sup>

Finally, the normalized scattering intensity is given by<sup>[316]</sup>

$$I(q) = \left(\frac{d\Sigma}{d\Omega}\right)_{sample} = \frac{1}{F_{sc}} \left(\frac{d\Sigma}{d\Omega}\right)_{H_2O} \frac{\left[\frac{I_{sample} - I_{B_4C}}{Tr_{sample}} - \frac{I_{empty cell} - I_{B_4C}}{Tr_{empty cell}}\right] \frac{1}{D_{sample}}}{\left[\frac{I_{H_2O} - I_{B_4C}}{Tr_{H_2O}} - \frac{I_{empty cell} - I_{B_4C}}{Tr_{empty cell}}\right] \frac{1}{D_{H_2O}}}, \quad (6.17)$$

where the intensities  $I_{sample}$ ,  $I_{B_4C}$ ,  $I_{empty cell}$  and  $I_{H_2O}$  are normalized with regard to the respective measuring time. The normalized intensity from the 2D detector is radially averaged for powder-oriented samples (or sector averaged for anisotropic scattering patterns) to obtain the total intensity  $I(q)$  as a function of  $q$ .

To cover a large  $q$ -range, different measurement settings, *i.e.* different sample-to-detector distances with different collimations, are used. The obtained intensity for the high  $q$ -range (short sample-to-detector distance) and the low  $q$ -range (large sample-to-detector distance) can be slightly inaccurate

since high  $q$ -values are cut-off by the detector edge and for low  $q$ -values the small number of pixels leads to a poor resolution. Usually, the intensity obtained for the different  $q$ -ranges differs slightly in the overlap region. Hence, the intensity measured for the high  $q$ -range and the low  $q$ -range are shifted to meet the intensity of the middle  $q$ -range.

The obtained scattering intensity is the sum of the coherent scattering intensity and the incoherent scattering intensity which does not contain structural information about the sample. The incoherent background is calculated from the measurement at the highest possible  $q$ -values since the scattering objects are usually too large to produce significant coherent scattering at high  $q$ .<sup>[316]</sup>

In summary, the protocol for the data reduction procedure is:

- a) calculate the beam center
- b) calculate the transmissions
- c) subtract the scattering from the empty cell
- d) calibrate to absolute units
- e) perform radial averaging
- f) merge all measured  $q$ -ranges
- g) subtract the incoherent background.

In this study, data reduction was performed using the software provided by the neutron facilities ILL and NIST, *i.e.* LAMP and IGOR Pro, respectively.

### 6.1.3 Neutron scattering from lamellar phases

The  $L_\alpha$  phase consists of infinite planar 2D surfactant bilayers which are stacked periodically in one dimension separated by water sub-layers (see Figure 3.9a). The bilayers are fluid and can thus be deformed elastically resulting in a layer curvature. Thermally induced out-of-layer fluctuations of the fluid bilayers, so-called undulations, stabilize the lamellar structure. The steric hindrance of mutually undulating bilayers leads to a repulsive interaction known as Helfrich interaction<sup>[322]</sup> which competes with the attractive van der Waals interaction (even though in unscreened ionic bilayers the electrostatic repulsion dominates and stabilizes the lamellar order).<sup>[323]</sup>

The model evolved by Nallet *et al.*<sup>[324]</sup> was chosen to describe the scattering of a lamellar phase. The Nallet model combines a static (“geometrical”) scattering contribution from planar surfactant bilayers

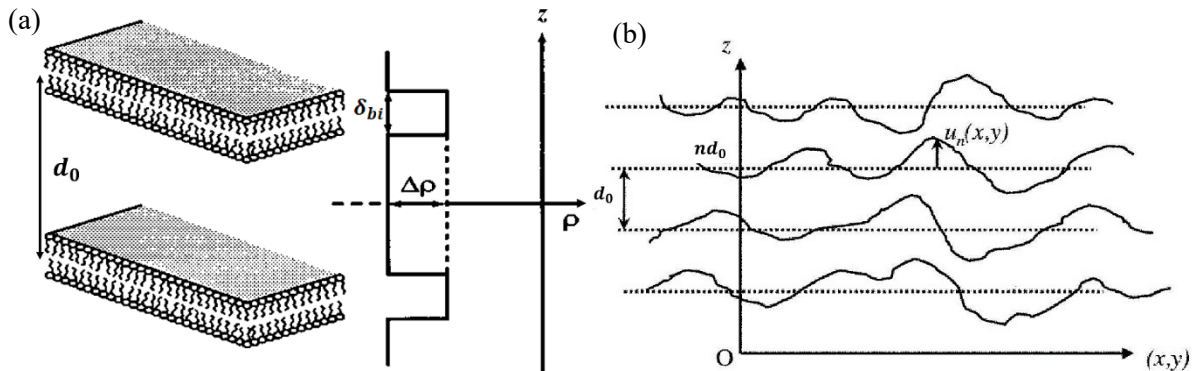
with a dynamic contribution from thermal layer displacement fluctuations. According to the Nallet model, the powder averaged scattering intensity is

$$I(q) = 2\pi \frac{V}{d_0} \cdot \frac{P(q) \cdot S(q)}{q^2}, \quad (6.18)$$

with the irradiated volume  $V$ , the layer repeat unit  $d_0$ , the form factor  $P(q)$  and the structure factor  $S(q)$ . The bilayer form factor  $P(q)$ , which is based on the geometrical model of  $N$  identical bilayers of thickness  $\delta_{bi}$  stacked regularly in the  $z$ -direction with a period  $d_0$  is given by

$$P(q) = \frac{2\Delta\rho^2}{q^2} [1 - \cos(q \cdot \delta_{bi}) \cdot e^{-q^2\sigma_{bi}^2/2}]. \quad (6.19)$$

The polydispersity of the bilayer thickness is taken into account by a Gaussian distribution of  $\delta_{bi}$  with width  $\sigma_{bi}$  (due to the poor resolution at high  $q$ ,  $\sigma_{bi}$  is rather a damping parameter and  $\sigma_{bi} = \delta_{bi}/3.5$  was chosen for all fits). As shown in Figure 6.4a,  $\Delta\rho$  is the scattering length density difference between the surfactant bilayers and the water sub-layers.



**Figure 6.4:** *a)* Geometry of the  $L_\alpha$  phase and the corresponding neutron scattering length density profile along the layer normal. Adapted by permission from Springer Nature, G. Bouglet, C. Ligoure, *EPJB* **1999**, *9*, 137.<sup>[325]</sup> Copyright 1999. *b)* Schematic drawing of the undulations of the stacked bilayers in a  $L_\alpha$  phase. Adapted by permission from Springer Nature, F. Castro-Roman, L. Porcar, G. Porte, C. Ligoure, *EPJE* **2005**, *18*, 259.<sup>[326]</sup> Copyright 2005.

The dynamic contribution to the scattering intensity stems from thermally induced layer displacement fluctuations. It is assumed that the  $n$ -th layer may fluctuate around its equilibrium position  $nd_0$  by an amount  $u_n$  (see Figure 6.4b).<sup>[324]</sup> Following the continuum theory for smectic liquid crystals, the elastic free energy density corresponding to layer displacement is<sup>[327,328]</sup>

$$F = \frac{1}{2} \left[ B \left( \frac{\partial u}{\partial z} \right)^2 + K \left( \frac{\partial^2 u}{\partial x^2} + \frac{\partial^2 u}{\partial y^2} \right)^2 \right], \quad (6.20)$$

with the layer displacement in the  $z$ -direction (normal to the layers)  $u(x, y, z)$  and the bulk moduli of the layer curvature  $K$  and the layer compressibility  $B$ . In lyotropic smectics  $K$  and  $B$  are a measure for the bilayer flexibility and the interactions between the bilayers, respectively.<sup>[329]</sup>

The Landau-Peierls instability states that the thermal layer displacement fluctuations destroy true (infinite) long-range translational order in a 1D periodic medium since the mean square layer displacements  $\langle (u_n - u_0)^2 \rangle$  diverge logarithmically with the sample size.<sup>[330,331]</sup> The resulting quasi-long-range translational order considerably affects the scattering curves of smectic liquid crystals, as described by the Caillé theory.<sup>[332]</sup> Conventional  $\delta$ -function Bragg peaks (as for 3D solids) at  $q_m = m q_0 = \frac{2\pi m}{d_0}$  are replaced with weaker singularities, since the positional correlation function in smectic liquid crystals decays algebraically as  $r^{-\eta}$  with  $\eta$  being the Caillé parameter. Hence, the structure factor parallel and perpendicular to the layers follows an asymptotic power-law behavior

$$S(q_{\perp} = 0, q_{\parallel}) \sim (q_{\parallel} - q_m)^{-2+\eta_m} \quad (6.21)$$

and

$$S(q_{\perp}, q_{\parallel} = q_m) \sim q_{\perp}^{-4+2\eta_m}. \quad (6.22)$$

For powder-oriented samples the averaged structure factor is<sup>[333]</sup>

$$S(q) \sim (q - q_m)^{-1+\eta_m}. \quad (6.23)$$

The power-law exponent  $\eta_m$  is related to the elasticity of the lamellar layers by

$$\eta_m = m^2 \frac{k_B T q_0^2}{8\pi \sqrt{KB}} \quad (6.24)$$

and the exponent  $\eta_1$  of the first harmonic ( $m = 1$ ) is commonly called the Caillé parameter  $\eta$ .

As described above, the tails of the pseudo-Bragg peaks decay following the power-law of equation (6.23) and thus peak shape analysis of high-resolution synchrotron X-ray data was performed to determine  $\eta$  for thermotropic<sup>[334]</sup> and lyotropic<sup>[323,333,335]</sup> smectic phases.

The Nallet model expands the Caillé theory by combining the layer displacement fluctuations with

the geometry of the lamellar phase. The powder-averaged, resolution-limited structure factor of a lamellar stack then reads

$$S(q) = 1 + 2 \sum_1^{N-1} \left(1 - \frac{n}{N}\right) \cos \frac{qd_0 n}{1 + 2\Delta q^2 d_0^2 \alpha(n)} \cdot e^{-\frac{2q^2 d_0^2 \alpha(n) + \Delta q^2 d_0^2 n^2}{2(1 + 2\Delta q^2 d_0^2 \alpha(n))}} \frac{1}{\sqrt{1 + 2\Delta q^2 d_0^2 \alpha(n)}} \quad (6.25)$$

with the correlation function

$$\alpha(n) = \frac{\langle (u_n - u_0)^2 \rangle}{2d_0^2} = \frac{\eta}{4\pi^2} [\ln(\pi n) + \gamma]. \quad (6.26)$$

$N$  is the number of correlated layers in a stack,  $\gamma$  is the Euler's constant and  $\Delta q$  the instrumental resolution function (provided by the respective neutron scattering facility).

In addition to the detailed Nallet model we also used in a second approach simply the sum of two commensurable Lorentzians

$$I(q) = \frac{2A}{\pi} \frac{\xi_0}{4(q - q_0)^2 + \xi_0^2} \quad (6.27)$$

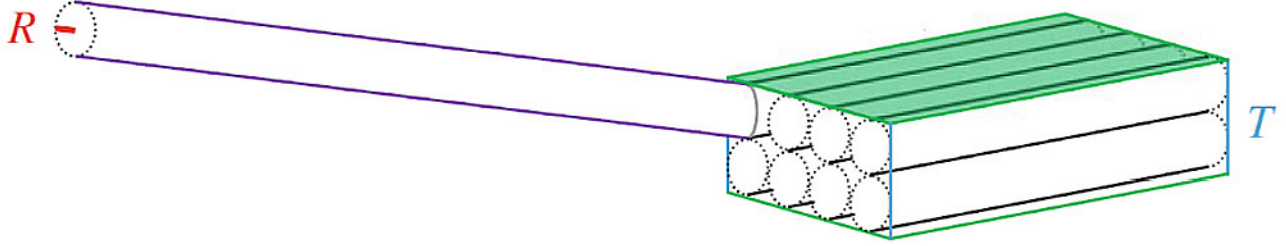
to fit the pseudo-Bragg peaks of the lamellar layers  $q_0$  is the position of the pseudo-Bragg peak,  $\xi_0$  is the full width at half maximum (FWHM) and  $A$  is the area of the peak.

#### 6.1.4 Neutron scattering from fibrillar networks

To describe the scattering of the gel fiber network the model evolved by Terech *et al.*<sup>[258]</sup> and further developed by Laupheimer *et al.*<sup>[267]</sup> was applied. The gel network is treated as a combination of “free” gel fibers considered as stiff cylindrical rods and gel fibers bundled together in a network node (*i.e.* the network junction zones), which are considered as stacked layers of parallel running fibers. The suggested gel network structure is shown in Figure 6.5. It is further assumed that the effective structure factor of the network is  $S_{\text{eff}}(q) = 0$  and only the form factor of the gel fibers and network nodes contribute to the scattering intensity of the gel network.

The scattering intensity of the gel network is thus described by the sum of two independent scattering contributions, the one of the “free” gelator fibers  $I_{\text{fbr}}$  and the one of the nodes  $I_{\text{nds}}$

$$I_{\text{net}} = I_{\text{fbr}} + I_{\text{nds}} \cdot \quad (6.28)$$



**Figure 6.5:** Schematic drawing of the gel network structure consisting of free cylindrical fibers of radius  $R$  and fibers agglomerated in nodes of thickness  $T$ . Adapted from Ref.<sup>[267]</sup> with permission from The Royal Society of Chemistry, Copyright 2014.

Actually, one should add the respective scattering amplitudes and calculate the square of this sum to obtain the total scattering intensity. The cross-term resulting from this is neglected for the sake of simplicity.

The scattering contribution of the gel fibers is given by

$$I_{\text{fbr}} = f \frac{V_{\text{fbr}}}{V} (1 - g) \int_{R=0}^{\infty} \frac{1}{qR^2} \cdot P_{\text{fcs}}(q) \cdot W(R, R_0) dR \quad (6.29)$$

and the one of nodes is described by

$$I_{\text{nds}} = (1 - f) \frac{V_{\text{fbr}}}{V} (1 - g) \cdot \int_{T=0}^{\infty} \frac{8}{Tq^2} \cdot P_{\text{nth}}(q) \cdot W(T, T_0) dT. \quad (6.30)$$

The volume of the fibers formed in the sample  $V_{\text{fbr}}$  is calculated by

$$V_{\text{fbr}} = \frac{m_{12\text{HOA}}}{M_{12\text{HOA}}} N_A \cdot \frac{V_{\text{cell}}}{N_{\text{cell}}} \quad (6.31)$$

with  $V_{\text{cell}} = 1897.3 \text{ \AA}^3$  and  $N_{\text{cell}} = 4$  taken from the monoclinic elementary cell of 12-HOA in the neat crystal.<sup>[336]</sup> The assumption that the crystalline packing of 12-HOA in the gel fibers is the same as in the neat crystal is valid since the (001) and (003) reflections of the “lamellar” 12-HOA structure are visible at the same position in both, the scattering curve of the neat crystal and the gel<sup>[258]</sup> (see also X-ray data in Figure 4.3 of chapter 4.1.2).

The parameter  $f$  describes the fraction of the “free” gel fibers, *i.e.* the part of fibers not agglomerated in nodes. The fraction of gelator, which is not forming fibers but being dissolved monomerically in the solvent is given by the parameter  $g$ . The form factor of the fiber cross section  $P_{\text{fcs}}(R)$  is given by

$$P_{\text{fcs}}(R) = \left( \frac{R2\pi\Delta\rho \cdot J_1(qR)}{q} \right)^2 \quad (6.32)$$

and the form factor of a lamellar node  $P_{\text{nth}}(T)$  is

$$P_{\text{nth}}(T) = \left( \frac{2\Delta\rho}{q} \sin\left(\frac{qT}{2}\right) \right)^2. \quad (6.33)$$

$\Delta\rho$  is the scattering length density difference between the fiber network and the respective solvent. The polydispersity of the mean gel fiber radius  $R_0$  and the mean thickness of a lamellar node  $T_0$  is taken into account by a Gaussian distribution as size distribution function

$$W(X, X_0) = \frac{1}{\sigma_X \sqrt{2\pi}} e^{-\frac{(X-X_0)^2}{2\sigma_X^2}}. \quad (6.34)$$

The measure for the polydispersity is the standard deviation  $\sigma_X$ .

## 6.2 Results and Discussion

This section is organized in three parts. First, the SANS results are discussed qualitatively with regard to the question whether and how the structure of the lamellar phase is modified in the gelled state. The differences in the scattering curves of the  $L_\alpha$  phase gelled with either DBS or 12-HOA are addressed and we compare them to the scattering curves of the reference systems, namely the gelator-free  $L_\alpha$  phase, the binary gel and the gelled isotropic micellar phase.

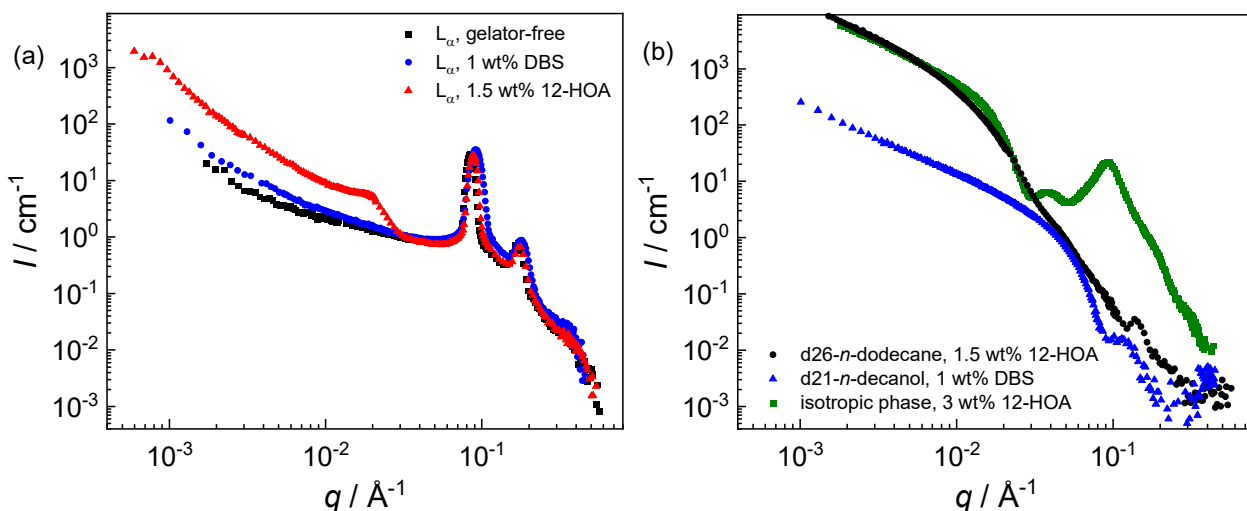
In the second part, the SANS data is analyzed quantitatively using different models in order to compare structural parameters of the gelled  $L_\alpha$  phase with its reference systems. Finally, a model for the synergistic structure present in lamellar gels is evolved.

### 6.2.1 Indications of a new synergistic structure in lyotropic lamellar gels

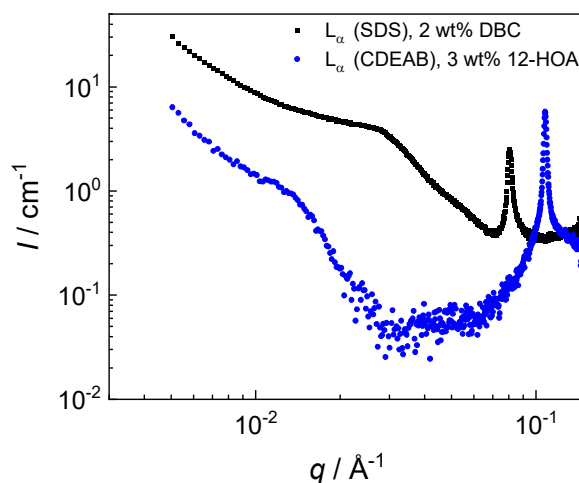
In Figure 6.6a the bulk contrast SANS curves of the gelator-free  $L_\alpha$  phase and the corresponding lamellar gels obtained with DBS (blue) or 12-HOA (red) are shown. The  $I(q)$ -curve of the DBS gelled  $L_\alpha$  phase more or less exactly matches the curve of the gelator-free lamellar phase. This leads to the conclusion that the lamellar structure is not significantly disturbed by the presence of the DBS gel fibers. It seems like the relatively thin DBS gel fibers (4 – 8 nm), which match the lamellar repeat unit (7.5 nm), can be incorporated in the lamellar layer stacking without breaking too many layers.

In contrast, the SANS curve of the  $L_\alpha$  phase gelled with 12-HOA shows a remarkable difference to both the curve of the gelator-free and the DBS gelled  $L_\alpha$  phase: at  $q \approx 0.017 \text{ \AA}^{-1}$  a pronounced shoulder is observed. As shown in Figure 6.7, similar observations are made in other gelled  $L_\alpha$  phases as well. Figure 6.6b shows the SANS curves of the gelled reference systems, namely the binary gel (d26-*n*-dodecane / 12-HOA and isotropic micellar phase of the same lyotropic system gelled with 12-HOA. The latter was chosen for comparison since its polarity is similar to the one of the  $L_\alpha$  phase. The polarity of a solvent can have strong impact on structure and properties of a formed gel network.<sup>[224,226,228,230,251,264,337]</sup> By gelling samples of similar polarity, differences between a gelled isotropic phase and a gelled  $L_\alpha$  phase can be attributed to the difference between an isotropic and an anisotropic solvent. None of the scattering curves of the different isotropic gels shows a broad shoulder at low  $q$ -values. These findings thus indicate the formation of a new synergistic structure in the lamellar gel, which is neither present in the gelator-free  $L_\alpha$  phase nor in the isotropic gel, in case the fiber diameter significantly exceeds the lamellar repeat unit.





**Figure 6.6:** Double logarithmic representation of the SANS curves (total coherent scattering intensity  $I(q)$  vs  $q$ ) of *a*) the gelator-free  $L_\alpha$  phase of the system  $D_2O - n\text{-decanol} - SDS$  ( $\phi_w = 0.675$  and  $\phi_{DOH/SDS} = 0.5$ , black squares), the corresponding  $L_\alpha$  phase gelled with 1 wt% DBS (blue circles) and the  $L_\alpha$  phase gelled with 1.5 wt% 12-HOA (blue triangles) and *b*) the binary gel d26-*n*-dodecane / 12-HOA ( $\mu = 0.015$ , black circles), the binary gel d21-*n*-decanol / DBS ( $\mu = 0.01$ , blue triangles) and the isotropic micellar phase of the system  $D_2O - n\text{-decanol} - SDS$  gelled with 3 wt% 12-HOA ( $\phi_w = 0.75$  and  $\phi_{DOH/SDS} = 0.17$ , green squares). Adapted from Ref.<sup>[164]</sup> with permission from The Royal Society of Chemistry, Copyright 2020.



**Figure 6.7:** Double logarithmic representation of the SAXS curves (total coherent scattering intensity  $I(q)$  vs  $q$ ) of the  $L_\alpha$  phase of the system  $H_2O - n\text{-decanol} - SDS$  gelled with 2 wt% DBC (black squares) and the  $L_\alpha$  phase of the system  $H_2O - n\text{-decanol} - CDEAB$  gelled with 3 wt% 12-HOA (blue circles). Since the fiber diameter of DBC gel fibers ( $\sim 15$  nm) is smaller than of 12-HOA gel fibers ( $\sim 25$  nm), the broad shoulder of the DBC gelled  $L_\alpha$  phase is at higher  $q$ -values.

### 6.2.2 Detailed analysis of SANS data

Basically, there are three scattering contributions to the bulk scattering curves  $I(q)$  of the  $L_\alpha$  phase gelled with 12-HOA to be considered: Besides the scattering of the lamellar liquid-crystalline structure  $I_{\text{lam}}(q)$  and the scattering of the gel network fibers  $I_{\text{net}}(q)$ , the scattering contribution of the synergistic structure has to be taken into account. Thus, in a first approximation the total coherent scattering intensity is described as the weighted sum of the three contributions while neglecting all cross-terms between these contributions

$$I(q) = I_{\text{lam}}(q) + w_{\text{net}}I_{\text{net}}(q) + w_{\text{syn}}I_{\text{syn}}(q). \quad (6.35)$$

The weighting factors  $w_{\text{net}}$  and  $w_{\text{syn}}$  reflect the volume fraction and the scattering length density difference of the gel fiber network and the synergistic structure, respectively.

The scattering contribution of the lamellar structure  $I_{\text{lam}}(q)$  is taken into account by two different models. In the first approach, the elaborate model developed by Nallet *et al.*<sup>[324]</sup> is used, which combines the geometry of a lyotropic lamellar phase with its thermodynamics, to be precise with the thermally induced layer displacement fluctuations. From the fit of the experimental scattering data with the Nallet model (Figure 6.8a) we obtain the bilayer thickness  $\delta_{bi}$ , the layer repeat period  $d_0$  and the Caillé parameter  $\eta$ . The Caillé parameter is a measure for the elasticity of the bilayers since  $\eta$  is related to the layer curvature modulus  $K$  and the layer compressibility modulus  $B$  by equation (6.24). The Nallet model is known to poorly reproduce the SANS data in the low- $q$  regime since it predicts a strong increase in diffuse scattering intensity in this regime. This shortcoming can also be observed in our case (see the green curve in Figure 6.8a). Nevertheless, the Nallet model was proven to give reasonable values for the Caillé parameter<sup>[326]</sup>, at least in the case of small thermal fluctuations, *i.e.* “hard smectic order”, which also applies for the here investigated  $L_\alpha$  phase.

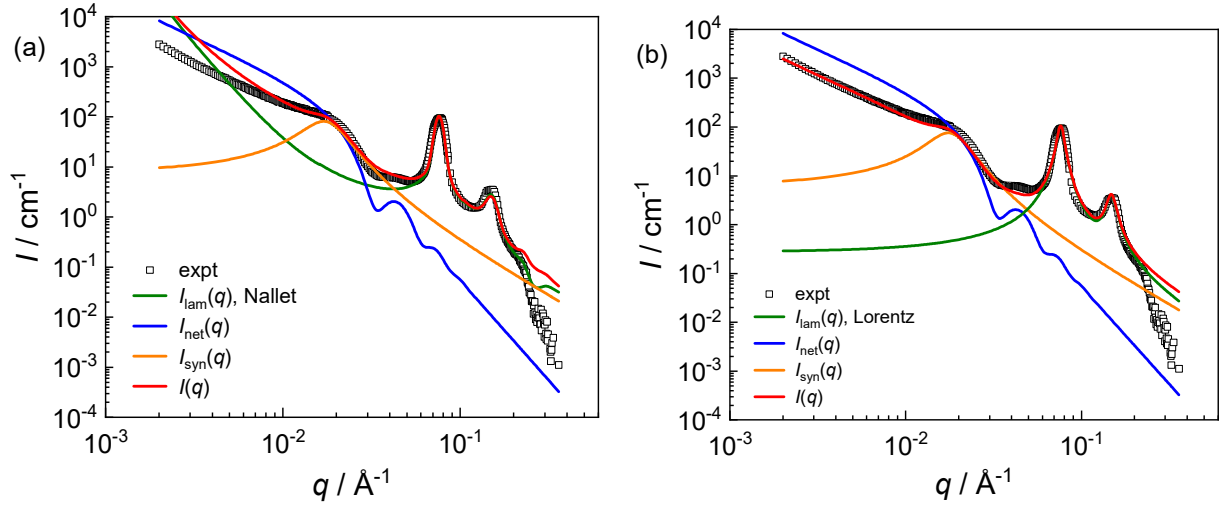
For the lamellar gel however, the scattering intensity at low  $q$ -values is dominated by the gel network contribution. Thus, a second approach was used to describe the scattering contribution  $I_{\text{lam}}(q)$  of the  $L_\alpha$  phase. To better reproduce the scattering at low  $q$ , the sum of two Lorentzians at  $q = 2\pi/d_0$  and  $4\pi/d_0$  was used to fit the two orders of pseudo-Bragg layer peaks in the experimental SANS data.

The scattering contribution of the fiber network  $I_{\text{net}}(q)$  was modeled using the approach of Téreché *et al.*<sup>[258]</sup>, as outlined in section 6.1.4. According to Téreché, the gel network can be considered as a combination of “free” gelator fibers and fibers which are agglomerated in the network nodes. The

fit parameters to reproduce the experimental SANS data are the fraction of “free” gelator fibers  $f$  not involved in nodes, the fraction of monomerically dissolved gelator  $g$  not forming fibers, the mean radius of the fibers  $R_0$  and the mean thickness of the nodes  $T_0$ . The polydispersity of  $R_0$  and  $T_0$  is included by the standard deviations  $\sigma_R$  and  $\sigma_T$ , respectively. It was found that most fibers are free and not bundled in nodes. To decrease the number of fit parameters, the parameters  $T_0$  and  $\sigma_T$  were fixed at reasonably constant values, since  $T_0$  and  $\sigma_T$  have no considerable impact on the scattering contribution  $I_{\text{net}}(q)$ . Finally, the scattering contribution of the new synergistic structure  $I_{\text{syn}}(q)$  was considered in a phenomenological way by a Lorentzian with a peak position  $q_c$  and a full width at half maximum (FWHM)  $\xi_c$ .

In Figure 6.8 the individual scattering contributions  $I_{\text{lam}}(q)$ ,  $I_{\text{net}}(q)$  and  $I_{\text{syn}}(q)$  to the full fit reproducing the scattering of the  $L_\alpha$  phase gelled with 3 wt% 12-HOA are shown. To compare the two models chosen to describe the scattering from the lamellar structure, the Nallet model and the sum of two commensurable Lorentzians are shown in Figure 6.8a and b, respectively. Both models reproduce the lamellar layer peaks almost quantitatively providing similar values for the layer repeat unit  $d_0$  (see fit parameters in Table 6.1). Choosing one of the models does not affect the fit parameters of the other scattering contributions, neither the one of the fiber network  $I_{\text{net}}(q)$  nor the one of the synergistic structure  $I_{\text{syn}}(q)$ . Hence, only the far simpler analyses obtained with Lorentz fits for  $I_{\text{lam}}(q)$  are discussed in the following. The corresponding analysis containing the Nallet model can be found in the Supplementary Information of reference<sup>[164]</sup>.

The key message from the analysis with the Nallet model is that the Caillé parameter  $\eta$  and thus the bilayer elasticity is not considerably altered in the gelled state regardless whether the used gelator is 12-HOA or DBS ( $\eta = 0.11$  for the  $L_\alpha$  phase gelator-free,  $\eta = 0.11$  for the  $L_\alpha$  phase gelled with 1.5 wt% 12-HOA,  $\eta = 0.13$  for the  $L_\alpha$  phase gelled with 3 wt% 12-HOA and  $\eta = 0.11$  for the  $L_\alpha$  phase gelled with 1 wt% DBS).



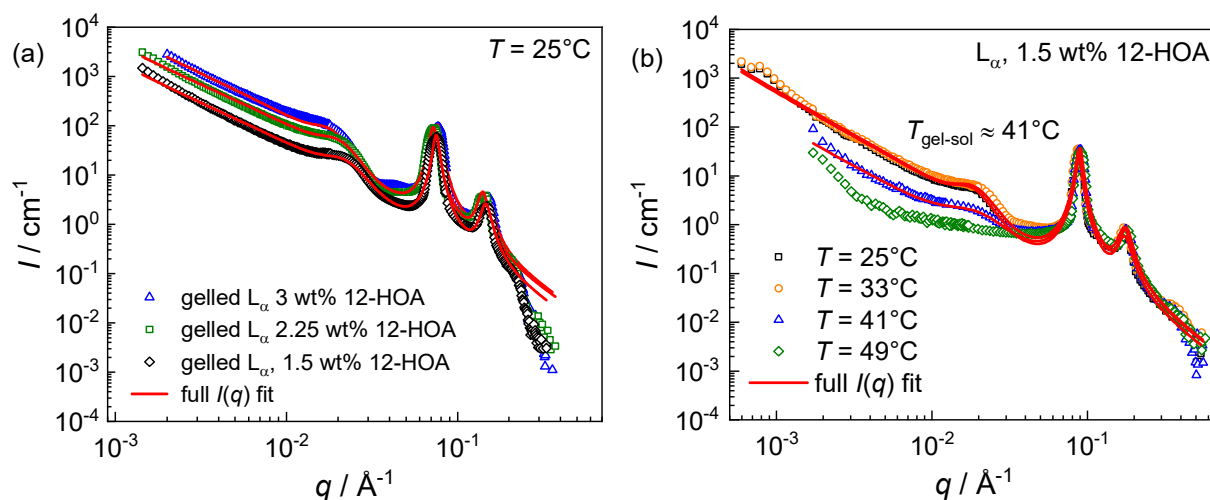
**Figure 6.8:** Analysis of the total coherent scattering intensity  $I(q)$  of the lamellar phase ( $\phi_w = 0.675$  and  $\phi_{DOH/SDS} = 0.5$ ) gelled with 3 wt% 12-HOA.  $I_{\text{lam}}(q)$ ,  $I_{\text{net}}(q)$  and  $I_{\text{syn}}(q)$  are the calculated scattering contributions from the lamellar liquid-crystalline structure, the gel fiber network and the synergistic structure, respectively.  $I_{\text{lam}}(q)$  is calculated using the Nallet model in *a*) and by two commensurable Lorentzians in *b*). All fit parameters are listed in Table 6.1. Adapted from Ref.<sup>[164]</sup> with permission from The Royal Society of Chemistry, Copyright 2020.

**Table 6.1:** Fit parameters obtained from the analysis of the SANS data shown in Figure 6.8. Parameters of the scattering contribution  $I_{\text{lam}}(q)$  of the lamellar structure are the bilayer thickness  $\delta_{bi}$ , the Caillé parameter  $\eta$ , the lamellar repeat distance  $d_0$  and the layer peak FWHM  $\xi_0$ . Parameters of the contribution from the gel fiber network  $I_{\text{net}}(q)$  are the mean fiber radius  $R_0$  and its distribution  $\sigma_R$ , the fraction  $f$  of gel fibers not bundled in nodes and the fraction  $g$  of monomerically dissolved gelator. Parameters of the contribution  $I_{\text{syn}}(q)$  from the synergistic structure are the characteristic length  $d_c$  and the distribution parameter  $\xi_c$ . Contributions of  $I_{\text{net}}(q)$  and  $I_{\text{syn}}(q)$  are weighted with the parameters  $w_{\text{net}}$  and  $w_{\text{syn}}$ , respectively. All fits are performed with fixed values of the node thickness  $T_0 = 40$  nm and its distribution  $\sigma_T = 5$  nm. Reproduced from Ref.<sup>[164]</sup> with permission from The Royal Society of Chemistry, Copyright 2020.

	$I_{\text{lam}}(q)$				$I_{\text{net}}(q)$				$I_{\text{syn}}(q)$			
	$\delta_{bi} /$ nm	$\eta$	$d_0$ nm	$\xi_0 /$ $\text{nm}^{-1}$	$w_{\text{net}}$	$R_0 /$ nm	$\sigma_R /$ nm	$f$	$g$	$w_{\text{syn}}$	$d_c /$ nm	$\xi_c /$ $\text{nm}^{-1}$
Figure 6.8a (Nallet)	2.4	0.13	8.2	-	0.3	11.5	1.3	0.87	0.10	0.7	37	0.011
Figure 6.8 b (Lorentz)	-	-	8.3	0.009	0.3	11.5	1.3	0.87	0.10	0.7	37	0.011

Now the impact of gelator content and temperature on the SANS curves of the  $L_\alpha$  phase with 12-HOA is discussed. As shown in Figure 6.9a, with increasing gelator mass fraction  $\mu$  the scattering intensity at low and intermediate  $q$  ( $q < 0.05 \text{ \AA}^{-1}$ ) is systematically increasing, indicating that both the contribution from the gel fiber network and the contribution from the synergistic structure are increasing. Additionally, the position of the shoulder is shifted to lower  $q$ -values with increasing  $\mu$  and thus the characteristic length of the synergistic structure  $d_c$  increases as  $\mu$  increases (see Table 6.2). Accordingly, the mean fiber radius  $R_0$  increases with increasing  $\mu$  as well.

The temperature dependent SANS measurements clearly support the observation that the new synergistic structure exists in the lamellar gel only. Below the gel-sol transition temperature of  $T_{\text{gel-sol}} = 41^\circ\text{C}$  the characteristic shoulder originating from  $I_{\text{syn}}(q)$  is visible in the SANS curves with the characteristic length  $d_c$  not showing any systematic variation with  $T$ . However, when  $T$  approaches  $T_{\text{gel-sol}}$  the shoulder related to the synergistic structure decreases significantly and vanishes completely above  $T_{\text{gel-sol}}$ . Accordingly, the amount of gelator  $g$  monomerically dissolved in the  $L_\alpha$  phase considerably increases at  $T_{\text{gel-sol}}$ .



**Figure 6.9:** a) Total coherent scattering intensity  $I(q)$  at  $25^\circ\text{C}$  of the  $L_\alpha$  phase ( $\phi_w = 0.675$  and  $\phi_{\text{DOH/SDS}} = 0.5$ ) gelled with different mass fractions of the gelator 12-HOA (symbols) and the corresponding  $I(q)$  fits (lines). Fit parameters are listed in Table 6.2. b)  $I(q)$  of the  $L_\alpha$  phase ( $\phi_w = 0.675$  and  $\phi_{\text{DOH/SDS}} = 0.5$ ) with fixed 12-HOA gelator mass fraction of  $\mu = 0.015$  at different temperatures  $T$  and the corresponding  $I(q)$  fits. Fit parameters are listed in Table 6.3. At temperatures above the gel-sol transition temperature  $T_{\text{gel-sol}}$  the shoulder of the synergistic structure disappears. Reproduced from Ref.<sup>[164]</sup> with permission from The Royal Society of Chemistry, Copyright 2020.

**Table 6.2:** Fit parameters from the analyses of SANS data in Figure 6.9a ( $L_\alpha$  phase ( $\phi_w = 0.675$  and  $\phi_{DOH/SDS} = 0.5$ ) gelled with different mass fractions  $\mu$  of gelator 12-HOA). Parameters of the contribution  $I_{\text{lam}}(q)$  of the lamellar structure are the lamellar repeat distance  $d_0$  and the layer peak FWHM  $\xi_0$ . Parameters of the contribution from the gel fiber network are the mean fiber radius  $R_0$  and its distribution  $\sigma_R$ , the fraction  $f$  of gel fibers not bundled in nodes and the fraction  $g$  of monomerically dissolved gelator. Parameters of the contribution  $I_{\text{syn}}(q)$  from the synergistic structure are the characteristic length  $d_c$  and the distribution parameter  $\xi_c$ . Contributions of  $I_{\text{net}}(q)$  and  $I_{\text{syn}}(q)$  are weighted with the parameters  $w_{\text{net}}$  and  $w_{\text{syn}}$ , respectively. All fits are performed with fixed values of the node thickness  $T_0 = 40$  nm and its distribution  $\sigma_T = 5$  nm. Reproduced from Ref.<sup>[164]</sup> with permission from The Royal Society of Chemistry, Copyright 2020.

$\mu$	$I_{\text{lam}}(q)$		$w_{\text{net}}$	$I_{\text{net}}(q)$				$w_{\text{syn}}$	$I_{\text{syn}}(q)$	
	$d_0/\text{nm}$	$\xi_0/\text{nm}^{-1}$		$R_0/\text{nm}$	$\sigma_R/\text{nm}$	$f$	$g$		$d_c/\text{nm}$	$\xi_c/\text{nm}^{-1}$
0.015	8.4	0.09	0.28	10.5	1.7	0.90	0.10	0.72	31	0.16
0.0225	8.7	0.09	0.28	11.0	1.5	0.90	0.10	0.72	33	0.135
0.03	8.3	0.09	0.30	11.5	1.3	0.87	0.10	0.7	37	0.11

**Table 6.3:** Fit parameters from the analyses of SANS data in Figure 6.9b ( $L_\alpha$  phase ( $\phi_w = 0.675$  and  $\phi_{DOH/SDS} = 0.5$ ) with fixed 12-HOA gelator mass fraction of  $\mu = 0.015$  at different temperatures  $T$ ). Parameters of the contribution  $I_{\text{lam}}(q)$  of the lamellar structure are the lamellar repeat distance  $d_0$  and the layer peak FWHM  $\xi_0$ . Parameters of the contribution from the gel fiber network are the mean fiber radius  $R_0$  and its distribution  $\sigma_R$ , the fraction  $f$  of gel fibers not bundled in nodes and the fraction  $g$  of monomerically dissolved gelator. Parameters of the contribution  $I_{\text{syn}}(q)$  from the synergistic structure are the characteristic length  $d_c$  and the distribution parameter  $\xi_c$ . Contributions of  $I_{\text{net}}(q)$  and  $I_{\text{syn}}(q)$  are weighted with the parameters  $w_{\text{net}}$  and  $w_{\text{syn}}$ , respectively. All fits are performed with fixed values of the node thickness  $T_0 = 40$  nm and its distribution  $\sigma_T = 5$  nm. Reproduced from Ref.<sup>[164]</sup> with permission from The Royal Society of Chemistry, Copyright 2020.

$T / ^\circ\text{C}$	$I_{\text{lam}}(q)$		$w_{\text{net}}$	$I_{\text{net}}(q)$				$w_{\text{syn}}$	$I_{\text{syn}}(q)$	
	$d_0/\text{nm}$	$\xi_0$		$R_0/\text{nm}$	$\sigma_R/\text{nm}$	$f$	$g$		$d_c/\text{nm}$	$\xi_c$
25	7.1	0.12	0.1	10.5	1.7	0.84	0.10	0.9	36	0.12
33	7.1	0.12	0.1	11.0	1.7	0.84	0.10	0.9	36	0.13
41	7.0	0.12	0.1	11.5	2.0	0.82	0.80	0.9	38	0.23

### 6.2.3 Model for the new synergistic structure

The SANS measurements show that the spatial coexistence of gel fibers and lamellar layers lead to the formation of a synergistic structure, *i.e.* a structure that neither exist in the non-gelled  $L_\alpha$  phase

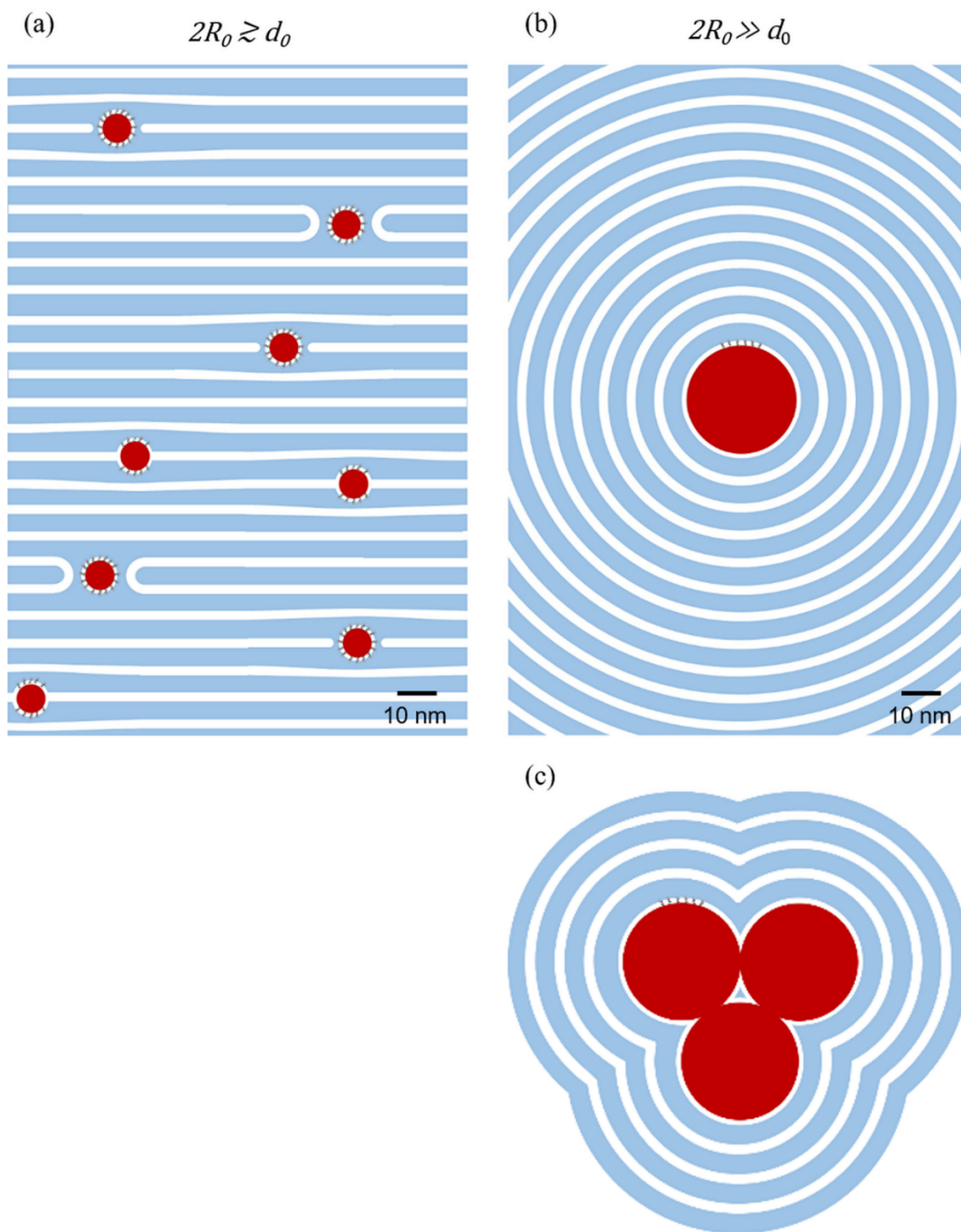
nor in the isotropic gel, in case the fiber diameter significantly exceeds the lamellar repeat unit. The synergistic structure is indicated by a broad Lorentzian-shaped scattering peak at a characteristic length  $d_c$  which is considerably larger than the gel fiber diameter.

What does this synergistic structure look like? First, one has to keep in mind that the  $L_\alpha$  phase is a 1D periodic, anisotropic medium and fibers running through this phase can be considered as a kind of topological defects. The natural response of LCs to such defects is an elastic response and the elastic deformation that cost the least energy in smectic or lamellar liquid crystals is the layer bending. The layer bending corresponds to the director splay, which is the only deformation that conserves the lamellar repeat unit and satisfies the condition that the director is normal to the layers everywhere.<sup>[338]</sup> Hence, each fiber is most likely surrounded by cylindrical lamellar layers, as shown in Figure 6.10b. In this structure, the layers experience pure layer bend and equally important, energy-costly layer ends are avoided. A surfactant monolayer directly attached to the fiber ensures the compatibility of the hydrophobic fiber with the water sub-layers.

Since the elastic energy of the layer bending increases as the square of the layer curvature increases, the energy penalty of the layer bending thus decreases with increasing thickness of the gel fiber. More important, the gel fibers can bundle together to further decrease the elastic energy of the layer bending (see Figure 6.10c). This effect might create the source of a sort of pseudo force which tends to arrange the fibers in bundles.

In contrast, if the length scale of the deformation is small in comparison with the molecular length scale, set for instance by the thickness of the surfactant bilayer  $\delta_{bi}$  or the lamellar spacing  $d_0$ , the elastic response of the liquid crystal breaks down since the layer curvature and thus the elastic bending energy would be far too high.<sup>[339]</sup> In such case, the fibers rather interrupt the lamellar structure causing energy-costly layer ends, *i.e.* the fibers appear like dislocations (see Figure 6.10a). In an energetically more favorable spatial arrangement the hydrophobic fibers can either be surrounded by a surfactant monolayer or cause a passage in the bilayer.

In case of the gelator 12-HOA the fiber diameter  $2R_0$  exceeds the lamellar spacing  $d_0$ , *i.e.*  $2R_0 \gg d_0 > \delta_{bi}$  with  $2R_0 \approx 24$  nm,  $d_0 \approx 8$  nm and  $\delta_{bi} \approx 2.4$  nm and the structure proposed in Figure 6.10b and Figure 6.10c is most likely formed. Contrary, for the gelator DBS the fiber diameter comes close to the molecular length scale, *i.e.*  $2R_0 \approx d_0$  with  $2R_0 \approx 8 \dots 16$  nm and  $d_0 \approx 8$  nm, so that the resulting structure is probably the one suggested in Figure 6.10a.



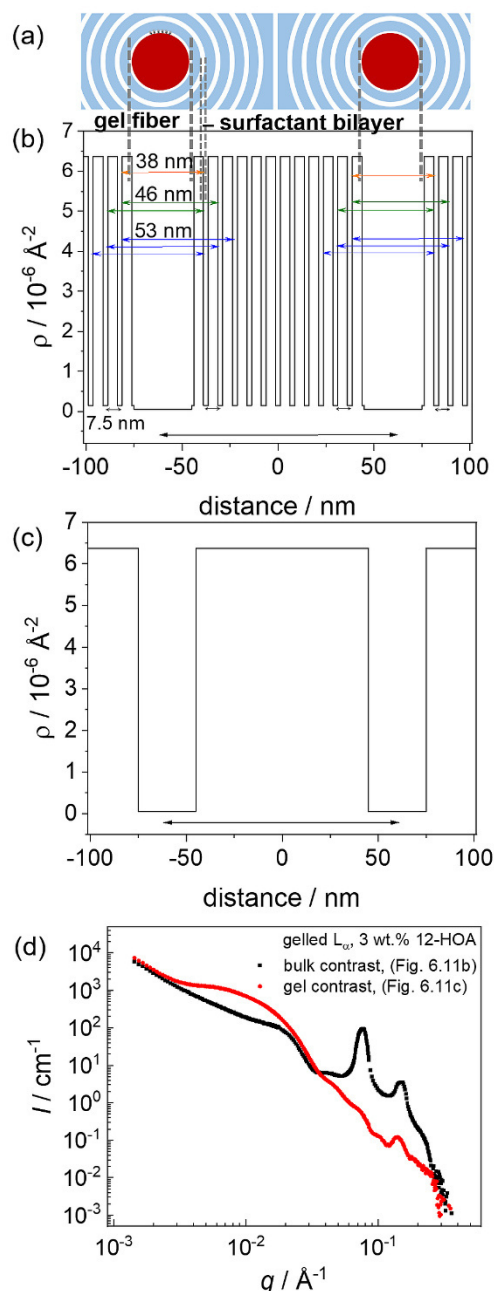
**Figure 6.10:** Comparison of structures formed in lamellar gels if *a*) the gel fiber diameter  $2R_0$  is in the order of the lamellar repeat period  $d_0$  or *b*) substantially exceeds  $d_0$ . In *c*) three fibers bundle together to further reduce the lamellar layer curvature in *(b)*. Cross sections of fibers are colored in red, surfactant bilayers in white and solvent layers in blue. Figures are drawn to scale for the cases of *(a)* DBS fibers and *(b)*, *(c)* 12-HOA fibers. Reproduced from Ref.<sup>[164]</sup> with permission from The Royal Society of Chemistry, Copyright 2020.



But how does a synergistic structure as sketched in Figure 6.10b give rise to a broad Lorentzian shaped scattering maxima indicating a characteristic length of the structure being larger than both, the fiber diameter and the lamellar repeat period? To answer this question, the scattering length density profiles of the proposed synergistic structure in a lamellar gel (Figure 6.11a) in the bulk contrast (Figure 6.11b) and in the “gel contrast” (Figure 6.11c) are compared with their corresponding SANS curves (Figure 6.11d).

As can be seen in the bulk contrast scattering length density profile of the synergistic structure, the periodic lamellar layer stacking is disturbed by the gel fibers. The regular lamellar layer structure and the rather coincidental distance between the gel fibers are incommensurable. But new recurring distances between the lamellar layers appear around the fibers (highlighted by colored arrows in Figure 6.11b), which we believe to be the reason for the broad Lorentzian peak in the bulk scattering curves of 12-HOA lamellar gels.

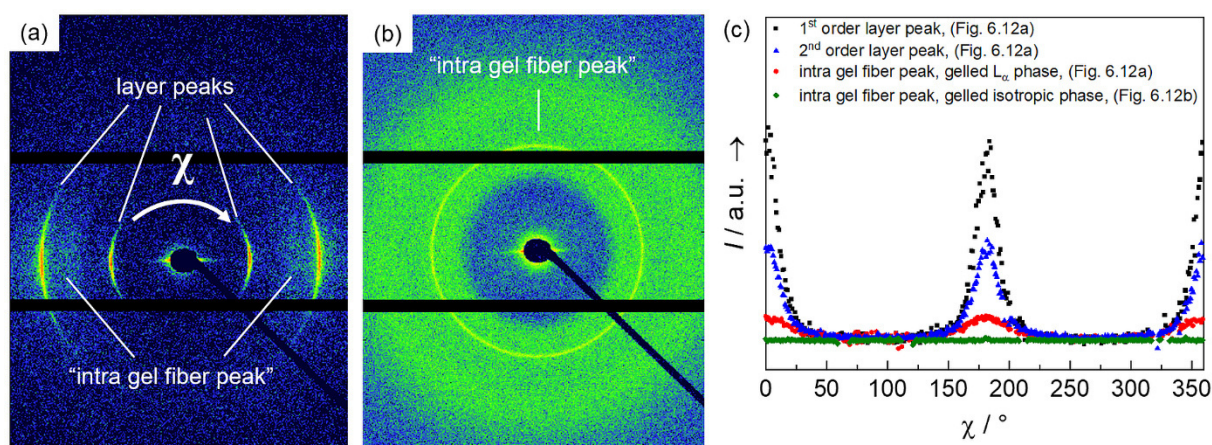
To selectively observe the gel network structure in the lamellar gel, the “gel contrast” is used, in which the contrast between the surfactant bilayers and the water sub-layers is eliminated (Figure 6.11c). The gel contrast is realized by using a mixture of mainly deuterated surfactant (and cosurfactant) with partly protonated surfactant (and cosurfactant), such that the scattering length density of the bilayers match the one of D<sub>2</sub>O. Thus, instead of pseudo-Bragg peaks due to the lamellar layer structure only small bumps remain at high  $q$ -values of the corresponding SANS curve proving our contrast adjustment to be successful (Figure 6.11d). Only the contrast between the gel fibers and the surrounding L <sub>$\alpha$</sub>  phase remains and the only occurring distance in the scattering length density profile is the one between adjacent gel fibers. In the SANS curve of the 12-HOA lamellar gel a very broad shoulder is seen at even lower  $q$ -values in the gel contrast than in the bulk contrast. This indicates that the distance between the gel fibers is considerably larger than the predominant distances in the bulk contrast and its width can be explained due to the even broader distribution of distances between gel fibers. The SANS data of the gelled L <sub>$\alpha$</sub>  phase in the gel contrast thus clearly support our model for the synergistic structure.



**Figure 6.11:** *a)* Synergistic structure in lyotropic lamellar gels with the gel fiber diameter considerably exceeding the lamellar repeat unit. A surfactant monolayer (white) is adsorbed at the surface of the hydrophobic gel fiber (red) and the subsequent layers are circularly wrapped around the fibers. *b)* Scattering length density profile of the suggested synergistic structure. The orange, green and blue arrows indicate the recurring distances leading to the broad Lorentzian peak (“shoulder”) in the SANS profile. *c)* Scattering length density profile for the “gel contrast”, a contrast where due to the use of deuterated surfactant and deuterated cosurfactant only the gel network sub-structure is monitored by the neutrons. *d)* SANS curves of the  $L_{\alpha}$  phase ( $\phi_w = 0.675$  and  $\phi_{DOH/SDS} = 0.5$ ) gelled with 3 wt% 12-HOA in bulk contrast (black squares) and in the gel contrast (red circles). In the gel contrast a mixture of deuterated and protonated surfactant (16.7 v% / 2.4 v%) and cosurfactant (9.6 v% / 0.5 v%) is used to match the scattering length density of  $D_2O$ . Reproduced from Ref.<sup>[164]</sup> with permission from The Royal Society of Chemistry, Copyright 2020.

The suggested model for the synergistic structure with lamellar layers circularly wrapped around the gel fibers requires the gel fibers to run along the layers. To prove that the fiber axis is normal to the lamellar layer normal 2D SAXS experiments were performed. The 12-HOA gel fibers have a layered structure (see chapter 4.1.2), which gives rise to a “intra-fiber” scattering maximum at  $q \approx 0.14 \text{ \AA}^{-1}$  in the direction normal to the fiber axis. In the SANS scattering curves this intra-fiber peak is superimposed by the second order layer peak (but is visible in the gel contrast), since the intra-fiber peak is weak due to the low content of gel fibers (in the range of a few wt%) and broad due to the limited number of layers in the fiber.

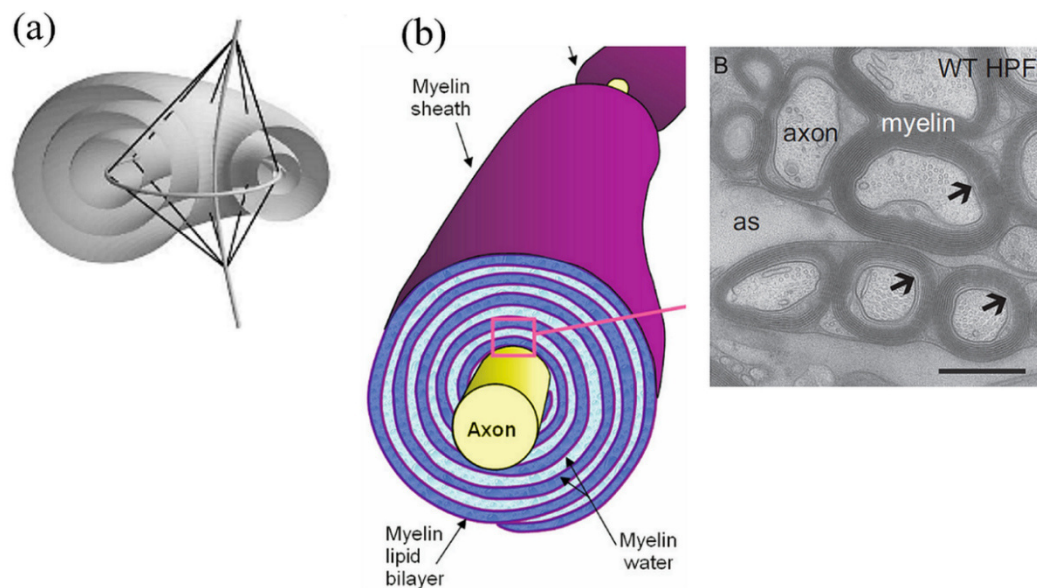
With SAXS however, the resolution is high enough to separate the layer peaks from the intra-fiber peak. The intra-fiber peak should be observed in the same direction than the lamellar layer peaks in an aligned domain of a lamellar gel in accordance with the proposed model for the synergistic structure. As shown in Figure 6.12, the intra-fiber peak is indeed found in the same direction as the lamellar layer peaks in the 2D SAXS pattern of a small aligned domain of the  $L_\alpha$  phase gelled with 12-HOA. Contrary, the intra-fiber peak is randomly distributed in the 2D SAXS pattern of an isotropic micellar gel. While in the isotropic micellar gel the fibers form a more or less random gel network, the fibers in the lamellar gel are oriented in directions along the lamellar layers with the layer normal of the  $L_\alpha$  phase perpendicular to the long axis of the gel fiber, thus giving rise to an anisotropic gel network.



**Figure 6.12:** 2D SAXS pattern of *a*) an aligned domain of the gelled  $L_\alpha$  phase ( $\phi_w = 0.675$  and  $\phi_{DOH/SDS} = 0.5$ ,  $\mu(12HOA) = 0.03$ ), *b*) the gelled isotropic phase ( $\phi_w = 0.75$  and  $\phi_{DOH/SDS} = 0.17$ ,  $\mu(12HOA) = 0.03$ ) and *c*) the azimuthal peak profiles integration thereof. Reproduced from Ref.<sup>[164]</sup> with permission from The Royal Society of Chemistry, Copyright 2020.

### 6.3 Conclusion

A new synergistic structure in lyotropic lamellar gels is observed, which neither exist in the non-gelled  $L_\alpha$  phase nor in the isotropic micellar gel. Those synergistic structures appear in cases the gel fiber diameter is considerably larger than the lamellar repeat unit as an elastic response of the lamellar layers to the presence of a relatively thick gel fiber. The lamellar layers bend into closed cylinders which coaxially enclose the fiber to avoid the appearance of energy-costly layer ends. In focal conic textures of smectic and lamellar liquid crystals the same elastic response is found, since the layers are bent into Dupin cyclids (Figure 6.13a)<sup>[340,341]</sup>, the formation of which is well understood in the elasticity theory of thermotropic smectics.<sup>[327,342]</sup> Hence, the synergistic structure is the natural response of a 1D layered fluid medium to topological defects. In future, the relation between the lamellar repeat unit, the bilayer rigidity and the gel fiber diameter has to be investigated in more detail. Interestingly, the observed synergistic structure mimics similar biological patterns, namely the structure of neural cells in which the axon is coaxially enclosed by the lamellar layers of myelin lipid bilayers and water (see Figure 6.13b). Lyotropic lamellar gels can thus be considered as a new kind of complex soft matter spontaneously forming biomimetic structures.



**Figure 6.13:** Analogies to the new synergistic structure in lyotropic lamellar gels: *a)* Bend layers in Dupin cyclids of the focal conic domains found in thermotropic smectic liquid crystals.<sup>[343]</sup> *b)* In nerve cells the axons are coaxially enclosed by myelin sheets, as can be seen in the schematic drawing<sup>[344]</sup> (*left*), as well as in the electron microscopy image<sup>[345]</sup> (*right*). Reproduced from Ref.<sup>[164]</sup> with permission from The Royal Society of Chemistry, Copyright 2020.

## 7 Concluding discussion and outlook

Surfactant-based LLC gels in the sense that genuine micellar LLC phases are immobilized by an interpenetrating gel network were practically unknown until 2016. This “blind spot” in the landscape of anisotropic gels has now been filled to a certain extent by the results of this thesis. Following the rational design strategy to gel surfactant-based LLC phases with the help of low-molecular mass gelators (LMWGs), not only lamellar  $L_\alpha$  and hexagonal  $H_1$  LLC gels but also the very first example of micellar nematic ( $N_d$  and  $N_c$ ) gels were obtained. The richness of self-assembled LLC structures together with the increasing availability of LMWGs now opens an avenue to new anisotropic hydrogels, the properties of which can be tailored individually by the composition of the LLC phase and the choice of the LMWG.

Furthermore, this work has led to first important insights into how the self-assembly of the gel is directed and how the gel network and the LLC phase mutually influence each other in terms of structure and morphology. It turned out that lamellar gels are the easiest to obtain, even though a strong mutual interaction between gel network and lamellar phase was noticed for lamellar gels obtained with the gelator 12-HOA. A thorough small angle neutron and X-ray study demonstrated that the lamellar gels are not orthogonal self-assembled systems, since an arrested lamellar layer spacing, an orientation of the gel fibers along the lamellar layers and the formation of a new synergistic structure, which is neither present in the gelator-free  $L_\alpha$  phase nor in an isotropic micellar gel, were observed.

The thickness of the fibers in relation to the lamellar repeat unit is the crucial criterion for the formation of the synergistic structure. The structure of the obtained lyotropic gel is determined by how, or how well the gel fibers are integrated in the respective liquid-crystalline phase. This is one reason why lamellar gels are the easiest to obtain since the lamellar phase can show an elastic response to the disturbance the gel fibers constitute. The lamellar layers bend into closed cylinders coaxially surrounding the fiber which avoids the appearance of energy-costly layer ends. This is the natural response of a 1D layered fluid medium, as it occurs in the Dupin cyclids of the focal-conic textures observed in smectic liquid crystals. However, for fibers with a diameter in the range of the lamellar layer thickness or smaller such a described elastic response of the lamellar layers is no longer possible since the layer curvature and thus the elastic bending energy would be far too high. In the case of small gel fibers, the energetic cost of layer ends is favored over a bending of the lamellar layers into closed cylinders and the structure of the resulting lamellar gel is similar to the one of the gelator-free

lamellar phase, as it was shown for lamellar gels obtained with the gelator DBS.

The thickness of the gel fibers and thus the compatibility of gel network and LLC phase is also the critical factor for the formation of lyotropic hexagonal gels. In cases the gel fibers are significantly larger than the intermicellar distance of the long cylindrical micelles in the hexagonal phase, the 2D translational long-range order of the  $H_1$  phase is incompatible with the formation of a 3D network and an isotropic gel is obtained, as it was shown when gelling the  $H_1$  phase with 12-HOA. However, gelling the hexagonal phase with the gelator DBS, which forms fibers with a thickness in the order of the diameter of the cylindrical micelles leads to a lyotropic hexagonal gel. In conclusion, the first requirement a LMWG has to fulfill in order to be able to successfully gel LLC phases is that the thickness of the formed gel fibers is compatible with the structure of the respective liquid-crystalline phase. Even if the lyotropic liquid-crystalline phase is able to adapt to the gel network, the structure of the LLC gel is determined by the relation of the gel fiber diameter and the LLC repeat unit.

The second, and more important requirement a gelator has to meet in order to obtain lyotropic nematic gels in particular is that its molecular structure has to be non-amphiphilic. If this condition is not satisfied, a part of the gelator molecules is incorporated into the micelles acting as a cosurfactant and flattens the micelle curvature, as it was shown for the gelling of the  $N_d$  and  $N_c$  phase with the gelator 12-HOA, where lamellar gels were obtained. Using the bulky gelators DBS and DBC the first examples of micellar lyotropic nematic gels were realized. In a 2D SAXS study it was even shown that macroscopically aligned micellar nematic gels can be achieved, although not yet in a reproducible way.

Micellar lyotropic liquid crystalline gels can be regarded as the lyotropic counterpart to the thermotropic LCEs, which are today the workhorses in the field of soft robotics and biomimetic actuation.<sup>[101,104,107,108,346–348]</sup> With LLC gels as a new kind of anisotropic hydrogels, soft actuators which are compatible to aqueous media and responsive to a different range of external stimuli such as water activity, pH-value, vapor pressure, ion or solute concentration are conceivable.

In LLC physical gels, two kinds of responsiveness are possible. First, the use of responsive gelators can be applied for a switchable and reversible gel network formation.<sup>[144,145,154,157]</sup> Second, and more important, the coupling of the macroscopic shape and the global orientational order may lead to a macroscopic shape change when external stimuli alter or destroy the global orientational long-range order.<sup>[100,101]</sup> The main requirement for a macroscopic shape response of a LLC gel sample to an external stimulus is the fabrication of macroscopically aligned LLC gels with a well-defined and macroscopically anisotropic director configuration. Additionally, an anisotropic swelling in water

might be observed for macroscopically aligned LLC hydrogels. Macroscopically aligned LLC (mainly nematic) gels may be achieved via field-assisted methods (alignment in a magnetic field), mechanical methods (shear- and flow alignment) or via surface interactions in restricted geometries (*e.g.* droplets). If temperature is chosen to be the stimulus, the LLC gels must meet a second condition. The sol-gel transition temperature has to be above the clearing temperature. However, this complicates the fabrication of aligned nematic gels, since during cooling down the gel network forms first. Thus, the kinetics of the gel network formation must be slow enough to allow a proper alignment of the nematic phase before the gel network forms. Another possibility is here the use of an LMWG responsive to *e.g.* UV light, which enables the alignment of the LLC phase during the exposure to UV light and a gel formation in the aligned LLC sample after the UV light is turned off. All in all, to obtain well-defined macroscopically aligned lyotropic nematic gels, the kinetics of the gel network formation, the orientational order parameter of the nematic phase, the relative orientation of the director and the gel fibers, as well as the respective sol-gel transition temperature  $T_{\text{sol-gel}}$  and the nematic to isotropic temperature  $T_{\text{NI}}$  have to be determined and tailored via the choice of the LLC system, the choice of the low molecular weight gelator and the choice of the fabrication conditions.

In conclusion, the key result of this thesis work is the success in introducing micellar lyotropic liquid crystal gels as a new class of anisotropic soft materials. By rational design, namely the gelation of micellar liquid crystal phases by low-molecular weight gelators, lamellar and hexagonal gels as well as first examples of micellar nematic gels were obtained. The requirements for a successful transfer of the LLC phases into the corresponding LLC gels were revealed and the knowledge on the structure of LLC gels was considerably deepened. Interestingly, structures that mimics biological schemes such as nerve cells were observed in lyotropic lamellar gels. Like their thermotropic counterparts (LCEs), micellar lyotropic gels are most interesting as stimuli-responsive water-based systems for applications in sensing and actuation, although the challenge remains to reproducibly obtain macroscopically aligned LLC gels.

## 8 References

- [1] D. Jordan Lloyd in *Theory and Methods* (Ed.: J. Alexander), *Vol. 1*, The Chemical Catalog Co., New York, **1926**, pp.767–782.
- [2] M. Nič, J. Jirát, B. Košata, A. Jenkins, A. McNaught (Eds.), *IUPAC Compendium of Chemical Terminology*, IUPAC, Research Triangle Park, NC, **2009**.
- [3] P. H. Hermans in *Colloid Science* (Ed.: H. R. Kruyt), *Vol. II*, Elsevier, Amsterdam, **1949**, p. 484.
- [4] P. J. Flory, Introductory lecture, *Faraday Discuss. Chem. Soc.* **1974**, *57*, 7.
- [5] R. G. Weiss, P. Terech in *Molecular Gels. Materials with Self-Assembled Fibrillar Networks* (Eds.: R. G. Weiss, P. Terech), Springer, Dordrecht, **2006**, pp. 1–13.
- [6] C. Stubenrauch, F. Giesselmann, Gelled Complex Fluids: Combining Unique Structures with Mechanical Stability, *Angew. Chem. Int. Ed.* **2016**, *55*, 3268.
- [7] K. Almdal, J. Dyre, S. Hvidt, O. Kramer, Towards a phenomenological definition of the term ‘gel’, *Polym. Gels Networks* **1993**, *1*, 5.
- [8] W. S. Gosal, A. H. Clark, S. B. Ross-Murphy, Fibrillar beta-lactoglobulin gels, *Biomacromolecules* **2004**, *5*, 2408.
- [9] U. Shimanovich, I. Efimov, T. O. Mason, P. Flagmeier, A. K. Buell, A. Gedanken, S. Linse, K. S. Åkerfeldt, C. M. Dobson, D. A. Weitz, T. P. J. Knowles, Protein microgels from amyloid fibril networks, *ACS nano* **2015**, *9*, 43.
- [10] J. B. Jones, C. R. Safinya, Interplay between Liquid Crystalline and Isotropic Gels in Self-Assembled Neurofilament Networks, *Biophys. J.* **2008**, *95*, 823.
- [11] N. M. Sangeetha, U. Maitra, Supramolecular gels, *Chem. Soc. Rev.* **2005**, *34*, 821.
- [12] J. I. Dawson, J. M. Kanczler, X. B. Yang, G. S. Attard, R. O. C. Oreffo, Clay gels for the delivery of regenerative microenvironments, *Adv. Mater.* **2011**, *23*, 3304.
- [13] R. Nigmatullin, M. A. Johns, J. C. Muñoz-García, V. Gabrielli, J. Schmitt, J. Angulo, Y. Z. Khimyak, J. L. Scott, K. J. Edler, S. J. Eichhorn, Hydrophobization of Cellulose Nanocrystals for Aqueous Colloidal Suspensions and Gels, *Biomacromolecules* **2020**, *21*, 1812.
- [14] L. Lewis, M. Derakhshandeh, S. G. Hatzikiriakos, W. Y. Hamad, M. J. MacLachlan, Hydrothermal Gelation of Aqueous Cellulose Nanocrystal Suspensions, *Biomacromolecules* **2016**, *17*, 2747.
- [15] P. Davidson, C. Bourgaux, L. Schouffet, P. Sergot, C. Williams, J. Livage, A Structural Study of the Lyotropic Nematic Phase of Vanadium Pentoxide Gels, *J. Phys. II France* **1995**, *5*, 1577.
- [16] J. Livage, Vanadium pentoxide gels, *Chem. Mater.* **1991**, *3*, 578.
- [17] M. Nordenström, A. Fall, G. Nyström, L. Wågberg, Formation of Colloidal Nanocellulose Glasses and Gels, *Langmuir* **2017**, *33*, 9772.
- [18] H. Tanaka, J. Meunier, D. Bonn, Nonergodic states of charged colloidal suspensions, *Phys. Rev. E: Stat., Nonlinear, Soft Matter Phys.* **2004**, *69*, 31404.



- [19] C. Schütz, J. R. Bruckner, C. Honorato-Rios, Z. Tosheva, M. Anyfantakis, J. P. F. Lagerwall, From Equilibrium Liquid Crystal Formation and Kinetic Arrest to Photonic Bandgap Films Using Suspensions of Cellulose Nanocrystals, *Crystals* **2020**, *10*, 199.
- [20] Y. Xu, A. D. Atrens, J. R. Stokes, “Liquid, gel and soft glass” phase transitions and rheology of nanocrystalline cellulose suspensions as a function of concentration and salinity, *Soft Matter* **2018**, *14*, 1953.
- [21] K. N. Pham, A. M. Puertas, J. Bergenholtz, S. U. Egelhaaf, A. Moussaïd, P. N. Pusey, A. B. Schofield, M. E. Cates, M. Fuchs, W. C. K. Poon, Multiple glassy states in a simple model system, *Science* **2002**, *296*, 104.
- [22] P. F. Fahey, W. W. Webb, Lateral diffusion in phospholipid bilayer membranes and multilamellar liquid crystals, *Biochemistry* **1978**, *17*, 3046.
- [23] E. S. Wu, K. Jacobson, D. Papahadjopoulos, Lateral diffusion in phospholipid multibilayers measured by fluorescence recovery after photobleaching, *Biochemistry* **1977**, *16*, 3936.
- [24] C.-Y. Cheng, T.-Y. Wang, S.-H. Tung, Biological Hydrogels Formed by Swollen Multilamellar Liposomes, *Langmuir* **2015**, *31*, 13312.
- [25] H. E. Warriner, S. L. Keller, S. H. J. Idziak, N. L. Slack, P. Davidson, J. A. Zasadzinski, C. R. Safinya, The Influence of Polymer Molecular Weight in Lamellar Gels Based on PEG-Lipids, *Biophys. J.* **1998**, *75*, 272.
- [26] H. E. Warriner, P. Davidson, N. L. Slack, M. Schellhorn, P. Eiselt, S. H. J. Idziak, H.-W. Schmidt, C. R. Safinya, Lamellar biogels comprising fluid membranes with a newly synthesized class of polyethylene glycol-surfactants, *J. Chem. Phys.* **1997**, *107*, 3707.
- [27] H. E. Warriner, S. H. J. Idziak, N. L. Slack, P. Davidson, C. R. Safinya, Lamellar Biogels, *Science* **1996**, *271*, 969.
- [28] J. Niu, D. Wang, H. Qin, X. Xiong, P. Tan, Y. Li, R. Liu, X. Lu, J. Wu, T. Zhang, W. Ni, J. Jin, Novel polymer-free iridescent lamellar hydrogel for two-dimensional confined growth of ultrathin gold membranes, *Nat. Commun.* **2015**, *5*, 3313.
- [29] G. Ben Messaoud, P. Le Griel, S. Prévost, D. Hermida-Merino, W. Soetaert, S. L. K. W. Roelants, C. V. Stevens, N. Baccile, Single-molecule lamellar hydrogels from bolaform microbial glucolipids, *Soft Matter* **2020**, *16*, 2528.
- [30] T. Kato, T. Kutsuna, K. Yabuuchi, N. Mizoshita, Anisotropic Self-Aggregation of an Anthracene Derivative, *Langmuir* **2002**, *18*, 7086.
- [31] J. M. McCracken, B. R. Donovan, T. J. White, Materials as Machines, *Adv. Mater.* **2020**, *32*, e1906564.
- [32] L. Ionov, Biomimetic Hydrogel-Based Actuating Systems, *Adv. Funct. Mater.* **2013**, *23*, 4555.
- [33] P. Calvert, Hydrogels for Soft Machines, *Adv. Mater.* **2009**, *21*, 743.
- [34] K. Sano, Y. Ishida, T. Aida, Synthesis of Anisotropic Hydrogels and Their Applications, *Angew. Chem. Int. Ed.* **2018**, *57*, 2532.
- [35] A. F. Mejia, R. Ng, P. Nguyen, M. Shuai, H. Y. Acosta, M. S. Mannan, Z. Cheng, Thermo-responsive discotic nematic hydrogels, *Soft Matter* **2013**, *9*, 10257.
- [36] N. Miyamoto, M. Shintate, S. Ikeda, Y. Hoshida, Y. Yamauchi, R. Motokawa, M. Annaka, Liquid crystalline inorganic nanosheets for facile synthesis of polymer hydrogels with

- anisotropies in structure, optical property, swelling/deswelling, and ion transport/fixation, *Chem. Commun.* **2013**, *49*, 1082.
- [37] L. Chen, Q. Wu, J. Zhang, T. Zhao, X. Jin, M. Liu, Anisotropic thermoresponsive hydrogels by mechanical force orientation of clay nanosheets, *Polymer* **2020**, *192*, 122309.
- [38] Z. Zhu, G. Song, J. Liu, P. G. Whitten, L. Liu, H. Wang, Liquid crystalline behavior of graphene oxide in the formation and deformation of tough nanocomposite hydrogels, *Langmuir* **2014**, *30*, 14648.
- [39] J. Ramón-Azcón, S. Ahadian, M. Estili, X. Liang, S. Ostrovidov, H. Kaji, H. Shiku, M. Ramalingam, K. Nakajima, Y. Sakka, A. Khademhosseini, T. Matsue, Dielectrophoretically aligned carbon nanotubes to control electrical and mechanical properties of hydrogels to fabricate contractile muscle myofibers, *Adv. Mater.* **2013**, *25*, 4028.
- [40] Y. Tanaka, A. Kubota, M. Matsusaki, T. Duncan, Y. Hatakeyama, K. Fukuyama, A. J. Quantock, M. Yamato, M. Akashi, K. Nishida, Anisotropic mechanical properties of collagen hydrogels induced by uniaxial-flow for ocular applications, *J. Biomater. Sci., Polym. Ed.* **2011**, *22*, 1427.
- [41] M. Hayakawa, T. Onda, T. Tanaka, K. Tsujii, Hydrogels Containing Immobilized Bilayer Membranes, *Langmuir* **1997**, *13*, 3595.
- [42] K. Mito, M. A. Haque, T. Nakajima, M. Uchiumi, T. Kurokawa, T. Nonoyama, J. P. Gong, Supramolecular hydrogels with multi-cylindrical lamellar bilayers, *Polymer* **2017**, *128*, 373.
- [43] M. Ilyas, M. A. Haque, Y. Yue, T. Kurokawa, T. Nakajima, T. Nonoyama, J. P. Gong, Water-Triggered Ductile–Brittle Transition of Anisotropic Lamellar Hydrogels and Effect of Confinement on Polymer Dynamics, *Macromolecules* **2017**, *50*, 8169.
- [44] K. Tsujii, M. Hayakawa, T. Onda, T. Tanaka, A Novel Hybrid Material of Polymer Gels and Bilayer Membranes, *Macromolecules* **1997**, *30*, 7397.
- [45] J. E. Stumpel, E. R. Gil, A. B. Spoelstra, C. W. M. Bastiaansen, D. J. Broer, A. P. H. J. Schenning, Stimuli-Responsive Materials Based on Interpenetrating Polymer Liquid Crystal Hydrogels, *Adv. Funct. Mater.* **2015**, *25*, 3314.
- [46] F. A. Aouada, M. R. de Moura, P. R.G. Fernandes, A. F. Rubira, E. C. Muniz, Optical and morphological characterization of polyacrylamide hydrogel and liquid crystal systems, *Eur. Polym. J.* **2005**, *41*, 2134.
- [47] R. S. Kularatne, H. Kim, M. Ammanamanchi, H. N. Hayenga, T. H. Ware, Shape-Morphing Chromonic Liquid Crystal Hydrogels, *Chem. Mater.* **2016**, *28*, 8489.
- [48] F. Kleinschmidt, M. Hickl, K. Saalwächter, C. Schmidt, H. Finkelmann, Lamellar Liquid Single Crystal Hydrogels, *Macromolecules* **2005**, *38*, 9772.
- [49] S. A. Willis, G. R. Dennis, G. Zheng, W. S. Price, Preparation and physical properties of a macroscopically aligned lyotropic hexagonal phase templated hydrogel, *React. Funct. Polym.* **2013**, *73*, 911.
- [50] F. A. Aouada, M. R. de Moura, A. F. Rubira, E. C. Muniz, P. R. G. Fernandes, H. Mukai, A. C.F. da Silveira, R. Itri, Birefringent hydrogels based on PAAm and lyotropic liquid crystal, *Eur. Polym. J.* **2006**, *42*, 2781.

- [51] D. T. McCormick, K. D. Stovall, C. A. Guymon, Photopolymerization in Pluronic Lyotropic Liquid Crystals, *Macromolecules* **2003**, *36*, 6549.
- [52] C. L. Lester, S. M. Smith, C. D. Colson, C. A. Guymon, Physical Properties of Hydrogels Synthesized from Lyotropic Liquid Crystalline Templates, *Chem. Mater.* **2003**, *15*, 3376.
- [53] B. S. Forney, C. Baguenard, C. A. Guymon, Effects of Controlling Polymer Nanostructure Using Photopolymerization within Lyotropic Liquid Crystalline Templates, *Chem. Mater.* **2013**, *25*, 2950.
- [54] S. Wang, D. P. Maruri, J. M. Boothby, X. Lu, L. K. Rivera-Tarazona, V. D. Varner, T. H. Ware, Anisotropic, porous hydrogels templated by lyotropic chromonic liquid crystals, *J. Mater. Chem. B* **2020**, *8*, 6988.
- [55] J. D. Clapper, C. A. Guymon, Physical Behavior of Cross-Linked PEG Hydrogels Photopolymerized within Nanostructured Lyotropic Liquid Crystalline Templates, *Macromolecules* **2007**, *40*, 1101.
- [56] M. A. DePierro, K. G. Carpenter, C. A. Guymon, Influence of Polymerization Conditions on Nanostructure and Properties of Polyacrylamide Hydrogels Templated from Lyotropic Liquid Crystals, *Chem. Mater.* **2006**, *18*, 5609.
- [57] H. Zhang, I. Hussain, M. Brust, M. F. Butler, S. P. Rannard, A. I. Cooper, Aligned two- and three-dimensional structures by directional freezing of polymers and nanoparticles, *Nat. Mater.* **2005**, *4*, 787.
- [58] R. Takahashi, Z. L. Wu, M. Arifuzzaman, T. Nonoyama, T. Nakajima, T. Kurokawa, J. P. Gong, Control superstructure of rigid polyelectrolytes in oppositely charged hydrogels via programmed internal stress, *Nat. Commun.* **2014**, *5*, 4490.
- [59] I. Bihannic, L. J. Michot, B. S. Lartiges, D. Vantelon, J. Labille, F. Thomas, J. Susini, M. Salomé, B. Fayard, First Direct Visualization of Oriented Mesostructures in Clay Gels by Synchrotron-Based X-ray Fluorescence Microscopy, *Langmuir* **2001**, *17*, 4144.
- [60] B. J. Lemaire, P. Panine, J. C. P. Gabriel, P. Davidson, The measurement by SAXS of the nematic order parameter of laponite gels, *EPL* **2002**, *59*, 55.
- [61] E. Loizou, P. Butler, L. Porcar, G. Schmidt, Dynamic Responses in Nanocomposite Hydrogels, *Macromolecules* **2006**, *39*, 1614.
- [62] P. Schexnailder, E. Loizou, L. Porcar, P. Butler, G. Schmidt, Heterogeneity in nanocomposite hydrogels from poly(ethylene oxide) cross-linked with silicate nanoparticles, *Phys. Chem. Chem. Phys.* **2009**, *11*, 2760.
- [63] J.-H. Ryu, M. Lee, Transformation of Isotropic Fluid to Nematic Gel Triggered by Dynamic Bridging of Supramolecular Nanocylinders, *J. Am. Chem. Soc.* **2005**, *127*, 14170.
- [64] M. Zhang, C. Fives, K. C. Waldron, X. X. Zhu, Self-Assembly of a Bile Acid Dimer in Aqueous Solutions, *Langmuir* **2017**, *33*, 1084.
- [65] D. Zhang, Q. Liu, R. Visvanathan, M. R. Tuchband, G. H. Sheetah, B. D. Fairbanks, N. A. Clark, I. I. Smalyukh, C. N. Bowman, A supramolecular hydrogel prepared from a thymine-containing artificial nucleolipid, *Soft Matter* **2018**, *14*, 7045.
- [66] J. S. Park, S. Jeong, D. W. Chang, P. K. Jae, K. Kim, E.-K. Park, K.-W. Song, Lithium-induced supramolecular hydrogel, *Chem. Commun.* **2011**, *47*, 4736.

- [67] Z. Huang, H. Lee, E. Lee, S.-K. Kang, J.-M. Nam, M. Lee, Responsive nematic gels from the self-assembly of aqueous nanofibres, *Nat. Commun.* **2011**, *2*, 459.
- [68] J. Zhou, X. Du, Y. Gao, J. Shi, B. Xu, Aromatic-aromatic interactions enhance interfiber contacts for enzymatic formation of a spontaneously aligned supramolecular hydrogel, *J. Am. Chem. Soc.* **2014**, *136*, 2970.
- [69] A. Aggeli, M. Bell, L. M. Carrick, C. W. G. Fishwick, R. Harding, P. J. Mawer, S. E. Radford, A. E. Strong, N. Boden, pH as a trigger of peptide beta-sheet self-assembly and reversible switching between nematic and isotropic phases, *J. Am. Chem. Soc.* **2003**, *125*, 9619.
- [70] S. M. Chin, C. V. Synatschke, S. Liu, R. J. Nap, N. A. Sather, Q. Wang, Z. Álvarez, A. N. Edelbrock, T. Fyrner, L. C. Palmer, I. Szleifer, M. O. de la Cruz, S. I. Stupp, Covalent-supramolecular hybrid polymers as muscle-inspired anisotropic actuators, *Nat. Commun.* **2018**, *9*, 2395.
- [71] F. Zhao, Y. Gao, J. Shi, H. M. Browdy, B. Xu, Novel anisotropic supramolecular hydrogel with high stability over a wide pH range, *Langmuir* **2011**, *27*, 1510.
- [72] A. Aggeli, I. A. Nyrkova, M. Bell, R. Harding, L. Carrick, T. C. McLeish, A. N. Semenov, N. Boden, Hierarchical self-assembly of chiral rod-like molecules as a model for peptide beta-sheet tapes, ribbons, fibrils, and fibers, *Proc. Natl. Acad. Sci. U. S. A.* **2001**, *98*, 11857.
- [73] H. A. Behanna, J. J. J. M. Donners, A. C. Gordon, S. I. Stupp, Coassembly of Amphiphiles with Opposite Peptide Polarities into Nanofibers, *J. Am. Chem. Soc.* **2005**, *127*, 1193.
- [74] J. D. Hartgerink, E. Beniash, S. I. Stupp, Peptide-amphiphile nanofibers, *Proc. Natl. Acad. Sci. U. S. A.* **2002**, *99*, 5133.
- [75] S. Zhang, M. A. Greenfield, A. Mata, L. C. Palmer, R. Bitton, J. R. Mantei, C. Aparicio, M. O. de La Cruz, S. I. Stupp, A self-assembly pathway to aligned monodomain gels, *Nat. Mater.* **2010**, *9*, 594.
- [76] M. T. McClendon, S. I. Stupp, Tubular hydrogels of circumferentially aligned nanofibers to encapsulate and orient vascular cells, *Biomaterials* **2012**, *33*, 5713.
- [77] J. Campbell, M. Kuzma, M. M. Labes, A Nonaqueous Lyotropic Nematic Gel, *Mol. Cryst. Liq. Cryst.* **2011**, *95*, 45.
- [78] P. Terech in *Orientation of rods formed by aggregated surfactants in organic media: the steroid-cyclohexane physical gel case. Trends in Colloid and Interface Science III* (Eds.: P. Bothorel, E. J. Dufourc), *Vol. 79*, Steinkopff, **1989**, pp. 81–87.
- [79] P. Terech, Optical birefringence and dichroism in physical steroid organogels, *Liq. Cryst.* **1991**, *9*, 59.
- [80] M. A. Firestone, J. A. Dzielawa, P. Zapol, L. A. Curtiss, S. Seifert, M. L. Dietz, Lyotropic Liquid-Crystalline Gel Formation in a Room-Temperature Ionic Liquid, *Langmuir* **2002**, *18*, 7258.
- [81] I. Dierking, A Review of Polymer-Stabilized Ferroelectric Liquid Crystals, *Materials* **2014**, *7*, 3568.
- [82] R. A. M. Hikmet, J. Lub, Anisotropic networks and gels obtained by photopolymerisation in the liquid crystalline state, *Prog. Polym. Sci.* **1996**, *21*, 1165.

- [83] I. Dierking, Recent developments in polymer stabilised liquid crystals, *Polym. Chem.* **2010**, *1*, 1153.
- [84] R. A. M. Hikmet, Anisotropic gels in liquid crystal devices, *Adv. Mater.* **1992**, *4*, 679.
- [85] R. A. M. Hikmet, Anisotropic gels and plasticized networks formed by liquid crystal molecules, *Liq. Cryst.* **1991**, *9*, 405.
- [86] C. Huang, Q. M. Zhang, A. Jáklí, Nematic Anisotropic Liquid-Crystal Gels—Self-Assembled Nanocomposites with High Electromechanical Response, *Adv. Funct. Mater.* **2003**, *13*, 525.
- [87] A. Y.-G. Fuh, M.-S. T. M.-S. Tsai, C.-Y. H. C.-Y. Huang, Polymer Network Formed in Liquid Crystals, *Jpn. J. Appl. Phys.* **1996**, *35*, 3960.
- [88] P. Xie, R. Zhang, Liquid crystal elastomers, networks and gels, *J. Mater. Chem.* **2005**, *15*, 2529.
- [89] R. A. M. Hikmet in *Molecular Gels. Materials with Self-Assembled Fibrillar Networks* (Eds.: R. G. Weiss, P. Terech), Springer, Dordrecht, **2006**, pp. 773–792.
- [90] K. Urayama, S. Honda, T. Takigawa, Electrooptical Effects with Anisotropic Deformation in Nematic Gels, *Macromolecules* **2005**, *38*, 3574.
- [91] R. A. M. Hikmet, Electrically induced light scattering from anisotropic gels, *J. Appl. Phys.* **1990**, *68*, 4406.
- [92] R. A. M. Hikmet, H. Kemperman, Electrically switchable mirrors and optical components made from liquid-crystal gels, *Nature* **1998**, *392*, 476.
- [93] I. Dierking, L. L. Kosbar, A. Afzali-Ardakani, A. C. Lowe, G. A. Held, Two-stage switching behavior of polymer stabilized cholesteric textures, *J. Appl. Phys.* **1997**, *81*, 3007.
- [94] R. A. M. Hikmet, B. H. Zwerver, Structure of cholesteric gels and their electrically induced light scattering and colour changes, *Liq. Cryst.* **1992**, *12*, 319.
- [95] R.A.M. Hikmet, R. Polesso, Patterned Multicolor Switchable Cholesteric Liquid Crystal Gels, *Adv. Mater.* **2002**, *14*, 502.
- [96] P. Archer, I. Dierking, Electro-optic properties of polymer-stabilized ferroelectric liquid crystals before, during and after photo-polymerization, *J. Opt. A: Pure Appl. Opt.*, *11*, 24022.
- [97] M. Petit, A. Daoudi, M. Ismaili, J. M. Buisine, Distortion and unwinding of the helical structure in polymer-stabilized short-pitch ferroelectric liquid crystal, *Eur. Phys. J. E* **2006**, *20*, 327.
- [98] J. Pirš, P. Bos, R. Petkovšek, S. Kralj, S. Pirš, S. Žumer, T. Matuszczyk, Influence of the Polymer Network on the Switching Behaviors in the Polymer Stabilized Ferroelectric Liquid Crystals, *Jpn. J. Appl. Phys.*, *41*, 6011.
- [99] C. Ohm, M. Brehmer, R. Zentel, Liquid crystalline elastomers as actuators and sensors, *Adv. Mater.* **2010**, *22*, 3366.
- [100] P.-G. de Gennes, M. Hébert, R. Kant, Artificial muscles based on nematic gels, *Macromol. Symp.* **1997**, *113*, 39.
- [101] M.-H. Li, P. Keller, Artificial muscles based on liquid crystal elastomers, *Philos. Trans. R. Soc., A* **2006**, *364*, 2763.
- [102] T. Ikeda, J.-i. Mamiya, Y. Yu, Photomechanics of liquid-crystalline elastomers and other polymers, *Angew. Chem. Int. Ed.* **2007**, *46*, 506.

- [103] Y. Yu, T. Ikeda, Soft Actuators Based on Liquid-Crystalline Elastomers, *Angew. Chem. Int. Ed.* **2006**, *45*, 5416.
- [104] E.-K. Fleischmann, H.-L. Liang, N. Kapernaum, F. Giesselmann, J. Lagerwall, R. Zentel, One-piece micropumps from liquid crystalline core-shell particles, *Nat. Commun.* **2012**, *3*, 1178.
- [105] M. Yamada, M. Kondo, J.-i. Mamiya, Y. Yu, M. Kinoshita, C. J. Barrett, T. Ikeda, Photomobile Polymer Materials, *Angew. Chem. Int. Ed.* **2008**, *47*, 4986.
- [106] D. L. Thomsen, P. Keller, J. Naciri, R. Pink, H. Jeon, D. Shenoy, B. R. Ratna, Liquid Crystal Elastomers with Mechanical Properties of a Muscle, *Macromolecules* **2001**, *34*, 5868.
- [107] A. Buguin, M.-H. Li, P. Silberzan, B. Ladoux, P. Keller, Micro-actuators, *J. Am. Chem. Soc.* **2006**, *128*, 1088.
- [108] M. Rogó z, H. Zeng, C. Xuan, D. S. Wiersma, P. Wasylczyk, Light-Driven Soft Robot Mimics Caterpillar Locomotion in Natural Scale, *Adv. Opt. Mater.* **2016**, *4*, 1689.
- [109] M. Yamada, M. Kondo, R. Miyasato, Y. Naka, J.-i. Mamiya, M. Kinoshita, A. Shishido, Y. Yu, C. J. Barrett, T. Ikeda, Photomobile polymer materials—various three-dimensional movements, *J. Mater. Chem.* **2009**, *19*, 60.
- [110] J. M. Boothby, H. Kim, T. H. Ware, Shape changes in chemoresponsive liquid crystal elastomers, *Sens. Actuators, B* **2017**, *240*, 511.
- [111] G. R. Mitchell, W. Guo, F. J. Davis, Liquid crystal elastomers based upon cellulose derivatives, *Polymer* **1992**, *33*, 68.
- [112] J. M. Boothby, T. H. Ware, Dual-responsive, shape-switching bilayers enabled by liquid crystal elastomers, *Soft Matter* **2017**, *13*, 4349.
- [113] R. Verduzco, N. R. Scruggs, S. Sprunt, P. Palffy-Muhoray, J. A. Kornfield, Director dynamics in liquid-crystal physical gels, *Soft Matter* **2007**, *3*, 993.
- [114] M. D. Kempe, N. R. Scruggs, R. Verduzco, J. Lal, J. A. Kornfield, Self-assembled liquid-crystalline gels designed from the bottom up, *Nat. Mater.* **2004**, *3*, 177.
- [115] M. D. Kempe, R. Verduzco, N. R. Scruggs, J. A. Kornfield, Rheological study of structural transitions in triblock copolymers in a liquid crystal solvent, *Soft Matter* **2006**, *2*, 422.
- [116] T. Kato, T. Kutsuna, K. Hanabusa, M. Ukon, Gelation of Room-Temperature Liquid Crystals by the Association of a trans-1,2-Bis(amino)cyclohexane Derivative, *Adv. Mater.* **1998**, *10*, 606.
- [117] L. Guan, Y. Zhao, Self-Assembly of a Liquid Crystalline Anisotropic Gel, *Chem. Mater.* **2000**, *12*, 3667.
- [118] N. Mizoshita, T. Kutsuna, T. Kato, K. Hanabusa, Smectic liquid-crystalline physical gels. Anisotropic self-aggregation of hydrogen-bonded molecules in layered structures, *Chem. Commun.* **1999**, 781.
- [119] T. Kato, Y. Hirai, S. Nakaso, M. Moriyama, Liquid-crystalline physical gels, *Chem. Soc. Rev.* **2007**, *36*, 1857.
- [120] N. Mizoshita, Y. Suzuki, K. Kishimoto, K. Hanabusa, T. Kato, Electrooptical properties of liquid-crystalline physical gels, *J. Mater. Chem.* **2002**, *12*, 2197.

- [121] T. Kato, Self-Assembly of Phase-Segregated Liquid Crystal Structures, *Science* **2002**, *295*, 2414.
- [122] R. H.C. Janssen, V. Stümpflen, M. C.W. van Boxtel, C. W.M. Bastiaansen, D. J. Broer, T. A. Tervoort, P. Smith, Thermo-reversible gelation of liquid crystals using di-benzylidene-D-sorbitol, *Macromol. Symp.* **2000**, *154*, 117.
- [123] W. L. Leaw, C. R. Mamat, S. Triwahyono, A. A. Jalil, N. Bidin, Liquid crystal physical gel formed by cholesteryl stearate for light scattering display material, *J. Colloid Interface Sci.* **2016**, *483*, 41.
- [124] C. Tolksdorf, R. Zentel, Reversible Physical Network Stabilized Ferroelectric Liquid Crystals, *Adv. Mater.* **2001**, *13*, 1307.
- [125] P. Deindörfer, A. Eremin, R. Stannarius, R. Davis, R. Zentel, Gelation of smectic liquid crystal phases with photosensitive gel forming agents, *Soft Matter* **2006**, *2*, 693.
- [126] N. Mizoshita, K. Hanabusa, T. Kato, Self-Aggregation of an Amino Acid Derivative in a Liquid-Crystalline Physical Gel—Faster Response to Electric Fields, *Adv. Mater.* **1999**, *11*, 392.
- [127] N. Mizoshita, K. Hanabusa, T. Kato, Fast and High-Contrast Electro-optical Switching of Liquid-Crystalline Physical Gels, *Adv. Funct. Mater.* **2003**, *13*, 313.
- [128] N. Mizoshita, K. Hanabusa, T. Kato, Nematic liquid-crystalline physical gels exhibiting faster responses to electric fields in twisted nematic cells, *Displays* **2001**, *22*, 33.
- [129] W. L. Leaw, C. R. Mamat, S. Triwahyono, A. A. Jalil, N. Bidin, Effect of temperature on the morphology and electro-optical properties of liquid crystal physical gel, *Mater. Chem. Phys.* **2016**, *184*, 197.
- [130] N. Mizoshita, H. Monobe, M. Inoue, M. Ukon, T. Watanabe, Y. Shimizu, K. Hanabusa, T. Kato, The positive effect on hole transport behaviour in anisotropic gels consisting of discotic liquid crystals and hydrogen-bonded fibres, *Chem. Commun.* **2002**, 428.
- [131] L. Guan, Y. Zhao, Self-assembled gels of liquid crystals, *J. Mater. Chem.* **2001**, *11*, 1339.
- [132] R. H. C. Janssen, J.-P. Teunissen, S. J. Picken, C. W. M. Bastiaansen, D. J. Broer, T. A. Tervoort, P. Smith, Cholesteric Thermo-reversible Liquid-Crystal Gels, *Jpn. J. Appl. Phys.* **2001**, *40*, 2372.
- [133] M. Moriyama, N. Mizoshita, T. Yokota, K. Kishimoto, T. Kato, Photoresponsive Anisotropic Soft Solids, *Adv. Mater.* **2003**, *15*, 1335.
- [134] F. Crucenau, D. Liang, R. L. Leheny, G. S. Iannacchione, Calorimetric study of the isotropic to nematic phase transition in an aligned liquid crystal nano-colloidal gel, *Liq. Cryst.* **2008**, *35*, 1061.
- [135] D. Liang, M. A. Borthwick, R. L. Leheny, Smectic liquid crystals in anisotropic colloidal silica gels, *J. Phys.: Condens. Matter* **2004**, *16*, S1989-S2002.
- [136] Y. Xu, M. Laupheimer, N. Preisig, T. Sottmann, C. Schmidt, C. Stubenrauch, Gelled Lyotropic Liquid Crystals, *Langmuir* **2015**, *31*, 8589.
- [137] P. Prang, R. Müller, A. Eljaouhari, K. Heckmann, W. Kunz, T. Weber, C. Faber, M. Vroemen, U. Bogdahn, N. Weidner, The promotion of oriented axonal regrowth in the injured spinal cord by alginate-based anisotropic capillary hydrogels, *Biomaterials* **2006**, *27*, 3560.

- [138] L. E. Millon, H. Mohammadi, W. K. Wan, Anisotropic polyvinyl alcohol hydrogel for cardiovascular applications, *J. Biomed. Mater. Res., Part B* **2006**, *79*, 305.
- [139] H. Tseng, D. S. Puperi, E. J. Kim, S. Ayoub, J. V. Shah, M. L. Cuchiara, J. L. West, K. J. Grande-Allen, Anisotropic poly(ethylene glycol)/polycaprolactone hydrogel-fiber composites for heart valve tissue engineering, *Tissue Eng., Part A* **2014**, *20*, 2634.
- [140] H. Wermter, H. Finkelmann, Liquid crystalline elastomers as artificial muscles, *e-Polym.* **2001**, *1*.
- [141] T. J. White, D. J. Broer, Programmable and adaptive mechanics with liquid crystal polymer networks and elastomers, *Nat. Mater.* **2015**, *14*, 1087.
- [142] D. J. Abdallah, R. G. Weiss, Organogels and Low Molecular Mass Organic Gelators, *Adv. Mater.* **2000**, *12*, 1237.
- [143] P. Terech, R. G. Weiss, Low Molecular Mass Gelators of Organic Liquids and the Properties of Their Gels, *Chem. Rev.* **1997**, *97*, 3133.
- [144] M. Ayabe, T. Kishida, N. Fujita, K. Sada, S. Shinkai, Binary organogelators which show light and temperature responsiveness, *Org. Biomol. Chem.* **2003**, *1*, 2744.
- [145] X. Yang, G. Zhang, D. Zhang, Stimuli responsive gels based on low molecular weight gelators, *J. Mater. Chem.* **2012**, *22*, 38.
- [146] S. A. Ahmed, X. Sallenave, F. Fages, G. Mieden-Gundert, W. M. Müller, U. Müller, F. Vögtle, J.-L. Pozzo, Multiaddressable Self-Assembling Organogelators Based on 2 H - Chromene and N -Acyl-1, $\omega$ -amino Acid Units, *Langmuir* **2002**, *18*, 7096.
- [147] C. Wang, D. Chen, X. Jiao, Lyotropic liquid crystal directed synthesis of nanostructured materials, *Sci. Technol. Adv. Mater.* **2009**, *10*, 23001.
- [148] S. H. Tolbert, A. Firouzi, G. D. Stucky, B. F. Chmelka, Magnetic Field Alignment of Ordered Silicate-Surfactant Composites and Mesoporous Silica, *Science* **1997**, *278*, 264.
- [149] T. Kato, From nanostructured liquid crystals to polymer-based electrolytes, *Angew. Chem. Int. Ed.* **2010**, *49*, 7847.
- [150] L. Kang, H. H. Cheong, S. Y. Chan, P. F. C. Lim in *Soft fibrillar materials-Fabrication and applications. Applications of Small-Molecule Gels - Drug Delivery* (Eds.: X. Y. Liu, J.-L. Li), John Wiley & Sons, Ltd, Weinheim, Germany, **2013**, pp. 115–128.
- [151] D.-H. Kim, A. Jahn, S.-J. Cho, J. S. Kim, M.-H. Ki, D.-D. Kim, Lyotropic liquid crystal systems in drug delivery, *J. Pharm. Invest.* **2015**, *45*, 1.
- [152] K. Murata, M. Aoki, T. Nishi, A. Ikeda, S. Shinkai, New cholesterol-based gelators with light- and metal-responsive functions, *J. Chem. Soc., Chem. Commun.* **1991**, 1715.
- [153] K. Murata, M. Aoki, T. Suzuki, T. Harada, H. Kawabata, T. Komori, F. Ohseto, K. Ueda, S. Shinkai, Thermal and Light Control of the Sol-Gel Phase Transition in Cholesterol-Based Organic Gels. Novel Helical Aggregation Modes As Detected by Circular Dichroism and Electron Microscopic Observation, *J. Am. Chem. Soc.* **1994**, *116*, 6664.
- [154] J.-L. Pozzo, G. M. Clavier, J.-P. Desvergne, Rational design of new acid-sensitive organogelators, *J. Mater. Chem.* **1998**, *8*, 2575.
- [155] A. Friggeri, B. L. Feringa, J. H. van Esch, Entrapment and release of quinoline derivatives using a hydrogel of a low molecular weight gelator, *J. Controlled Release* **2004**, *97*, 241.



- [156] Z. Yang, B. Xu, A simple visual assay based on small molecule hydrogels for detecting inhibitors of enzymes, *Chem. Commun.* **2004**, 2424.
- [157] Z. Yang, B. Xu, Using Enzymes to Control Molecular Hydrogelation, *Adv. Mater.* **2006**, *18*, 3043.
- [158] K. J. C. van Bommel, M. C. A. Stuart, B. L. Feringa, J. van Esch, Two-stage enzyme mediated drug release from LMWG hydrogels, *Org. Biomol. Chem.* **2005**, *3*, 2917.
- [159] D. D. Díaz, E. Morin, E. M. Schön, G. Budin, A. Wagner, J.-S. Remy, Tailoring drug release profile of low-molecular-weight hydrogels by supramolecular co-assembly and thiol–ene orthogonal coupling, *J. Mater. Chem.* **2010**, *21*, 641.
- [160] B. Alberts, A. Johnson, J. Lewis, M. Raff, K. Roberts, P. Walter, *Molecular biology of the cell*, Garland Science Taylor & Francis Group, New York, NY, **2002**.
- [161] G. Vereb, J. Szöllosi, J. Matkó, P. Nagy, T. Farkas, L. Vigh, L. Mátyus, T. A. Waldmann, S. Damjanovich, Dynamic, yet structured: The cell membrane three decades after the Singer-Nicolson model, *Proc. Natl. Acad. Sci. U. S. A.* **2003**, *100*, 8053.
- [162] S. Dieterich, T. Sottmann, F. Giesselmann, Gelation of Lyotropic Liquid-Crystal Phases-The Interplay between Liquid Crystalline Order and Physical Gel Formation, *Langmuir* **2019**, *35*, 16793.
- [163] S. Dieterich, F. Stemmler, N. Preisig, F. Giesselmann, Micellar Lyotropic Nematic Gels, *Adv. Mater.* **2021**, *33*, 2007340.
- [164] S. Dieterich, S. Prévost, C. Dargel, T. Sottmann, F. Giesselmann, Synergistic structures in lyotropic lamellar gels, *Soft Matter* **2020**, *16*, 10268.
- [165] M. Barón, Definitions of basic terms relating to low-molar-mass and polymer liquid crystals (IUPAC Recommendations 2001), *Pure Appl. Chem.* **2001**, *73*, 845.
- [166] H.-D. Dörfler, *Grenzflächen und kolloid-disperse Systeme*, Springer, Berlin, **2002**, p. 475.
- [167] H. Stegemeyer, *Lyotrope Flüssigkristalle. Grundlagen Entwicklung Anwendung*, Springer-Verlag, Berlin, **1999**.
- [168] A. L. Lehninger, D. L. Nelson, M. M. Cox in *Lehninger principles of biochemistry*, 4<sup>th</sup> edition, W.H. Freeman, New York, **2005**, p. 53.
- [169] J. N. Israelachvili, D. J. Mitchell, B. W. Ninham, Theory of self-assembly of hydrocarbon amphiphiles into micelles and bilayers, *J. Chem. Soc., Faraday Trans. 2* **1976**, *72*, 1525.
- [170] J. N. Israelachvili, *Intermolecular and surface forces*, Academic Press, Burlington, MA, **2011**, pp. 535-576.
- [171] A. M. Figueiredo Neto, S. R. A. Salinas, *The physics of lyotropic liquid crystals. Phase transitions and structural properties*, Oxford Univ. Press, Oxford, **2005**.
- [172] I. Dierking, S. Al-Zangana, Lyotropic Liquid Crystal Phases from Anisotropic Nanomaterials, *Nanomaterials* **2017**, *7*, 305.
- [173] N. Boden in *Partially Ordered Systems* (Eds.: W. M. Gelbart, A. Ben-Shaul, D. Roux), Springer, New York, NY, **1994**, pp. 153–217.
- [174] Y. Hendriks, J. Charvolin, Structural relations between lyotropic phases in the vicinity of the nematic phases, *J. Phys. France* **1981**, *42*, 1427.

- [175] K. D. Lawson, T. J. Flautt, Magnetically oriented lyotropic liquid crystalline phases, *J. Am. Chem. Soc.* **1967**, *89*, 5489.
- [176] A. M. Figueiredo Neto, Y. Galerne, A. M. Levelut, L. Liebert, Pseudo-lamellar ordering in uniaxial and biaxial lyotropic nematics, *J. Physique Lett.* **1985**, *46*, 499.
- [177] P. J. Collings, J. W. Goodby, *Introduction to liquid crystals. Chemistry and physics*, 2<sup>nd</sup> edition, CRC Press, Taylor & Francis Group, **2020**.
- [178] E. Akpınar, A. Figueiredo Neto, Experimental Conditions for the Stabilization of the Lyotropic Biaxial Nematic Mesophase, *Crystals* **2019**, *9*, 158.
- [179] V. Hendriks, J. Charvolin, M. Rawiso, L. Liebert, M. C. Holmes, Anisotropic aggregates of amphiphilic molecules in lyotropic nematic phases, *J. Phys. Chem.* **1983**, *87*, 3991.
- [180] N. Boden, K. Radley, M. C. Holmes, On the relationship between the micellar structure and the diamagnetic anisotropy of amphiphilic nematic mesophases, *Mol. Phys.* **1981**, *42*, 493.
- [181] K. Lonsdale, Diamagnetic Anisotropy of Organic Molecules, *Proc. R. Soc. A* **1939**, *171*, 541.
- [182] F. Fujiwara, L. W. Reeves, M. Suzuki, J. A. Vanin in *Solution Chemistry of Surfactants* (Ed.: K. L. Mittal), *Vol. 1*, Springer New York, Boston, MA, **1979**, pp. 63–77.
- [183] D. Demus, L. Richter, *Textures of liquid crystals*, Verl. Chemie, Weinheim, **1978**.
- [184] I. Dierking, *Textures of liquid crystals*, Wiley-VCH, Weinheim, **2003**.
- [185] J. Als-Nielsen, Des McMorrow, *Elements of modern X-ray physics*, Wiley, Chichester, **2011**.
- [186] W. H. de Jeu, *Basic x-ray scattering for soft matter*, Oxford University Press, Oxford, **2016**.
- [187] M. C. Holmes, N. Boden, K. Radley, Characterization of Lyotropic Nematics by Microscopy, *Mol. Cryst. Liq. Cryst.* **1983**, *100*, 93.
- [188] K. Berger, K. Hiltrop, Characterization of structural transitions in the SLS/decanol/water system, *Colloid Polym. Sci.* **1996**, *274*, 269.
- [189] Y. Galerne, A. M. F. Neto, L. Liébert, Microscopical structure of the uniaxial and biaxial lyotropic nematics, *J. Chem. Phys.* **1987**, *87*, 1851.
- [190] A. G. Oliveira-Filho, E. Akpınar, D. Reis, A. M. Figueiredo Neto, A survey on the phase diagram of the system sodium dodecyl sulphate/1-decanol /D 2 O concerning an eventual coexistence of uniaxial nematic phases, *Liq. Cryst.* **2017**, *46*, 1.
- [191] D. Roux, C. R. Safinya, F. Nallet in *Partially Ordered Systems* (Eds.: W. M. Gelbart, A. Ben-Shaul, D. Roux), Springer, New York, NY, **1994**, pp. 303–346.
- [192] G. S. Smith, E. B. Sirota, C. R. Safinya, N. A. Clark, Structure of the  $L_{\beta}$  phases in a hydrated phosphatidylcholine multimembrane, *Phys. Rev. Lett.* **1988**, *60*, 813.
- [193] G. S. Smith, E. B. Sirota, C. R. Safinya, R. J. Plano, N. A. Clark, X-ray structural studies of freely suspended ordered hydrated DMPC multimembrane films, *J. Chem. Phys.* **1990**, *92*, 4519.
- [194] A. Firouzi, D. J. Schaefer, S. H. Tolbert, G. D. Stucky, B. F. Chmelka, Magnetic-Field-Induced Orientational Ordering of Alkaline Lyotropic Silicate–Surfactant Liquid Crystals, *J. Am. Chem. Soc.* **1997**, *117*, 9466.
- [195] F. B. Rosevear, The microscopy of the liquid crystalline neat and middle phases of soaps and synthetic detergents, *J. Am. Oil Chem. Soc.* **1954**, *31*, 628.

- [196] D. W. Deamer, R. Leonard, A. Tardieu, D. Branton, Lamellar and hexagonal lipid phases visualized by freeze-etching, *Biochim. Biophys. Acta* **1970**, *219*, 47.
- [197] M. Chabre, A. Cavaggioni, H. B. Osborne, T. Gulik-Krzywicki, J. Olive, A rhodopsin-lipid-water lamellar system, *FEBS Lett.* **1972**, *26*, 197.
- [198] P. Holmqvist, P. Alexandridis, B. Lindman, Modification of the Microstructure in Poloxamer Block Copolymer–Water–“Oil” Systems by Varying the “Oil” Type, *Macromolecules* **1997**, *30*, 6788.
- [199] P. Kékicheff, B. Cabane, M. Rawiso, Structural defects of a lamellar lyotropic mesophase, *J. Phys., Lett* **1984**, *45*, 813.
- [200] B. J. Forrest, L. W. Reeves, New lyotropic liquid crystals composed of finite nonspherical micelles, *Chem. Rev.* **1981**, *81*, 1.
- [201] S. H. J. Idziak, I. Koltover, P. Davidson, M. Ruths, Y. Li, J. N. Israelachvili, C. R. Safinya, Structure under confinement in a smectic-A and lyotropic surfactant hexagonal phase, *Phys. B* **1996**, *221*, 289.
- [202] D. Varade, K. Aramaki, C. Stubenrauch, Phase diagrams of water–alkyltrimethylammonium bromide systems, *Colloids Surf., A* **2008**, *315*, 205.
- [203] L. E. Buerkle, S. J. Rowan, Supramolecular gels formed from multi-component low molecular weight species, *Chem. Soc. Rev.* **2012**, *41*, 6089.
- [204] L. A. Estroff, A. D. Hamilton in *Molecular Gels. Materials with Self-Assembled Fibrillar Networks* (Eds.: R. G. Weiss, P. Terech), Springer, Dordrecht, **2006**, pp. 721–742.
- [205] M. Hermansson, The fluidity of hydrocarbon regions in organo-gels, studied by NMR, *Colloids Surf., A* **1999**, *154*, 303.
- [206] M. George, R. G. Weiss, Molecular organogels. Soft matter comprised of low-molecular-mass organic gelators and organic liquids, *Acc. Chem. Res.* **2006**, *39*, 489.
- [207] R. G. Weiss, The past, present, and future of molecular gels. What is the status of the field, and where is it going?, *J. Am. Chem. Soc.* **2014**, *136*, 7519.
- [208] R.-Y. Wang, X.-Y. Liu, J. Narayanan, J.-Y. Xiong, J.-L. Li, Architecture of fiber network, *J. Phys. Chem. B* **2006**, *110*, 25797.
- [209] R. Lam, L. Quaroni, T. Pedersen, M. A. Rogers, A molecular insight into the nature of crystallographic mismatches in self-assembled fibrillar networks under non-isothermal crystallization conditions, *Soft Matter* **2010**, *6*, 404.
- [210] R. Wang, X.-Y. Liu, J. Xiong, J. Li, Real-time observation of fiber network formation in molecular organogel, *J. Phys. Chem. B* **2006**, *110*, 7275.
- [211] M. A. Rogers, T. Pedersen, L. Quaroni, Hydrogen-Bonding Density of Supramolecular Self-Assembled Fibrillar Networks Probed Using Synchrotron Infrared Spectromicroscopy, *Cryst. Growth Des.* **2009**, *9*, 3621.
- [212] J.-M. Guenet in *Organogels. SpringerBriefs in Materials* (Ed.: J.-M. Guenet), Springer, **2016**, pp. 1–5.
- [213] X. Du, J. Zhou, J. Shi, B. Xu, Supramolecular Hydrogelators and Hydrogels: From Soft Matter to Molecular Biomaterials, *Chem. Rev.* **2015**, *115*, 13165.

- [214] M. de Loos, B. L. Feringa, J. H. van Esch, Design and Application of Self-Assembled Low Molecular Weight Hydrogels, *Eur. J. Org. Chem.* **2005**, 2005, 3615.
- [215] N. Fujita, S. Shinkai in *Molecular Gels. Materials with Self-Assembled Fibrillar Networks* (Eds.: R. G. Weiss, P. Terech), Springer, Dordrecht, **2006**, pp. 553–575.
- [216] R. Oda in *Molecular Gels. Materials with Self-Assembled Fibrillar Networks* (Eds.: R. G. Weiss, P. Terech), Springer, Dordrecht, **2006**, pp. 577–609.
- [217] J. H. van Esch, We can design molecular gelators, but do we understand them?, *Langmuir* **2009**, 25, 8392.
- [218] Y. Jeong, K. Hanabusa, H. Masunaga, I. Akiba, K. Miyoshi, S. Sakurai, K. Sakurai, Solvent/gelator interactions and supramolecular structure of gel fibers in cyclic bis-urea/primary alcohol organogels, *Langmuir* **2005**, 21, 586.
- [219] M. Basta, V. Picciarelli, R. Stella, An introduction to percolation, *Eur. J. Phys.*, 15, 97.
- [220] X. Huang, P. Terech, S. R. Raghavan, R. G. Weiss, Kinetics of 5 $\alpha$ -cholestan-3 $\beta$ -yl N-(2-naphthyl)carbamate/n-alkane organogel formation and its influence on the fibrillar networks, *J. Am. Chem. Soc.* **2005**, 127, 4336.
- [221] M. A. Rogers, A. G. Marangoni, Non-Isothermal Nucleation and Crystallization of 12-Hydroxystearic Acid in Vegetable Oils, *Cryst. Growth Des.* **2008**, 8, 4596.
- [222] M. Lescanne, A. Colin, O. Mondain-Monval, F. Fages, J.-L. Pozzo, Structural Aspects of the Gelation Process Observed with Low Molecular Mass Organogelators, *Langmuir* **2003**, 19, 2013.
- [223] M. George, R. G. Weiss in *Molecular Gels. Materials with Self-Assembled Fibrillar Networks* (Eds.: R. G. Weiss, P. Terech), Springer, Dordrecht, **2006**, pp. 449–551.
- [224] G. Zhu, J. S. Dordick, Solvent Effect on Organogel Formation by Low Molecular Weight Molecules, *Chem. Mater.* **2006**, 18, 5988.
- [225] N. Zweep, J. H. van Esch in *Functional Molecular Gels* (Eds.: B. Escuder, J. F. Miravet), **2013**, pp. 1–29.
- [226] S. Wu, J. Gao, T. J. Emge, M. A. Rogers, Solvent-Induced Polymorphic Nanoscale Transitions for 12-Hydroxyoctadecanoic Acid Molecular Gels, *Cryst. Growth Des.* **2013**, 13, 1360.
- [227] Y. Lan, M. G. Corradini, X. Liu, T. E. May, F. Borondics, R. G. Weiss, M. A. Rogers, Comparing and correlating solubility parameters governing the self-assembly of molecular gels using 1,3:2,4-dibenzylidene sorbitol as the gelator, *Langmuir* **2014**, 30, 14128.
- [228] J. Li, K. Fan, X. Guan, Y. Yu, J. Song, Self-assembly mechanism of 1,3:2,4-di(3,4-dichlorobenzylidene)-D-sorbitol and control of the supramolecular chirality, *Langmuir* **2014**, 30, 13422.
- [229] W. Edwards, C. A. Lagadec, D. K. Smith, Solvent–gelator interactions—using empirical solvent parameters to better understand the self-assembly of gel-phase materials, *Soft Matter* **2011**, 7, 110.
- [230] Y. Lan, M. G. Corradini, R. G. Weiss, S. R. Raghavan, M. A. Rogers, To gel or not to gel: correlating molecular gelation with solvent parameters, *Chem. Soc. Rev.* **2015**, 44, 6035.

- [231] N. Yan, Z. Xu, K. K. Diehn, S. R. Raghavan, Y. Fang, R. G. Weiss, How do liquid mixtures solubilize insoluble gelators? Self-assembly properties of pyrenyl-linker-glucono gelators in tetrahydrofuran-water mixtures, *J. Am. Chem. Soc.* **2013**, *135*, 8989.
- [232] K. K. Diehn, H. Oh, R. Hashemipour, R. G. Weiss, S. R. Raghavan, Insights into organogelation and its kinetics from Hansen solubility parameters. Toward a priori predictions of molecular gelation, *Soft Matter* **2014**, *10*, 2632.
- [233] L. Feng, K. A. Cavicchi, Investigation of the relationships between the thermodynamic phase behavior and gelation behavior of a series of tripodal trisamide compounds, *Soft Matter* **2012**, *8*, 6483.
- [234] X. Huang, S. R. Raghavan, P. Terech, R. G. Weiss, Distinct kinetic pathways generate organogel networks with contrasting fractality and thixotropic properties, *J. Am. Chem. Soc.* **2006**, *128*, 15341.
- [235] M. A. Rogers, A. G. Marangoni, Kinetics of 12-Hydroxyoctadecanoic Acid SAFiN Crystallization Rationalized Using Hansen Solubility Parameters, *Langmuir* **2016**, *32*, 12833.
- [236] P. d. La Iglesia, D. C. Pozzo, Effects of supersaturation on the structure and properties of poly(9,9-dioctyl fluorene) organogels, *Soft Matter* **2013**, *9*, 11214.
- [237] J.-L. Li, X.-Y. Liu, R.-Y. Wang, J.-Y. Xiong, Architecture of a biocompatible supramolecular material by supersaturation-driven fabrication of its fiber network, *J. Phys. Chem. B* **2005**, *109*, 24231.
- [238] G. Chinga-Carrasco, Cellulose fibres, nanofibrils and microfibrils, *Nanoscale Res. Lett.* **2011**, *6*, 417.
- [239] T. J. Wess, Collagen Fibril Form and Function, *Adv. Protein Chem.* **2005**, *70*, 341.
- [240] K. J. C. van Bommel, C. van der Pol, I. Muizebelt, A. Friggeri, A. Heeres, A. Meetsma, B. L. Feringa, J. van Esch, Responsive cyclohexane-based low-molecular-weight hydrogelators with modular architecture, *Angew. Chem. Int. Ed.* **2004**, *43*, 1663.
- [241] P. Terech, D. Pasquier, V. Bordas, C. Rossat, Rheological Properties and Structural Correlations in Molecular Organogels, *Langmuir* **2000**, *16*, 4485.
- [242] F. M. Menger, K. L. Caran, Anatomy of a Gel. Amino Acid Derivatives That Rigidify Water at Submillimolar Concentrations, *J. Am. Chem. Soc.* **2000**, *122*, 11679.
- [243] S. Koitani, S. Dieterich, N. Preisig, K. Aramaki, C. Stubenrauch, Gelling Lamellar Phases of the Binary System Water-Didodecyldimethylammonium Bromide with an Organogelator, *Langmuir* **2017**, *33*, 12171.
- [244] P.-O. Quist, First order transitions to a lyotropic biaxial nematic, *Liq. Cryst.* **1995**, *18*, 623.
- [245] L. Q. Amaral, O. R. Santos, W. S. Braga, N. M. Kimura, A. J. Palangana, Biaxial phase and coexistence of the two uniaxial nematic phases in the system sodium dodecyl sulphate–decanol–D<sub>2</sub>O, *Liq. Cryst.* **2015**, *42*, 240.
- [246] Y. Galerne, J. P. Marcerou, Temperature Behavior of the Order-Parameter Invariants in the Uniaxial and Biaxial Nematic Phases of a Lyotropic Liquid Crystal, *Phys. Rev. Lett.* **1983**, *51*, 2109.
- [247] L. Q. Amaral, M. E. Marcondes Helene, Nematic domain in the sodium lauryl sulfate/water/decanol system, *J. Phys. Chem.* **1988**, *92*, 6094.

- [248] C. V. Teixeira, R. Itri, L. Q. do Amaral, Micellar Shape Transformation Induced by Decanol, *Langmuir* **2000**, *16*, 6102.
- [249] P.-O. Quist, B. Halle, Curvature defects in a lamellar phase revealed by nuclear-spin-relaxation anisotropy, *Phys. Rev. E* **1993**, *47*, 3374.
- [250] T. Tachibana, T. Mori, K. Hori, New type of twisted mesophase in jellies and solid films of chiral 12-hydroxyoctadecanoic acid, *Nature* **1979**, *278*, 578.
- [251] J. Gao, S. Wu, T. J. Emge, M. A. Rogers, Nanoscale and microscale structural changes alter the critical gelator concentration of self-assembled fibrillar networks, *CrystEngComm* **2013**, *15*, 4507.
- [252] H. Sato, K. Hori, T. Sakurai, A. Yamagishi, Long distance chiral transfer in a gel, *Chem. Phys. Lett.* **2008**, *467*, 140.
- [253] H. Sato, T. Sakurai, A. Yamagishi, Comparison of Vibrational Circular Dichroism between the Langmuir–Blodgett Films and Gels of 12-Hydroxyoctadecanoic Acid, *Chem. Lett.* **2011**, *40*, 25.
- [254] P. Terech, 12-D-Hydroxyoctadecanoic acid organogels, *J. Phys. II France* **1992**, *2*, 2181.
- [255] T. Tachibana, T. Mori, K. Hori, Chiral mesophases of 12-hydroxyoctadecanoic acid in jelly and in the solid state. I. A new type of lyotropic mesophase in jelly with organic solvents, *Bull. Chem. Soc. Jpn.* **1980**, *53*, 1714.
- [256] Ricky Lam, Luca Quaroni, Tor Pedersen, M. A. Rogers, A molecular insight into the nature of crystallographic mismatches in self-assembled fibrillar networks under non-isothermal crystallization conditions, *Soft Matter* **2010**, *6*, 404.
- [257] H. Takeno, T. Mochizuki, K. Yoshiba, S. Kondo, T. Dobashi, Self-assembling Structures and Sol-Gel Transition of Optically Active and Racemic 12-Hydroxystearic Acids in Organic Solvents, *Pogr. Colloid Polym. Sci.* **2009**, *136*, 47.
- [258] P. Terech, V. Rodriguez, J. D. Barnes, G. B. McKenna, Organogels and Aerogels of Racemic and Chiral 12-Hydroxyoctadecanoic Acid, *Langmuir* **1994**, *10*, 3406.
- [259] P. Terech, Small-angle-scattering study of 12-hydroxystearic physical organogels and lubricating greases, *Colloid Polym. Sci.* **1991**, *269*, 490.
- [260] T. Tachibana, H. Kambara, The sense of twist in the fibrous aggregates from 12-hydroxystearic acid and its alkali metal soaps, *J. Colloid Interface Sci.* **1968**, *28*, 173.
- [261] T. Sakurai, Y. Masuda, H. Sato, A. Yamagishi, H. Kawaji, T. Atake, K. Hori, A Comparative Study on Chiral and Racemic 12-Hydroxyoctadecanoic Acids in the Solutions and Aggregation States, *Bull. Chem. Soc. Jpn.* **2010**, *83*, 145.
- [262] D. A. S. Grahame, C. Olauson, R. S. H. Lam, T. Pedersen, F. Borondics, S. Abraham, R. G. Weiss, M. A. Rogers, Influence of chirality on the modes of self-assembly of 12-hydroxystearic acid in molecular gels of mineral oil, *Soft Matter* **2011**, *7*, 7359.
- [263] J. Gao, S. Wu, M. A. Rogers, Harnessing Hansen solubility parameters to predict organogel formation, *J. Mater. Chem.* **2012**, *22*, 12651.
- [264] M. Burkhardt, S. Kinzel, M. Gradzielski, Macroscopic properties and microstructure of HSA based organogels: sensitivity to polar additives, *J. Colloid Interface Sci.* **2009**, *331*, 514.

- [265] T. Tamura, M. Ichikawa, Effect of lecithin on organogel formation of 12-hydroxystearic acid, *J. Am. Oil Chem. Soc.* **1997**, *74*, 491.
- [266] M. Laupheimer, K. Jovic, F. E. Antunes, da Graça Martins Miguel, Maria, C. Stubenrauch, Studying orthogonal self-assembled systems, *Soft Matter* **2013**, *9*, 3661.
- [267] M. Laupheimer, T. Sottmann, R. Schweins, C. Stubenrauch, Studying orthogonal self-assembled systems: microstructure of gelled bicontinuous microemulsions, *Soft Matter* **2014**, *10*, 8744.
- [268] R. H. C. Janssen, V. Stümpflen, C. W. M. Bastiaansen, D. J. Broer, T. A. Tervoort, P. Smith, Thermo-reversible Liquid-Crystal Gels: Towards a New Processing Route for Twisted Nematic Displays, *Jpn. J. Appl. Phys.* **2000**, *39*, 2721.
- [269] H.-C. Lin, C.-H. Wang, J.-K. Wang, S.-F. Tsai, Fast Response and Spontaneous Alignment in Liquid Crystals Doped with 12-Hydroxystearic Acid Gelators, *Materials* **2018**, *11*, 745.
- [270] A.-L. Fameau, F. Cousin, A. Saint-Jalmes, Morphological Transition in Fatty Acid Self-Assemblies, *Langmuir* **2017**, *33*, 12943.
- [271] A.-L. Fameau, B. Houinsou-Houssou, B. Novales, L. Navailles, F. Nallet, J.-P. Douliez, 12-Hydroxystearic acid lipid tubes under various experimental conditions, *J. Colloid Interface Sci.* **2010**, *341*, 38.
- [272] A.-L. Fameau, A. Saint-Jalmes, Yielding and flow of solutions of thermoresponsive surfactant tubes, *Soft Matter* **2014**, *10*, 3622.
- [273] A.-L. Fameau, M. A. Rogers, The curious case of 12-hydroxystearic acid — the Dr. Jekyll & Mr. Hyde of molecular gelators, *Curr. Opin. Colloid Interface Sci.* **2020**, *45*, 68.
- [274] J.-P. Douliez, L. Navailles, F. Nallet, C. Gaillard, Self-assembly of unprecedented swollen multilamellar twisted ribbons from a racemic hydroxy fatty acid, *ChemPhysChem* **2008**, *9*, 74.
- [275] E. O. Kraemer, S. T. Dexter, The Light-Scattering Capacity (Tyndall Effect) and Colloidal Behavior of Gelatine Sols and Gels, *J. Phys. Chem.* **1927**, *31*, 764.
- [276] J.-L. Li, R.-Y. Wang, X.-Y. Liu, H.-H. Pan, Nanoengineering of a biocompatible organogel by thermal processing, *J. Phys. Chem. B* **2009**, *113*, 5011.
- [277] T. G. Mezger, *The rheology handbook. For users of rotational and oscillation rheometers*, Vincentz Network, Hannover, **2006**.
- [278] S. R. Raghavan, B. H. Cipriano in *Molecular Gels. Materials with Self-Assembled Fibrillar Networks* (Eds.: R. G. Weiss, P. Terech), Springer, Dordrecht, **2006**, pp. 241–252.
- [279] G. Dimonte, D. Nelson, S. Weaver, M. Schneider, E. Flower-Maudlin, R. Gore, J. R. Baumgardner, M. S. Sahota, Comparative study of viscoelastic properties using virgin yogurt, *J. Rheol.* **1998**, *42*, 727.
- [280] K. Steck, C. Schmidt, C. Stubenrauch, The Twofold Role of 12-Hydroxyoctadecanoic Acid (12-HOA) in a Ternary Water—Surfactant—12-HOA System, *Gels* **2018**, *4*, 78.
- [281] M. Laupheimer, N. Preisig, C. Stubenrauch, The molecular organogel n-decane/12-hydroxyoctadecanoic acid: Sol–gel transition, rheology, and microstructure, *Colloids Surf., A* **2015**, *469*, 315.
- [282] M. Watase, Y. Nakatani, H. Itagaki, On the Origin of the Formation and Stability of Physical Gels of Di- O -benzylidene- d -sorbitol, *J. Phys. Chem. B* **1999**, *103*, 2366.

- [283] M. d. C. Núñez-Santiago, A. Tecante, Rheological and calorimetric study of the sol–gel transition of  $\kappa$ -carrageenan, *Carbohydr. Polym.* **2007**, *69*, 763.
- [284] N. Amanokura, K. Yoza, H. Shinmori, S. Shinkai, D. N. Reinhoudt, New sugar-based gelators bearing a p-nitrophenyl chromophore, *J. Chem. Soc., Perkin Trans. 2* **1998**, 2585.
- [285] J. E. Eldridge, J. D. Ferry, Studies of the Cross-linking Process in Gelatin Gels. III. Dependence of Melting Point on Concentration and Molecular Weight, *J. Phys. Chem.* **1954**, *58*, 992.
- [286] M. Tokita, K. Nishinari (Eds.), *Some Thoughts on The Definition of a Gel. Gels: Structures, Properties, and Functions*, Springer Berlin Heidelberg, **2009**.
- [287] B. Nystroem, H. Walderhaug, F. K. Hansen, B. Lindman, Rheological Behavior during Thermoreversible Gelation of Aqueous Mixtures of Ethyl(hydroxyethyl)cellulose and Surfactants, *Langmuir* **1995**, *11*, 750.
- [288] P. Terech, C. Rossat, F. Volino, On the Measurement of Phase Transition Temperatures in Physical Molecular Organogels, *J. Colloid Interface Sci.* **2000**, *227*, 363.
- [289] S. Kirchner, G. Cevc, Temperature Variation of Lipid Membrane Structure and the Hydration Force in Fluid Lamellar Phase, *Europhys. Lett.*, *23*, 229.
- [290] H.-D. Dörfler, C. Görgens, Mizellpolymorphie lyotroper Mesophasen, *Tenside, Surfactants, Deterg.* **1999**, *36*, 314.
- [291] H.-D. Dörfler, C. Görgens, X-ray structural studies of lyotropic-nematic phases in the ternary system hexadecyl dimethylethyl ammonium bromide/water/n-decanol, *Tenside, Surfactants, Deterg.* **2000**, *37*, 17.
- [292] C. Görgens, "Strukturelle Charakterisierung lyotroper Mesophasen, insbesondere lyotrop-nematischer und lyotrop-cholesterischer Phasen, mittels Röntgenkleinwinkeluntersuchungen in binären, ternären und quaternären Systemen", *Dissertation*, Dresden, **1996**.
- [293] F. M. Menger, Y. Yamasaki, K. K. Catlin, T. Nishimi, X-Ray Structure of a Self-Assembled Gelating Fiber, *Angew. Chem. Int. Ed.* **1995**, *34*, 585.
- [294] A. M. Brizard, M. C. A. Stuart, J. H. van Esch, Self-assembled interpenetrating networks by orthogonal self assembly of surfactants and hydrogelators, *Faraday Discuss.* **2009**, *143*, 345.
- [295] B. O. Okesola, V. M. P. Vieira, D. J. Cornwell, N. K. Whitelaw, D. K. Smith, 1,3:2,4-Dibenzylidene-D-sorbitol (DBS) and its derivatives--efficient, versatile and industrially-relevant low-molecular-weight gelators with over 100 years of history and a bright future, *Soft Matter* **2015**, *11*, 4768.
- [296] S. Yamasaki, Y. Ohashi, H. Tsutsumi, K. Tsujii, The Aggregated Higher-Structure of 1,3:2,4-Di- O -benzylidene-D-sorbitol in Organic Gels, *Bull. Chem. Soc. Jpn.* **1995**, *68*, 146.
- [297] K. Steck, N. Preisig, C. Stubenrauch, Gelling Lyotropic Liquid Crystals with the Organogelator 1,3:2,4-Dibenzylidene-d-sorbitol Part II: Microstructure, *Langmuir* **2019**, *35*, 17142.
- [298] K. Steck, C. Stubenrauch, Gelling Lyotropic Liquid Crystals with the Organogelator 1,3:2,4-Dibenzylidene-d-sorbitol Part I: Phase Studies and Sol-Gel Transitions, *Langmuir* **2019**, *35*, 17132.
- [299] R. A. Gortner, W. F. Hoffmann, An interesting colloid gel, *J. Am. Chem. Soc.* **1921**, *43*, 2199.



- [300] C. G. L. Wolf, E. K. Rideal, The Properties of Dibenzoylcystine, *Biochem. J.* **1922**, *16*, 548.
- [301] I. Ziemecka, G. J. M. Koper, A. G. L. Olive, J. H. van Esch, Chemical-gradient directed self-assembly of hydrogel fibers, *Soft Matter* **2013**, *9*, 1556.
- [302] A. Heeres, C. van der Pol, M. Stuart, A. Friggeri, B. L. Feringa, J. van Esch, Orthogonal self-assembly of low molecular weight hydrogelators and surfactants, *J. Am. Chem. Soc.* **2003**, *125*, 14252.
- [303] E. Fan, J. Yang, S. J. Geib, T. C. Stoner, M. D. Hopkins, A. D. Hamilton, Hydrogen-bonding control of molecular aggregation, *J. Chem. Soc., Chem. Commun.* **1995**, 1251.
- [304] K. Hanabusa, A. Kawakami, M. Kimura, H. Shirai, Small Molecular Gelling Agents to Harden Organic Liquids, *Chem. Lett.* **1997**, *26*, 191.
- [305] A. Brizard, M. Stuart, K. van Bommel, A. Friggeri, M. de Jong, J. van Esch, Preparation of nanostructures by orthogonal self-assembly of hydrogelators and surfactants, *Angew. Chem. Int. Ed.* **2008**, *47*, 2063.
- [306] F. Stemmler, "Lassen sich lyotrop nematische Flüssigkristalle gelieren? Untersuchungen am Beispiel des Tensidsystems N,N-dimethyl-N-ethylhexadecylammoniumbromid/ n-Decanol/ Wasser", *Bachelor Thesis*, University of Stuttgart, Stuttgart, **2019**.
- [307] A. G. Oliveira-Filho, E. Akpınar, D. Reis, A. M. F. Neto, On the coexistence of uniaxial nematic phases in the lyotropic mixture sodium dodecyl sulphate/1-decanol/D<sub>2</sub>O, *Mol. Cryst. Liq. Cryst.* **2018**, *657*, 1.
- [308] P.-G. de Gennes, An analogy between superconductors and smectics A, *Solid State Commun.* **1972**, *10*, 753.
- [309] S. Chakraborty, J. T. Gleeson, A. Jakli, S. Sprunt, A comparison of short-range molecular order in bent-core and rod-like nematic liquid crystals, *Soft Matter* **2013**, *9*, 1817.
- [310] G. Albertini, M. Corinaldesi, S. Mazkedian, S. Melone, M. G. Ponzì Bossi, F. Rustichelli, Evidence for cybotactic cluster pretransition formation in TBBA liquid crystal, *Solid State Commun.* **1977**, *24*, 433.
- [311] P. E. Laibinis, J. J. Hickman, M. S. Wrighton, G. M. Whitesides, Orthogonal self-assembled monolayers, *Science* **1989**, *245*, 845.
- [312] J. Boekhoven, A. M. Brizard, M. C. A. Stuart, L. Florusse, G. Raffy, A. Del Guerzo, J. H. van Esch, Bio-inspired supramolecular materials by orthogonal self-assembly of hydrogelators and phospholipids, *Chem. Sci.* **2016**, *7*, 6021.
- [313] P. Lindner, T. Zemb (Eds.), *Neutrons, X-rays and light. Scattering methods applied to soft condensed matter*, North-Holland Elsevier, Amsterdam, **2002**.
- [314] <https://www.ill.eu/users/instruments/instruments-list/d11/description/instrument-layout>, last access 05.02.2021.
- [315] <https://www.nist.gov/ncnr/ng7-sans-small-angle-neutron-scattering>, last access 05.02.2021.
- [316] I. Grillo in *Soft Matter Characterization* (Eds.: R. Borsali, R. Pecora), Springer Netherlands, Dordrecht, **2008**, pp. 723–782.
- [317] M. Engel, T. Spehr, B. Stühn, Small-Angle X-ray and Neutron Scattering, *Bunsen-Magazin* **2001**, *13*, 4.
- [318] O. Spalla in *Neutrons, X-rays and light: Scattering methods applied to soft condensed matter* (Eds.: P. Lindner, T. Zemb), **2002**, pp. 49–71.

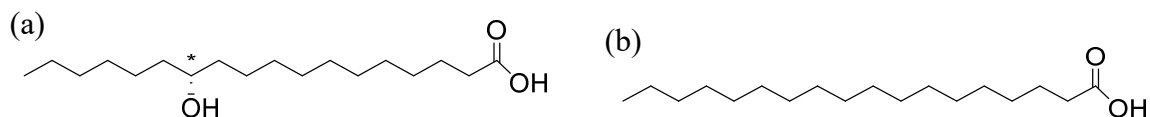
- [319] A. J. Jackson, "Introduction to Small-Angle Neutron Scattering and Neutron Reflectometry", NIST Center for Neutron Research, **2008**.
- [320] P. Schurtenberger in *Neutrons, X-rays and light: Scattering methods applied to soft condensed matter* (Eds.: P. Lindner, T. Zemb), **2002**, pp. 145–170.
- [321] P. Lindner in *Neutrons, X-rays and light: Scattering methods applied to soft condensed matter* (Eds.: P. Lindner, T. Zemb), **2002**, pp. 23–48.
- [322] W. Helfrich, Steric Interaction of Fluid Membranes in Multilayer Systems, *Zeitschrift für Naturforschung A* **1978**, *33*, 305.
- [323] D. Roux, C. R. Safinya, A synchrotron X-ray study of competing undulation and electrostatic interlayer interactions in fluid multimembrane lyotropic phases, *J. Phys. France* **1988**, *49*, 307.
- [324] F. Nallet, R. Laversanne, D. Roux, Modelling X-ray or neutron scattering spectra of lyotropic lamellar phases, *J. Phys. II France* **1993**, *3*, 487.
- [325] G. Bouglet, C. Ligoure, Polymer-mediated interactions of fluid membranes in a lyotropic lamellar phase, *EPJ B* **1999**, *9*, 137.
- [326] F. Castro-Roman, L. Porcar, G. Porte, C. Ligoure, Quantitative analysis of lyotropic lamellar phases SANS patterns in powder oriented samples, *EPJ E* **2005**, *18*, 259.
- [327] P. G. de Gennes, Conjectures sur L'État Smectique, *J. Phys. Colloques* **1969**, *30*, C4-65.
- [328] F. Brochard, P. G. de Gennes in *Series in modern condensed matter physics*, (Ed.: P.-G. de Gennes), *Vol. 12*, WORLD SCIENTIFIC, River Edge, NJ, **2003**, pp. 86–107.
- [329] F. Nallet, D. Roux, J. Prost, Hydrodynamics of lyotropic smectics, *J. Phys. France* **1989**, *50*, 3147.
- [330] R. E. Peierls, Remarks on transition temperatures, *Proc. Cambridge Philos. Soc.* **1934**, *32*, 477.
- [331] L. D. Landau, On the theory of phase transitions, *Phys. Z. Sowjetunion* **1937**, *11*, 26.
- [332] A. Caillé, Remarques sur la diffusion des rayons X dans les smectiques A, *C.R. Acad. Sci. Paris* **1972**, 891.
- [333] C. R. Safinya, D. Roux, G. S. Smith, S. K. Sinha, P. Dimon, N. A. Clark, A. M. Bellocq, Steric Interactions in a Model Multimembrane System, *Phys. Rev. Lett.* **1986**, *57*, 2718.
- [334] J. Als-Nielsen, J. D. Litster, R. J. Birgeneau, M. Kaplan, C. R. Safinya, A. Lindegaard-Andersen, S. Mathiesen, Observation of algebraic decay of positional order in a smectic liquid crystal, *Phys. Rev. B* **1980**, *22*, 312.
- [335] C. R. Safinya, E. B. Sirota, D. Roux, G. S. Smith, Universality in interacting membranes, *Phys. Rev. Lett.* **1989**, *62*, 1134.
- [336] T. Kuwahara, H. Nagase, T. Endo, H. Ueda, M. Nakagaki, Crystal Structure of DL-12-Hydroxystearic Acid, *Chem. Lett.* **1996**, *25*, 435.
- [337] S. Wu, J. Gao, T. J. Emge, M. A. Rogers, Influence of solvent on the supramolecular architectures in molecular gels, *Soft Matter* **2013**, *9*, 5942.
- [338] G. Vertogen, W. H. Jeu, *Thermotropic Liquid Crystals, Fundamentals*, Springer, Berlin, Heidelberg, **1988**.
- [339] P.-G. de Gennes, J. Prost, *The physics of liquid crystals*, Clarendon Press, Oxford, **1993**.

- [340] Y. Bouligand, Recherches sur les textures des états mésomorphes - 1. Les arrangements focaux dans les smectiques, *J. Phys. France* **1972**, *33*, 525.
- [341] C. E. Williams, M. Kléman, Dislocations, Grain Boundaries and Focal Conics in Smectics A, *J. Phys. Colloques* **1975**, *36*, C1-315.
- [342] A. Saupe, On Molecular Structure and Physical Properties of Thermotropic Liquid Crystals, *Mol. Cryst.* **1969**, *7*, 59.
- [343] W.K. Schief, M. Kléman, C. Rogers, On a nonlinear elastic shell system in liquid crystal theory, *Proc. R. Soc. A* **2005**, *461*, 2817.
- [344] C. Laule, I. M. Vavasour, S. H. Kolind, D. K.B. Li, T. M. Traboulsee, G. M. W. Moore, A. L. MacKay, Magnetic Resonance Imaging of Myelin, *Neurotherapeutics* **2007**, *4*, 460.
- [345] W. Möbius, K.-A. Nave, H. B. Werner, Electron microscopy of myelin, *Brain Res.* **2016**, *1641*, 92.
- [346] M. Camacho-Lopez, H. Finkelmann, P. Palffy-Muhoray, M. Shelley, Fast liquid-crystal elastomer swims into the dark, *Nat. Mater.* **2004**, *3*, 307.
- [347] S. Schuhladen, F. Preller, R. Rix, S. Petsch, R. Zentel, H. Zappe, Iris-like tunable aperture employing liquid-crystal elastomers, *Adv. Mater.* **2014**, *26*, 7247.
- [348] O. M. Wani, H. Zeng, A. Priimagi, A light-driven artificial flytrap, *Nat. Commun.* **2017**, *8*, 15546.
- [349] M. Herbst, "Stearic acid as a cosurfactant in the lyotropic system SDS/DOH/H<sub>2</sub>O - a comparison with the gelator 12-HOA", *research report*, University of Stuttgart, Stuttgart, **2020**.
- [350] M. H. F. Wilkins, A. E. Blaurock, D. M. Engelmann, Bilayer Structure in Membranes, *Nature, New Biol.* **1971**, *230*, 72.
- [351] A. J. Leadbetter, E. K. Norris, Distribution functions in three liquid crystals from X-ray diffraction measurements, *Mol. Phys.* **1979**, *38*, 669.
- [352] A. J. Leadbetter, P. G. Wrighton, Order Parameters in SA, SC AND N Phases by X-Ray Diffraction, *J. Phys. Colloques* **1979**, *40*, C3-234.
- [353] P. Davidson, L. Strzelecki, Synthesis, Characterization and X-Ray Diffraction Studies of a New Homologous Series of Cyano-Substituted Mesomorphic Side Chain Polyacrylates, *Liq. Cryst.* **1988**, *3*, 1583.
- [354] P. Davidson, A. M. Levelut, M. F. Achard, F. Hardouin, X-ray diffraction study of the smectic A phases of some side-chain polysiloxanes, *Liq. Cryst.* **1989**, *4*, 561.
- [355] M. J. Buerger, G. E. Klein, Correction of X-Ray Diffraction Intensities for Lorentz and Polarization Factors, *J. Appl. Phys.* **1945**, *16*, 408.
- [356] M. J. Buerger, The Correction of X-Ray Diffraction Intensities for Lorentz and Polarization Factors, *Proc. Natl. Acad. Sci. U. S. A.* **1940**, *26*, 637.

## 9 Appendix

### 9.1 Comparative study on the cosurfactant effect of 12-HOA

In chapter 4 it was shown that the gelator 12-HOA - besides its gelling properties - acts also partly as cosurfactant. To better understand the influence of 12-HOA on the LLC phases, the phase behavior of the LLC phases after gelation was compared with the phase behavior of the LLC phases after addition of stearic acid. This was studied in the research internship of Michael Herbst under my supervision.<sup>[349]</sup> As shown in Figure 9.1, the molecular structures of 12-HOA and stearic acid differ only in the presence of the OH-group at the C12 position in the case of 12-HOA. As described above, the 12-hydroxyl group of 12-HOA is substantial for the formation of gel fibers. Thus, stearic acid should show a comparable influence as cosurfactant on the LLC phases, while not inducing gelation. In fact, the absence of the hydroxyl group reduces steric hindrance and makes the alkyl chain more hydrophobic, all of which should make stearic acid a more effective cosurfactant than 12-HOA. Hence, by comparing the influence of stearic acid or 12-HOA on the LLC phases, effects due to the cosurfactant behavior can be distinguished from effects of the gel fiber network for 12-HOA.

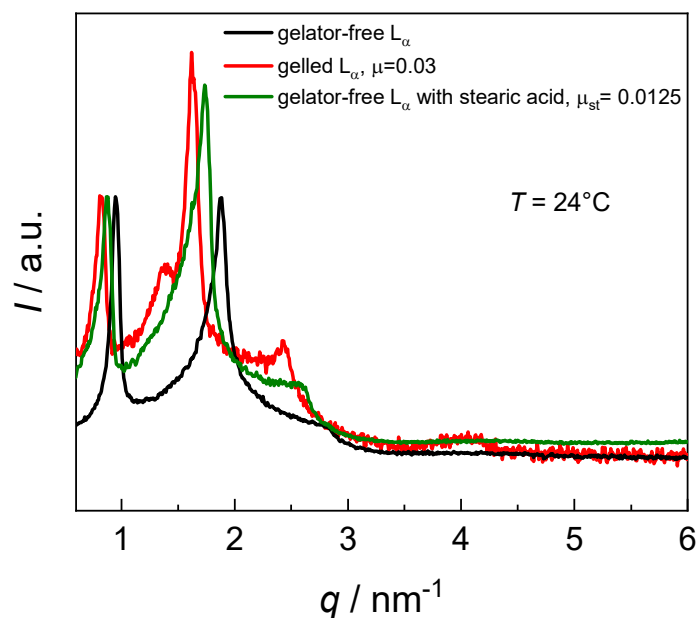


**Figure 9.1:** Molecular structure of *a)* 12-HOA and *b)* stearic acid. Both have a carboxylic head group and a C18 alkyl tail, but 12-HOA additionally has a hydroxyl group at the C12 position.

Since the DSC results indicate that about 1.25 wt% of 12-HOA are incorporated into the micelles, also 1.25 wt% stearic acid were added to the ternary lyotropic mixtures. For the  $N_d$  phase after addition of stearic acid, a two-phase region of  $N_d + L_\alpha$  phase was found at room temperature. However, the  $N_c$  phase is still nematic after addition of stearic acid, although the diffuse scattering maxima are slightly sharper than for the ternary  $N_c$  phase, indicating a larger correlation length of clusters with local translational ordering in the nematic phase.<sup>[349]</sup> To conclude, 12-HOA has a greater impact on the nematic phases by shifting them completely into the lamellar regime than stearic acid has as a cosurfactant. Since the cosurfactant effect should be similar or even slightly better for stearic acid, we assume that not only the cosurfactant effect but additionally a soft templating effect by the gel fibers lead to the surprising stabilization of the lamellar structure.

One effect of the gel network on the structure of the lamellar phase is that the lamellar layer spacing is “arrested”, i.e. independent of temperature (section 4.2.3, Figure 4.20). That this surprising behavior is truly a network effect and not a cosurfactant effect of 12-HOA was confirmed by measuring the temperature dependent lamellar repeat unit for a  $L_\alpha$  phase in which stearic acid was added as cosurfactant, which shows the same behavior than the “regular” gelator-free  $L_\alpha$  phase, namely a decreasing lamellar repeat unit with increasing temperature.<sup>[349]</sup>

As shown in chapter 4 (see Figure 4.21), gelling the  $L_\alpha$  phase leads to an enhanced lamellar order in comparison to the non-gelled lamellar phase, since in X-ray scattering the intensity of higher order layer peaks increases. In the X-ray curve of the  $L_\alpha$  phase with stearic acid the higher order layer peaks are also intensified in comparison with the gelator-free  $L_\alpha$  phase but are less intense than in the lamellar gel.



**Figure 9.2:** Comparison of the X-ray curves of the gelator-free  $L_\alpha$  phase ( $\omega_{H_2O} = 0.70$ ,  $\gamma_{DOH/SDS} = 0.30$ , black), the corresponding gelled  $L_\alpha$  phase ( $\mu = 0.03$ , red) and the corresponding  $L_\alpha$  phase with stearic acid as cosurfactant ( $\mu_{st} = 0.0125$ , green). The intensity is normalized to the respective intensity of the first order layer peak. An increase in intensity of the higher order reflections indicates a higher translational order for the gelled than for the gelator-free  $L_\alpha$  phase.

All measurements in Figure 9.2 were recorded with a cell holder in which the capillary is rotated along its long axis to obtain perfect powder diffractograms. It is noted that in the case of the gelator-free  $L_\alpha$  phase the intensity of the second order peak  $I_{002}$  is already as high as for the first order one ( $I_{001}$ ), while for the lamellar gel even  $I_{002} > I_{001}$  applies. The reason for this behavior lies in the electron density contrast along the lamellar repeat unit (electron density  $\rho(z)$  for one lamellar layer spacing  $d_0$

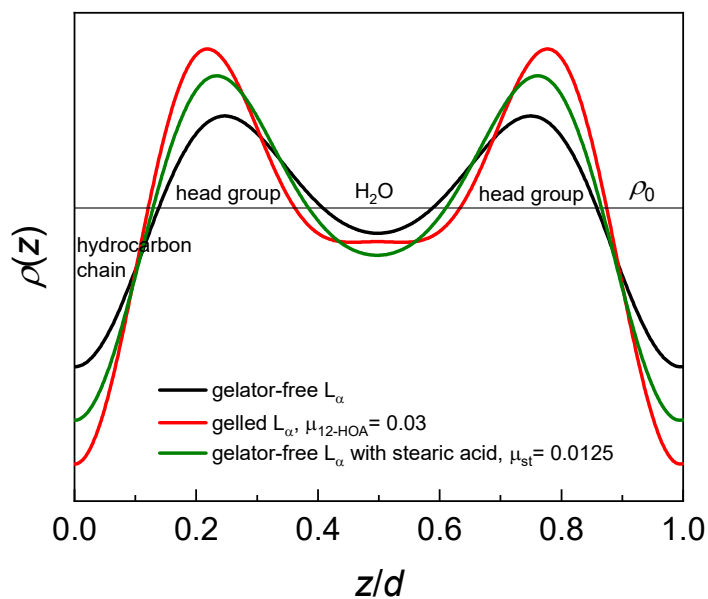
along the director  $\mathbf{n}$ ). The surfactant head groups have an electron density higher than that of water, while the hydrocarbon chains have an electron density lower than water.<sup>[350]</sup> Thus, a description of the electron density as a sinusoidal modulation of period  $d_0$  along the director as for typical thermotropic SmA phases<sup>[339]</sup> is not valid for lyotropic lamellar phases and an estimation of the translational order parameter from the ratio of the intensities of the layer peaks as suggested by Leadbetter *et al.*<sup>[351,352]</sup> is not straightforward for  $L_\alpha$  phases. The electron density profile however can be calculated from the intensities of the layer peaks as was shown for LC polymers by Davidson *et al.*<sup>[353,354]</sup> The modulation of the electron density  $\rho(z)$  around the mean electron density  $\rho_0$  is a symmetric and periodic function of period  $d_0$  and hence  $\rho(z)$  can be expanded in a Fourier series with only the cosine terms being relevant

$$\rho(z) = \sum_{n=1}^{\infty} a_n \cos\left(2\pi n \frac{z}{d_0}\right). \quad (9.1)$$

The intensity of the  $n^{\text{th}}$  order layer peak is directly proportional to  $|a_n^2|$ , with  $|a_n|$  being the modulus of the coefficient  $a_n$ . The intensities were corrected with the Lorentz factor ( $L = \frac{1}{\sin 2\theta}$ )<sup>[355,356]</sup> and since no absolute scattering intensities were measured, the ratio of the amplitude of the  $n^{\text{th}}$  order layer peak to the first one  $a_n/a_1$  are used. The coefficients  $a_n$  may be positive or negative, so the phase problem constitutes in determining the correct combination of the algebraic signs for the coefficients  $a_n$  ( $\frac{2^n}{2}$  distinctive possibilities).<sup>[353,354]</sup> The physical probability of the obtained electron density profiles has to be evaluated. In our case, only one combination of algebraic signs for the coefficients  $a_n$ , namely  $\rho_{---}(z)$  (meaning that  $a_1$ ,  $a_2$  and  $a_3$  are negative) shows two maxima in an appropriate distance.

The electron density profile along the layer normal with the origin being in the center of the bilayer calculated from the measurements shown in Figure 9.2 can be seen in Figure 9.3. A period of very roughly  $d_0/2$  in the electron density profile leads to the high intensity of the second order reflection. The more defined electron density profile for the lamellar gel shows that the lamellar order is increased in comparison with the gelator-free  $L_\alpha$  phase. For the  $L_\alpha$  phase in which stearic acid is added as cosurfactant to imitate the cosurfactant effect of 12-HOA, the modulation of electron density profile is better than for the gelator-free  $L_\alpha$  phase but worse than in the lamellar gel. This underlines that the

increased translational order is mainly the consequence of the fiber network and only secondary the result of the cosurfactant effect.



**Figure 9.3:** Projection of the electron density profile  $\rho(z)$  along the layer normal  $z$  using the combination  $\rho_{\text{---}}(z)$  calculated from the scattering data shown in Figure 9.2 for the gelator-free  $L_\alpha$  phase (black), the corresponding gelled  $L_\alpha$  phase ( $\mu = 0.03$ , red) and the  $L_\alpha$  phase with stearic acid as cosurfactant ( $\mu_{\text{st}} = 0.0125$ , green). The origin is chosen to be in the center of the bilayer.

## 9.2 Publications



## Publication I



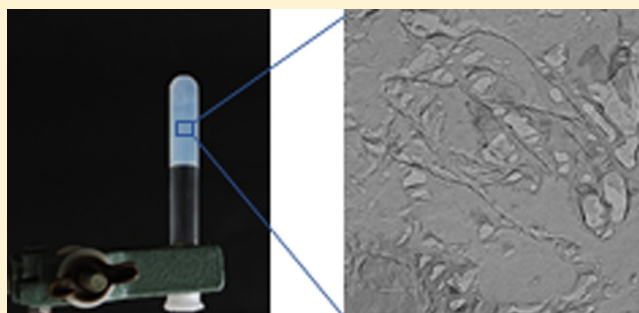
# Gelation of Lyotropic Liquid-Crystal Phases—The Interplay between Liquid Crystalline Order and Physical Gel Formation

Sonja Dieterich, Thomas Sottmann,<sup>1b</sup> and Frank Giesselmann\*<sup>1b</sup>

Institute of Physical Chemistry, University of Stuttgart, Pfaffenwaldring 55, 70569 Stuttgart, Germany

## Supporting Information

**ABSTRACT:** We present a systematic investigation of gelled lyotropic liquid crystals (LLCs). This new class of soft materials combines the anisotropy of LLCs with the mechanical stability of a physical gel. The studied LLC system consists of sodium dodecyl sulfate as a surfactant, *n*-decanol as a cosurfactant, and water as a solvent. At room temperature, four liquid crystalline phases (lamellar  $L_w$ , nematic  $N_d$  and  $N_o$  and hexagonal  $H_1$ ) are formed depending on the composition. We were successful in gelling the lyotropic lamellar phase with the low-molecular-weight organogelator 12-hydroxyoctadecanoic acid (12-HOA). The obtained gelled lamellar phase shows optical birefringence, elastic response, and no macroscopic flow. However, we were not able to obtain gels with hexagonal or nematic structure. These findings can be explained twofold. When gelling the hexagonal phase, the long-range hexagonal order was destroyed and an isotropic gel was formed. The reason might be the incompatibility between the gel fiber network and the two-dimensional long-range translational order of the cylindrical micelles in the hexagonal phase. Otherwise, the lyotropic nematic phase was transformed into an anisotropic gel with the lamellar structure during gelation. Evidently, the addition of the gelator 12-HOA to the lyotropic system considerably widens the lamellar regime because the integration of the surface-active 12-HOA gelator molecules into the nematic micelles flattens out the micelle curvature. We further investigated the successfully gelled  $L_w$  phase to examine the impacts of the gel network and the remaining monomeric gelator on both the structure and properties of the gelled lamellar phase. Small-angle X-ray scattering results showed an arrested lamellar layer spacing in the gelled state, which indicates a higher translational order for the gelled lamellar phases in comparison with their gelator-free counterparts.



## INTRODUCTION

The gelation of lyotropic liquid crystals (LLCs) combines the unique properties of a physical gel and an anisotropic fluid which leads to a new class of soft anisotropic materials. LLCs show various degrees of orientational and translational order and are of interest because of their appearance in various biological structures such as lysosomes or the eukaryotic cell membrane. Physical gels are soft solids in which the solvent is trapped in a three-dimensional (3D) fibrous network (the so-called self-assembled fibrillar networks). This network is built by a small amount of a low-molecular-weight gelator. The gelator molecules self-organize via highly selective noncovalent interactions such as H-bonds or  $\pi$ - $\pi$ -stacking leading to a one-dimensional growth of the fibers, which then entangle to form the 3D network.<sup>1–6</sup> An important example of a low-molecular-weight gelator is 12-hydroxyoctadecanoic acid (12-HOA), whose molecular structure and fiber formation are shown in Figure 1. 12-HOA gels various organic solvents<sup>7–9</sup> and is thus known as an organogelator.

Applications of elastic physical gels as new functional materials can be found in various fields.<sup>1,5,16–23</sup> The thermoreversible sol–gel phase transition and their responsiveness to external stimuli<sup>24</sup> such as pH value,<sup>25</sup> light,<sup>26–29</sup>

enzymes,<sup>30–33</sup> or ion concentration<sup>26</sup> make physical gels to proper matrices for cosmetics, inks, and drugs, where on-demand release is necessary.<sup>3,6,34</sup>

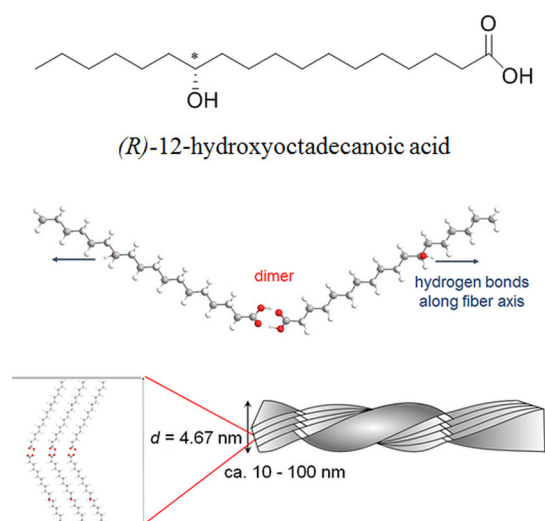
It has been shown that some organogelators are able to gel thermotropic liquid crystals (LCs), thus forming anisotropic soft solids.<sup>35–42</sup> The gel structure can enhance anisotropic properties such as electro-optical response in twisted nematic cells<sup>43</sup> or hole mobility.<sup>44</sup> Additionally, it is found that the gel network stabilizes the liquid-crystal (LC) alignment and director patterns.<sup>45,46</sup> If the liquid crystalline phase is formed before the gel network structure, the LC can serve as a soft template for the gel, resulting in well-aligned fibers.<sup>47–50</sup> If the fiber structure is formed first, randomly oriented fibers result in a polydomain LC morphology. Applying an electric field to such a liquid crystalline physical gel leads to a macroscopic alignment of the LC director and thereby switches a light-scattering material into a transparent one<sup>51,52</sup> (or the other way round for a homeotropically aligned nematic pattern as a template for the physical gel<sup>53</sup>).

Received: August 20, 2019

Revised: October 10, 2019

Published: October 17, 2019

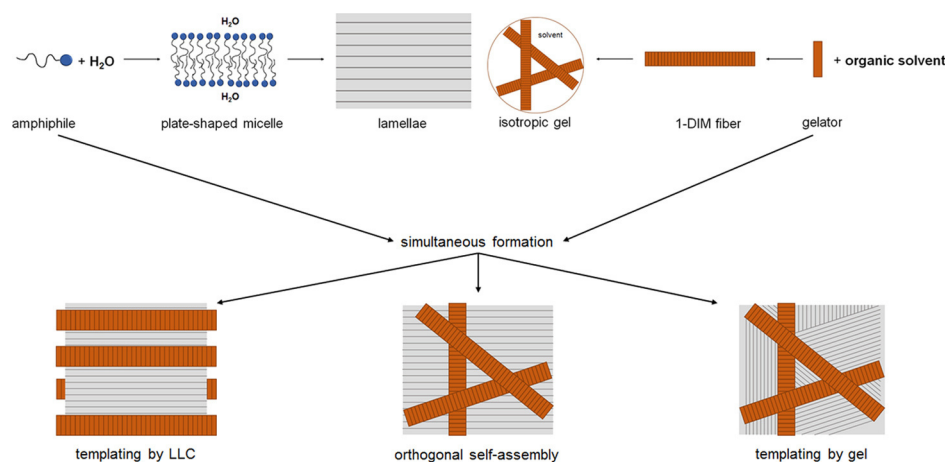




**Figure 1.** Molecular structure of (*R*)-12-HOEA, as well as the arrangement of 12-HOEA molecules into the gel fibers. In nonpolar solvents, the 12-HOEA molecules form cyclic bent dimers via the carboxylic head groups.<sup>10,11</sup> Aggregation of the dimers due to hydrogen bonds between the hydroxyl groups at the C<sub>12</sub> position leads to a one-dimensional fiber growth.<sup>12,13</sup> X-ray investigations showed that the dimers are organized in layers of a thickness of 4.67 nm.<sup>14,15</sup> Freeze-fracture electron microscopy (FFEM) showed that the fibers exhibit a helical twist and revealed a fiber thickness of 10–100 nm,<sup>14</sup> indicating that there are 2–20 layers per fiber.

In contrast to these soft templating scenarios, two coexisting self-assembled structures might also form independently from each other within the same system. This concept is called orthogonal self-assembly<sup>54,55</sup> which can be found in biological cells, where amphiphiles, proteins, biopolymers, and other self-assembling components form coexisting structures such as membranes, cytoskeleton, and ribosomes.<sup>56–58</sup> Hence, there is an intensive research to form complex biomimetic architectures by orthogonal self-assembly,<sup>59</sup> where a physical gel coexists with liposomes,<sup>56</sup> micellar solutions,<sup>60,61</sup> and bicontinuous microemulsions.<sup>62,63</sup>

In Figure 2, the three possible scenarios (soft templating by either a LC or a gel network and orthogonal self-assembly) are portrayed for the case of gelled LLCs.



**Figure 2.** LLCs (here the  $L_{\alpha}$  phase is shown as an example) as well as fibrillar gel networks self-assemble in two steps. A simultaneous formation of both structures can either result in an orthogonal self-assembled system or one of the two structures guides the orientation of the other one leading to a templating mechanism by either the LLC or the gel network.

A soft templating mechanism has already been reported to fabricate ultrathin polyacrylamide nanosheets, where lamellar bilayer membranes served as a two-dimensional (2D) template.<sup>64</sup> In contrast to the previously described physical gels formed by low-molecular-weight gelators, the monomers are linked via chemical bonds in this case. Another way to form chemical gels in combination with LCs are liquid-crystal elastomers (LCEs). In LCEs, the mesogenic units can be covalently linked via flexible spacers to the polymer backbone (side-chain polymers) or can be part of the polymer backbone itself (main-chain polymers).<sup>67,68</sup> Therefore, LCEs are chemically cross-linked gels that do not form via self-assembly. LCEs are of eminent importance in the field of biomimetic actuation because LCEs can reversibly change their shape in response to external stimuli, such as temperature, light, or electric fields, because of the changes in the order (parameter) of the liquid crystalline phase. They are actuators that convert external energy into directed mechanical motion.<sup>65–68</sup> Examples for biomimetic motion are artificial muscles,<sup>69–73</sup> biological locomotion,<sup>74–76</sup> the iris of the human eye,<sup>77</sup> or an artificial flytrap.<sup>78</sup> In addition, applications such as micropumps<sup>79</sup> or motors<sup>80</sup> are possible with LCEs.

Lamellar hydrogels, in which surfactant bilayers are decorated with short poly(ethylene glycol)-based amphiphilic block copolymers, have already been reported.<sup>81,82</sup> So far, there are only a few examples of a LLC coexisting with a 3D physical network<sup>83–86</sup> and no gelled lyotropic nematic phase is reported until now. What is lacking so far is a systematic investigation of various liquid crystalline phases of the same lyotropic system gelled by the same self-assembling low-molecular-weight gelator.

In the present paper, we now try to transfer the concept of liquid crystalline physical gels to physically cross-linked LLCs. Similar to LCEs, macroscopically aligned monodomains of such gelled LLCs may respond to external stimuli such as temperature, pH value, or vapor pressure of the solvent by a macroscopic change in shape. The advantage of gelled LLCs over LCEs is the cheap and easy fabrication of a functional elastic material. Further possible applications of gelled LLCs are in the field of transdermal drug delivery,<sup>18,87</sup> or they may serve as soft templates for the synthesis of highly oriented and macroscopic-

cally aligned nanostructured materials, such as mesoporous silica materials.<sup>88–92</sup>

Here, we report the gelation of the system consisting of sodium dodecyl sulfate (SDS) as a surfactant, *n*-decanol (DOH) as a cosurfactant, and water as a solvent. Depending on the composition, four liquid crystalline phases (lamellar  $L_{\alpha}$  nematic  $N_d$  and  $N_c$ , and hexagonal  $H_1$ ) are formed at room temperature. The organogelator 12-HOA was used as a gelator. The two questions under considerations are as follows:

- (1) Are we able to gel the lyotropic liquid crystalline phases? This means that the particular liquid crystalline order is conserved during gelation and coexists with the gel network.
- (2) Do the two structures form independently from each other (orthogonal self-assembly)? Or, and more important how, does the gel network influences the structure and properties of the LC and vice versa?

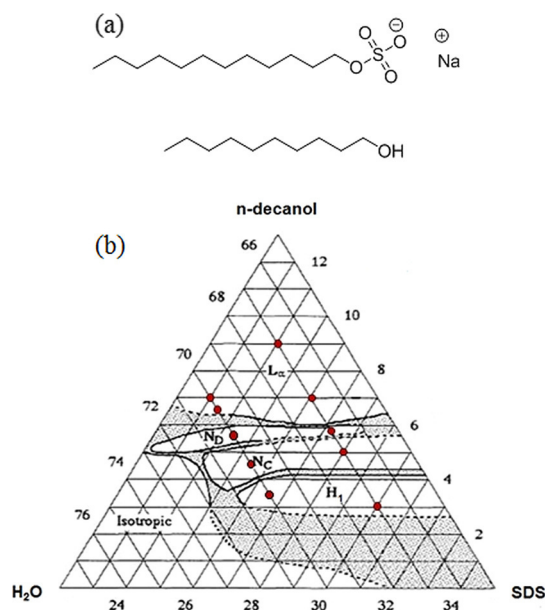
This paper is organized in two parts. In the first part, we report our attempts to gel the four liquid crystalline phases (lamellar  $L_{\alpha}$  nematic  $N_d$  and  $N_c$ , and hexagonal  $H_1$ ) of our LLC system. We found that the gelation strongly stabilizes the  $L_{\alpha}$  phase, while the structure of the other phases is not conserved during gelation. A gel with hexagonal liquid crystalline order could not be obtained because it seems like the 3D fiber growth destroys the 2D translational order of the  $H_1$  phase, leading to an isotropic gel. When gelling the lyotropic nematic phases, we received anisotropic gels with lamellar order. In the second part of the paper, we studied the successfully gelled lamellar phase in more detail. Small-angle X-ray scattering (SAXS) results demonstrate a higher translational order and an arrested lamellar layer spacing for the gelled lamellar phase in comparison with the gelator-free phase. This clearly shows that our gelled lamellar phase is not an orthogonal self-assembled system.

## EXPERIMENTAL SECTION

**Materials and Sample Preparation.** As a lyotropic liquid crystalline system, a ternary system containing SDS as surfactant, DOH as cosurfactant, and bidistilled water as solvent is used. SDS was purchased from Sigma-Aldrich (BioUltra,  $\geq 99.0\%$ ). The cosurfactant DOH was obtained from Merck ( $\geq 99.0\%$ ). SDS and DOH were used without further purification, and their molecular structures are shown in Figure 3a. At room temperature, four liquid crystalline phases (lamellar  $L_{\alpha}$  nematic  $N_d$  and  $N_c$ , and hexagonal  $H_1$ ) are formed, depending on the cosurfactant-to-surfactant mass ratio  $\phi_{\text{DOH/SDS}}$ . We prepared samples at two fixed water contents, 70 and 67 wt %  $\text{H}_2\text{O}$ . The phase diagram is well established in the literature<sup>93</sup> and shown in Figure 3b, the examined samples are highlighted as red dots.

The low-molecular-weight gelator 12-HOA (see Figure 1) was purchased from ChemCruz and used without further purification. Because no chirality information was available, melting temperature and optical activity were measured to confirm that the *R*-configuration is present, as 12-HOA is obtained by hydrogenation of the naturally occurring chiral compound ricinolic acid.<sup>13</sup> The melting point was measured via differential scanning calorimetry (DSC) (PerkinElmer, DSC 8000) to be 79.5 °C, which is in good agreement with values of 79.8<sup>13</sup> and 80.3 °C<sup>14</sup> found in the literature and clearly higher than the value 76.2 °C of the racemate.<sup>13</sup> The specific rotation of 12-HOA  $[\alpha]$  was measured with a polarimeter (PerkinElmer, 241 MC) at room temperature in pyridine at  $\lambda = 589$  nm (Na-D line) and in benzene at  $\lambda = 365$  nm (Hg-lamp). We found  $[\alpha]_{\text{D}} = -0.39$  (literature  $[\alpha]_{\text{D}} = -0.46$ )<sup>14</sup> and  $[\alpha]_{365} = -0.99$  [literature  $[\alpha]_{365} = -0.84$  (Kanto Chemicals, purified) and  $[\alpha]_{365} = -1.0$  (Sigma-Aldrich)].<sup>13</sup> Hence, the used 12-HOA is clearly present in its *R*-configuration.

The handedness of the chiral 12-HOA is of importance because there is an ongoing scientific discussion whether the racemic form is able to



**Figure 3.** (a) Molecular structure of SDS (on top) and DOH (below). (b) Phase diagram of the investigated lyotropic liquid crystalline system. The red dots indicate the sample compositions. Reprinted with permission from [Quist, P.-O.; Halle, B. Curvature defects in a lamellar phase revealed by nuclear-spin-relaxation anisotropy. *Phys. Rev. E* 1993, 47, 3374–3395. Copyright 1993, American Physical Society].

gel organic solvents or not. Sakurai et al. claimed that the racemic form does not form gels,<sup>13</sup> whereas Grahame et al. described the gelating ability of the racemic form as significantly worse than that of the enantiopure compound.<sup>12</sup> The reason for this is different H-bond geometries, which lead in organic solvents to twisted fibers in the case of enantiopure 12-HOA and platelets in the case of racemate.<sup>12</sup> Additionally, it was found that (*R*)-12-HOA forms left-handed fibers, whereas the fibers formed by (*S*)-12-HOA show a right-handed twist.<sup>94</sup>

The composition of the investigated samples is specified by the quantities listed below.

The water mass fraction is defined as

$$\omega_{\text{H}_2\text{O}} = \frac{m_{\text{H}_2\text{O}}}{m_{\text{H}_2\text{O}} + m_{\text{SDS}} + m_{\text{DOH}} + m_{12\text{-HOA}}} \quad (1)$$

and is either  $\omega_{\text{H}_2\text{O}} = 0.70$  or  $\omega_{\text{H}_2\text{O}} = 0.67$  for all samples. The DOH-to-SDS ratio is given by

$$\phi_{\text{DOH/SDS}} = \frac{m_{\text{DOH}}}{m_{\text{SDS}}} \quad (2)$$

The amount of gelator used to gel the sample is specified by the gelator mass fraction

$$\eta = \frac{m_{12\text{-HOA}}}{m_{\text{H}_2\text{O}} + m_{\text{SDS}} + m_{\text{DOH}} + m_{12\text{-HOA}}} \quad (3)$$

The properties of the gelled lyotropic liquid crystalline phases are compared with two parent systems, namely, (i) the gelator-free LLC with the same  $\omega_{\text{H}_2\text{O}}$  and  $\phi_{\text{DOH/SDS}}$  as the gelled LLC and (ii) the binary gel formed by dodecane and the same amount  $\eta$  of 12-HOA as in the gelled LLC. Dodecane was chosen for comparison because it has the same chain length as the hydrophobic part of the surfactant SDS.

The gelled LLC phases were prepared by dissolving proper amounts of SDS and 12-HOA in  $\text{H}_2\text{O}$  and DOH, respectively. For the dissolution of 12-HOA, elevated temperatures (60–70 °C) in a thermoshaker (Hettich, MHR-23) are necessary. The two solutions are combined by adding the SDS/ $\text{H}_2\text{O}$  solution to 12-HOA/DOH by means of a syringe with a thick needle and concurrent but cautious vortex (ika VORTEX 3) to ensure a proper mixing while preventing

foam formation. For fast gel network growth, the mixture was quenched in an ice bath for 0.5 h. Afterward, the sample is kept 1 day at room temperature to complete the gel formation. To probe whether or not the sample was gelled, the vial was put upside down for at least 4 h. If no flow was observed, the sample was considered as gelled.

The parent systems were obtained as follows. To prepare the gelator-free LLC, SDS and water were weighed into a glass vial sealed with a screw plug and the mixture was kept at 40 °C in a thermoshaker (Biosan, PST-60HL) until SDS was completely dissolved (about 1 h). DOH was added and the vial was placed on a roll mixer (Phoenix Instruments, RS-TR05) until the sample was homogenized (at least 2 days). The formation of the liquid crystalline phases was confirmed by the observation of characteristic textures in the polarizing optical microscope (Leica, DMLP). To obtain the binary gel, 12-HOA and dodecane (Sigma-Aldrich,  $\geq 99.0\%$ , used without further purification) were weighed into a vial, which were heated in a thermoshaker (Hettich, MHR-23) until 12-HOA was dissolved (60–70 °C, 500 rpm). Afterward, the hot solution was quenched in an ice bath and kept overnight at room temperature. Gel formation was tested as described above.

**Methods.** Polarizing microscopy was performed at room temperature using a Leica DMLP polarizing microscope. Photographs of the textures were taken by a Nikon D5300 camera. Samples were filled into flat capillaries (Camlab UK) of dimensions of  $0.4 \times 4$  mm and flame sealed.

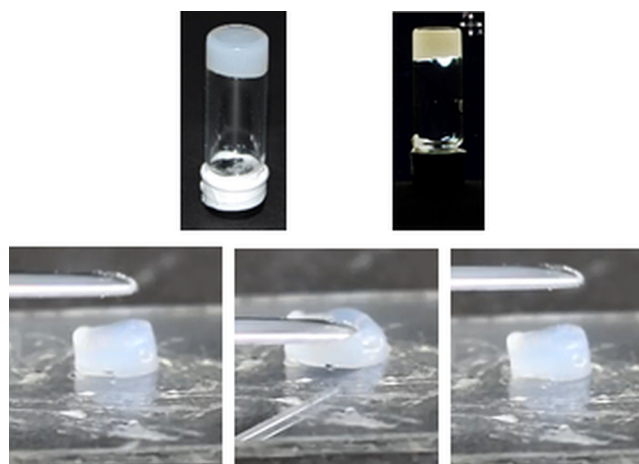
Dynamic scanning calorimetry was performed with a power compensating PerkinElmer DSC8000 instrument using a heating rate of 5 K/min to heat from 20 to 80 °C. Samples were filled into aluminum pans (PerkinElmer, Part no. B016-9321) which were sealed afterward.

Small-angle X-ray studies were carried out with a SAXSess system (Anton Paar). The X-ray radiation (Cu K $\alpha$ ,  $\lambda = 0.15418$  nm) was generated by an ISO-DEBYEFLEX 3003 X-ray generator (GE Inspection Technologies GmbH) and the X-ray scattering was recorded using either a CMOS detector (Dectris, Mythen 2 1K) or a CCD detector (Princeton instruments, SCX-TE:4300K/2). Temperature was controlled by the sample holder unit TSC 120. Samples were placed into Mark capillary tubes (Hilgenberg, glass no. 14) with an outer diameter of 0.7 mm and a wall thickness of 0.01 mm.

FFEM replicas of the gelled LC samples were prepared with a freeze fracture and etching system EM BAF060 from Leica. At room temperature, a small amount of each specimen was placed on two copper grids (hexagonal 360 mesh) and two copper plates (4.5 mm  $\times$  3.0 mm), which were assembled to a so-called sandwich. The sandwich was then plunged into liquid ethane cooled by liquid nitrogen. The frozen and fractured specimen was quickly transferred into the vacuum chamber of BAF060. At  $-150$  °C, the surface was replicated by a layer of Pt/C ( $\sim 2$  nm) deposited at an angle of 45° and stabilized by a layer of pure carbon ( $\sim 20$  nm) at 90°. After cleaning the replicas with warm ethanol, they were examined using a Tecnai G2 Sphera FEI TEM (FEI, Eindhoven, Netherlands) at 200 kV. TEM images were recorded by a 16-megapixel camera (TemCam-F416 [4k  $\times$  4k], TVIPS, Gauting, Germany).

## RESULTS AND DISCUSSION

**Gelling the Different Lyotropic Liquid Crystalline Phases.** Characteristic gel properties are elasticity (at least in a certain stress range) and the absence of macroscopic flow. To probe whether our gelled LLCs show this behavior, the vial containing the sample was put upside down for several hours. No flow was observed for the gelled  $L_\alpha$  phase ( $\eta = 0.015$ ), as seen in Figure 4. The shape persistency was proven by applying stress by means of a spatula on the sample and releasing it afterward. As shown in Figure 4, the deformation is reversible, clearly confirming the elastic properties of the gelled  $L_\alpha$  phase. Between crossed polarizers, the gelled  $L_\alpha$  phase shows optical birefringence, which was not observed for the corresponding binary gel (dodecane gelled with 1.5 wt % 12-HOA). This



**Figure 4.** (On top) Picture of the gelled lyotropic lamellar phase outside and between crossed polarizers. The gel shows no flow but strong optical birefringence. (Below) The pictures show the elasticity of the gelled lamellar phase. The gel returns to its original shape when the stress is released.

confirms the anisotropy originating from the presence of the liquid crystalline phase.

When gelling the liquid crystalline phases, we noticed that at least 1.5 wt % 12-HOA are needed to gel the lamellar phase. However, 1.8 and 2.0 wt % are necessary to gel the nematic phases and the hexagonal phase, respectively. In contrast, the critical gelation concentration (cgc) to gel dodecane is much less, 0.2 wt % only. It was reported that the cgc increases with increasing polarity and increasing ability of the solvent to form hydrogen bonds.<sup>95</sup>

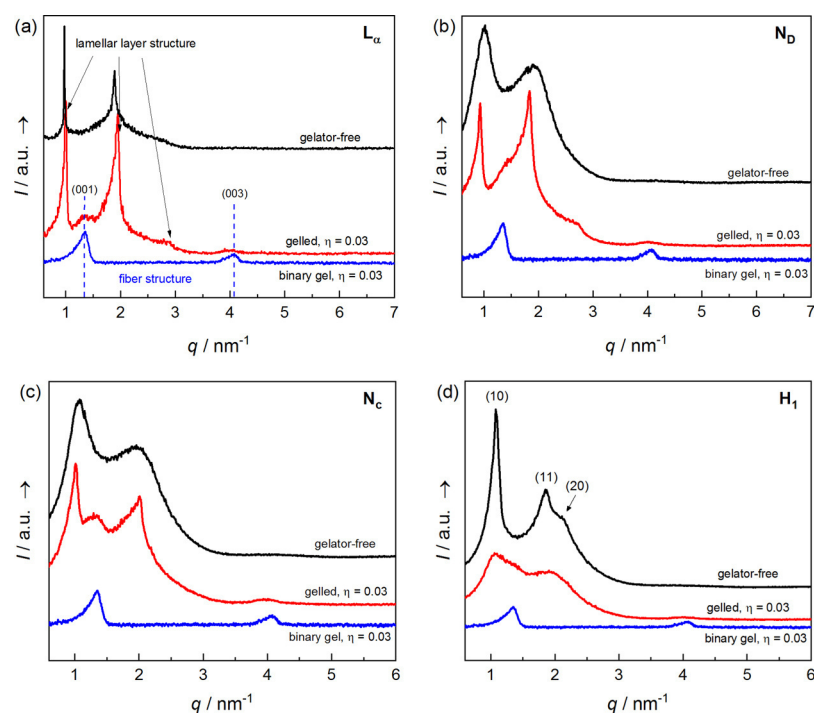
We now examined by X-ray diffraction (XRD) and POM whether or not the structures of the four different liquid crystalline phases are conserved in their gelled states.

The X-ray diffractograms of the gelled and gelator-free  $L_\alpha$ ,  $N_d$ ,  $N_c$ , and  $H_1$  phase as well as of the binary gel are shown in Figure 5. Because of the layer structure of the lamellar phase, pseudo-Bragg peaks arise at the same positions in both cases, the gelator-free and the gelled ( $\eta = 0.03$ )  $L_\alpha$  phase. In addition, small broad peaks at  $q = 1.33 \text{ nm}^{-1}$  and  $q = 3.99 \text{ nm}^{-1}$  appear in the SAXS curve of the binary gel and the gelled  $L_\alpha$  phase. These are known to be the (001) and (003) reflections of the bilayers of bent cyclic 12-HOA dimers of which the fiber consists.<sup>14,15</sup> The considerable width of these peaks corresponds to small correlation lengths because a single twisted fiber is formed by a limited number of layers. All in all, the SAXS results in Figure 5a clearly confirm the formation and coexistence of the lamellar layer structure and the gel fiber structure in the gelled  $L_\alpha$  phase.

In the case of the gelator-free nematic phases  $N_d$  and  $N_c$ , broad scattering peaks due to the short-range translational order of nematic phases are observed. However, the gelled materials obtained thereof show the characteristic  $I(q)$  profiles of lamellar phases with 2 orders of sharp layer peaks. This observation suggests that the gelation transforms the lyotropic nematic phases into lamellar phases. Further support is given by FFEM, which indeed confirms the presence of lamellar layer steps in the gelled material (S1). Hence, gelling the nematic phases with 12-HOA leads to gelled lamellar phases.

The gelator-free  $H_1$  phase shows three sharp peaks with a  $q$ -ratio of  $1:\sqrt{3}:2$ , which is characteristic for 2D hexagonal order. In the gelled state, however, just two diffuse peaks remain, which indicates that only short-range order is left. In addition, the





**Figure 5.** XRD profiles of the gelator-free (black) and gelled (red) (a)  $L_{\alpha}$ , (b)  $N_D$ , (c)  $N_C$ , and (d)  $H_1$  phases ( $\omega_{\text{H}_2\text{O}} = 0.70$  in all four phases). The formation of the lamellar layer structure is confirmed by the presence of 2 orders of sharp pseudo-Bragg peaks in both the gelator-free and the gelled  $L_{\alpha}$  phase. In the binary gel (blue), the diffuse and weak (001) and (003) peaks from the layered structure of the 12-HOA fibers are seen. These peaks are also found in the gelled  $L_{\alpha}$  phase, which confirms the coexistence of lamellar layers and gel fibers in the gelled  $L_{\alpha}$  phase. In the case of nematic phases, the gelator-free phases show two diffuse peaks because of the short-range order present in nematic phases. In the gelled materials obtained thereof, two sharp peaks with a  $q$ -ratio of 1:2 are observed together with the gel peaks from the 12-HOA fibers. This reveals that not a gelled nematic phase but instead a gelled lamellar phase is formed. For the gelator-free hexagonal phase, three characteristic pseudo-Bragg peaks with a  $q$ -ratio of  $1:\sqrt{3}:2$  are found because of the 2D hexagonal long-range order. After gelation with 12-HOA, only two broad peaks remain, which reveals that there is only short-range order left.

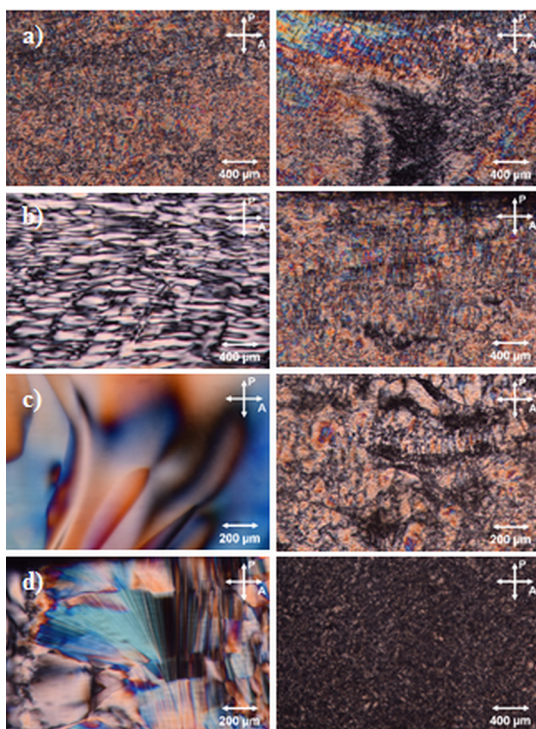
gelled phase shows no optical birefringence between crossed polarizers. Thus, gelling a hexagonal phase with 12-HOA does not result in a gelled  $H_1$  phase, but in an isotropic gel.

For a further identification of the gelled lyotropic liquid crystalline phases, we used polarized optical microscopy (POM) (Figure 6). The textures of the gelator-free and the gelled ( $\eta = 0.015$ ) lamellar phase resemble each other, both show an oily streak texture in a planar matrix. This is another proof that the lamellar structure is maintained in the gelled state. On the contrary, the POM images of the other gelled lyotropic liquid crystalline phases prove that it was not possible to gel the lyotropic  $N_C$ ,  $N_D$ , and  $H_1$  structures. The gelator-free  $N_C$  and  $N_D$  phase exhibit a schlieren texture typical for nematic phases. In line with the XRD results, the gelled phases ( $\eta = 0.018$ ) show textures similar to the one of the  $L_{\alpha}$  phase. In the gelator-free  $H_1$  phase, a typical fanlike texture can be observed, whereas it is not birefringent in the gelled state ( $\eta = 0.02$ ) anymore. The weak birefringence occurring in some parts of the gelled  $H_1$  phase arises because of a dense gel network. The results of POM thus confirm all findings of SAXS. The 2D translational order of the hexagonal phase is destroyed by the growth of the gel network. In the case of nematic phases, a lamellar phase is obtained after the gelation procedure.

What is the reason for the surprising stabilization of the lamellar phase? An explanation may lie in the molecular structure of the gelator 12-HOA. Apart from the 12-hydroxy group, 12-HOA has a typical surface-active structure with a polar head group and a nonpolar alkyl tail (see Figure 1). Thus, 12-HOA might also act as a cosurfactant and might be incorporated

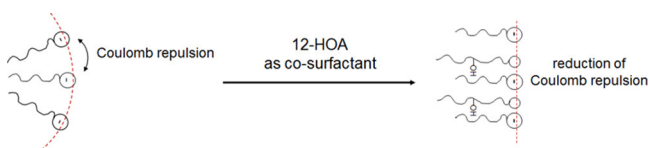
into the amphiphilic film. According to Israelachvili, the curvature of the micelle as well as the liquid crystalline phase formed thereof depend on the ratio of the effective cross-sectional area occupied by the alkyl tail and the effective cross-sectional area occupied by the head group.<sup>96</sup> The effective head group area of anionic surfactants such as SDS is determined by repulsive Coulomb interactions between the charged head groups. The incorporation of a nonionic cosurfactant reduces the Coulomb repulsion between the head groups, leads to a smaller effective head group area, and thus to a smaller curvature resulting in a transition from the nematic to the lamellar phase, as shown in Scheme 1. Furthermore, 12-HOA as a cosurfactant is much more hydrophobic as SDS because of its less polar head and much longer hydrophobic chain and by this potentially a more effective cosurfactant as DOH. In addition, because 12-HOA is a hydrophobic cosurfactant, the bending rigidity of the amphiphilic film should be increased. The surface activity of 12-HOA was already observed for gelled bicontinuous microemulsions and gelled LLCs.<sup>63,84,86</sup>

Now the question arises how large is the concentration of 12-HOA integrated into the micelles? We roughly estimate this amount by DSC. The sol–gel transition enthalpy  $\Delta_{\text{sol-gel}}H$  is determined from the area of the endothermic peak. As expected,<sup>97</sup>  $\Delta_{\text{sol-gel}}H$  increases linearly with increasing gelator concentration for all observed samples. However, the linear regression does not pass through the origin but intersects the abscissa at a gelator content between 1.23 and 1.35 wt % of 12-HOA, as shown in Figure 7. This applies for all samples ( $\omega_{\text{H}_2\text{O}} =$



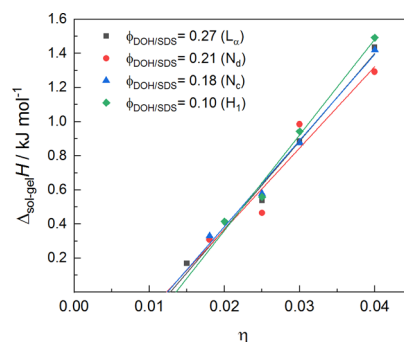
**Figure 6.** (Left) Texture images obtained by POM of the gelator-free (a)  $L_\alpha$ , (b)  $N_b$ , (c)  $N_c$  and (d)  $H_1$  phase ( $\omega_{\text{H}_2\text{O}} = 0.70$  in all four phases) and their gelled counterparts (right). While the gelator-free nematic phases show a typical schlieren texture, the corresponding gelled phases exhibit characteristics of the lamellar phase. The hexagonal phase is not birefringent in the gelled state, and the observed texture arises from aggregation of gel fibers.

### Scheme 1. Incorporation of Nonionic 12-HOA Molecules into the Micelles Leads to a Reduction of the Coulomb Repulsion between the Anionic Surfactant Molecules Which Results in a Decreased Film Curvature



0.67) independent of the cosurfactant-to-surfactant ratio  $\phi_{\text{DOH/SDS}}$  (for clarification, the corresponding gelator-free phase is given in parenthesis, even if the samples are in a different state after gelation). The amount of 12-HOA incorporated into the amphiphilic film can thus be estimated as between 1.2 and 1.4 wt %. Remembering the fact that the nematic  $N_b$  and  $N_c$  phases differ in cosurfactant concentration by roughly 1 wt % (see phase diagram in Figure 3), the estimated amount of  $1.3 \pm 0.1$  wt % 12-HOA incorporated into the micelles seems enough to substantially change the micelle curvature and thus the phase behavior.

The fact that a considerable amount of 12-HOA is incorporated into the amphiphilic film (and thus do not form fibers) in the liquid crystalline phases can also explain why the SAXS peaks of the fibers are higher in intensity for the binary gel than for the gelled  $L_\alpha$  phase (Figure 5a). In other words, even though the same amount of gelator is added to the sample, the actual gel fiber concentration is less in the gelled  $L_\alpha$  phase than in the binary gel. Otherwise, this cosurfactant effect of 12-HOA



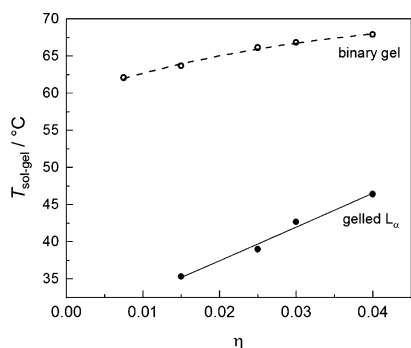
**Figure 7.** Sol-gel transition enthalpy  $\Delta_{\text{sol-gel}}H$  as a function of the gelator mass fraction  $\eta$  for gelled phases of the composition  $\omega_{\text{H}_2\text{O}} = 0.67$  and  $\phi_{\text{DOH/SDS}} = 0.27$  (squares),  $\phi_{\text{DOH/SDS}} = 0.21$  (circles),  $\phi_{\text{DOH/SDS}} = 0.18$  (triangles), and  $\phi_{\text{DOH/SDS}} = 0.10$  (diamonds). For clarification, the corresponding gelator-free phase is given in parenthesis.  $\Delta_{\text{sol-gel}}H$  increases linearly with  $\eta$ . The linear extrapolation to  $\Delta_{\text{sol-gel}}H = 0$  leads to an intersection with the abscissa for a gelator content between 1.23 and 1.35 wt %. Because  $\Delta_{\text{sol-gel}}H = 0$  should be found at  $\eta = 0$ , the obtained value can be interpreted as a rough estimate of the fraction of 12-HOA incorporated into the micelles.

does not explain why the  $H_1$  phase transforms during gelation into an isotropic gel because an increase in cosurfactant content should drive the hexagonal phase into the nematic or lamellar regimes (see the effect of DOH in Figure 3). Instead, we believe that in general the formation of gel fibers destroys the high degree of 2D translational order present in a lyotropic  $H_1$  phase.

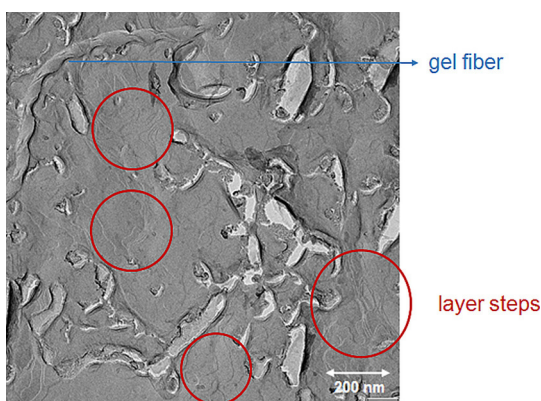
**Coexistence and Mutual Impact of Gel Network and Lamellar Structure.** Because the lamellar phase is the only phase which was successfully transferred into the gelled state, we focused on the  $L_\alpha$  phase to explore the influence of the gel fiber network on the structure and properties of the gelled phase and vice versa. The gel-sol transition of the gelled  $L_\alpha$  phase and the binary gel was studied with DSC, and broad endothermic peaks over a range of up to 10 K were observed on heating. This reflects that several processes take place during the melting of the gel on a molecular scale: the interfiber interactions in the nodes and junction zones as well as the hydrogen bonds holding together one single fiber have to be broken. We thus did not take the onset but the maximum of a peak as sol-gel transition temperature  $T_{\text{sol-gel}}$  and  $T_{\text{sol-gel}}$  was found to have a reproducibility in the order of  $\pm 1.5$  K.

With gelator concentrations increasing from  $\eta = 0.015$  to 0.04,  $T_{\text{sol-gel}}$  increases from 35 to 46  $^\circ\text{C}$  in the case of the gelled  $L_\alpha$  phase ( $\omega_{\text{H}_2\text{O}} = 0.67$ ) and from 64 to 68  $^\circ\text{C}$  in the case of binary gel (Figure 8). An increase in the sol-gel transition temperature with increasing gelator amount is expected because of more and/or thicker gel fibers. Because the  $T_{\text{sol-gel}}$  of the gelled lamellar phase is about 25 K lower than for the binary gel, the gelled  $L_\alpha$  phase is the weaker gel. Interactions of 12-HOA with the polar parts of the surrounding solvent may reduce the gel forming ability of 12-HOA and thus be the reason for the observed lower sol-gel transition temperatures. The low sol-gel transition temperatures of the gelled  $L_\alpha$  phase in comparison with those of the binary gel can also be explained with the surface activity of 12-HOA. If parts of the gelator molecules are incorporated into the micelles, the effective gelator concentration is reduced, which should result in a lower  $T_{\text{sol-gel}}$ .

FFEM images as the one shown in Figure 9 show layer steps typical of a  $L_\alpha$  phase which appear next to twisted gelator fibers. This observation further confirms that both structures actually



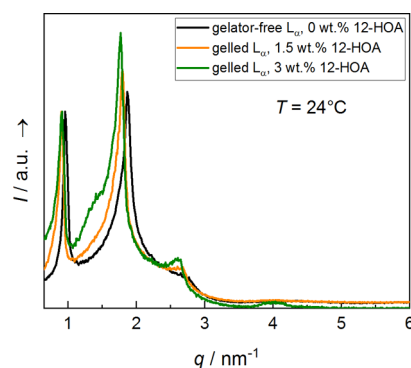
**Figure 8.** Sol–gel transition temperature  $T_{\text{sol-gel}}$  vs the gelator mass fraction  $\eta$  for the gelled  $L_{\alpha}$  phase ( $\omega_{\text{H}_2\text{O}} = 0.67$ ,  $\phi_{\text{DOH/SDS}} = 0.27$ , filled circles) and the binary gel *n*-dodecane/12-HOA (open circles) measured via DSC. For both, the binary gel and the gelled lamellar phase, the sol–gel transition temperature increases with increasing gelator content. The sol–gel transition temperatures are about 25° lower for the gelled  $L_{\alpha}$  phase, indicating that the gelled  $L_{\alpha}$  phase is a weaker gel than the binary gel.



**Figure 9.** FFEM image of the  $L_{\alpha}$  phase ( $\omega_{\text{H}_2\text{O}} = 0.67$ ,  $\phi_{\text{DOH/SDS}} = 0.38$ ) gelled with 3 wt % of 12-HOA. A helically twisted gel fiber and lamellar layer steps (highlighted by the red circles) were found next to each other, which proves the coexistence of the lamellar layer structure and the gel network.

have formed and exist next to each other. The fibers have a thickness of 40–50 nm, which is in the same range as in the corresponding binary gel (30–60 nm, see S1). All fibers observed in the replica show a right-handed twist, which means all fibers are actually left-handed, as expected for (*R*)-12-HOA<sup>94</sup> gels. However, this result is in clear contrast to the observation of nontwisted fibers of (*R*)-12-HOA in gelled lamellar phases of the system  $\text{D}_2\text{O}$ –*n*-decane– $\text{C}_{10}\text{E}_4$  presented by Xu et al.<sup>83</sup>

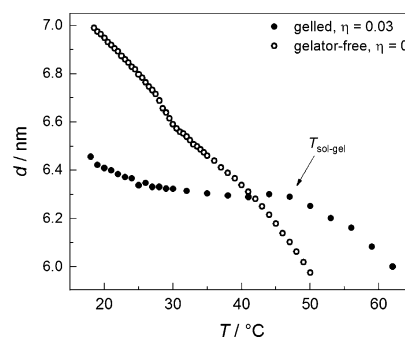
To further analyze the structure of the gelled lamellar phase, we performed SAXS. When comparing the SAXS data of the gelator-free  $L_{\alpha}$  phase with the  $L_{\alpha}$  phase gelled with 1.5 and 3 wt % in Figure 10, it is striking that for the gelled lamellar phases, a third-order layer peak emerges, which is more pronounced for 3 wt % than for 1.5 wt %. In addition, a second-order layer peak is enhanced for the gelled  $L_{\alpha}$  phases as well. The appearance and intensification of higher-order layer peaks indicates that the quality of lamellar ordering is clearly enhanced by the presence of the gel network fibers, which leads to the general conclusion that both structures, lamellar layers and gel fibers, do not coexist independently of each other. For the gelled  $L_{\alpha}$  phases, a shift of the layer peaks to lower  $q$  in comparison with the corresponding gelator-free  $L_{\alpha}$  phase is often observed. This is a common, but



**Figure 10.** Comparison of XRD curves obtained for the gelator-free  $L_{\alpha}$  phase ( $\omega_{\text{H}_2\text{O}} = 0.70$ ,  $\phi_{\text{DOH/SDS}} = 0.30$ , black line) and for the  $L_{\alpha}$  phases gelled with 1.5 (orange line) and 3 wt % (green line) 12-HOA. The intensity is normalized to the intensities of the first-order layer peaks. With increasing gelator amount, an enhancement of the second-order layer peak and even a third-order layer peak due to the lamellar structure can be observed. This indicates a higher translational order for the gelled phase than for the gelator-free  $L_{\alpha}$  phase.

not the general behavior, and this trend is not systematic in its magnitude. The X-ray experiments show that the gel network increases the degree of liquid crystalline order. On the one hand, the appearance of higher-order Bragg peaks indicates a higher degree of translational order. On the other hand, an increase in the layer repeat unit points toward a higher degree of orientational order.

When monitoring the temperature-dependent lamellar layer spacing of the gelator-free and the corresponding gelled ( $\eta = 0.03$ )  $L_{\alpha}$  phase, another striking difference is observed in Figure 11. For the gelator-free lamellar phase, the layer spacing



**Figure 11.** Lamellar layer spacing  $d$  of the gelator-free (open circles) and the corresponding gelled  $L_{\alpha}$  phase ( $\omega_{\text{H}_2\text{O}} = 0.70$ ,  $\phi_{\text{DOH/SDS}} = 0.28$ , filled circles) vs temperature measured by SAXS. For the gelled  $L_{\alpha}$  phase, an arrested layer spacing is observed below the sol–gel transition temperature  $T_{\text{sol-gel}}$ .

decreases with increasing temperature as it is expected because of enhanced fluctuations of the surfactant molecules and thus decreasing orientational order. In contrast, the layer spacing of the gelled lamellar phase is almost independent of temperature at low temperatures. Above a certain temperature, a decrease of the layer spacing as in the gelator-free case can be observed. The temperature at which the behavior changes coincides with the sol–gel transition temperature. Above the sol–gel transition temperature, the layer spacing is free; below the sol–gel transition temperature, the layer spacing is arrested. The gel network seems to freeze the lamellar liquid crystalline order leading to stiffer lamellar bilayers.



Above  $T_{\text{sol-gel}}$ , the lamellar repeat distance  $d$  is found to be larger in the case of gelled  $L_{\alpha}$  phase than in the case of gelator-free  $L_{\alpha}$  phase. This observation might be explained by the incorporation of 12-HOA molecules into the bilayers because the long  $C_{18}$  chains of 12-HOA might enlarge the lamellar bilayers ( $C_{12}$  chains of SDS).

The arrested layer spacing in the gelled  $L_{\alpha}$  phase shown in Figure 11 is frequent and typical but not of the general behavior. When the composition of the  $L_{\alpha}$  phase is altered, a systematic arrested layer spacing cannot always be observed. The mutual influence of lamellar layer structure and gel morphology has to be investigated in more detail in future.

## CONCLUSIONS

The present study shows one of the first examples of a physically gelled LLC. By gelling LLCs with a low-molecular-weight gelator, we obtain new mechanically stable, elastic, and anisotropic soft solids. It is possible to transfer all three observed liquid crystalline phases (lamellar, nematic, and hexagonal) into the gelled state, but only for the  $L_{\alpha}$  phase, the lamellar structure is maintained. In contrast, nematic phases have a lamellar structure in the gelled state, and the hexagonal phase was found to be isotropic after gelation. It seems that the high order of the hexagonal phase is incompatible with the gel network structure. On the contrary, the gel network interacts with the lyotropic phases in such a way that the lamellar structure is stabilized. Thus, gelling is most straightforward for the  $L_{\alpha}$  phase. Because of the strong tendency to the lamellar phase, gelling of nonlayered phases, such as nematic phases, was not successful. Furthermore, the gelator 12-HOA was found to be surface-active, acting partly as a cosurfactant in our LLC system. This reduces the micelle curvature and thus broadens the lamellar regime. The obtained results clearly demonstrate that the two combined structures, liquid crystalline phase and gel fiber network, do not coexist independently of each other, indicating that our gelled lyotropic liquid crystalline phases are not orthogonal self-assembled systems.

Nevertheless, gelled LLCs are promising new materials on the way to elastic LLCs to be used as stimuli-responsive actuators. To separate the previously described disadvantageous influences of 12-HOA on the lyotropic system for further studies, we are currently searching for new low-molecular-weight gelators that are able to gel our lyotropic liquid crystalline system.

## ASSOCIATED CONTENT

### Supporting Information

The Supporting Information is available free of charge on the ACS Publications website at DOI: 10.1021/acs.langmuir.9b02621.

FFEM images of the binary gel and gelled nematic phase (PDF)

## AUTHOR INFORMATION

### Corresponding Author

\*E-mail: f.giesselmann@ipc.uni-stuttgart.de.

### ORCID

Thomas Sottmann: 0000-0003-3679-3703

Frank Giesselmann: 0000-0002-9974-9470

## Funding

The authors gratefully acknowledge the financial support from the Deutsche Forschungsgemeinschaft (DFG Gi 243/9-1) and Fonds der Chemischen Industrie (FCI).

## Notes

The authors declare no competing financial interest.

## ACKNOWLEDGMENTS

The authors thank Cosima Stubenrauch for helpful discussion and Natalie Preisig for the fabrication of the FFEM images.

## REFERENCES

- (1) Abdallah, D. J.; Weiss, R. G. Organogels and Low Molecular Mass Organic Gelators. *Adv. Mater.* **2000**, *12*, 1237–1247.
- (2) Brinksma, J.; Feringa, B. L.; Kellogg, R. M.; Vreeker, R.; van Esch, J. Rheology and Thermotropic Properties of Bis-Urea-Based Organogels in Various Primary Alcohols. *Langmuir* **2000**, *16*, 9249–9255.
- (3) George, M.; Weiss, R. G. Molecular Organogels. Soft Matter Comprised of Low-Molecular-Mass Organic Gelators and Organic Liquids. *Acc. Chem. Res.* **2006**, *39*, 489–497.
- (4) Liu, X. Y.; Sawant, P. D. Mechanism of the Formation of Self-Organized Microstructures in Soft Functional Materials. *Adv. Mater.* **2002**, *14*, 421–426.
- (5) Terech, P.; Weiss, R. G. Low Molecular Mass Gelators of Organic Liquids and the Properties of Their Gels. *Chem. Rev.* **1997**, *97*, 3133–3160.
- (6) van Esch, J. H.; Feringa, B. L. New Functional Materials Based on Self-Assembling Organogels: From Serendipity towards Design. *Angew. Chem., Int. Ed.* **2000**, *39*, 2263–2266.
- (7) Tachibana, T.; Mori, T.; Hori, K. New type of twisted mesophase in jellies and solid films of chiral 12-hydroxyoctadecanoic acid-hydroxyoctadecanoic acid. *Nature* **1979**, *278*, 578–579.
- (8) Burkhardt, M.; Kinzel, S.; Gradzielski, M. Macroscopic properties and microstructure of HSA based organogels: sensitivity to polar additives. *J. Colloid Interface Sci.* **2009**, *331*, 514–521.
- (9) Terech, P.; Rodriguez, V.; Barnes, J. D.; McKenna, G. B. Organogels and Aerogels of Racemic and Chiral 12-Hydroxyoctadecanoic Acid. *Langmuir* **1994**, *10*, 3406–3418.
- (10) Sato, H.; Hori, K.; Sakurai, T.; Yamagishi, A. Long distance chiral transfer in a gel: Experimental and ab initio analyses of vibrational circular dichroism spectra of R- and S-12-hydroxyoctadecanoic acid gels. *Chem. Phys. Lett.* **2008**, *467*, 140–143.
- (11) Sato, H.; Sakurai, T.; Yamagishi, A. Comparison of Vibrational Circular Dichroism between the Langmuir-Blodgett Films and Gels of 12-Hydroxyoctadecanoic Acid. *Chem. Lett.* **2011**, *40*, 25–27.
- (12) Grahame, D. A. S.; Olauson, C.; Lam, R. S. H.; Pedersen, T.; Borondics, F.; Abraham, S.; Weiss, R. G.; Rogers, M. A. Influence of chirality on the modes of self-assembly of 12-hydroxystearic acid in molecular gels of mineral oil. *Soft Matter* **2011**, *7*, 7359–7365.
- (13) Sakurai, T.; Masuda, Y.; Sato, H.; Yamagishi, A.; Kawaji, H.; Atake, T.; Hori, K. A Comparative Study on Chiral and Racemic 12-Hydroxyoctadecanoic Acids in the Solutions and Aggregation States: Does the Racemic Form Really Form a Gel? *Bull. Chem. Soc. Jpn.* **2010**, *83*, 145–150.
- (14) Tachibana, T.; Mori, T.; Hori, K. Chiral mesophases of 12-hydroxyoctadecanoic acid in jelly and in the solid state. I. A new type of lyotropic mesophase in jelly with organic solvents. *Bull. Chem. Soc. Jpn.* **1980**, *53*, 1714–1719.
- (15) Terech, P. Small-angle-scattering study of 12-hydroxystearic physical organogels and lubricating greases. *Colloid Polym. Sci.* **1991**, *269*, 490–500.
- (16) Weiss, R. G. The past, present, and future of molecular gels. What is the status of the field, and where is it going? *J. Am. Chem. Soc.* **2014**, *136*, 7519–7530.
- (17) Hirst, A. R.; Escuder, B.; Miravet, J. F.; Smith, D. K. High-Tech Applications of Self-Assembling Supramolecular Nanostructured Gel-

Phase Materials: From Regenerative Medicine to Electronic Devices. *Angew. Chem., Int. Ed.* **2008**, *47*, 8002–8018.

(18) Liu, X. Y.; Li, J.-L. *Soft Fibrillar Materials: Fabrication and Applications*; Wiley-VCH Verlag GmbH & Co. KGaA: Weinheim, Germany, 2013.

(19) Sangeetha, N. M.; Maitra, U. Supramolecular gels: Functions and uses. *Chem. Soc. Rev.* **2005**, *34*, 821–836.

(20) *Molecular Gels: Materials with Self-Assembled Fibrillar Networks*; Weiss, R. G., Terech, P., Eds.; Springer: Dordrecht, 2006.

(21) Murdan, S.; Gregoriadis, G.; Florence, A. T. Sorbitan monostearate/polysorbate 20 organogels containing niosomes: A delivery vehicle for antigens? *Eur. J. Pharm. Sci.* **1999**, *8*, 177–185.

(22) Ibrahim, M. M.; Hafez, S. A.; Mahdy, M. M. Organogels, hydrogels and bigels as transdermal delivery systems for diltiazem hydrochloride. *Asian J. Pharm. Sci.* **2013**, *8*, 48–57.

(23) Majumder, J.; Deb, J.; Das, M. R.; Jana, S. S.; Dastidar, P. Designing a simple organic salt-based supramolecular topical gel capable of displaying in vivo self-delivery application. *Chem. Commun.* **2014**, *50*, 1671–1674.

(24) Ahmed, S. A.; Sallenave, X.; Fages, F.; Mieden-Gundert, G.; Müller, W. M.; Müller, U.; Vögtle, F.; Pozzo, J.-L. Multiaddressable Self-Assembling Organogelators Based on 2H-Chromene and N-Acyl-1, $\omega$ -amino Acid Units. *Langmuir* **2002**, *18*, 7096–7101.

(25) Pozzo, J.-L.; Clavier, G. M.; Desvergne, J.-P. Rational design of new acid-sensitive organogelators. *J. Mater. Chem.* **1998**, *8*, 2575–2577.

(26) Murata, K.; Aoki, M.; Nishi, T.; Ikeda, A.; Shinkai, S. New cholesterol-based gelators with light- and metal-responsive functions. *J. Chem. Soc., Chem. Commun.* **1991**, 1715–1718.

(27) Ayabe, M.; Kishida, T.; Fujita, N.; Sada, K.; Shinkai, S. Binary organogelators which show light and temperature responsiveness. *Org. Biomol. Chem.* **2003**, *1*, 2744–2747.

(28) de Jong, J. J. D.; Lucas, L. N.; Kellogg, R. M.; van Esch, J. H.; Feringa, B. L. Reversible optical transcription of supramolecular chirality into molecular chirality. *Science* **2004**, *304*, 278–281.

(29) Murata, K.; Aoki, M.; Suzuki, T.; Harada, T.; Kawabata, H.; Komori, T.; Ohseto, F.; Ueda, K.; Shinkai, S. Thermal and Light Control of the Sol-Gel Phase Transition in Cholesterol-Based Organic Gels. Novel Helical Aggregation Modes As Detected by Circular Dichroism and Electron Microscopic Observation. *J. Am. Chem. Soc.* **1994**, *116*, 6664–6676.

(30) Li, J.; Gao, Y.; Kuang, Y.; Shi, J.; Du, X.; Zhou, J.; Wang, H.; Yang, Z.; Xu, B. Dephosphorylation of D-peptide derivatives to form biofunctional, supramolecular nanofibers/hydrogels and their potential applications for intracellular imaging and intratumoral chemotherapy. *J. Am. Chem. Soc.* **2013**, *135*, 9907–9914.

(31) Yang, Z.; Xu, B. A simple visual assay based on small molecule hydrogels for detecting inhibitors of enzymes. *Chem. Commun.* **2004**, 2424–2425.

(32) Ulijn, R. V.; Bibi, N.; Jayawarna, V.; Thornton, P. D.; Todd, S. J.; Mart, R. J.; Smith, A. M.; Gough, J. E. Bioresponsive hydrogels. *Mater. Today* **2007**, *10*, 40–48.

(33) Yang, Z.; Xu, B. Using Enzymes to Control Molecular Hydrogelation. *Adv. Mater.* **2006**, *18*, 3043–3046.

(34) Yamanaka, M. Urea derivatives as low-molecular-weight gelators. *J. Inclusion Phenom. Macrocylic Chem.* **2013**, *77*, 33–48.

(35) Kato, T.; Kutsuna, T.; Hanabusa, K.; Ukon, M. Gelation of Room-Temperature Liquid Crystals by the Association of *trans*-1,2-Bis(amino)cyclohexane Derivative. *Adv. Mater.* **1998**, *10*, 606–608.

(36) Moriyama, M.; Mizoshita, N.; Yokota, T.; Kishimoto, K.; Kato, T. Photoresponsive Anisotropic Soft Solids: Liquid-Crystalline Physical Gels Based on a Chiral Photochromic Gelator. *Adv. Mater.* **2003**, *15*, 1335–1338.

(37) Yabuuchi, K.; Rowan, A. E.; Nolte, R. J. M.; Kato, T. Liquid-Crystalline Physical Gels: Self-Aggregation of a Gluconamide Derivative in Mesogenic Molecules for the Formation of Anisotropic Functional Composites. *Chem. Mater.* **2000**, *12*, 440–443.

(38) Guan, L.; Zhao, Y. Self-Assembly of a Liquid Crystalline Anisotropic Gel. *Chem. Mater.* **2000**, *12*, 3667–3673.

(39) Guan, L.; Zhao, Y. Self-assembled gels of liquid crystals: Hydrogen-bonded aggregates formed in various liquid crystalline textures. *J. Mater. Chem.* **2001**, *11*, 1339–1344.

(40) Janssen, R. H. C.; Stümpflen, V.; Bastiaansen, C. W. M.; Broer, D. J.; Tervoort, T. A.; Smith, P. Thermo-reversible Liquid-Crystal Gels: Towards a New Processing Route for Twisted Nematic Displays. *Jpn. J. Appl. Phys.* **2000**, *39*, 2721–2726.

(41) Lin, H.-C.; Wang, C.-H.; Wang, J.-K.; Tsai, S.-F. Fast Response and Spontaneous Alignment in Liquid Crystals Doped with 12-Hydroxystearic Acid Gelators. *Materials* **2018**, *11*, 745.

(42) Zhao, Y.; Guan, L. Use of a gelator in a ferroelectric liquid crystal: Pitch compensation and nanofibres. *Liq. Cryst.* **2003**, *30*, 81–86.

(43) Mizoshita, N.; Hanabusa, K.; Kato, T. Self-Aggregation of an Amino Acid Derivative in a Liquid-Crystalline Physical Gel-Faster Response to Electric Fields. *Adv. Mater.* **1999**, *11*, 392–394.

(44) Mizoshita, N.; Monobe, H.; Inoue, M.; Ukon, M.; Watanabe, T.; Shimizu, Y.; Hanabusa, K.; Kato, T. The positive effect on hole transport behaviour in anisotropic gels consisting of discotic liquid crystals and hydrogen-bonded fibres. *Chem. Commun.* **2002**, 428–429.

(45) Tolksdorf, C.; Zentel, R. Reversible Physical Network Stabilized Ferroelectric Liquid Crystals. *Adv. Mater.* **2001**, *13*, 1307–1310.

(46) Deindörfer, P.; Eremin, A.; Stannarius, R.; Davis, R.; Zentel, R. Gelation of smectic liquid crystal phases with photosensitive gel forming agents. *Soft Matter* **2006**, *2*, 693–698.

(47) Kato, T.; Hirai, Y.; Nakaso, S.; Moriyama, M. Liquid-crystalline physical gels. *Chem. Soc. Rev.* **2007**, *36*, 1857–1867.

(48) Mizoshita, N.; Kutsuna, T.; Kato, T.; Hanabusa, K. Smectic liquid-crystalline physical gels. Anisotropic self-aggregation of hydrogen-bonded molecules in layered structures. *Chem. Commun.* **1999**, 781–782.

(49) Kato, T.; Kutsuna, T.; Yabuuchi, K.; Mizoshita, N. Anisotropic Self-Aggregation of an Anthracene Derivative: Formation of Liquid-Crystalline Physical Gels in Oriented States. *Langmuir* **2002**, *18*, 7086–7088.

(50) Mizoshita, N.; Hanabusa, K.; Kato, T. Fast and High-Contrast Electro-optical Switching of Liquid-Crystalline Physical Gels: Formation of Oriented Microphase-Separated Structures. *Adv. Funct. Mater.* **2003**, *13*, 313–317.

(51) Kato, T. Self-Assembly of Phase-Segregated Liquid Crystal Structures. *Science* **2002**, *295*, 2414–2418.

(52) Mizoshita, N.; Suzuki, Y.; Kishimoto, K.; Hanabusa, K.; Kato, T. Electrooptical properties of liquid-crystalline physical gels: A new oligo(amino acid) gelator for light scattering display materials. *J. Mater. Chem.* **2002**, *12*, 2197–2201.

(53) Suzuki, Y.; Mizoshita, N.; Hanabusa, K.; Kato, T. Homeotropically oriented nematic physical gels for electrooptical materials. *J. Mater. Chem.* **2003**, *13*, 2870–2874.

(54) Stubenrauch, C.; Giesselmann, F. Gelled Complex Fluids: Combining Unique Structures with Mechanical Stability. *Angew. Chem., Int. Ed.* **2016**, *55*, 3268–3275.

(55) Laibinis, P. E.; Hickman, J. J.; Wrighton, M. S.; Whitesides, G. M. Orthogonal self-assembled monolayers: Alkanethiols on gold and alkane carboxylic acids on alumina. *Science* **1989**, *245*, 845–847.

(56) Boekhoven, J.; Brizard, A. M.; Stuart, M. C. A.; Florusse, L.; Raffy, G.; Del Guerso, A.; van Esch, J. H. Bio-inspired supramolecular materials by orthogonal self-assembly of hydrogelators and phospholipids. *Chem. Sci.* **2016**, *7*, 6021–6031.

(57) Vereb, G.; Szöllösi, J.; Matkó, J.; Nagy, P.; Farkas, T.; Vigh, L.; Mátyus, L.; Waldmann, T. A.; Damjanovich, S. Dynamic, yet structured: The cell membrane three decades after the Singer-Nicolson model. *Proc. Natl. Acad. Sci. U.S.A.* **2003**, *100*, 8053–8058.

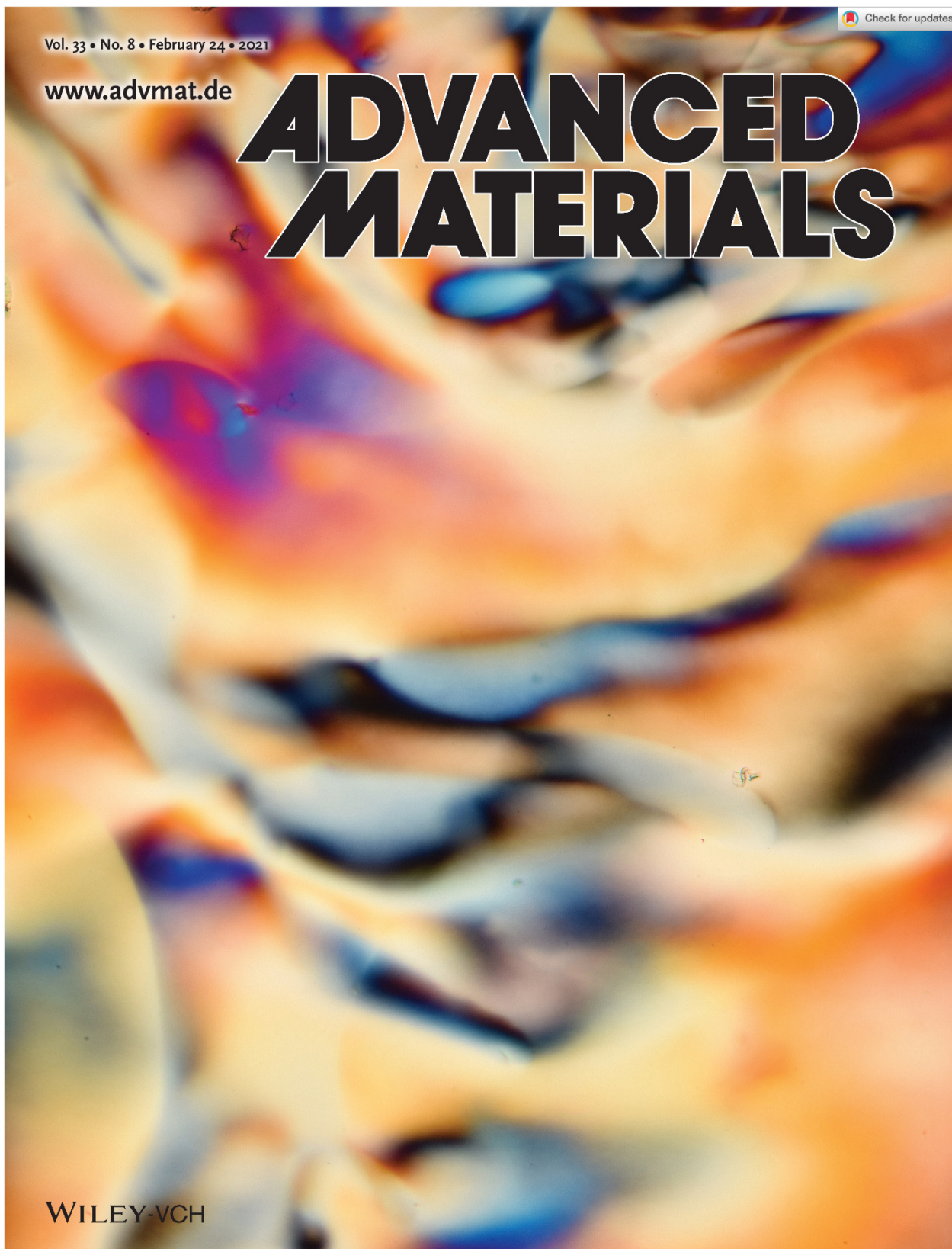
(58) Alberts, B.; Johnson, A.; Lewis, J.; Raff, M.; Roberts, K.; Walter, P. *Molecular Biology of the Cell*; Garland Science Taylor & Francis Group: New York, NY, 2002.

(59) Brizard, A.; Stuart, M.; van Bommel, K.; Friggeri, A.; de Jong, M.; van Esch, J. Preparation of nanostructures by orthogonal self-assembly of hydrogelators and surfactants. *Angew. Chem., Int. Ed.* **2008**, *47*, 2063–2066.

- (60) Brizard, A. M.; Stuart, M. C. A.; van Esch, J. H. Self-assembled interpenetrating networks by orthogonal self assembly of surfactants and hydrogelators. *Faraday Discuss.* **2009**, *143*, 345–357.
- (61) Heeres, A.; van der Pol, C.; Stuart, M.; Friggeri, A.; Feringa, B. L.; van Esch, J. Orthogonal self-assembly of low molecular weight hydrogelators and surfactants. *J. Am. Chem. Soc.* **2003**, *125*, 14252–14253.
- (62) Laupheimer, M.; Jovic, K.; Antunes, F. E.; da Graça Martins Miguel, M.; Stubenrauch, C. Studying orthogonal self-assembled systems: Phase behaviour and rheology of gelled microemulsions. *Soft Matter* **2013**, *9*, 3661–3670.
- (63) Laupheimer, M.; Sottmann, T.; Schweins, R.; Stubenrauch, C. Studying orthogonal self-assembled systems: microstructure of gelled bicontinuous microemulsions. *Soft Matter* **2014**, *10*, 8744–8757.
- (64) Qin, H.; Li, F.; Wang, D.; Lin, H.; Jin, J. Organized Molecular Interface-Induced Noncrystallizable Polymer Ultrathin Nanosheets with Ordered Chain Alignment. *ACS Nano* **2016**, *10*, 948–956.
- (65) Ikeda, T.; Mamiya, J.-i.; Yu, Y. Photomechanics of liquid-crystalline elastomers and other polymers. *Angew. Chem., Int. Ed.* **2007**, *46*, 506–528.
- (66) Yu, Y.; Ikeda, T. Soft Actuators Based on Liquid-Crystalline Elastomers. *Angew. Chem., Int. Ed.* **2006**, *45*, 5416–5418.
- (67) Ohm, C.; Brehmer, M.; Zentel, R. Liquid crystalline elastomers as actuators and sensors. *Adv. Mater.* **2010**, *22*, 3366–3387.
- (68) Xie, P.; Zhang, R. Liquid crystal elastomers, networks and gels: Advanced smart materials. *J. Mater. Chem.* **2005**, *15*, 2529–2550.
- (69) Thomsen, D. L.; Keller, P.; Naciri, J.; Pink, R.; Jeon, H.; Shenoy, D.; Ratna, B. R. Liquid Crystal Elastomers with Mechanical Properties of a Muscle. *Macromolecules* **2001**, *34*, 5868–5875.
- (70) Wermter, H.; Finkelmann, H. Liquid crystalline elastomers as artificial muscles. *e-Polym.* **2001**, *1*. DOI: 10.1515/epoly.2001.1.1.111
- (71) Li, M.-H.; Keller, P.; Yang, J.; Albouy, P.-A. An Artificial Muscle with Lamellar Structure Based on a Nematic Triblock Copolymer. *Adv. Mater.* **2004**, *16*, 1922–1925.
- (72) Buguin, A.; Li, M.-H.; Silberzan, P.; Ladoux, B.; Keller, P. Microactuators: When artificial muscles made of nematic liquid crystal elastomers meet soft lithography. *J. Am. Chem. Soc.* **2006**, *128*, 1088–1089.
- (73) Naciri, J.; Srinivasan, A.; Jeon, H.; Nikolov, N.; Keller, P.; Ratna, B. R. Nematic Elastomer Fiber Actuator. *Macromolecules* **2003**, *36*, 8499–8505.
- (74) Rogó, M.; Zeng, H.; Xuan, C.; Wiersma, D. S.; Wasylczyk, P. Light-Driven Soft Robot Mimics Caterpillar Locomotion in Natural Scale. *Adv. Opt. Mater.* **2016**, *4*, 1689–1694.
- (75) Camacho-Lopez, M.; Finkelmann, H.; Palfy-Muhoray, P.; Shelley, M. Fast liquid-crystal elastomer swims into the dark. *Nat. Mater.* **2004**, *3*, 307–310.
- (76) Yamada, M.; Kondo, M.; Miyasato, R.; Naka, Y.; Mamiya, J.-i.; Kinoshita, M.; Shishido, A.; Yu, Y.; Barrett, C. J.; Ikeda, T. Photomobile polymer materials-various three-dimensional movements. *J. Mater. Chem.* **2009**, *19*, 60–62.
- (77) Schuhl, S.; Preller, F.; Rix, R.; Petsch, S.; Zentel, R.; Zappe, H. Iris-like tunable aperture employing liquid-crystal elastomers. *Adv. Mater.* **2014**, *26*, 7247–7251.
- (78) Wani, O. M.; Zeng, H.; Priimagi, A. A light-driven artificial flytrap. *Nat. Commun.* **2017**, *8*, 15546.
- (79) Fleischmann, E.-K.; Liang, H.-L.; Kapernaum, N.; Giesselmann, F.; Lagerwall, J.; Zentel, R. One-piece micropumps from liquid crystalline core-shell particles. *Nat. Commun.* **2012**, *3*, 1178.
- (80) Yamada, M.; Kondo, M.; Mamiya, J.-i.; Yu, Y.; Kinoshita, M.; Barrett, C. J.; Ikeda, T. Photomobile Polymer Materials: Towards Light-Driven Plastic Motors. *Angew. Chem.* **2008**, *120*, 5064–5066.
- (81) Warriner, H. E.; Idziak, S. H. J.; Slack, N. L.; Davidson, P.; Safinya, C. R. Lamellar Biogels: Fluid-Membrane-Based Hydrogels Containing Polymer Lipids. *Science* **1996**, *271*, 969–973.
- (82) Slack, N. L.; Schellhorn, M.; Eiselt, P.; Chibbaro, M. A.; Schulze, U.; Warriner, H. E.; Davidson, P.; Schmidt, H.-W.; Safinya, C. R. Synthesis and Phase Behavior of New Amphiphilic PEG-Based Triblock Copolymers as Gelling Agents for Lamellar Liquid Crystalline Phases. *Macromolecules* **1998**, *31*, 8503–8508.
- (83) Xu, Y.; Laupheimer, M.; Preisig, N.; Sottmann, T.; Schmidt, C.; Stubenrauch, C. Gelled Lyotropic Liquid Crystals. *Langmuir* **2015**, *31*, 8589–8598.
- (84) Koitani, S.; Dieterich, S.; Preisig, N.; Aramaki, K.; Stubenrauch, C. Gelling Lamellar Phases of the Binary System Water-Didodecyltrimethylammonium Bromide with an Organogelator. *Langmuir* **2017**, *33*, 12171–12179.
- (85) Steck, K.; van Esch, J. H.; Smith, D. K.; Stubenrauch, C. Tuning gelled lyotropic liquid crystals (LLCs) - probing the influence of different low molecular weight gelators on the phase diagram of the system H<sub>2</sub>O/NaCl-Genapol LA070. *Soft Matter* **2019**, *15*, 3111–3121.
- (86) Steck, K.; Schmidt, C.; Stubenrauch, C. The Twofold Role of 12-Hydroxyoctadecanoic Acid (12-HOA) in a Ternary Water-Surfactant-12-HOA System: Gelator and Co-Surfactant. *Gels* **2018**, *4*, 78.
- (87) Kim, D.-H.; Jahn, A.; Cho, S.-J.; Kim, J. S.; Ki, M.-H.; Kim, D.-D. Lyotropic liquid crystal systems in drug delivery: A review. *J. Pharm. Invest.* **2015**, *45*, 1–11.
- (88) Wang, C.; Chen, D.; Jiao, X. Lyotropic liquid crystal directed synthesis of nanostructured materials. *Sci. Technol. Adv. Mater.* **2009**, *10*, 023001.
- (89) Tolbert, S. H.; Firouzi, A.; Stucky, G. D.; Chmelka, B. F. Magnetic Field Alignment of Ordered Silicate-Surfactant Composites and Mesoporous Silica. *Science* **1997**, *278*, 264–268.
- (90) Kresge, C. T.; Leonowicz, M. E.; Roth, W. J.; Vartuli, J. C.; Beck, J. S. Ordered mesoporous molecular sieves synthesized by a liquid-crystal template mechanism. *Nature* **1992**, *359*, 710–712.
- (91) Shopsowitz, K. E.; Qi, H.; Hamad, W. Y.; MacLachlan, M. J. Free-standing mesoporous silica films with tunable chiral nematic structures. *Nature* **2010**, *468*, 422–425.
- (92) Lin, H.-P.; Mou, C.-Y. Structural and Morphological Control of Cationic Surfactant-Templated Mesoporous Silica. *Acc. Chem. Res.* **2002**, *35*, 927–935.
- (93) Quist, P.-O.; Halle, B. Curvature defects in a lamellar phase revealed by nuclear-spin-relaxation anisotropy. *Phys. Rev. E* **1993**, *47*, 3374–3395.
- (94) Tachibana, T.; Kambara, H. The sense of twist in the fibrous aggregates from 12-hydroxystearic acid and its alkali metal soaps. *J. Colloid Interface Sci.* **1968**, *28*, 173–174.
- (95) Gao, J.; Wu, S.; Emge, T. J.; Rogers, M. A. Nanoscale and microscale structural changes alter the critical gelator concentration of self-assembled fibrillar networks. *CrystEngComm* **2013**, *15*, 4507–4515.
- (96) Findenegg, G. H. J. N. Israelachvili: Intermolecular and Surface Forces (With Applications to Colloidal and Biological Systems). Academic Press, London, Orlando, San Diego, New York, Toronto, Montreal, Sydney, Tokyo 1985. 296 Seiten, Preis: \$ 65.00. *Berichte der Bunsengesellschaft für Physikalische Chemie* **1986**, *90*, 1241–1242.
- (97) Raghavan, S. R.; Cipriano, B. H. Gel Formation: Phase Diagrams Using Tabletop Rheology and Calorimetry. In *Molecular Gels: Materials with Self-Assembled Fibrillar Networks*; Weiss, R. G., Terech, P., Eds.; Springer: Dordrecht, 2006, pp 241–252.



Publication II



# Micellar Lyotropic Nematic Gels

Sonja Dieterich, Friedrich Stemmler, Natalie Preisig, and Frank Giesselmann\*

**Lyotropic liquid crystal (LLC) gels are a new class of liquid crystal (LC) networks that combine the anisotropy of micellar LLCs with the mechanical stability of a gel. However, so far, only micellar LLC gels with lamellar and hexagonal structures have been obtained by the addition of gelators to LLCs. Here, the first examples of lyotropic nematic gels are presented. The key to obtain these nematic gels is the use of gelators that have a non-amphiphilic molecular structure and thus leave the size and shape of the micellar aggregates essentially unchanged. By adding these gelators to lyotropic nematic phases, an easy and reproducible way to obtain large amounts of lyotropic nematic gels is established. These nematic gels preserve the long-range orientational order and optical birefringence of a lyotropic nematic phase but have the mechanical stability of a gel. LLC nematic gels are promising new materials for elastic and anisotropic hydrogels to be applied as water-based stimuli-responsive actuators and sensors.**

The coupling of orientational order and macroscopic shape<sup>[1,2]</sup> is the striking feature of liquid crystalline networks, such as liquid-crystalline elastomers<sup>[3–5]</sup> (LCEs) and LC gels (LCGs).<sup>[6–8]</sup> Today, thermotropic LCEs and LCGs are the backbone of the rapidly emerging field of soft robotics and biomimetic actuation.<sup>[9–14]</sup> External stimuli (e.g., temperature, light) modify or destroy the LC orientational order leading to macroscopic shape changes. Drawbacks of LCEs are their often complicated and expensive fabrication as well as the limitation in the choice of external stimuli. In contrast, lyotropic liquid crystal (LLC) physical gels, which are the lyotropic counterpart to thermotropic LCEs and LCGs, are comparatively easy in fabrication and compatible to aqueous systems. Thus, they might find biomedical applications (e.g., artificial tissues) and respond to a broad range of biological and chemical stimuli such as pH-value, salt concentration, solutes, vapor pressure, and temperature, as it was shown for anisotropic hydrogels.<sup>[15–26]</sup> LLC gels are a new approach to anisotropic hydrogels: instead of a water-swollen polymer network, a genuine LLC phase formed by micelles is

gelled by low-molecular-weight gelators (LMWGs).<sup>[27–30]</sup> Via physical interactions, such as  $\pi$ - $\pi$  interactions and hydrogen bonds, LMWGs form self-assembled 3D fibrillar networks (SAFINs), which arrest the fluidity of the LLC phase as a result of the gelation. The anisotropy of the LLC is thus combined with the elasticity of a gel network enabling potential applications where some mechanical stability is needed such as stimuli-responsive actuation,<sup>[22,24,31]</sup> transdermal drug delivery<sup>[32,33]</sup> as well as non-fluid templates for the synthesis of macroscopically aligned nanostructured materials.<sup>[34,35]</sup>

In recent years few studies on LLC gels as a new kind of LC networks were presented.<sup>[36–40]</sup> It was shown that the anisotropic order of the surfactant-based LLCs


is combined with the mechanical stability and elasticity of a 3D physical gel network. Lyotropic lamellar and hexagonal phases were successfully gelled by LMWGs, but so far no lyotropic nematic physical gel was obtained. In comparison to lamellar and hexagonal lyotropics, lyotropic nematic phases are less common. In recent years however the understanding of their stability has been much improved and, as a result, the pool of lyotropic nematic systems was significantly enlarged by the work of Akpınar et al.<sup>[41–43]</sup>

Nematics are the structurally simplest LC phase due to the absence of any long-range translational order, which is also the reason for their low viscosity enabling easy alignment of lyotropic nematics before gelation. This makes lyotropic nematic gels essential for demonstrating fundamental principles in LLC gels and straightforward for the application in stimuli-responsive actuators. In a former paper we showed that lyotropic nematic physical gels are not as easily achievable as lamellar gels since the used gelator 12-HOA acts partly as cosurfactant and thus gelation of lyotropic LLCs with 12-HOA lead to lamellar gels only.<sup>[40]</sup>

In this paper we restrict the term lyotropic nematic gels to the genuine nematic LLC phases formed by rod- or disk-like micelles and gelled by a fibrillar network. Please note that the term lyotropic nematic gel is also used in other contexts where the building blocks of the nematic phase are interacting with each other so that they form a gel network. This was for instance found for orientationally ordered dispersions of rigid fibers,<sup>[44,45]</sup> nanoparticles,<sup>[46]</sup> inverse micelles,<sup>[47]</sup> or (bio)polymers<sup>[48,49]</sup> in either water or organic solvents.

Here, we present the first examples of gelator-based micellar lyotropic nematic networks. We gelled the nematic  $N_d$  and  $N_c$  phases of the two surfactant systems  $H_2O$ -*n*-decanol-sodium dodecyl sulfate (SDS) and  $H_2O$ -*n*-decanol-*N,N*-dimethyl-*N*-ethylhexadecylammonium bromide (CDEAB) with the three

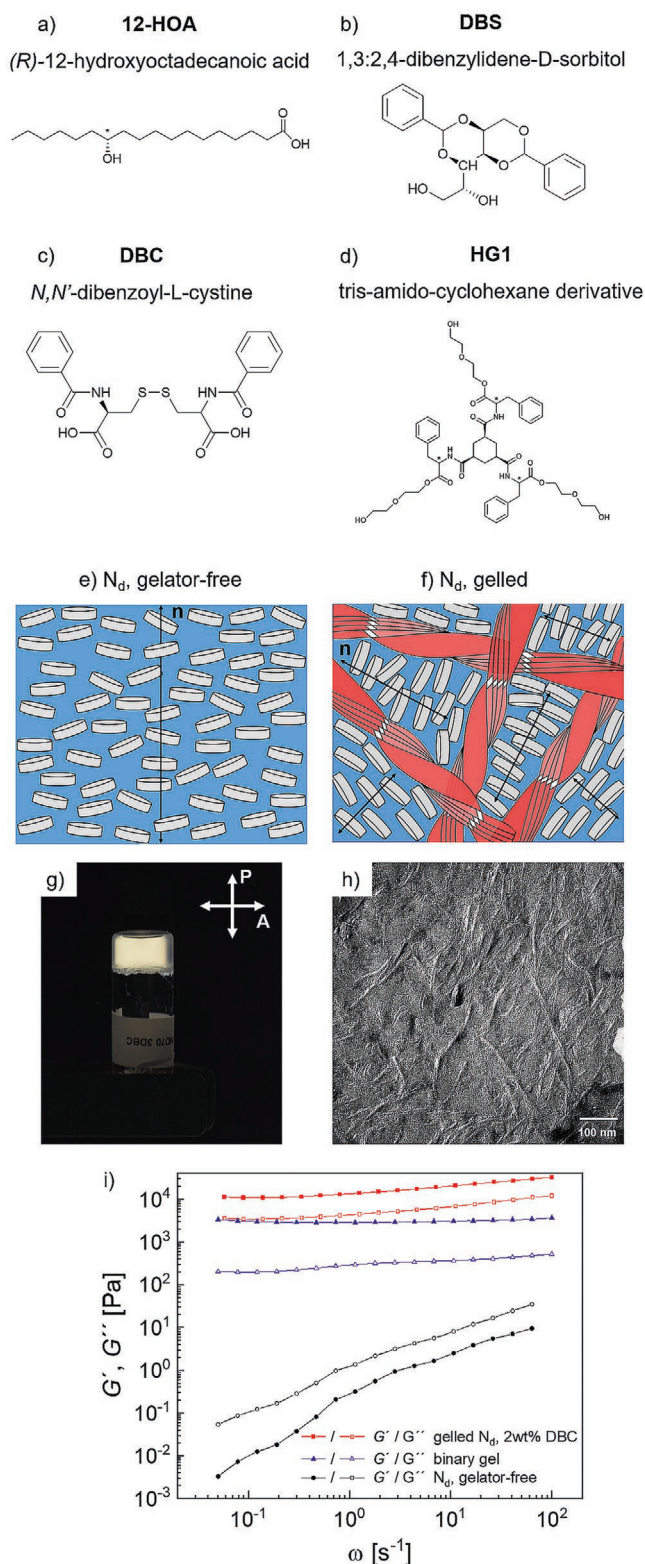
S. Dieterich, F. Stemmler, Dr. N. Preisig, Prof. F. Giesselmann  
Institute of Physical Chemistry  
University of Stuttgart  
Pfaffenwaldring 55, 70569 Stuttgart, Germany  
E-mail: frank.giesselmann@ipc.uni-stuttgart.de

 The ORCID identification number(s) for the author(s) of this article can be found under <https://doi.org/10.1002/adma.202007340>.

© 2021 The Authors. Advanced Materials published by Wiley-VCH GmbH. This is an open access article under the terms of the Creative Commons Attribution-NonCommercial License, which permits use, distribution and reproduction in any medium, provided the original work is properly cited and is not used for commercial purposes.

DOI: 10.1002/adma.202007340





**Figure 1.** a–d) Molecular structure of the used LMWGs 12-HOA (a), DBS (b), DBC (c), and HG1 (d). While 12-HOA has an amphiphilic structure, the molecular structure of the other gelators is bulky, thus an incorporation of gelator molecules into the micelles is not possible for DBS, DBC, and HG1. e, f) Schematic drawings of the structure of a fluid gelator-free  $N_d$  phase (e) and the proposed structure of a gelled  $N_d$  phase (f),

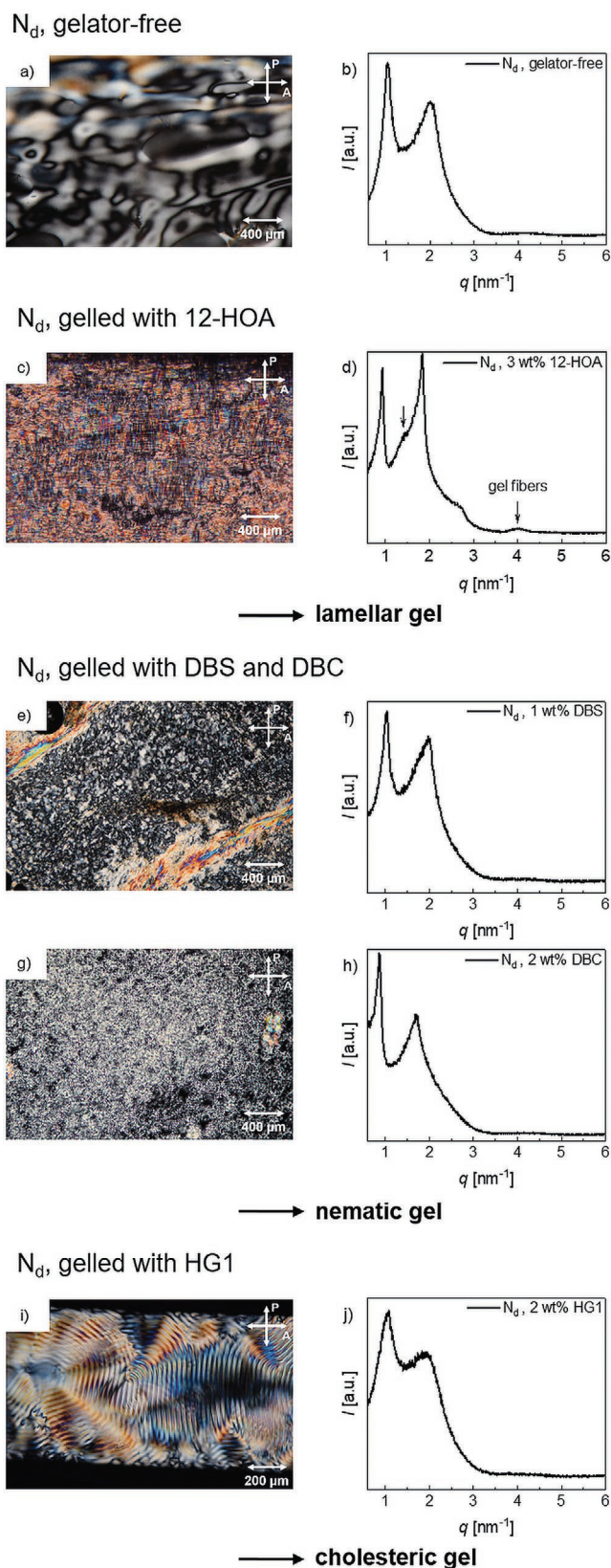
low-molecular-weight gelators DBS, DBC, and HG1 (see molecular structures in **Figure 1**). Gels were achieved for all combinations with the exception of the nematic phases of the system  $H_2O$ –*n*-decanol–CDEAB with the gelator DBC. All obtained gels were nematic with the exception of the system  $H_2O$ –*n*-decanol–SDS gelled with HG1, where starting from the  $N_c$  phase an isotropic gel was received. All in all, we were able to obtain nine different lyotropic nematic gels, which are to the best of our knowledge the first examples of this new kind of water-based micellar LC networks. A complete overview on our experiments to obtain lyotropic nematic gels with these surfactant systems and gelators is found in Table S1 in the Supporting Information.

As a representative example, we will now discuss the properties of lyotropic nematic gels using the  $N_d$  phase of the surfactant system  $H_2O$ –*n*-decanol–SDS transferred into the gelled state by the gelators DBS, DBC and HG1, and make a comparison to previous results obtained with the gelator 12-HOA.<sup>[40]</sup>

A schematic drawing of a lyotropic  $N_d$  phase and its gelled state is shown in **Figure 1e,f**, respectively. For the nematic gel, the observed sol–gel transition temperature  $T_{sol-gel}$  lies above the nematic clearing temperature (the same is true for all obtained nematic gels, see Table S2, Supporting Information). Thus, in the absence of external influences, a random gel fiber network is formed upon cooling. As in the case of thermotropic nematic gels,<sup>[8]</sup> the gel fibers probably serve as a soft template for the nematic phase leading to a nematic polydomain structure. **Figure 1g** demonstrates that the lyotropic nematic gel combines the anisotropic properties of a nematic phase with the mechanical stability of a gel since an upside down sample between crossed polarizers shows optical birefringence and no flow. A freeze-fracture electron microscopy image of the same sample reveals the gel fiber network, where twisted gel fibers with a diameter of 8–12 nm run arbitrarily through the nematic phase. The rheological measurements (**Figure 1i**) clearly reveal the solid-like elastic behavior of the nematic gel. Similar to what is observed in the binary gel, the storage modulus  $G'$  exceeds the loss modulus  $G''$  over the full frequency range from  $\omega = 0.05$  to  $100\text{ s}^{-1}$ . This is in clear contrast to the fluid-like behavior of the gelator-free nematic phase with  $G'' > G'$  and both moduli at least three orders of magnitude smaller than in the nematic gel.

The molecular structure of the used LMWGs (see **Figure 1c–f**) shows a distinct difference between that of 12-HOA and the other gelators. While DBS, DBC, and HG1 are bulky, 12-HOA has a typical amphiphilic structure with a long hydrophobic alkyl chain and a polar head group. As reported before<sup>[40]</sup> and shown in **Figure 2** the molecular structure of 12-HOA

with *n* being the director. In the nematic gel, the micellar lyotropic nematic phase coexists with the gel fiber network. g, h) Gel formation is confirmed since no flow is observed when turning the sample ( $N_d$  phase with 3 wt% DBC) upside down, but the nematic gel shows optical birefringence between crossed polarizers (g) and the gel fibers are visible in electron microscopy images (h). An example is shown for the  $N_c$  phase gelled with 2 wt% DBC. i) Storage modulus  $G'$  (filled symbols) and loss modulus  $G''$  (open symbols) for the gelator-free  $N_d$  phase (black circles), the nematic gel ( $N_d$  phase gelled with 2 wt% DBC, red squares) and the binary gel ( $H_2O$  gelled with 0.5 wt% DBC, blue triangles), obtained via oscillation frequency ( $\omega$ ) sweeps at constant shear stress and temperature.



**Figure 2.** a–j) Comparison of the gelator-free  $N_d$  phase with the  $N_d$  phase gelled with the different LMWGs. (left) POM images of the gelator-free  $N_d$  phase (a) and of the gels obtained with 12-HOA (c), DBS (e), DBC

significantly influences its gelling properties since 12-HOA is partly incorporated into the micelles, acting as a cosurfactant and thus reducing the micelle curvature. As a result, the nematic phase is transferred into a lamellar gel, as proven by POM and X-ray investigations.<sup>[40]</sup> The challenge is thus to find gelators that are not incorporated into the micelles and leave the LLC phase unchanged upon gelation.

In fact, gelation of the  $N_d$  phase with DBS and DBC successfully leads to nematic gels, as proven by the schlieren textures observed in POM examinations and X-ray profiles that resemble the one of the gelator-free  $N_d$  phase (see Figure 2e–h). In all cases, a relatively sharp first order and a diffuse second order scattering maxima are observed indicating the presence of a pseudo-lamellar structure. The peak shape analysis (Figure S9 and Table S3, Supporting Information) reveals that the correlation length is about 150 Å and remains practically in the same range for the gelled  $N_d$  phases. The SAXS study thus demonstrates that the nematic structure remains essentially unchanged in the gelled state and a comparison with the X-ray profile of a  $L_\alpha$  phase (Figure 2d), which exhibits significantly sharper peaks confirms the nematic nature of all samples.

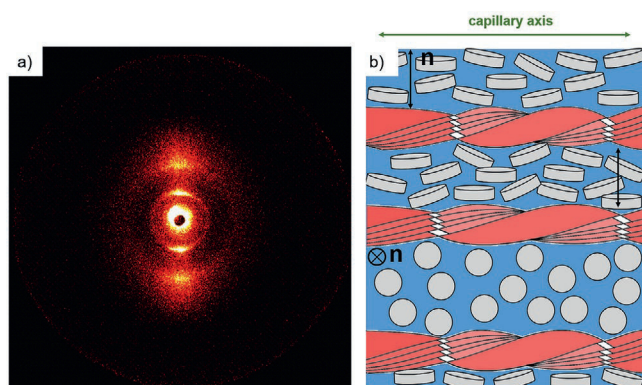
The X-ray curve of the  $N_d$  phase gelled with HG1 also clearly proves the absence of translational order, but the POM image reveals a fingerprint texture, typical of a chiral nematic phase (see Figure 2j). Obviously, gelation of the  $N_d$  phase with HG1 leads to a lyotropic cholesteric gel, due to (heterogenous) chiral induction by the twisted gel fibers.

To gain further insights into the structure of the lyotropic nematic gels we performed 2D small angle X-ray scattering (2D SAXS). In many cases, a uniform director configuration is observed (Figure 3). Even though the gel fiber network forms first, not a nematic polydomain structure (as sketched in Figure 1b) but a macroscopically aligned nematic gel is obtained. We assume that in thin capillaries (700 μm) the fibers grow along the capillary axis and thus the director of the  $N_d$  phase is aligned perpendicular to it. Like in other types of anisotropic hydrogels<sup>[22,31,50]</sup> and LCEs,<sup>[51–53]</sup> such monodomains of lyotropic nematic networks are essential, for the potential use of LLC gels as actuators and sensors. However, a director alignment as shown in Figure 3b is not always reproducible. In some cases, nematic polydomain gels were observed as well. Similar investigations on the  $N_c$  phase gelled with DBS, DBC and HG1 are found in the Supporting Information.

In conclusion, we have shown that anisotropic hydrogels are available relatively easy by gelling micellar lyotropic nematic host phases with gelators which do not have an amphiphilic structure and thus do not act as a cosurfactant. In certain cases, a chirality transfer from the helical gel fibers to the LC phase might also result in cholesteric gels. Similar to their

(g), and HG1 (j). (right) X-ray diffraction profiles of the gelator-free  $N_d$  phase (b) and of the gels obtained with 12-HOA (d), DBS (f), DBC (h), and HG1 (j). Gelation of the lyotropic nematic  $N_d$  phase with the gelator 12-HOA leads to a lamellar gel. Contrary, gelation of the  $N_d$  phase with the LMWGs DBS and DBC results in a nematic gel. When using HG1 to gel the  $N_d$  phase, the formation of a chiral nematic gel is observed. The layered structure of the 12-HOA fibers<sup>[55,56]</sup> reveals itself by two small and broad maxima at  $q = 1.35 \text{ nm}^{-1}$  and  $q = 4.04 \text{ nm}^{-1}$ . Contrary, the presence of gel fibers of DBS, DBC, and HG1 is not reflected in the X-ray profiles.





**Figure 3.** a) 2D SAXS diffractogram of the  $N_d$  phase gelled with 2 wt% DBC. Although the gel fibers form first, an oriented director configuration is observed. Probably, the capillary surface guides a linear growth of the gel fibers which in turn serve as a soft template for the  $N_d$  phase, as shown in (b), the schematic drawing of the gelled  $N_d$  phase.

thermotropic counterparts (LCs), micellar lyotropic nematic gels are most interesting as stimuli-responsive water-based systems for applications in sensing and actuation.

## Experimental Section

**Sample Preparation:** The lyotropic nematic phases  $N_d$  and  $N_c$  of the ternary system sodium dodecylsulfate (SDS, SigmaAldrich, BioUltra,  $\geq 99\%$ ) as surfactant, *n*-decanol (DOH, Merck,  $\geq 99\%$ ) as co-surfactant and bidistilled water, as well as of a second ternary system containing *N,N*-dimethyl-*N*-ethylhexadecylammonium bromide (CDEAB, Merck,  $> 98\%$ ) as surfactant, DOH as cosurfactant and water were studied. To transfer the nematic phases into the gel state the LMWGs 1,3:2,4-dibenzylidene-*D*-sorbitol (DBS, NJC Europe), *N,N'*-dibenzoyl-L-cystine (DBC, Santa Cruz) and the tris-amido-cyclohexane derivative HG1 (kindly provided by the group of van Esch, TU Delft, synthesized as described in ref. [54]) were used. All chemicals were used without further purification. The nematic gels were prepared with the same water mass fraction ( $\omega_{H_2O} = \frac{m_{H_2O}}{m_{tot}} = \text{const.}$ ) and the same cosurfactant to surfactant ratio ( $\gamma = \frac{m_{\text{cosurfactant}}}{m_{\text{surfactant}}} = \text{const.}$ ) than the gelator-free nematic phases by adding the LMWG ( $\text{wt}\%_{\text{LMWG}} = \frac{m_{\text{LMWG}}}{m_{\text{tot}}} \times 100$ ). Please consult the Supporting Information for the exact composition of the respective samples. The gelator-free nematic phases were prepared by weighing surfactant and water into a glass vial sealed by a screw plug and subsequent shaking of the mixture for about 1 h at 40 °C (thermoshaker Biosan, PST-60HL) until the surfactant was dissolved. DOH was added and the sample was placed on a roll mixer (Phoenix Instruments, RS-TR05) at room temperature for one day to ensure homogenization of the sample.  $N_d$  and  $N_c$  phases were differentiated by the way they attach to a polar glass surface and align in a magnetic field (see Figures S2 and S3, Supporting Information). To obtain nematic gels the proper amount of LMWG was added to the sample and dissolved by heating the sample up in a thermoshaker (Hettich, MHR-23, 95 °C, 500 rpm, 10 min). Afterward, the sample was kept at room temperature for one day until gelation was completed. Samples were considered gelled when no flow occurred in an inverted vessel for at least 8 h. Please consult Table S1 in the Supporting Information for the respective critical gelation concentrations (cgc), which is for a given sample the minimal gelator concentration necessary to obtain a gel.

**Methods:** Polarizing microscopy was performed at room temperature using a Leica DMLP polarizing microscope. Photographs of the textures were taken by a Nikon D5300 camera. Samples were filled into flat capillaries (Camlab UK) with a cross-section of 0.3 mm  $\times$  3 mm

and were flame sealed. 1D small-angle X-ray studies were carried out with a SAXSess system (Anton Paar). The X-ray radiation ( $\text{Cu-K}\alpha$ ,  $\lambda = 0.15418$  nm) was generated by an ISO-DEBYEFLEX 3003 X-ray generator (GE Inspection Technologies GmbH) and the X-ray scattering was recorded using a CMOS detector (Dectris, Mythen 2 1K). Temperature was controlled by the sample holder unit TSC 120. 2D small angle X-ray scattering was carried out on a Bruker AXS Nanostar X-ray diffractometer ( $\text{Cu-K}\alpha$  radiation,  $\lambda = 0.15418$  nm, generated by a Kristalloflex 770 generator, 100  $\mu\text{m}$  point-collimated X-ray beam, 60 cm sample to detector distance, VANTEC 500 2D digital Mikrogap area detector and a home-build temperature-controlled sample holder with a magnetic field of 0.7 T). Samples were filled into Mark capillary tubes (Hilgenberg, glass No. 14) with an outer diameter of 0.7 mm and a wall thickness of 0.01 mm. Freeze fracture electron microscopy replicas of the gelled samples were prepared with the freeze fracture and etching system EM BAF060 from Leica. After quenching the sample in liquid ethane and fracturing it, the surface was replicated by a layer of Pt/C ( $\approx 2$  nm) deposited at an angle of 45° and stabilized by a layer of pure carbon ( $\approx 20$  nm) at 90° in the vacuum chamber of the BAF060 at  $-150$  °C. The replicas were examined using a transmission electron microscope EM10 from Zeiss operated at 60 kV. Oscillating shear rheometry was measured using a Physica MCR 501 (Anton Paar) rheometer with a plate-plate geometry (diameter of upper plate 25 mm) and a constant gap size of 1 mm. For all measurements, temperature was set to 24 °C and water evaporation reduced by a solvent gap. To determine the limit of the linear viscoelastic range first amplitude sweeps at a constant angular frequency of  $\omega = 10$  s $^{-1}$  and an increasing shear stress  $\tau$  were carried out. Oscillation frequency sweeps were then executed at an appropriate constant shear stress ( $\tau = 2$  Pa for the gelator-free  $N_d$  phase and  $\tau = 40$  Pa for the gelled  $N_d$  phase and the binary gel) varying the angular frequency  $\omega$  from 100 to 0.05 s $^{-1}$ .

## Supporting Information

Supporting Information is available from the Wiley Online Library or from the author.

## Acknowledgements

The authors gratefully acknowledge financial support from the Deutsche Forschungsgemeinschaft (DFG Gi-243/9-1) and Fonds der Chemischen Industrie (FCI). The authors thank Tabea Pfister for the preparation of the samples studied in Figure S3 (Supporting Information). Many thanks to Ke Peng for the introduction into the rheometer.

Open access funding enabled and organized by Projekt DEAL.

## Conflict of Interest

The authors declare no conflict of interest.

## Keywords

low-molecular-weight gelators, lyotropic liquid crystals, lyotropic nematic gels, self-assembled fibrillar networks

Received: October 27, 2020

Revised: December 7, 2020

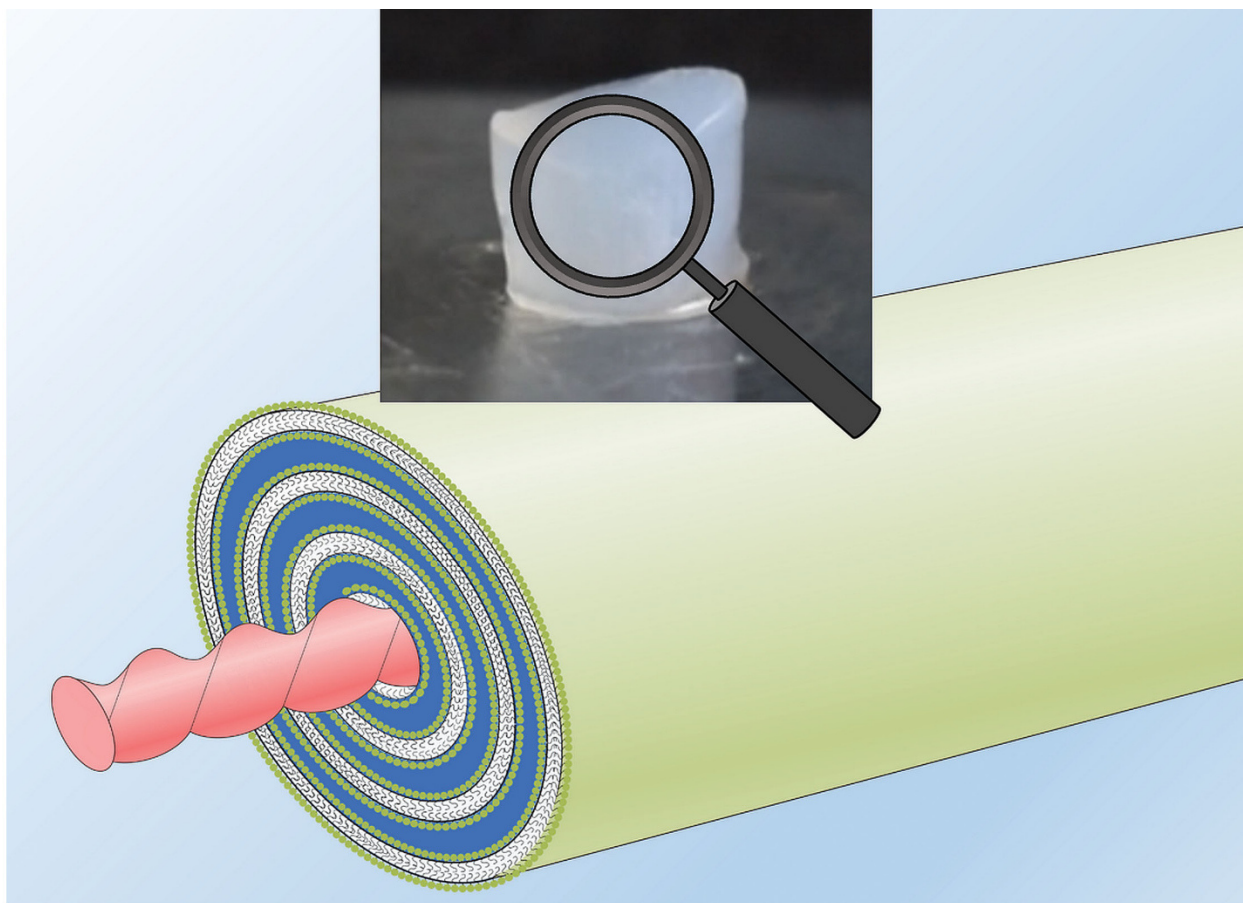
Published online: January 18, 2021

[1] P.-G. de Gennes, M. Hébert, R. Kant, *Macromol. Symp.* **1997**, 113, 39.



- [2] M.-H. Li, P. Keller, *Philos. Trans. R. Soc., A* **2006**, *364*, 2763.
- [3] F. J. Davis, *J. Mater. Chem.* **1993**, *3*, 551.
- [4] S. Mayer, R. Zentel, *Curr. Opin. Solid State Mater. Sci.* **2002**, *6*, 545.
- [5] T. J. White, D. J. Broer, *Nat. Mater.* **2015**, *14*, 1087.
- [6] T. Kato, T. Kutsuna, K. Hanabusa, M. Ukon, *Adv. Mater.* **1998**, *10*, 606.
- [7] L. Guan, Y. Zhao, *J. Mater. Chem.* **2001**, *11*, 1339.
- [8] T. Kato, Y. Hirai, S. Nakaso, M. Moriyama, *Chem. Soc. Rev.* **2007**, *36*, 1857.
- [9] E.-K. Fleischmann, H.-L. Liang, N. Kapernaum, F. Giesselmann, J. Lagerwall, R. Zentel, *Nat. Commun.* **2012**, *3*, 1178.
- [10] M. Rogósz, H. Zeng, C. Xuan, D. S. Wiersma, P. Wasylczyk, *Adv. Opt. Mater.* **2016**, *4*, 1689.
- [11] S. Schuhladen, F. Preller, R. Rix, S. Petsch, R. Zentel, H. Zappe, *Adv. Mater.* **2014**, *26*, 7247.
- [12] M.-H. Li, P. Keller, J. Yang, P.-A. Albouy, *Adv. Mater.* **2004**, *16*, 1922.
- [13] M. Camacho-Lopez, H. Finkelmann, P. Palffy-Muhoray, M. Shelley, *Nat. Mater.* **2004**, *3*, 307.
- [14] J. M. McCracken, B. R. Donovan, T. J. White, *Adv. Mater.* **2020**, *32*, 1906564.
- [15] K. Sano, Y. Ishida, T. Aida, *Angew. Chem., Int. Ed.* **2018**, *57*, 2532.
- [16] S. A. Willis, G. R. Dennis, G. Zheng, W. S. Price, *React. Funct. Polym.* **2013**, *73*, 911.
- [17] F. A. Aouada, M. R. de Moura, P. R. G. Fernandes, A. F. Rubira, E. C. Muniz, *Eur. Polym. J.* **2005**, *41*, 2134.
- [18] C. L. Lester, S. M. Smith, C. D. Colson, C. A. Guymon, *Chem. Mater.* **2003**, *15*, 3376.
- [19] M. Hayakawa, T. Onda, T. Tanaka, K. Tsujii, *Langmuir* **1997**, *13*, 3595.
- [20] F. Kleinschmidt, M. Hickl, K. Saalwächter, C. Schmidt, H. Finkelmann, *Macromolecules* **2005**, *38*, 9772.
- [21] C. Özdilek, E. Mendes, S. J. Picken, *Polymer* **2006**, *47*, 2189.
- [22] N. Miyamoto, M. Shintate, S. Ikeda, Y. Hoshida, Y. Yamauchi, R. Motokawa, M. Annaka, *Chem. Commun.* **2013**, *49*, 1082.
- [23] A. F. Mejia, R. Ng, P. Nguyen, M. Shuai, H. Y. Acosta, M. S. Mannan, Z. Cheng, *Soft Matter* **2013**, *9*, 10257.
- [24] L. Chen, Q. Wu, J. Zhang, T. Zhao, X. Jin, M. Liu, *Polymer* **2020**, *192*, 122309.
- [25] Z. Zhu, G. Song, J. Liu, P. G. Whitten, L. Liu, H. Wang, *Langmuir* **2014**, *30*, 14648.
- [26] M. F. Islam, A. M. Alsayed, Z. Dogic, J. Zhang, T. C. Lubensky, A. G. Yodh, *Phys. Rev. Lett.* **2004**, *92*, 88303.
- [27] D. J. Abdallah, R. G. Weiss, *Adv. Mater.* **2000**, *12*, 1237.
- [28] X. Du, J. Zhou, J. Shi, B. Xu, *Chem. Rev.* **2015**, *115*, 13165.
- [29] M. George, R. G. Weiss, *Acc. Chem. Res.* **2006**, *39*, 489.
- [30] L. E. Buerkle, S. J. Rowan, *Chem. Soc. Rev.* **2012**, *41*, 6089.
- [31] L. E. Millon, H. Mohammadi, W. K. Wan, *J. Biomed. Mater. Res., Part B* **2006**, *79*, 305.
- [32] D.-H. Kim, A. Jahn, S.-J. Cho, J. S. Kim, M.-H. Ki, D.-D. Kim, *J. Pharm. Invest.* **2015**, *45*, 1.
- [33] L. Kang, H. H. Cheong, S. Y. Chan, P. F. C. Lim, in *Soft Fibrillar Materials: Fabrication and Applications* (Eds: X. Y. Liu, J.-L. Li), Wiley-VCH, Weinheim, Germany **2013**, pp. 115–128.
- [34] C. Wang, D. Chen, X. Jiao, *Sci. Technol. Adv. Mater.* **2009**, *10*, 023001.
- [35] S. H. Tolbert, A. Firouzi, G. D. Stucky, B. F. Chmelka, *Science* **1997**, *278*, 264.
- [36] Y. Xu, M. Laupheimer, N. Preisig, T. Sottmann, C. Schmidt, C. Stubenrauch, *Langmuir* **2015**, *31*, 8589.
- [37] S. Koitani, S. Dieterich, N. Preisig, K. Aramaki, C. Stubenrauch, *Langmuir* **2017**, *33*, 12171.
- [38] K. Steck, C. Stubenrauch, *Langmuir* **2019**, *35*, 17132.
- [39] K. Steck, N. Preisig, C. Stubenrauch, *Langmuir* **2019**, *35*, 17142.
- [40] S. Dieterich, T. Sottmann, F. Giesselmann, *Langmuir* **2019**, *35*, 16793.
- [41] E. Akpınar, C. Canioz, M. Turkmen, D. Reis, A. M. Figueiredo Neto, *Liq. Cryst.* **2018**, *45*, 219.
- [42] E. Akpınar, K. Otluoğlu, M. Turkmen, C. Canioz, D. Reis, A. M. Figueiredo Neto, *Liq. Cryst.* **2016**, *43*, 1693.
- [43] E. Akpınar, M. Turkmen, C. Canioz, A. M. F. Neto, *Eur. Phys. J. E: Soft Matter Biol. Phys.* **2016**, *39*, 107.
- [44] D. Zhang, Q. Liu, R. Visvanathan, M. R. Tuchband, G. H. Sheeta, B. D. Fairbanks, N. A. Clark, I. I. Smalyukh, C. N. Bowman, *Soft Matter* **2018**, *14*, 7045.
- [45] P. Terech, *Liq. Cryst.* **2006**, *9*, 59.
- [46] B. J. Lemaire, P. Panine, J. C. P. Gabriel, P. Davidson, *Europhys. Lett.* **2002**, *59*, 55.
- [47] J. Campbell, M. Kuzma, M. M. Labes, *Mol. Cryst. Liq. Cryst.* **2011**, *95*, 45.
- [48] H. C. Yun, E. Y. Chu, Y. K. Han, J. L. Lee, T. K. Kwei, Y. Okamoto, *Macromolecules* **1997**, *30*, 2185.
- [49] J. B. Jones, C. R. Safinya, *Biophys. J.* **2008**, *95*, 823.
- [50] R. M. Erb, J. S. Sander, R. Grisch, A. R. Studart, *Nat. Commun.* **2013**, *4*, 1712.
- [51] O. M. Wani, H. Zeng, A. Priimagi, *Nat. Commun.* **2017**, *8*, 15546.
- [52] D. L. Thomsen, P. Keller, J. Naciri, R. Pink, H. Jeon, D. Shenoy, B. R. Ratna, *Macromolecules* **2001**, *34*, 5868.
- [53] C. Ohm, M. Brehmer, R. Zentel, *Adv. Mater.* **2010**, *22*, 3366.
- [54] K. J. C. van Bommel, C. van der Pol, I. Muizebelt, A. Friggeri, A. Heeres, A. Meetsma, B. L. Feringa, J. van Esch, *Angew. Chem., Int. Ed.* **2004**, *43*, 1663.
- [55] T. Tachibana, T. Mori, K. Hori, *Bull. Chem. Soc. Jpn.* **1980**, *53*, 1714.
- [56] P. Terech, *Colloid Polym. Sci.* **1991**, *269*, 490.

## Publication III



Highlighting research from the Liquid Crystal and Soft Matter group of Prof. Frank Gießelmann, obtained in cooperation with Prof. Thomas Sottmann, both from the Institute of Physical Chemistry, University of Stuttgart, Germany; including SANS experiments from the Institut Laue Langevin (ILL), Grenoble, France.

Synergistic structures in lyotropic lamellar gels

Gelled lamellar lyotropic liquid crystal phases ( $L_a$ ) were studied by means of small angle neutron scattering (SANS). Based on the SANS data, we report the formation of a new synergistic structure, which is neither present in the gelator-free lamellar phase nor in the isotropic 3D gel network and mimics similar schemes found in neural cells, where axons are surrounded by lamellar myelin sheets.

As featured in:



See Frank Giesselmann *et al.*,  
*Soft Matter*, 2020, **16**, 10268.



Cite this: *Soft Matter*, 2020, **16**, 10268

## Synergistic structures in lyotropic lamellar gels†

Sonja Dieterich,<sup>a</sup> Sylvain Prévost,<sup>ib</sup> Carina Dargel,<sup>c</sup> Thomas Sottmann<sup>id</sup><sup>a</sup> and Frank Giesselmann<sup>id</sup><sup>\*a</sup>

In this work we present a systematic study on the microstructure of soft materials which combine the anisotropy of lyotropic liquid crystals with the mechanical stability of a physical gel. Systematic small-angle neutron (SANS) and X-ray (SAXS) scattering experiments were successfully used to characterize the lyotropic lamellar phase ( $L_x$ ) of the system  $D_2O - n$ -decanol – SDS which was gelled by two low molecular weight organogelators, 1,3:2,4-dibenzylidene- $D$ -sorbitol (DBS) and 12-hydroxyoctadecanoic acid (12-HOA). Surprisingly, a pronounced shoulder appeared in the scattering curves of the lamellar phase gelled with 12-HOA, whereas the curves of the DBS-gelled  $L_x$  phase remained almost unchanged compared to the ones of the gelator-free  $L_x$  phase. The appearance of this additional shoulder strongly indicates the formation of a synergistic structure, which neither exists in the gelator-free  $L_x$  phase nor in the isotropic binary gel. By comparing the thicknesses of the 12-HOA (25–30 nm) and DBS (4–8 nm) gel fibers with the lamellar repeat distance (7.5 nm), we suggest that the synergistic structure originates from the minimization of the elastic free energy of the lamellar phase. In the case of 12-HOA, where the fiber diameter is significantly larger than the lamellar repeat distance, energetically unfavored layer ends can be prevented, when the layers cylindrically enclose the gel fibers. Interestingly, such structures mimic similar schemes found in neural cells, where axons are surrounded by lamellar myelin sheets.

Received 13th August 2020,  
Accepted 23rd September 2020

DOI: 10.1039/d0sm01473g

[rsc.li/soft-matter-journal](http://rsc.li/soft-matter-journal)

## Introduction

Lyotropic liquid crystal gels (LLCGs) are soft solids in which the mechanical stability of a physical 3D gel network is combined with the anisotropy of a lyotropic liquid crystal. In this study, the class of supramolecular physical gels are so-called self-assembled fibrillar networks (SAFINS) which are built up by small amounts of bio-inspired and thus biodegradable low molecular weight gelators (LMWGs, *e.g.* amino acid or fatty acid based). In an appropriate solvent, the LMWG molecules self-assemble into 1D fibers, which then entangle to form the 3D gel network able to immobilize the solvent (note that a physical gel is not at thermodynamic equilibrium).<sup>1–5</sup> Since in a SAFIN all interactions are non-covalent (mainly H-bonds and  $\pi$ – $\pi$  interactions), the gel can be reversibly transferred into the sol state by increasing the temperature above the gel–sol transition temperature  $T_{\text{gel-sol}}$ . SAFINS also show responsiveness to other external stimuli such as light,<sup>6–9</sup> pH-value<sup>10</sup> or ion concentration<sup>6</sup> allowing on-demand release of *e.g.* drugs or

inks.<sup>3,5,11</sup> LMWGs can be separated into hydro- and organogelators depending on whether they are able to gel water or organic solvents, respectively.

In this study two chiral organogelators, namely 1,3:2,4-dibenzylidene- $D$ -sorbitol (DBS) and (*R*)-12-hydroxyoctadecanoic acid (12-HOA), both well-known to gel various organic solvents<sup>12–15</sup> are investigated in their ability to gel LLCs. The one-dimensional fiber growth for DBS is mainly mediated *via* intermolecular hydrogen bonding from the OH-group at the C6 position to the acetal oxygen, although in polar solvents  $\pi$ – $\pi$  stacking between the aromatic rings plays a crucial role as well.<sup>16–19</sup> 12-HOA molecules form dimers *via* the carboxylic head group.<sup>20,21</sup> These dimers aggregate into one-dimensional helical fibers *via* H-bonds between the C12 OH-groups.<sup>22,23</sup> The fibers exhibit an internal layer structure.<sup>24,25</sup> While both gelators form twisted gel fibers, they substantially differ in the thickness of the fibers (see Fig. 1). DBS forms rather thin fibers (4–8 nm),<sup>26</sup> whereas 12-HOA results in thick fibers ( $27 \pm 6$  nm).<sup>27</sup> Both gelators, DBS and 12-HOA, were proven to gel thermotropic liquid crystals leading to anisotropic soft solids.<sup>28–30</sup> It was shown that the gel network is able to enhance anisotropic properties of the LC<sup>31,32</sup> and stabilizes the liquid-crystalline alignment.<sup>33,34</sup>

Surfactant-based lyotropic liquid crystals (LLCs) are anisotropic fluids, in which the micellar and lamellar building blocks possess at least a long-range orientational order. In addition to the long-range orientational order of lyotropic

<sup>a</sup> Institute of Physical Chemistry, University of Stuttgart, Pfaffenwaldring 55, 70569 Stuttgart, Germany. E-mail: [f.giesselmann@ipc.uni-stuttgart.de](mailto:f.giesselmann@ipc.uni-stuttgart.de)

<sup>b</sup> Institut Laue Langevin, LSS Group, 71 avenue des Martyrs CS 20156, 38042 Grenoble Cedex 9, France

<sup>c</sup> Physical and Biophysical Chemistry, Department of Chemistry, Bielefeld University, Universitätsstraße 25, 33615 Bielefeld, Germany

† Electronic supplementary information (ESI) available. See DOI: 10.1039/d0sm01473g



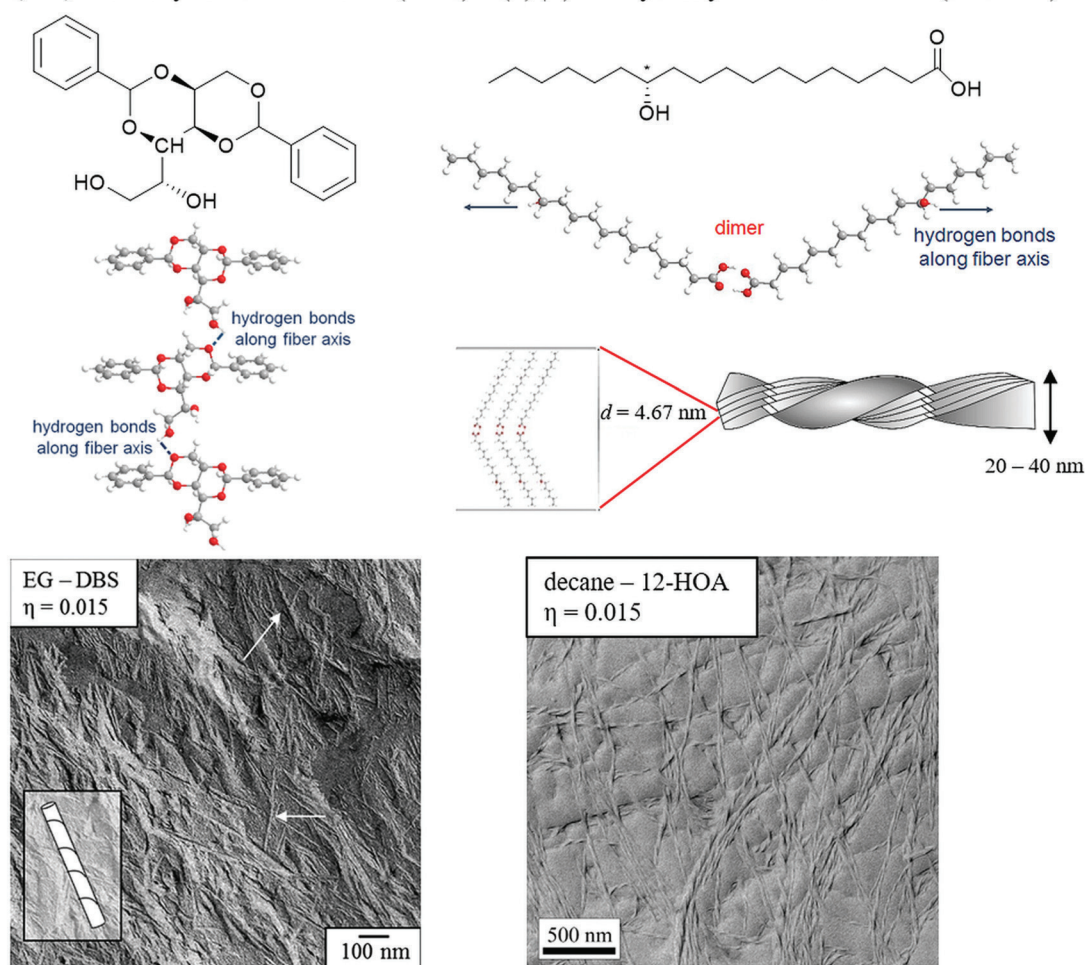
(a) 1,3:2,4-dibenzylidene-D-sorbitol (DBS) (b) (*R*)-12-hydroxyoctadecanoic acid (12-HOA)

Fig. 1 Molecular structure and gel fiber formation of the two organogelators (a) 1,3:2,4-dibenzylidene-D-sorbitol (DBS) and (b) (*R*)-12-hydroxyoctadecanoic acid (12-HOA), reprinted from<sup>35</sup> with the permission of American Chemical Society, Copyright 2020. DBS and 12-HOA both form twisted gel fibers in organic solvents. It was shown that DBS forms fibers of 4–8 nm thickness in ethyleneglycol<sup>26</sup> (electron microscopy image reprinted from<sup>26</sup> with the permission of American Chemical Society, Copyright 2020), whereas the thickness of 12-HOA fibers in *n*-decane is  $27 \pm 6$  nm<sup>27</sup> (electron microscopy image reprinted from<sup>27</sup> with the permission from Elsevier, Copyright 2020).

nematic phases, lamellar phases possess 1D quasi long-range translational order, while hexagonal phases possess 2D quasi long-range translational order. The fluid lamellar phase  $L_\alpha$  is characterized by a regular 1D stacking of surfactant bilayers separated by water layers.

The formation of a physical gel in a LLC, leads to anisotropic gels, which show no macroscopic flow, but elastic response to external stress and solid-like rheological properties. Their macroscopic anisotropy expresses itself in *e.g.* optical birefringence.<sup>35–37</sup> LLCs are thus the lyotropic counterparts of thermotropic liquid-crystalline gels (LCGs)<sup>38–40</sup> and elastomers (LCEs)<sup>41–44</sup> and might likewise be useful as stimuli-responsive materials in biomimetic actuation and motion.<sup>45–52</sup> Other possible LLC applications are in the field of trans-dermal drug delivery<sup>1,53</sup> or as templates in the synthesis of nanostructured silica materials.<sup>54–56</sup>

The present paper aims to investigate the structure of the lyotropic lamellar phase ( $L_\alpha$ ) of the system  $D_2O - n$ -decanol – SDS

which was gelled by DBS and 12-HOA. One goal is to clarify, whether the gel fiber network influence the structure of the  $L_\alpha$  phase and *vice versa*. In the case of thermotropic LCGs it was shown that the LC can serve as a soft template for the gel network leading to aligned fibers, in case the LC phase forms before the gel.<sup>40,57–59</sup> Otherwise, if the gel network forms first, the randomly oriented gel fibers direct a LC polydomain structure.<sup>60–62</sup>

If the two structures form independently from each other within the same system, the LLC would be an “orthogonal self-assembled system”.<sup>63–65</sup> There are few studies using the LMWGs DBS and 12-HOA to investigate whether or not LLCs are orthogonal self-assembled systems.<sup>26,35–37,66</sup> Most studies conclude that structure and properties of gel network and LLC remain essentially unchanged by the presence of each other,<sup>26,36,37,66</sup> although 12-HOA is known to be incorporated into the micelles due to its amphiphilic structure<sup>35,67</sup> (whereas the bulky DBS has no amphiphilic nature). It was shown that the chronology of DBS-gel and LLC formation has no

significant influence on the actual LLCG structure.<sup>26</sup> However, in a recent study we showed that the gelation of a  $L_{\alpha}$  phase with 12-HOA results in an arrested lamellar layer spacing and a higher degree of lamellar order clearly proving that in this particular case the lamellar gel is not an orthogonal self-assembled system.<sup>35</sup>

All these studies have in common that structural investigations were limited on length scales of up to 10 nm. To solve the question whether the gel network or LLC morphologies are changed by the presence of each other, also investigations on larger length scales are necessary. Thus, we here present the results of a small-angle neutron scattering (SANS) study, where structures with length scales up to 500 nm were examined. As a key result of our systematic SANS studies we report on the formation of a synergistic structure in the  $L_{\alpha}$  phase gelled with 12-HOA, which manifests in a broad shoulder in the respective SANS curves. This synergistic structure only exists in the combined system of lamellar layers pervaded by a fiber network and neither appear in the gelator-free  $L_{\alpha}$  phase nor in the isotropic binary gel. We suggest that the formation of the synergistic structure originates from the minimization of the  $L_{\alpha}$  elastic free energy in the presence of relatively thick gel fibers. In case of 12-HOA, the fiber diameter is significantly larger than the lamellar repeat distance. To prevent too many layer ends, the layers cylindrically enclose the gel fibers. Such a structural assembly mimics similar schemes found in neural cells, where axons are surrounded by lamellar myelin sheets. Contrary, the SANS curves of the lamellar phases gelled with DBS, which forms gel fibers with a diameter in the range of the lamellar spacing, exhibit no pronounced shoulder, but instead, resemble the scattering of gelator-free  $L_{\alpha}$  phases. Thus for the DBS-gelled  $L_{\alpha}$  phase, the lamellar layer structure remains almost unchanged by the presence of thin gel fibers. These results clearly indicate that the ratio of gel fiber thickness to lamellar layer spacing seems to be the crucial criterion whether or not synergistic structures are formed in lyotropic lamellar gels.

## Experimental

### Materials and sample preparation

In our experiments we studied the  $L_{\alpha}$  phase made of sodium dodecylsulfate (SDS, SigmaAldrich, BioUltra,  $\geq 99\%$ ) as surfactant, *n*-decanol (DOH, Merck,  $\geq 99\%$ ) as cosurfactant and water. Samples for SANS experiments were prepared by using  $D_2O$  (Eurisotop, 99.9% D), samples for SAXS experiments by using bidistilled water as solvent. For SANS contrast variation experiments d25-SDS (Eurisotop,  $\geq 98\%$  D) and d21-DOH (Eurisotop,  $\geq 98$  D) were used. The samples were gelled using the low molecular weight gelators 1,3:2,4-dibenzylidene- $D$ -sorbitol (DBS, NJC Europe) and (*R*)-12-hydroxyoctadecanoic acid (12-HOA, ChemCruz). All chemicals were used without further purification. Samples were prepared according to the following quantities using the respective components' densities and assuming ideal mixing behavior.

The water volume fraction is given by:

$$\phi_w = \frac{V_{H/D_2O}}{V_{H/D_2O} + V_{SDS} + V_{DOH} + V_{LMWG}}, \quad (1)$$

with  $\phi_w = 0.675$  for all lamellar and  $\phi_w = 0.75$  for all isotropic samples.

The DOH to SDS ratio is defined as:

$$\phi_{DOH/SDS} = \frac{V_{DOH}}{V_{SDS}}, \quad (2)$$

with  $\phi_{DOH/SDS} = 0.5$  in the  $L_{\alpha}$  phase and  $\phi_{DOH/SDS} = 0.17$  in the isotropic phase.

The amount of gelator is specified by:

$$\mu = \frac{m_{LMWG}}{m_{H/D_2O} + m_{SDS} + m_{DOH} + m_{LMWG}}. \quad (3)$$

The scattering curves of lamellar gels are compared with those of three reference systems, namely (i) the gelator-free  $L_{\alpha}$  phase with the same  $\phi_w$  and  $\phi_{DOH/SDS}$  as the gelled  $L_{\alpha}$  phase. (ii) the isotropic binary gel, *n*-decanol/DBS and *n*-dodecane/12-HOA respectively, each with the same gelator weight fraction  $\mu$  than the gelled  $L_{\alpha}$  phase and (iii) a gelled isotropic micellar phase of the same surfactant system gelled with the same weight fraction gelator  $\mu$  as the gelled  $L_{\alpha}$  phase.

The gelator-free  $L_{\alpha}$  phase was prepared by weighing SDS and water in a glass vial sealed by a screw plug and shaking the mixture for about 1 h at 40 °C (thermoshaker Biosan, PST-60HL) until SDS was completely dissolved. DOH was added and the vial was placed on a roll mixer (Phoenix Instruments, RS-TR05) for one day to homogenize the sample. To obtain gelled  $L_{\alpha}$  phases the proper amount of the LMWG was added to the sample and the sample was heated in a thermoshaker (Hettich, MHR-23) to dissolve the gelator (95 °C for DBS, 80 °C for 12-HOA, 500 rpm). Afterwards, the sample was quenched in an ice bath for 30 minutes and kept at room temperature for one day for complete gel formation. The  $L_{\alpha}$  phase was considered as gelled when the vial was put upside down and no flow occurred for eight hours.

The binary gels were prepared by weighing the DBS to d21-*n*-decanol and 12-HOA to d26-*n*-dodecane (Eurisotop,  $\geq 98\%$ ), using the thermoshaker (Hettich, MHR-23) to dissolve the gelator (90 °C for DBS, 70 °C for 12-HOA, 500 rpm), quenching the sample in an ice bath and keeping it at room temperature afterwards. Gel formation was verified as described before.

### Methods

SANS measurements on gelator-free and 12-HOA gelled samples were performed on the instrument D11 at the ILL in Grenoble, France during three beam times. The following settings were used. March 2017: wavelengths  $\lambda = 4.6$  Å and 13 Å, sample-detector distances  $d = 1.4$  m, 8 m and 39 m at sample-collimator distances of  $col = 20.5$  m, 20.5 m and 40.5 m, respectively. October 2018:  $\lambda = 5.3$  Å,  $d = 2$  m, 8 m and 39 m at  $col = 8$  m, 8 m and 40.5 m, respectively. July 2019:  $\lambda = 5.5$  Å,  $d = 1.5$  m, 8 m and 39 m at  $col = 20.5$  m, 20.5 m and

40.5 m, respectively. These settings result in the  $q$ -ranges:  $0.0006 < q / \text{\AA}^{-1} < 0.56$ ,  $0.0014 < q / \text{\AA}^{-1} < 0.37$  and  $0.0018 < q / \text{\AA}^{-1} < 0.47$  respectively.

DBS gelled samples were measured at the NIST Center for Neutron Research (Gaithersburg, Maryland, USA) on the instrument NG7 30 m SANS. Neutron wavelengths of  $\lambda = 6.0 \text{ \AA}$  and  $\lambda = 8.4 \text{ \AA}$  (using focusing biconcave lenses LENS), sample-detector distances of  $d = 1.3 \text{ m}$ ,  $4 \text{ m}$  and  $13.2 \text{ m}$  at sample-collimator distances of  $\text{col} = 5.4 \text{ m}$ ,  $8.5 \text{ m}$ ,  $14.7 \text{ m}$  and  $16.3 \text{ m}$  (for the LENS configuration) respectively were used resulting in a  $q$ -range:  $0.0010 < q / \text{\AA}^{-1} < 0.47$ . The ILL specified a wavelength distribution of  $\Delta\lambda/\lambda = 0.09$  for the D11 instrument, while on NG7 30 m SANS a  $\Delta\lambda/\lambda = 0.138$  was adjusted.

The experiments were carried out in Hellma cells of 1 mm neutron path length, which were placed in cell holders which allow for an accurate temperature control (accuracy of 0.1 K). All isotropic two-dimensional raw data were radially averaged and then normalized to absolute scale using the incoherent scattering intensity of  $\text{H}_2\text{O}$  as a secondary standard at the ILL and the empty beam intensity at NIST. Radial averaging and data normalisation were performed with softwares available at the ILL and NIST, *i.e.* LAMP and IGOR Pro, respectively. All measured intensities were background-corrected and the detector dead time included, yielding the differential cross-section  $d\sigma(q)/d\Omega$ .

2D-SAXS measurements were carried out at the University of Bielefeld on a Xeuss SAXS/WAXS System (1st generation) from Xenocs. The X-ray radiation (Cu-K $\alpha$ ,  $\lambda = 1.5418 \text{ \AA}$ ) was provided by a GeniX<sup>3D</sup> Cu Ultra Low Divergence tube (Xenocs) and the X-ray scattering was recorded by a PILATUS 300 K 20 Hz hybrid pixel detector from Dectris. A sample-detector distance of 833 mm was used. Detector images were acquired over a time period of either 10 minutes ( $L_\alpha$  phase) or 30 minutes (isotropic phase) in high resolution collimation. Samples were placed into Mark capillary tubes (Hilgenberg, glass No. 14) with an outer diameter of 0.7 mm and a wall thickness of 0.01 mm and measured at room temperature. The 2D data was analyzed using the Foxtrot software (V.3.3.4, Xenocs/Soleil Synchrotron).

## Results and discussion

This section is organized as follows: First, we qualitatively discuss the difference in the scattering curves of the  $L_\alpha$  phase gelled with either DBS or 12-HOA and compare them to the scattering curves of the reference systems, namely the gelator-free  $L_\alpha$  phase, the binary gel and the isotropic micellar phase with focus whether and how the structure of the  $L_\alpha$  phase is altered in the gelled state. In the second part we analyze the SANS data with different models to obtain quantitative values for the structural parameters of the gelled  $L_\alpha$  phases in comparison to their reference systems. Last, we devise a model for the synergistic structures found in the  $L_\alpha$  phase gelled with the comparably thick 12-HOA fibers.

### Qualitative discussion of SANS curves

Bulk contrast SANS curves of the  $L_\alpha$  phase gelled with DBS or 12-HOA, and the one of the corresponding gelator-free  $L_\alpha$  phase are shown in Fig. 2 in a double logarithmic representation.

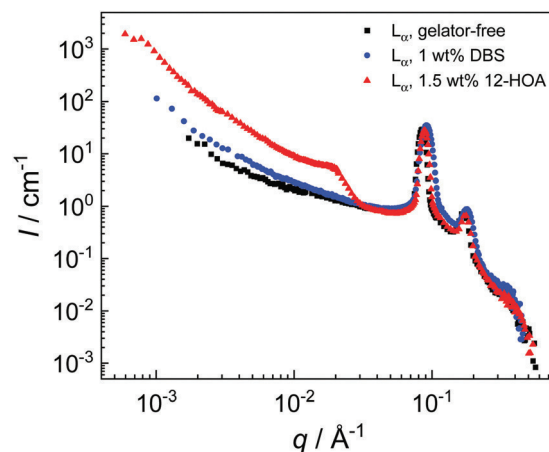


Fig. 2 SANS curves (total coherent scattering intensity  $I(q)$  vs.  $q$ ) of the gelator-free  $L_\alpha$  phase of the system  $\text{D}_2\text{O} - n$ -decanol – SDS ( $\phi_w = 0.675$  and  $\phi_{\text{DOH/SDS}} = 0.5$ , black squares), the corresponding  $L_\alpha$  phase gelled with 1 wt% DBS (blue circles) and the  $L_\alpha$  phase gelled with 1.5 wt% 12-HOA (red triangles). The curve of the DBS gelled  $L_\alpha$  phase resembles the one of the gelator-free  $L_\alpha$  phase almost quantitatively indicating that the DBS gel fiber network has no significant influence on the lamellar structure. In contrast, the curve of the 12-HOA gelled lamellar phase shows a pronounced shoulder at  $q \approx 0.017 \text{ \AA}^{-1}$  which is not present in the curve of the gelator-free  $L_\alpha$  phase.

All three curves show first and second order lamellar peaks as well as a strong increase of the scattering intensity at low  $q$ -values. As can be seen, the curve of the DBS gelled  $L_\alpha$  phase resembles the curve of the gelator-free lamellar phase almost quantitatively. From this we can conclude, that the structure of the  $L_\alpha$  phase seems not to be substantially disturbed by the relatively thin DBS gel fibers (4–8 nm) matching the lamellar repeat distance (7.5 nm). The fibers can thus be accommodated by the lamellar layer stacking without breaking too many layers. Note, that the wider lamellar peaks of the DBS gelled  $L_\alpha$  phase relate to the larger wavelength distribution at the NG-7 instrument at NIST ( $\Delta\lambda/\lambda = 0.138$ ) compared to the one of the instrument D11 at ILL ( $\Delta\lambda/\lambda = 0.09$ ), where the gelator-free  $L_\alpha$  phase and the  $L_\alpha$  phase gelled with 12-HOA were measured. In contrast, the SANS curve of the  $L_\alpha$  phase gelled with 12-HOA shows a remarkable difference to both the curve of the gelator-free and the DBS gelled  $L_\alpha$  phase: at  $q \approx 0.017 \text{ \AA}^{-1}$  a pronounced shoulder is observed. Even more remarkable, this shoulder is neither present in the curve of the binary gel (d26- $n$ -dodecane/12-HOA) nor in the one of the 12-HOA gelled isotropic micellar phase of the same lyotropic system (see Fig. S1, ESI<sup>†</sup>). This indicates the presence of a new “synergistic” structure in the lamellar gel, which does not exist in neither the gelator-free  $L_\alpha$  phase nor the isotropic gel.

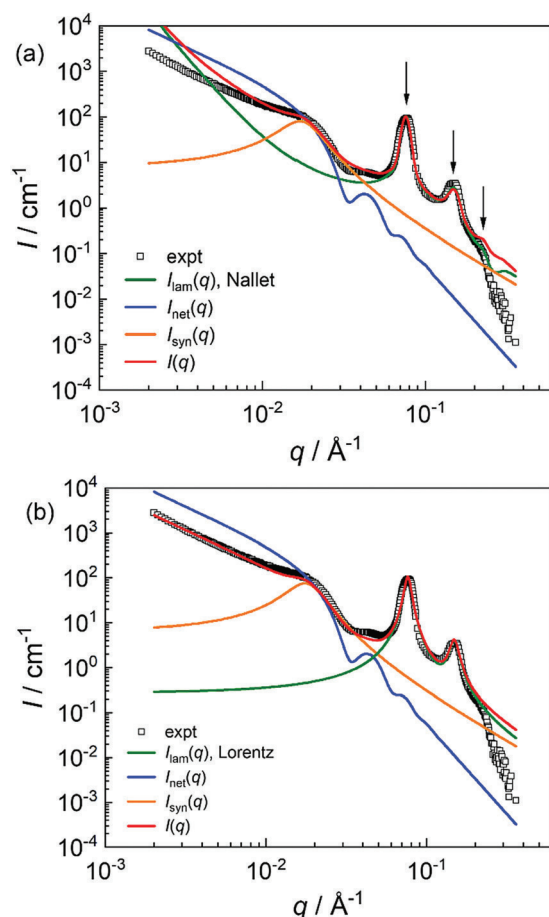
### Quantitative discussion of SANS curves

**$L_\alpha$  phase gelled with 12-HOA.** In this subsection we will analyze the bulk scattering curves  $I(q)$  of the  $L_\alpha$  phase gelled with 12-HOA by two slightly different fit models, both of which will allow us to separate the scattering contribution from the new synergistic structure  $I_{\text{syn}}(q)$  from other contributions,



namely the scattering from the gel network fibers  $I_{\text{net}}(q)$  and the scattering from the lamellar liquid-crystalline structure  $I_{\text{lam}}(q)$ . In a first approximation, we neglect any cross-terms between these three contributions and describe the total coherent scattering intensity in both models as a simple weighted sum of all three contributions:

$$I(q) = I_{\text{lam}}(q) + w_{\text{net}}I_{\text{net}}(q) + w_{\text{syn}}I_{\text{syn}}(q), \quad (4)$$



**Fig. 3** Analyses of the total coherent scattering intensity  $I(q)$  of the lamellar phase ( $\phi_w = 0.675$  and  $\phi_{\text{DOH/SDS}} = 0.5$ ,  $T = 25^\circ\text{C}$ ) gelled with 3 wt% 12-HOA.  $I_{\text{lam}}(q)$ ,  $I_{\text{net}}(q)$  and  $I_{\text{syn}}(q)$  are the calculated scattering contributions from the lamellar liquid-crystalline structure, the gel fiber network and the synergistic structure, respectively.  $I_{\text{lam}}(q)$  is calculated using the Nallet model in (a) and by two commensurable Lorentzians in (b). All fit parameters are listed in Table 1.

with weighting factors  $w_{\text{net}}$  and  $w_{\text{syn}}$  depending on the volume fraction and the scattering length density difference of the gel fiber network and the synergistic structure, respectively.

The fits of  $I(q)$  together with the separated contributions of the lamellar structure  $I_{\text{lam}}(q)$ , the gel network  $I_{\text{net}}(q)$  and the new synergistic structure  $I_{\text{syn}}(q)$  are shown in Fig. 3 and all parameters listed in Table 1. The models used in Fig. 3a and b to fit the experimental data differ in the way the scattering of the lamellar phase is described. In the first approach (Fig. 3a) we make use of the elaborate model developed by Nallet *et al.*<sup>68</sup> In the second approach we used simple Lorentzians (see ESI,† for equation) to fit the pseudo-Bragg peaks of the lamellar layers. For both models a comparable almost quantitative description of the lamellar layer peaks was achieved obtaining similar values of the layer spacing  $d_0$ .

The Nallet model<sup>68</sup> combines a static (“geometrical”) scattering contribution from planar surfactant bilayers with a dynamic contribution from thermal layer displacement fluctuations. The first (static) contribution assumes planar 2D-fluid surfactant bilayers of finite thickness  $\delta_{\text{bi}}$  that are regularly stacked in one dimension with period  $d_0$ . The second (dynamic) contribution originates from the Landau-Peierls instability which states that true (infinite) long-range translational order in a 1D-periodic medium is destroyed by thermal fluctuations.<sup>69,70</sup> Instead of an infinite correlation length in the direction normal to the layers, the positional correlation function in smectic and lamellar liquid crystals decays algebraically as  $r^{-\eta}$  with  $\eta$  being the Caillé parameter<sup>71</sup> which is in turn related to the elasticity of the lamellar layers, namely, the layer curvature modulus  $K_1$  and the layer compressibility  $B$ . In the Nallet model this effect is taken into account by the displacement  $u_n - nd_0$  of the  $n$ -th layer from its equilibrium position  $nd_0$  with a mean-square displacement  $\langle (u_n - u_0)^2 \rangle$  following the Caillé theory.<sup>71</sup> As a result, the tails of the pseudo-Bragg peak at  $q_0 = 2\pi/d_0$  decay according to the power law  $I_{\text{lam}}(q) \sim (q - q_0)^{2-\eta}$ .<sup>71,72</sup> The respective equations of the form and the structure factor are found in the ESI.† From the fit of the experimental scattering data with the Nallet model the bilayer thickness  $\delta_{\text{bi}}$ , the layer repeat period  $d_0$  and the Caillé parameter  $\eta$  are obtained.

The Nallet model is known to poorly reproduce the SANS data in the low- $q$  regime since it predicts a strong increase in diffuse scattering intensity at low  $q$ . This shortcoming can also be observed in our case (see the green curve in Fig. 3a).

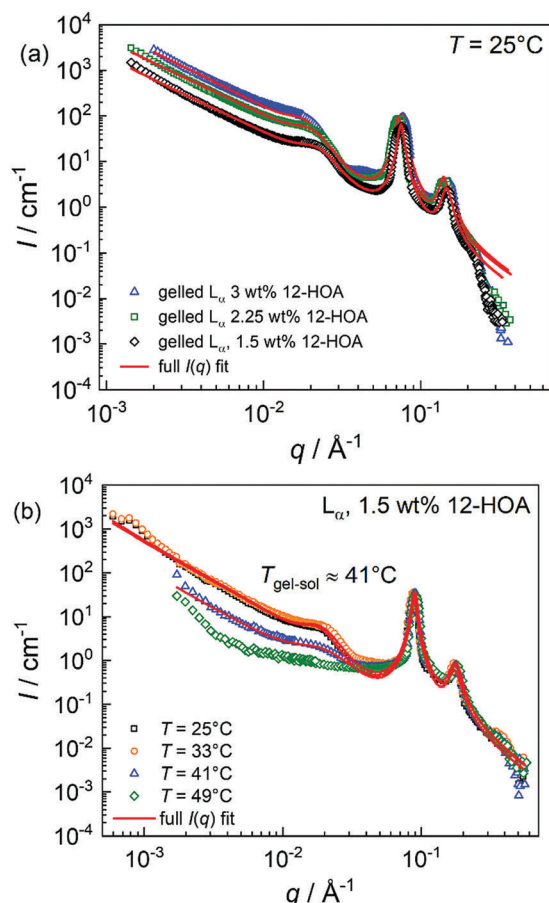
**Table 1** Fit parameters obtained from the analyses of the SANS data shown in Fig. 3. Parameters of the scattering contribution  $I_{\text{lam}}(q)$  of the lamellar structure are the bilayer thickness  $\delta_{\text{bi}}$ , the Caillé parameter  $\eta$ , the lamellar repeat distance  $d_0$  and the layer peak FWHM  $\xi_0$ . Parameters of the contribution from the gel fiber network  $I_{\text{net}}(q)$  are the mean fiber radius  $R_0$  and its distribution  $\sigma_R$ , the fraction  $f$  of gel fibers not bundled in nodes and the fraction  $g$  of monomerically dissolved gelator. Parameters of the contribution  $I_{\text{syn}}(q)$  from the synergistic structure are the characteristic length  $d_c$  and the distribution parameter  $\zeta_c$ . Contributions of  $I_{\text{net}}(q)$  and  $I_{\text{syn}}(q)$  are weighted with the parameters  $w_{\text{net}}$  and  $w_{\text{syn}}$ , respectively. All fits are performed with fixed values of the node thickness  $T_0 = 40$  nm and its distribution  $\sigma_T = 5$  nm

	$I_{\text{lam}}$				$I_{\text{net}}(q)$				$I_{\text{syn}}(q)$			
	$\delta_{\text{bi}}/\text{nm}$	$\eta$	$d_0/\text{nm}$	$\xi_0/\text{nm}^{-1}$	$w_{\text{net}}$	$R_0/\text{nm}$	$\sigma_R/\text{nm}$	$f$	$g$	$w_{\text{syn}}$	$d_c/\text{nm}$	$\zeta_c/\text{nm}^{-1}$
Fig. 3a (Nallet)	2.4	0.13	8.2	—	0.3	11.5	1.3	0.87	0.10	0.7	37	0.011
Fig. 3b (Lorentz)	—	—	8.3	0.009	0.3	11.5	1.3	0.87	0.10	0.7	37	0.011



Nevertheless, the Nallet model was proved to give reasonable values for the Caillé parameter,<sup>73</sup> at least in the case of “hard smectic order” which also applies for the here investigated  $L_\alpha$  phase.

To describe the scattering intensity in the low- $q$  regime quantitatively, we decided to model the scattering contribution



**Fig. 4** (a) Total coherent scattering intensity  $I(q)$  at 25 °C of the  $L_\alpha$  phase ( $\phi_w = 0.675$  and  $\phi_{\text{DOH/SDS}} = 0.5$ ) gelled with different mass fractions of the gelator 12-HOA (symbols) and the corresponding  $I(q)$  fits (lines). Fit parameters are listed in Table 2. (b)  $I(q)$  of the  $L_\alpha$  phase ( $\phi_w = 0.675$  and  $\phi_{\text{DOH/SDS}} = 0.5$ ) with fixed 12-HOA gelator mass fraction of  $\mu = 0.015$  at different temperatures  $T$  and the corresponding  $I(q)$  fits. Fit parameters are listed in Table 3. At temperatures above the gel–sol transition temperature  $T_{\text{gs}}$  the  $I(q)$ -shoulder of the synergistic structure disappears.

of the lamellar structure  $I_{\text{lam}}(q)$  by simply using the sum of two Lorentzians at  $q = 2\pi/d_0$  and  $4\pi/d_0$  to fit the two orders of pseudo-Bragg layer peaks in our experimental data (Fig. 3b). As seen in Fig. 3b, this simple approach describes the layer peaks equally well as the Nallet model in Fig. 3a but without the strong increase of the intensity at low  $q$ . Furthermore, both approaches provide within the measurement error the same value of the lamellar spacing, *i.e.*  $d_0 = 8.2$  nm (Nallet) and  $d_0 = 8.3$  nm (Lorentz). Note that the bilayer thickness  $\delta_{\text{bi}} = 2.4$  nm agrees with the value ( $\delta_{\text{bi}} \sim 2.5$  nm) found in ref. 74. The obtained Caillé parameter of  $\eta = 0.13$  is in good agreement with the prediction of  $\eta < 1/n^2$ ,<sup>73,75</sup> with  $n$  being the highest order of the pseudo-Bragg peaks visible, which is 3 in our samples (third order layer peak visible as a small bump (see arrows in Fig. 3a),  $1/3^2 = 0.11$ ).

The gel network can be described as a combination of “free” gelator fibers and of fibers agglomerated into nodes which are the networks junction zones.<sup>15</sup> The corresponding SANS intensity  $I_{\text{net}}(q)$  can be modelled by treating the gelator fibers as stiff cylindrical rods and the nodes as stacked layers of parallel running fibers. This leads to  $I_{\text{net}}(q)$  being the sum of two independent scattering contributions  $I_{\text{fbr}}$  and  $I_{\text{nds}}$ .<sup>15</sup> The model which we used to describe the gel network was evolved by Terech *et al.*<sup>15</sup> and further developed by Laupheimer *et al.*<sup>76</sup> A more detailed description of the gel network scattering contribution can be found in the ESI.† Fit parameters are the parameter  $f$  describing the fraction of “free” gel fibers not bundled in nodes, the parameter  $g$  describing the fraction of monomerically dissolved gelator not forming fibers, the mean radius  $R_0$  of the gel fibers and the mean thickness  $T_0$  of the nodes. In addition, Gaussian distributions of  $R_0$  and  $T_0$  are taken into account with standard deviations  $\sigma_R$  and  $\sigma_T$ , respectively. As it turned out, most of the gel fibers are “free” and not involved in nodes. Thus, the parameters  $T_0$  and  $\sigma_T$  have no significant impact on the scattering contributions. To reduce the number of fit parameters both parameters are fixed at reasonable constant values. The value of  $\sigma_R$  is found to have almost no impact on the full fit of  $I(q)$  and is thus taken in accordance to the value of  $\sigma_R$  found in a gelled isotropic micellar phase of the same system (see ESI†).

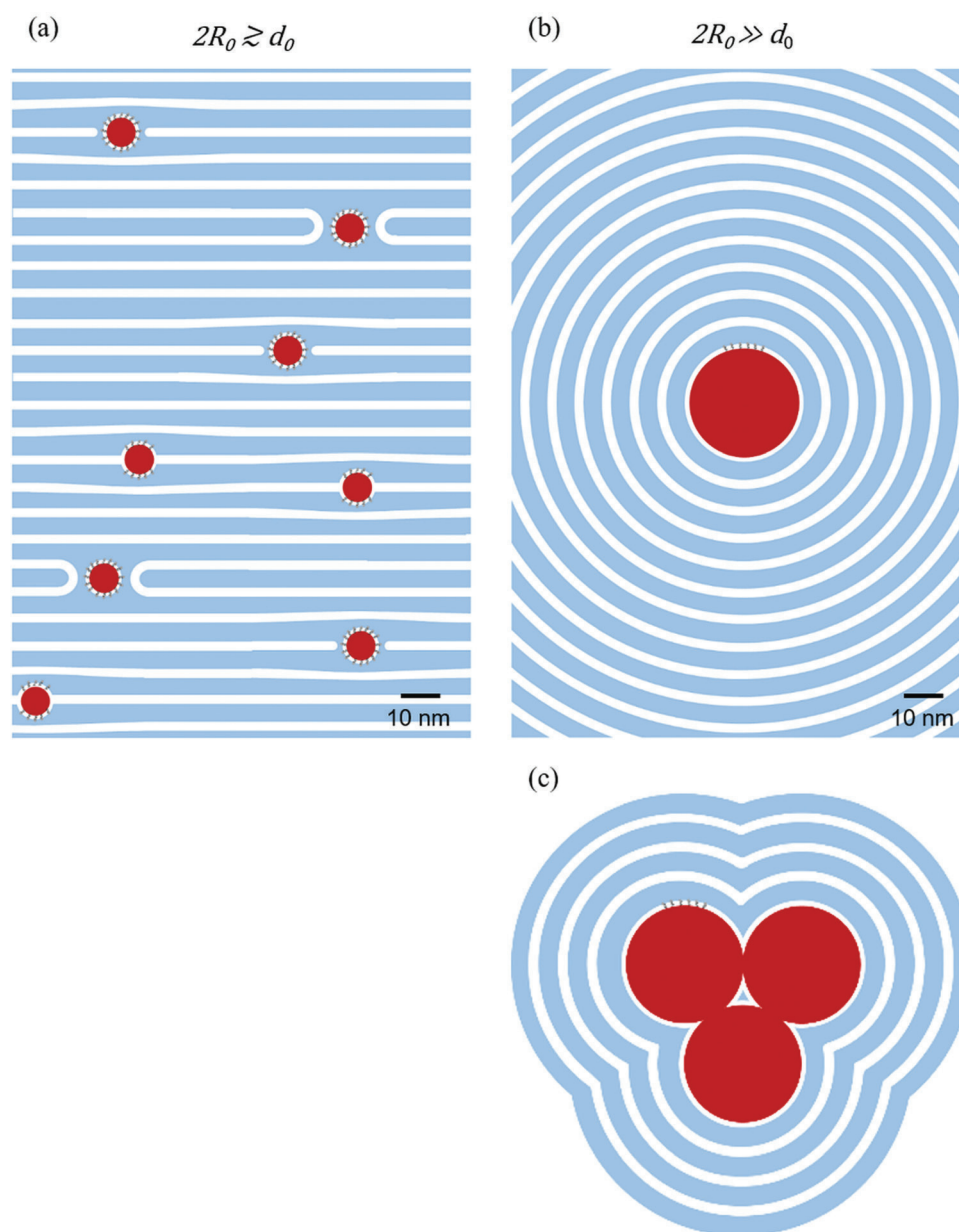
Finally, we described the scattering contribution of the synergistic structure in a phenomenological way by adding a Lorentzian  $I_{\text{syn}}(q)$  with a peak position  $q_c$  and a full width at half maximum (FWHM)  $\xi_c$ . From this analysis a characteristic

**Table 2** Fit parameters from the analyses of SANS data in Fig. 4a ( $L_\alpha$  phase ( $\phi_w = 0.675$  and  $\phi_{\text{DOH/SDS}} = 0.5$ ) gelled with different mass fractions  $\mu$  of gelator 12-HOA). Parameters of the contribution  $I_{\text{lam}}(q)$  of the lamellar structure are the lamellar repeat distance  $d_0$  and the layer peak FWHM  $\xi_0$ . Parameters of the contribution from the gel fiber network are the mean fiber radius  $R_0$  and its distribution  $\sigma_R$ , the fraction  $f$  of gel fibers not bundled in nodes and the fraction  $g$  of monomerically dissolved gelator. Parameters of the contribution  $I_{\text{syn}}(q)$  from the synergistic structure are the characteristic length  $d_c$  and the distribution parameter  $\xi_c$ . Contributions of  $I_{\text{net}}(q)$  and  $I_{\text{syn}}(q)$  are weighted with the parameters  $w_{\text{net}}$  and  $w_{\text{syn}}$ , respectively. All fits are performed with fixed values of the node thickness  $T_0 = 40$  nm and its distribution  $\sigma_T = 5$  nm

Fig. 4a $\mu$	$I_{\text{lam}}(q)$		$w_{\text{net}}$	$I_{\text{net}}(q)$			$g$	$w_{\text{syn}}$	$I_{\text{syn}}(q)$	
	$d_0/\text{nm}$	$\xi_0/\text{nm}^{-1}$		$R_0/\text{nm}$	$\sigma_R/\text{nm}$	$f$			$d_c/\text{nm}$	$\xi_c/\text{nm}^{-1}$
0.015	8.4	0.09	0.28	10.5	1.7	0.90	0.10	0.72	31	0.16
0.0225	8.7	0.09	0.28	11.0	1.5	0.90	0.10	0.72	33	0.135
0.03	8.3	0.09	0.30	11.5	1.3	0.87	0.10	0.7	37	0.11

**Table 3** Fit parameters from the analyses of SANS data in Fig. 4b ( $L_x$  phase ( $\phi_w = 0.675$  and  $\phi_{\text{DOH/SDS}} = 0.5$ ) with fixed 12-HOA gelator mass fraction of  $\mu = 0.015$  at different temperatures  $T$ ). Parameters of the contribution  $I_{\text{lam}}(q)$  of the lamellar structure are the lamellar repeat distance  $d_0$  and the layer structure peak FWHM  $\xi_0$ . Parameters of the contribution from the gel fiber network are the mean fiber radius  $R_0$  and its distribution  $\sigma_R$ , the fraction  $f$  of gel fibers not bundled in nodes and the fraction  $g$  of monomerically dissolved gelator. Parameters of the contribution  $I_{\text{syn}}(q)$  from the synergistic structure are the characteristic length  $d_c$  and the distribution parameter  $\xi_c$ . Contributions of  $I_{\text{net}}(q)$  and  $I_{\text{syn}}(q)$  are weighted with the parameters  $w_{\text{net}}$  and  $w_{\text{syn}}$ , respectively. All fits are performed with fixed values of the node thickness  $T_0 = 40$  nm and its distribution  $\sigma_T = 5$  nm

Fig. 4b $T/^\circ\text{C}$	$I_{\text{lam}}(q)$			$I_{\text{net}}(q)$				$I_{\text{syn}}(q)$		
	$d_0/\text{nm}$	$\xi_0/\text{nm}$	$w_{\text{net}}$	$R_0/\text{nm}$	$\sigma_R/\text{nm}$	$f$	$g$	$w_{\text{syn}}$	$d_c/\text{nm}$	$\xi_c/\text{nm}$
25	7.1	0.12	0.1	10.5	1.7	0.84	0.10	0.9	36	0.12
33	7.1	0.12	0.1	11.0	1.7	0.84	0.10	0.9	36	0.13
41	7.0	0.12	0.1	11.5	2.0	0.82	0.10	0.9	38	0.23



**Fig. 5** Comparison of structures formed in lamellar gels if (a) the gel fiber diameter  $2R_0$  is in the order of the lamellar repeat period  $d_0$  or (b) substantially exceeds  $d_0$ . In (c) three fibers bundle together to further reduce the lamellar layer curvature in (b). Cross sections of fibers are colored in red, surfactant bilayers in white and solvent layers in blue. Figures are drawn to scale for the cases of (a) DBS fibers and (b), (c) 12-HOA fibers.

length of the synergistic structure of the order of 37 nm was determined using the Bragg relation  $d_c = 2\pi/q_c$  and a peak position of  $q_c \approx 0.017 \text{ \AA}^{-1}$ . Due to the relatively large  $\xi_c$  in the order of  $0.013 \text{ nm}^{-1}$ ,  $d_c$  is considered to be broadly distributed.

Since the choice between the Nallet and Lorentz fits in Fig. 3 has no significant impact on the remaining fit parameters – neither those of the network contribution nor those of the synergistic structure (see Table 1) – we will further show and discuss the analyses obtained with Lorentz fits for  $I_{\text{lam}}(q)$  only. The corresponding analyses with the Nallet fit and the fit parameters thereof are found in the ESI.†

The impact of the gelator content on the SANS data of the gelled  $L_\alpha$  phase is shown in Fig. 4a with the corresponding fit parameters listed in Table 2. As a result of the increasing gelator mass fraction  $\mu$  the scattering intensity at low and intermediate  $q$  ( $q < 0.05 \text{ \AA}^{-1}$ ) is systematically increasing, indicating that both the contribution from the gel fiber network and the contribution from the synergistic structure are getting bigger. Furthermore, the position of the shoulder is found to shift to lower  $q$ -values. Accordingly, the mean radius of the gel fibers  $R_0$  and the characteristic length of the synergistic structure  $d_c$  increase as  $\mu$  increases (see Table 2).

Selected SANS curves of the temperature dependent measurements are shown in Fig. 4b with the corresponding fit parameters listed in Table 3. These measurements give another strong support that the new synergistic structure only exists in the lamellar gel. At temperatures below the gel–sol transition temperature of  $T_{\text{gs}} = 41 \text{ }^\circ\text{C}$ , the characteristic shoulder at  $q \approx 0.017 \text{ \AA}^{-1}$  originating from  $I_{\text{syn}}(q)$  is clearly observed in the SANS profiles. This shoulder however considerably decreases if  $T$  approaches  $T_{\text{gs}}$  and completely vanishes at temperatures  $T > T_{\text{gs}}$ , at which the gel fibers have melted and only the lamellar structure remains present. A melting of the gel fibers in this range of temperature was measured before by means of differential scanning calorimetry,<sup>35</sup> where a broad melting peak from 33 to 41  $^\circ\text{C}$  with a melting enthalpy of  $\Delta H_{\text{gs}} = 0.35 \text{ kJ mol}^{-1}$  was observed. As expected, the fraction  $g$  of monomeric gelator in the sample significantly increases towards  $T_{\text{gs}}$ . We further notice from Table 3 that the mean gel fiber radius  $R_0$  slightly increases with increasing temperature while the characteristic length  $d_c$  of the new synergistic structure does not show any systematic variation with  $T$ .

**Model for the new synergistic structure.** In the beginning of this section let us first summarize the experimental facts about the synergistic structure we observed in our lamellar gels:

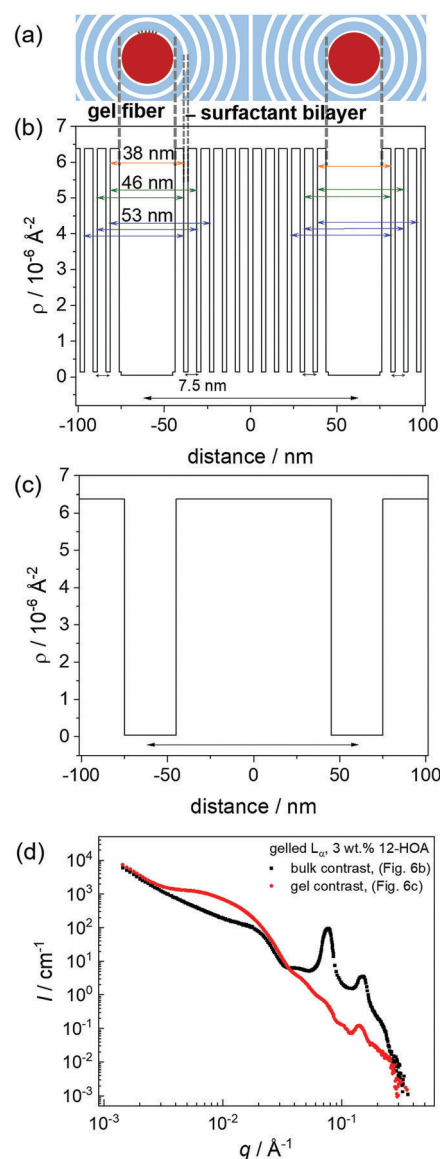
(1) The synergistic structure requires the spatial coexistence of gel fibers and a lamellar liquid crystalline structure; it is neither observed in the non-gelled lamellar phase nor in the isotropic gel.

(2) It is only observed if the gel fiber diameter considerably exceeds the lamellar repeat unit

(3) It gives rise to a broad Lorentzian-shaped scattering peak at a characteristic length which is significantly larger than the gel fiber diameter.

But what does this new synergistic structure look like? To solve this important question, we must take into account

that the gel fibers are running through a lamellar liquid crystal phase, an anisotropic, 1D-periodic medium. In this liquid-



**Fig. 6** (a) Synergistic structure in lyotropic lamellar gels with the gel fiber diameter considerably exceeding the lamellar repeat unit. A surfactant monolayer (white) is adsorbed at the surface of the hydrophobic gel fiber (red) and the subsequent layers are circularly wrapped around the fibers. (b) Scattering length density profile of the suggested synergistic structure. The orange, green and blue arrows indicate the recurring distances leading to the broad Lorentzian peak (“shoulder”) in the SANS profile. (c) Scattering length density profile for the “gel contrast”, a contrast where due to the use of deuterated surfactant and deuterated cosurfactant only the gel network sub-structure is monitored by the neutrons. (d) SANS curves of the  $L_\alpha$  phase ( $\phi_w = 0.675$  and  $\phi_{\text{DOH/SDS}} = 0.5$ ) gelled with 3 wt% 12-HOA in bulk contrast (black squares) and in the gel contrast (red circles). In the gel contrast a mixture of deuterated and protonated surfactant (16.7 v%/2.4 v%) and cosurfactant (9.6 v%/0.5 v%) is used to match the scattering length density of  $\text{D}_2\text{O}$ . In the bulk contrast, the scattering contributions of both fibers and surfactant bilayers are detected, while in the gel contrast the only scattering contribution arises from the gel fibers. In the gel contrast the shoulder shifts to lower  $q$ -values and is considerably broader than in the bulk contrast.



crystalline medium the fiber appears like the core of a topological defect and the natural response of a liquid crystal to this defect is an elastic response. This is at least true<sup>77</sup> as long as the length scale of the deformation, set by the fiber diameter  $2R_0$ , is large in comparison to the molecular length scale, set for instance by the thickness of the surfactant bilayer  $\delta_{bi}$  or the lamellar spacing  $d_0$ , *i.e.*  $2R_0 \gg d_0 > \delta_{bi}$  which is true in our 12-HOA case with  $2R_0 \approx 24$  nm,  $d_0 \approx 8$  nm and  $\delta_{bi} \approx 2.4$  nm.

How should the elastic response look like? It is well known that layer bending (corresponding to director splay) is the only “easy” elastic deformation allowed in smectic or lamellar liquid crystals since it is the only deformation which conserves the smectic or lamellar repeat unit.<sup>78</sup> Pure layer bending would lead to a synergistic structure of layers and fibers as shown in Fig. 5b where each fiber is enclosed by closed cylindrical layers of the lamellar phase. This synergistic structure avoids any energy-costly layer ends. Instead, it only requires a pure bend deformation of the layers, the elastic energy of which increases as the square of the layer curvature increases. The energy penalty of the layer bending thus decreases with increasing thickness of the gel fiber and – even more interesting – it can be further reduced if two or more fibers bundle together, as shown in Fig. 5c. This effect might create the source of a sort of pseudo force which tends to arrange the fibers in bundles.

Otherwise, if the fiber diameter comes close to the molecular length scale, *i.e.*  $2R_0 \approx d_0$  (which is true in our DBS case with  $2R_0 \approx 8.16$  nm and  $d_0 \approx 8$  nm) the elastic response of the liquid crystal breaks down since the layer curvature and thus the elastic bending energy would be far too high.<sup>77</sup> As shown in Fig. 5a, the fibers might now appear as a kind of dislocation since they interrupt the lamellar configuration and create (energy-costly) layer ends. In an energetically more favorable spatial arrangement the hydrophobic fibers can either be surrounded by a surfactant monolayer or cause the formation of passages in the bilayer.

These considerations explain very well the first two of the above-mentioned experimental observations on the appearance of synergistic structures. But does a synergistic structure such as the one sketched in Fig. 5b also explain the broad Lorentzian

scattering peak indicating a characteristic length of the structure being larger than both the fiber diameter and the lamellar repeat period?

Fig. 6b shows the profile of scattering length density in the lamellar gel around a synergistic structure (Fig. 6a). Obviously, the periodic lamellar structure is disturbed by the gel fibers. The regular stacking of lamellar layers and the rather coincidental distance between gel fibers are incommensurable. Around the fibers new recurring distances between surfactant bilayers appear, which are highlighted by the colored arrows in Fig. 6b. We believe these distances to be the reason for the broad Lorentzian peak appearing in the SANS curves of 12-HOA lamellar gels. The considerable width of the peak is owed to the broad distribution of distances between bilayers on opposite sides of a gel fibers.

This idea is further supported by SANS contrast variation experiments which allow to monitor the scattering contributions of the individual sub-structures in a lamellar gel. In all our measurements presented so far the bulk contrast (protonated gelator, surfactant and cosurfactant in D<sub>2</sub>O) was used which comprises the scattering contributions of both, gel fibers and surfactant bilayers and leads to the scattering length density profile shown in Fig. 6b. To selectively observe the gel network, the “gel contrast” was used. For the gel contrast a mixture of mostly deuterated and partly protonated surfactant (and cosurfactant) was used, such that the scattering length densities of SDS (and DOH) match the one of D<sub>2</sub>O leading to the scattering length profile shown in Fig. 6c. Since now the contrast between the surfactant bilayers and the water sub-layers vanishes, the only remaining contrast is the one between the gel fibers and the surrounding lamellar phase. The SANS data obtained from the gelled L<sub>α</sub> phase in the gel contrast is shown in Fig. 6d. Instead of pseudo-Bragg peaks due to the lamellar layer structure only small bumps can be observed at high *q*-values proving the contrast adjustment (no contrast between bilayers and D<sub>2</sub>O) to be successful.

The small peak at  $q \approx 0.14 \text{ \AA}^{-1}$  is the “intra-fiber peak” due to the layered structure of 12-HOA fibers (*cf.* Fig. 1b) which is

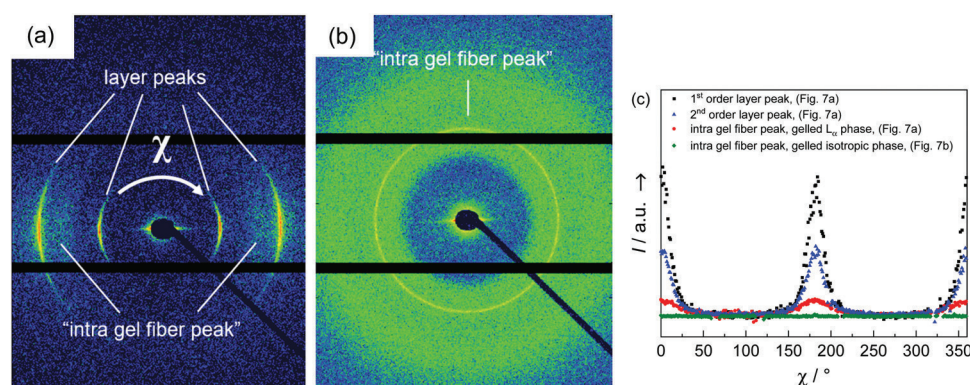


Fig. 7 2D-SAXS pattern of (a) an aligned domain of the gelled L<sub>α</sub> phase ( $\phi_w = 0.675$  and  $\phi_{DOH/SDS} = 0.5$ ,  $\mu(12HOA) = 0.03$ ), (b) the gelled isotropic phase ( $\phi_w = 0.75$  and  $\phi_{DOH/SDS} = 0.17$ ,  $\mu(12HOA) = 0.03$ ) and (c) the azimuthal peak profiles integration thereof. The 2D SAXS results prove that in a lamellar gel the fibers are oriented in directions along the lamellar layers with the layer normal of the L<sub>α</sub> phase perpendicular to the long axis of the gel fiber, whereas the fibers are uniformly distributed in a gelled isotropic phase.

superimposed by the second order layer peak in the bulk contrast. As can be seen in the scattering length density profile (Fig. 6c) the only remaining distance in the gel contrast is the one between adjacent gel fibers. This distance is considerably larger than the predominant distances in the bulk contrast (colored arrows in Fig. 6b). Thus, the broad shoulder in the bulk contrast appears at lower  $q$ -values in the gel contrast (see Fig. 6d) where it is also significantly broader due to the even broader distribution of distances between gel fibers. The SANS data of the gelled  $L_\alpha$  phase in the gel contrast thus clearly support our model for the synergistic structure.

In addition, our model of gel fibers coaxially enclosed by cylindrical lamellar layers requires that the gel fibers run along the lamellar layers, *i.e.* the fiber axis is normal to the lamellar layer normal. We have verified this mutual alignment of fibers and layers by 2D-SAXS experiments as follows: The 12-HOA fibers have a layered structure (see Fig. 1b) which gives rise to an “intra-fiber peak” at  $q \approx 0.14 \text{ \AA}^{-1}$  and in the direction normal to the fiber axis. In other words, this intra-fiber peak should be observed in the same direction as the lamellar layer peaks in an aligned domain of the lamellar gel with the proposed synergistic structure. The intra-fiber peak however is weak due to the low content of gel fibers (in the range of a few wt%) and the peak is broad due to the limited number of layers in the fiber (*cf.* Fig. 1b). While in our SANS experiments the intra-fiber peak is superimposed by the second-order lamellar layer peak, both peaks can be resolved in  $q$  by means of small-angle X-ray scattering (SAXS). Fig. 7a shows the 2D-SAXS pattern of a small aligned domain of our  $L_\alpha$  phase gelled with 12-HOA. As predicted from our model, the intra-fiber peak is found in the same directions as the lamellar layer peaks. This proves that the fibers run in directions along the lamellar layers with the layer normal of the  $L_\alpha$  phase perpendicular to the long axis of the gel fiber. In contrast, the intra gel fiber peak of a gelled isotropic micellar phase is randomly distributed in the “powder-like” 2D-SAXS pattern in Fig. 7b. This shows that the fibers form a more or less random gel network in the isotropic micellar phase, while in the  $L_\alpha$  phase a clearly anisotropic gel network is formed.

## Conclusion

In this paper we report the observation of so far unknown synergistic structures in lyotropic lamellar gels which are neither observed in the non-gelled  $L_\alpha$  phase nor in the isotropic micellar gel. The formation of these structures thus obviously requires the spatial coexistence of both lamellar liquid crystalline layers and gel fibers and, in addition, the diameter of the gel fibers has to be large in comparison to the lamellar repeat period.

We suggest that the synergistic structure originates from the elastic response of the lamellar layers to the presence of a relatively thick gel fiber which appears like the core of a topological defect that disturbs the regular lamellar order. As a result, the lamellar layers bend into closed cylinders which

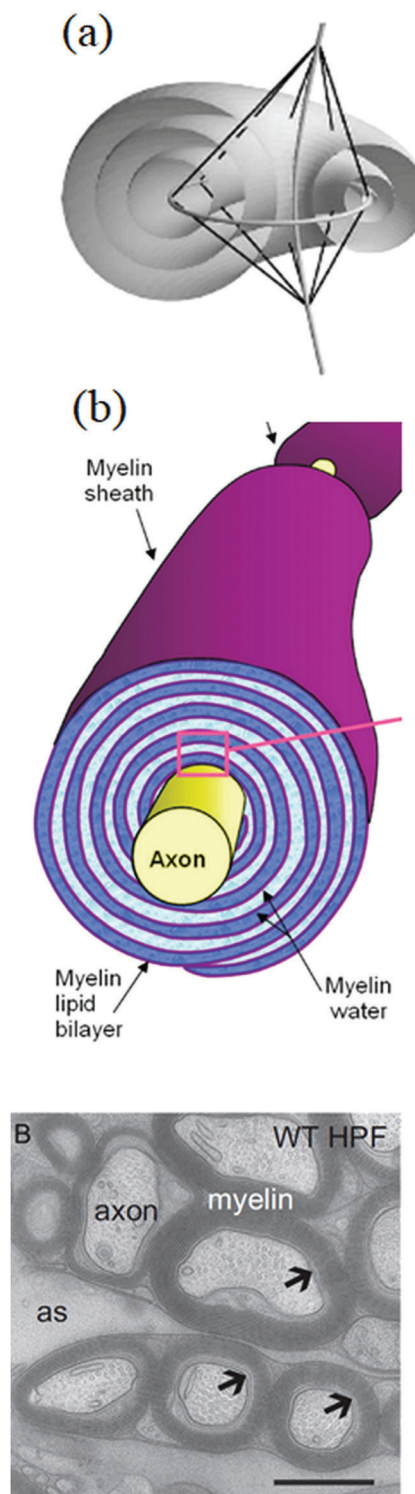


Fig. 8 Counterparts of the new synergistic structure found in lyotropic lamellar gels: (a) bend layers in Dupin cyclids of the focal conic domains found in thermotropic smectic liquid crystals. Reprinted from ref. 83 with the permission of the Royal Society of London, Copyright 2020. (b) In nerve cells the axons are coaxially enclosed by myelin sheets, as can be seen in the schematic drawing (top, reprinted from ref. 84 with the permission from Elsevier, Copyright 2020) as well as the electron microscopy image (bottom, reprinted from ref. 85 with the permission from Elsevier, Copyright 2020).

coaxially surround the fiber. Since the formation of closed cylindrical layers avoids the appearance of energy-costly layer ends, this is a natural response of a 1D-layered fluid medium. The same response is found in the characteristic focal-conic textures of smectic and lamellar liquid crystals where the layers are bent into Dupin cyclids<sup>79,80</sup> (Fig. 8a), the formation of which is well understood in the elasticity theory of thermotropic smectics.<sup>81,82</sup> All in all, the assumption of cylindrical lamellar layers around the gel fibers is in-line with all experimental observations and in particular with the SANS data presented in this study.

Last but not least, it has not escaped our notice that the new synergistic structure found in our lamellar gels has a famous biological counterpart, namely the structure of a nerve cell in which the axon is coaxially enclosed by the lamellar layers of myelin lipid bilayers and water. In the lamellar gel, the axon is replaced by the gel fiber and the myelin lipid bilayer by the surfactant bilayers. Lyotropic lamellar gels can thus be considered as a new kind of complex soft matter spontaneously forming biomimetic structures.

## Funding sources

The authors gratefully acknowledge financial support from the Deutsche Forschungsgemeinschaft (DFG Gi 243/9-1) and Fonds der Chemischen Industrie (FCI).

## Conflicts of interest

There are no conflicts to declare.

## Acknowledgements

The authors thank Thomas Hellweg for the possibility to carry out 2D-SAXS experiments on the Xeuss SAXS/WAXS system at the University of Bielefeld in the group of Physical and Biophysical Chemistry. We thank our local contacts Ralf Schweins and Yun Liu for help with the SANS experiments at the Institut Laue Langevin (Grenoble, France) and the NIST Center for Neutron Research (Gaithersburg, Maryland, USA), respectively. Furthermore, we would like to acknowledge the Institut Laue-Langevin (ILL) in Grenoble (France) for the allocation of beam-time under proposal 9-11-1882 [doi: 10.5291/ILL-DATA.9-11-1882] and David Bowyer for help with setting up the SANS environment. We also thank Diana Zauser, Kristina Schneider, Shih-Yu Tseng and Karina Abitav for valuable help with the SANS experiments and Christian Häge for help establishing the python fitting routine.

## References

- X. Y. Liu and J.-L. Li, eds., *Soft fibrillar materials. Fabrication and applications*, Wiley-VCH-Verl., Weinheim, 2013.
- D. J. Abdallah and R. G. Weiss, *Adv. Mater.*, 2000, **12**, 1237–1247.
- M. George and R. G. Weiss, *Acc. Chem. Res.*, 2006, **39**, 489–497.
- P. Terech and R. G. Weiss, *Chem. Rev.*, 1997, **97**, 3133–3160.
- J. H. van Esch and B. L. Feringa, *Angew. Chem., Int. Ed.*, 2000, **39**, 2263–2266.
- K. Murata, M. Aoki, T. Nishi, A. Ikeda and S. Shinkai, *J. Chem. Soc., Chem. Commun.*, 1991, 1715–1718.
- M. Ayabe, T. Kishida, N. Fujita, K. Sada and S. Shinkai, *Org. Biomol. Chem.*, 2003, **1**, 2744–2747.
- J. J. D. de Jong, L. N. Lucas, R. M. Kellogg, J. H. van Esch and B. L. Feringa, *Science*, 2004, **304**, 278–281.
- K. Murata, M. Aoki, T. Suzuki, T. Harada, H. Kawabata, T. Komori, F. Ohseto, K. Ueda and S. Shinkai, *J. Am. Chem. Soc.*, 1994, **116**, 6664–6676.
- J.-L. Pozzo, G. M. Clavier and J.-P. Desvergne, *J. Mater. Chem.*, 1998, **8**, 2575–2577.
- M. Yamanaka, *J. Inclusion Phenom. Macrocyclic Chem.*, 2013, **77**, 33–48.
- B. O. Okesola, V. M. P. Vieira, D. J. Cornwell, N. K. Whitelaw and D. K. Smith, *Soft Matter*, 2015, **11**, 4768–4787.
- T. Tachibana, T. Mori and K. Hori, *Nature*, 1979, **278**, 578–579.
- M. Burkhardt, S. Kinzel and M. Gradzielski, *J. Colloid Interface Sci.*, 2009, **331**, 514–521.
- P. Terech, V. Rodriguez, J. D. Barnes and G. B. McKenna, *Langmuir*, 1994, **10**, 3406–3418.
- S. Yamasaki, Y. Ohashi, H. Tsutsumi and K. Tsujii, *Bull. Chem. Soc. Jpn.*, 1995, **68**, 146–151.
- M. Watase, Y. Nakatani and H. Itagaki, *J. Phys. Chem. B*, 1999, **103**, 2366–2373.
- E. A. Wilder, R. J. Spontak and C. K. Hall, *Mol. Phys.*, 2003, **101**, 3017–3027.
- J. Li, K. Fan, X. Guan, Y. Yu and J. Song, *Langmuir*, 2014, **30**, 13422–13429.
- H. Sato, K. Hori, T. Sakurai and A. Yamagishi, *Chem. Phys. Lett.*, 2008, **467**, 140–143.
- H. Sato, T. Sakurai and A. Yamagishi, *Chem. Lett.*, 2011, **40**, 25–27.
- T. Sakurai, Y. Masuda, H. Sato, A. Yamagishi, H. Kawaji, T. Atake and K. Hori, *Bull. Chem. Soc. Jpn.*, 2010, **83**, 145–150.
- D. A. S. Grahame, C. Olauson, R. S. H. Lam, T. Pedersen, F. Borondics, S. Abraham, R. G. Weiss and M. A. Rogers, *Soft Matter*, 2011, **7**, 7359–7365.
- T. Tachibana, T. Mori and K. Hori, *Bull. Chem. Soc. Jpn.*, 1980, **53**, 1714–1719.
- P. Terech, *Colloid Polym. Sci.*, 1991, **269**, 490–500.
- K. Steck, N. Preisig and C. Stubenrauch, *Langmuir*, 2019, **35**, 17142–17149.
- M. Laupheimer, N. Preisig and C. Stubenrauch, *Colloids Surf., A*, 2015, **469**, 315–325.
- R. H. C. Janssen, V. Stümpflen, C. W. M. Bastiaansen, D. J. Broer, T. A. Tervoort and P. Smith, *J. Appl. Phys.*, 2000, **39**, 2721–2726.
- R. H. C. Janssen, V. Stümpflen, M. C. W. van Bortel, C. W. M. Bastiaansen, D. J. Broer, T. A. Tervoort and P. Smith, *Macromol. Symp.*, 2000, **154**, 117–126.



- 30 H.-C. Lin, C.-H. Wang, J.-K. Wang and S.-F. Tsai, *Materials*, 2018, **11**, 745.
- 31 N. Mizoshita, K. Hanabusa and T. Kato, *Adv. Mater.*, 1999, **11**, 392–394.
- 32 N. Mizoshita, H. Monobe, M. Inoue, M. Ukon, T. Watanabe, Y. Shimizu, K. Hanabusa and T. Kato, *Chem. Commun.*, 2002, 428–429.
- 33 C. Tolksdorf and R. Zentel, *Adv. Mater.*, 2001, **13**, 1307–1310.
- 34 P. Deindörfer, A. Eremin, R. Stannarius, R. Davis and R. Zentel, *Soft Matter*, 2006, **2**, 693–698.
- 35 S. Dieterich, T. Sottmann and F. Giesselmann, *Langmuir*, 2019, **35**, 16793–16802.
- 36 S. Koitani, S. Dieterich, N. Preisig, K. Aramaki and C. Stubenrauch, *Langmuir*, 2017, **33**, 12171–12179.
- 37 K. Steck and C. Stubenrauch, *Langmuir*, 2019, **35**(52), 17132–17141.
- 38 T. Kato, T. Kutsuna, K. Hanabusa and M. Ukon, *Adv. Mater.*, 1998, **10**, 606–608.
- 39 M. Moriyama, N. Mizoshita, T. Yokota, K. Kishimoto and T. Kato, *Adv. Mater.*, 2003, **15**, 1335–1338.
- 40 T. Kato, Y. Hirai, S. Nakaso and M. Moriyama, *Chem. Soc. Rev.*, 2007, **36**, 1857–1867.
- 41 H. Shahsavan, L. Yu, A. Jákl and B. Zhao, *Soft Matter*, 2017, **13**, 8006–8022.
- 42 M. Chambers, H. Finkelmann, M. Remškar, A. Sánchez-Ferrer, B. Zalar and S. Žumer, *J. Mater. Chem.*, 2009, **19**, 1524–1531.
- 43 C. Ohm, M. Brehmer and R. Zentel, *Adv. Mater.*, 2010, **22**, 3366–3387.
- 44 Y. Yu and T. Ikeda, *Angew. Chem., Int. Ed.*, 2006, **45**, 5416–5418.
- 45 D. L. Thomsen, P. Keller, J. Naciri, R. Pink, H. Jeon, D. Shenoy and B. R. Ratna, *Macromolecules*, 2001, **34**, 5868–5875.
- 46 M.-H. Li, P. Keller, J. Yang and P.-A. Albouy, *Adv. Mater.*, 2004, **16**, 1922–1925.
- 47 M. Rogóż, H. Zeng, C. Xuan, D. S. Wiersma and P. Wasylczyk, *Adv. Opt. Mater.*, 2016, **4**, 1689–1694.
- 48 M. Camacho-Lopez, H. Finkelmann, P. Palffy-Muhoray and M. Shelley, *Nat. Mater.*, 2004, **3**, 307–310.
- 49 S. Schuhl, F. Preller, R. Rix, S. Petsch, R. Zentel and H. Zappe, *Adv. Mater.*, 2014, **26**, 7247–7251.
- 50 O. M. Wani, H. Zeng and A. Priimagi, *Nat. Commun.*, 2017, **8**, 15546.
- 51 E.-K. Fleischmann, H.-L. Liang, N. Kapernaum, F. Giesselmann, J. Lagerwall and R. Zentel, *Nat. Commun.*, 2012, **3**, 1178.
- 52 S. Palagi, A. G. Mark, S. Y. Reigh, K. Melde, T. Qiu, H. Zeng, C. Parmeggiani, D. Martella, A. Sanchez-Castillo, N. Kapernaum, F. Giesselmann, D. S. Wiersma, E. Lauga and P. Fischer, *Nat. Mater.*, 2016, **15**, 647–653.
- 53 D.-H. Kim, A. Jahn, S.-J. Cho, J. S. Kim, M.-H. Ki and D.-D. Kim, *J. Pharm. Invest.*, 2015, **45**, 1–11.
- 54 S. H. Tolbert, A. Firouzi, G. D. Stucky and B. F. Chmelka, *Science*, 1997, **278**, 264–268.
- 55 C. T. Kresge, M. E. Leonowicz, W. J. Roth, J. C. Vartuli and J. S. Beck, *Nature*, 1992, **359**, 710–712.
- 56 C. Wang, D. Chen and X. Jiao, *Sci. Technol. Adv. Mater.*, 2009, **10**, 23001.
- 57 N. Mizoshita, T. Kutsuna, T. Kato and K. Hanabusa, *Chem. Commun.*, 1999, 781–782.
- 58 N. Mizoshita, K. Hanabusa and T. Kato, *Adv. Funct. Mater.*, 2003, **13**, 313–317.
- 59 T. Kato, T. Kutsuna, K. Yabuuchi and N. Mizoshita, *Langmuir*, 2002, **18**, 7086–7088.
- 60 T. Kato, *Science*, 2002, **295**, 2414–2418.
- 61 N. Mizoshita, Y. Suzuki, K. Kishimoto, K. Hanabusa and T. Kato, *J. Mater. Chem.*, 2002, **12**, 2197–2201.
- 62 Y. Suzuki, N. Mizoshita, K. Hanabusa and T. Kato, *J. Mater. Chem.*, 2003, **13**, 2870–2874.
- 63 P. E. Laibinis, J. J. Hickman, M. S. Wrighton and G. M. Whitesides, *Science*, 1989, **245**, 845–847.
- 64 C. Stubenrauch and F. Giesselmann, *Angew. Chem., Int. Ed.*, 2016, **55**, 3268–3275.
- 65 A. Brizard, M. Stuart, K. van Bommel, A. Friggeri, M. de Jong and J. van Esch, *Angew. Chem., Int. Ed.*, 2008, **47**, 2063–2066.
- 66 Y. Xu, M. Laupheimer, N. Preisig, T. Sottmann, C. Schmidt and C. Stubenrauch, *Langmuir*, 2015, **31**, 8589–8598.
- 67 K. Steck, C. Schmidt and C. Stubenrauch, *Gels*, 2018, **4**, 78.
- 68 F. Nallet, R. Laversanne and D. Roux, *J. Phys. II France*, 1993, **3**, 487–502.
- 69 R. E. Peierls, *Proc. Cambridge Philos. Soc.*, 1934, **32**, 477.
- 70 L. D. Landau, *Phys. Z. Sowjetunion*, 1937, **11**, 26.
- 71 A. Caillé, *Acad. Sci., Paris, C. R.*, 1972, 891.
- 72 J. Als-Nielsen, J. D. Litster, R. J. Birgeneau, M. Kaplan, C. R. Safinya, A. Lindegaard-Andersen and S. Mathiesen, *Phys. Rev. B: Condens. Matter Mater. Phys.*, 1980, **22**, 312–320.
- 73 F. Castro-Roman, L. Porcar, G. Porte and C. Ligoure, *Eur. Phys. J. E: Soft Matter Biol. Phys.*, 2005, **18**, 259–272.
- 74 P.-O. Quest, K. Fontell and B. Halle, *Liq. Cryst.*, 1994, **16**, 235–256.
- 75 C. R. Safinya, D. Roux, G. S. Smith, S. K. Sinha, P. Dimon, N. A. Clark and A. M. Bellocq, *Phys. Rev. Lett.*, 1986, **57**, 2718.
- 76 M. Laupheimer, T. Sottmann, R. Schweins and C. Stubenrauch, *Soft Matter*, 2014, **10**, 8744–8757.
- 77 P.-G. de Gennes and J. Prost, *The physics of liquid crystals*, Clarendon Press, Oxford, 2nd edn, 1993, ch. 8.3.
- 78 G. Vertogen and W. H. Jeu, *Thermotropic Liquid Crystals, Fundamentals*, Springer, Berlin, Heidelberg, 1988, ch. 5.3.
- 79 Y. Bouligand, *J. Phys.*, 1972, **33**, 525–547.
- 80 C. E. Williams and M. Kléman, *J. Phys. Colloques*, 1975, **36**, C1-315–C1-320.
- 81 P. G. de Gennes, *J. Phys. Colloques*, 1969, **30**, C4-65–C4-71.
- 82 A. Saupe, *Mol. Cryst.*, 1969, **7**, 59–74.
- 83 W. K. Schief, M. Kléman and C. Rogers, *Proc. R. Soc. A*, 2005, **461**, 2817–2837.
- 84 C. Laule, I. M. Vavasour, S. H. Kolind, D. K. B. Li, T. M. Trabousee, G. M. W. Moore and A. L. MacKay, *Neurotherapeutics*, 2007, **4**, 460–484.
- 85 W. Möbius, K.-A. Nave and H. B. Werner, *Brain Res.*, 2016, **1641**, 92–100.